

TWR-17542 Vol IV
Rev. A

FLIGHT SET 360L003 (STS-29)
SEALS FINAL REPORT
Volume IV

July 1989

Prepared for:

**NATIONAL AERONAUTICS AND SPACE ADMINISTRATION
GEORGE C. MARSHALL SPACE FLIGHT CENTER
MARSHALL SPACE FLIGHT CENTER, ALABAMA 35812**

Contract No. NAS8-30490

DR. No. 5-3

WBS.No. 4B601-04-01

(NASA-CR-183888) FLIGHT SET 360L003
(STS-29) SEALS, VOLUME 4 Final Report
(Thiokol Corp.) 239 p

N90-71175

Unclas
00/20 0271081

***Thiokol* CORPORATION**
SPACE OPERATIONS

P.O. Box 707, Brigham City, UT 84302-0707 (801) 863-3511

* DOC NO.

VOL

REV A

TITLE

TWR-17542, Volume IV

**Flight Set 360L003 (STS-29)
Seals Final Report
Volume IV**

July 1989

Prepared by:

Kelly S. Baker 8-4-89
K. S. Baker
Joints and Seals Design

Approved by:

Jerry Burn
J. Burn, Supervisor
Joints and Seals Design

J. V. Daines
J. V. Daines, Manager
Metallic Component Design

R. B. Crosbie
R. B. Crosbie
Seals Program Management

T. W. Morgan
T. W. Morgan
Flight Performance

G. D. Richards
Reliability

Phillip O. Greenhalgh
System Safety

Released by:

K. Sperry 10/11/89
K. Sperry, Supervisor
Metal Component/Fastener Design

P. C. Lydeck 10-24-89
Data Management
ECS# SS1011

MORTON THIOKOL, INC.

Aerospace Group

P.O. Box 524, Brigham City, Utah 84302 (801) 863-3511

ACKNOWLEDGMENTS

Contributions to this report were made by the following people:

Jeff Curry
Joints and Seals Design

David Gurney
Joints and Seals Design

CONTENTS

1.0	INTRODUCTION	1
2.0	SUMMARY AND CONCLUSIONS	12
2.1	Structural Performance Summary	12
2.2	Post-Test Inspection Summary	13
3.0	POST-FIRE INSPECTION OBJECTIVES, O-RING SQUEEZE AND LEAK CHECK RESULTS	16
4.0	STRUCTURAL ASSESSMENT.....	16
4.1	Instrumentation	20
4.2	Field Joint Performance	20
4.3	Case Membrane Girth Gage Response	32
4.4	Case Biaxial Stresses	36
4.4.1	Case Line Loads, Aft Field-to-ET Attach Joint	36
4.5	Nozzle-to-Case Joint Performance	43
4.5.1	Nozzle-to-Case Girth Gages	44
4.5.2	Nozzle-to-Case Biaxial Strain Gages	48
4.6	Moment, Shear, and Strut Forces	53
4.6.1	Bending Around the Y Axis	53
4.6.2	Bending Around the Z Axis	56
4.6.3	Axial Force, X Axis	58
4.6.4	Line Loads	60
4.6.5	Strut Forces	60
4.7	Flight Envelopes	63
4.7.1	Bending Around the Y Axis	63
4.7.2	Bending Around the Z Axis	64
4.7.3	Axial Force	65
5.0	POST-FIRE INSPECTION RESULTS	65
5.1	Left Motor "A" Disassembly Evaluation	66
5.1.1	External Walk Around	66
5.1.2	Safe and Arm Joint	66
5.1.3	Outer Igniter Joint	66
5.1.4	Inner Igniter Joint	68
5.1.5	Forward Field Joint	68
5.1.6	Center Field Joint	68
5.1.7	Aft Field Joint	68
5.1.8	Nozzle-to-Case Joint	70
5.1.9	Aft Exit Cone Joint	71
5.1.10	Forward End Ring-to-Nose Inlet Housing	71
5.1.11	Inlet Housing-to-Throat Support Housing	72
5.1.12	Forward Exit Cone-to-Throat Support Housing	72
5.1.13	Fixed Housing-to-Aft End Ring	73
5.1.14	Factory Joints.. ..	73
5.1.14.1	Forward Dome-to-Cylinder Factory Joint.....	73
5.1.14.2	Forward Cylinder-to-Cylinder Factory Joint.....	74
5.1.14.3	Center Forward Cylinder-to-Cylinder Factory Joint.....	74

CONTENTS (Continued)

5.1.14.4	Center Aft Cylinder-to-Cylinder Factory Joint.....	74
5.1.14.5	ET-to-Stiffener Factory Joint.....	75
5.1.14.6	Stiffener-to-Stiffener Factory Joint.....	75
5.1.14.7	Aft Dome-to-Stiffener Factory Joint.....	76
5.2	Right Motor Disassembly Evaluation	76
5.2.1	External Walk Around	76
5.2.2	Safe and Arm Joint	76
5.2.3	Outer Igniter Joint	76
5.2.4	Inner Igniter Joint	77
5.2.5	Forward Field Joint	77
5.2.6	Center Field Joint	78
5.2.7	Aft Field Joint	78
5.2.8	Nozzle-to-Case Joint	79
5.2.9	Aft Exit Cone Joint	80
5.2.10	Forward End Ring-to-Nose Inlet Housing	80
5.2.11	Nose Inlet Housing-to-Throat Support Housing	81
5.2.12	Forward Exit Cone-to-Throat Support Housing	81
5.2.13	Fixed Housing-to-Aft End Ring	82
5.2.14	Factory Joints	82
5.2.14.1	Forward Dome-to-Cylinder Factory Joint.....	82
5.2.14.2	Forward Cylinder-to-Cylinder Factory Joint.....	82
5.2.14.3	Center Forward Cylinder-to-Cylinder Factory Joint.....	82
5.2.14.4	Center Aft Cylinder-to-Cylinder Factory Joint.....	83
5.2.14.5	ET-to-Stiffener Factory Joint.....	83
5.2.14.6	Stiffener-to-Stiffener Factory Joint.....	83
5.2.14.7	Aft Dome-to-Stiffener Factory Joint.....	84
5.3	Leak Check and Vent Port Plug Post Flight Evaluations	84
5.4	Post-Fire Team Assessments.....	94
5.4.1	Remains Observation.....	95
5.4.2	Minor Anomalies.....	95
5.4.3	Major Anomalies.....	95
5.4.4	Critical Anomalies.....	95
5.5	RPRB Position.....	95
6.0	REFERENCES	97

CONTENTS (Continued)

TABLES

Table 1	Left SRM Forward Field Joint Girth Gages	21
Table 2	Left SRM Center Field Joint Girth Gages	22
Table 3	Left SRM Aft Field Joint Girth Gages	23
Table 4	Right SRM Forward Field Joint Girth Gage	24
Table 5	Right SRM Center Field Joint Girth Gages	25
Table 6	Right SRM Aft Field Joint Girth Gages	26
Table 7	Forward Field Joint Radial Growth Comparisons to 360L003 (STS-29)	28
Table 8	Center Field Joint Radial Growth Comparisons to 360L003 (STS-29)	29
Table 9	Aft Field Joint Radial Growth Comparisons to 360L003 (STS-27)	30
Table 10	Left SRM Case Radial Deflection Girth Gages	33
Table 11	Right SRM Case Radial Deflection Girth Gages	34
Table 12	Case Membrane Radial Growth Comparisons to 360L003 (STS-29)	35
Table 13	360L003 (STS-29) Comparison of Maximum Predicted Versus Measured Biaxial Strain Values (Zero to 3 Seconds) Left RSRM	37
Table 14	360L003 (STS-29) Comparison of Maximum Predicted Versus Measured Biaxial Strain Values (Zero to 3 Seconds) Right RSRM	39
Table 15	Maximum Measured Biaxial Stress Values (Zero to 120 Seconds)	41
Table 16	Left SRM Aft Dome, Fixed Housing Nozzle Case Girth Gages ...	45
Table 17	Right SRM Aft Dome, Fixed Housing Nozzle Case Girth Gages ..	46
Table 18	Nozzle-to-Case Joint Radial Growth Comparisons to 360L003 (STS-29)	47
Table 19	Left SRM Fixed Housing, Aft Dome Nozzle-to-Case Biaxial Gages	49
Table 20	Right SRM Fixed Housing, Aft Dome Nozzle-to-Case Biaxial Gages	50

CONTENTS (Continued)

Table 21	Left SRM Fixed Housing, Aft Dome Nozzle-to-Case Biaxial Gages Compared to Predictions	51
Table 22	Right SRM Fixed Housing, Aft Dome Nozzle-to-Case Biaxial Gages Compared to Predictions	52
Table 23	Flight Event Time Ranges	64
Table 24	Post Fire Inspection Definitions	67
Table 25	Leak Check and Vent Port Plug Post Fire Inspection Results ..	86
Table 26	Criteria for Classifying "Potential Anomalies"	96

FIGURES

Figure 1	RSRM Motor Configuration	2
Figure 2	RSRM Assembled Field Joint	3
Figure 3	Nozzle-to-Case Joint	4
Figure 4	Igniter Cross Section	5
Figure 5	Ignition System Seals	6
Figure 6	Forward Exit Cone-to-Aft Exit Cone Joint	7
Figure 7	Nose Inlet Housing-to-Throat Support Housing	8
Figure 8	Nose Inlet-to-Throat Housing Joint	9
Figure 9	Throat-to-Forward Exit Cone Joint	10
Figure 10	Flex Bearing-to-Fixed Housing Joint	11
Figure 11	Wiper O-ring Damage From Left Nozzle to Case Joint.....	14
Figure 12	Bending About the Y Axis, Station 1501	55
Figure 13	Bending About the Z Axis, Station 1196	57
Figure 14	Axial Force, Station 1466	59
Figure 17	Strut Forces, Y Axis	61
Figure 18	Strut Forces, Z Axis	62

CONTENTS (Continued)

APPENDICES

Appendix A	Developmental Flight Instrumentation Plots	A-1
Appendix B	RPRB Presentations	B-1

REVISION PAGE

Revision	Date	Description
A	07/27/89	Revised 1.0 to include structural assessment
A	07/27/89	Added 2.2
A	07/27/89	Revised 3.0 to include post-fire inspection objectives
A	07/27/89	Revised 2.1 to include post-fire Team Assessment
A	07/27/89	Added Section 4.0
A	07/27/89	Added Sections 5.1.14 and 5.2.14
A	07/27/89	Added Section 5.3, 5.4 and 5.5
A	07/27/89	Added Appendix A and B
A	07/27/89	Added Figures 12 - 18
A	07/27/89	Tables 1 - 26
A	07/27/89	Revised 6.0 to include Reference 1, 4, 5 and 8

1.0 INTRODUCTION

This report assesses the performance of the 360L003, Third Flight, Redesign Solid Rocket Motors (RSRM) in respect to joint sealing issues as seen from post-test inspection of the seals and sealing surfaces. The structural performance of the field, nozzle-to-case joints, and the case membrane are evaluated. In addition, all disassembly observations classified as potential anomalies are discussed, along with the Redesign Program Review Board (RPRB) position.

Figure 1 illustrates the RSRM, consisting of capture feature field joints with the J-joint insulation configuration (see Figure 2). Figure 3 illustrates the nozzle-to-case joint design, which includes 100, 7/8-inch radial bolts in conjunction with a wiper O-ring and modified insulation design. The ignition system seals and a cross section of the igniter are illustrated in Figures 4 and 5. Figures 6 through 10 show the configuration of all internal nozzle joints.

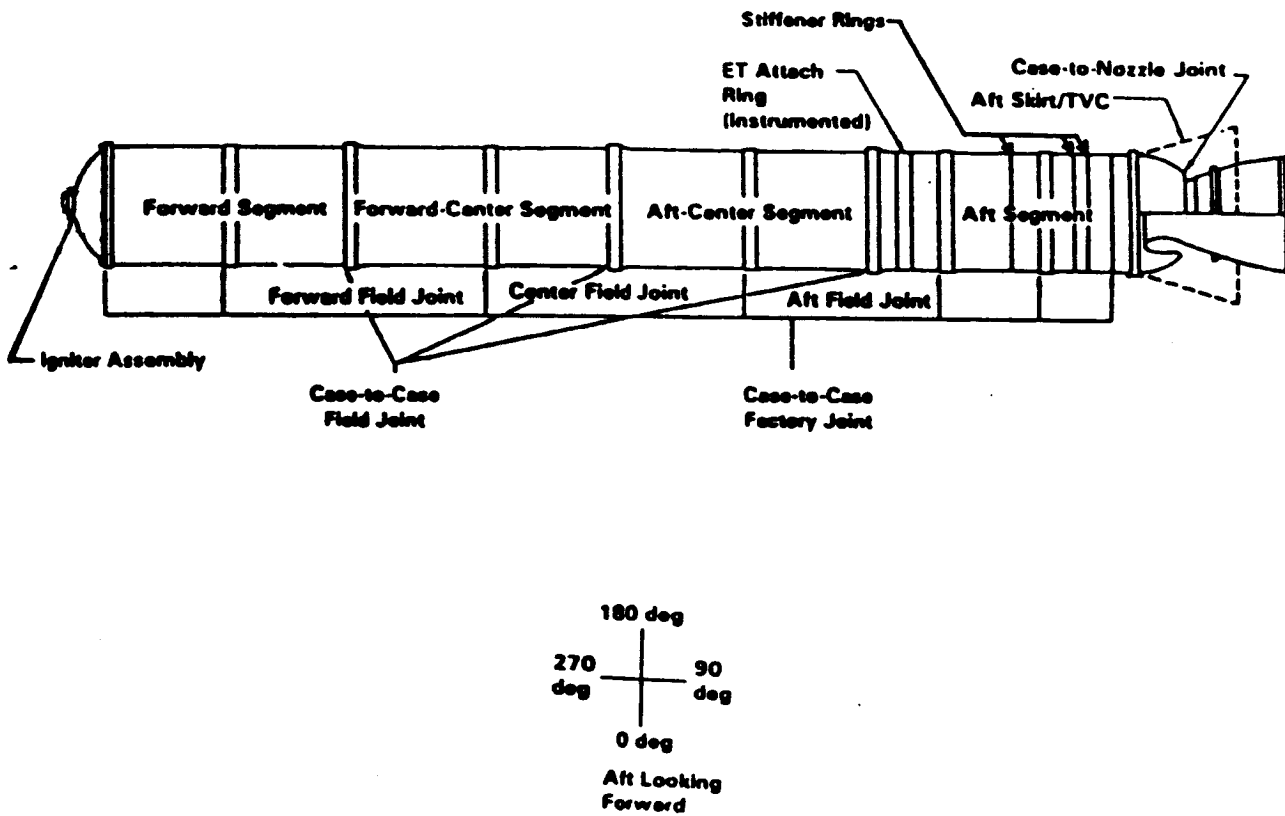


Figure 1
RSRM Motor Configuration

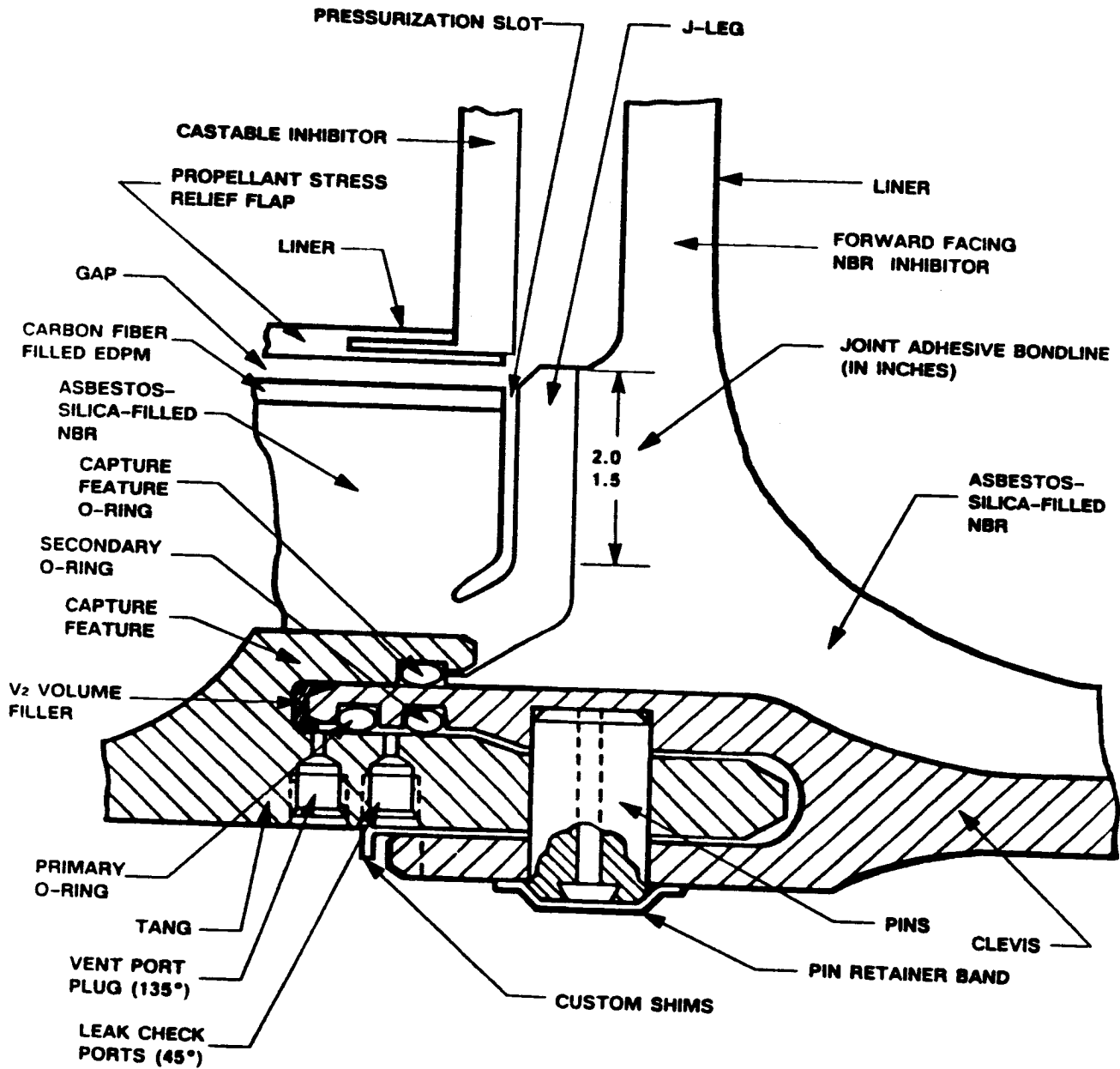


Figure 2
RSRM Assembled Field Joint

fig 3

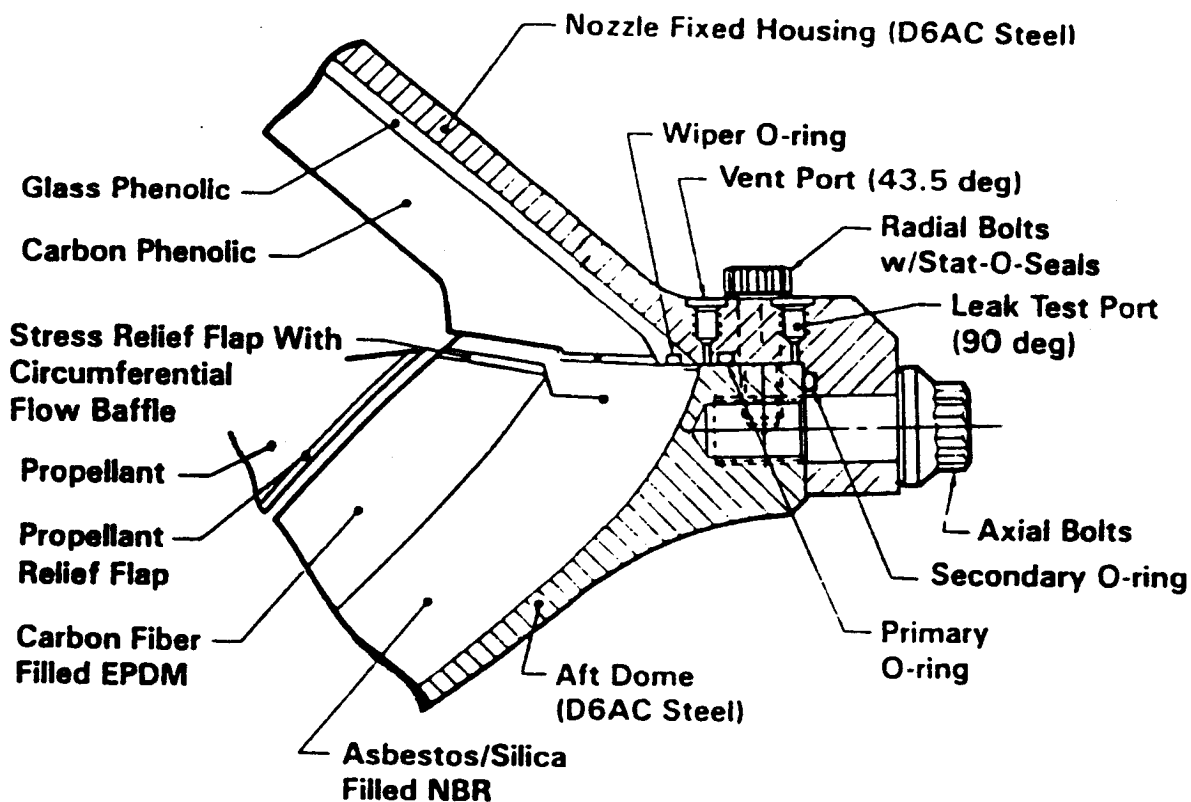


Figure 3
Nozzle-to-Case Joint

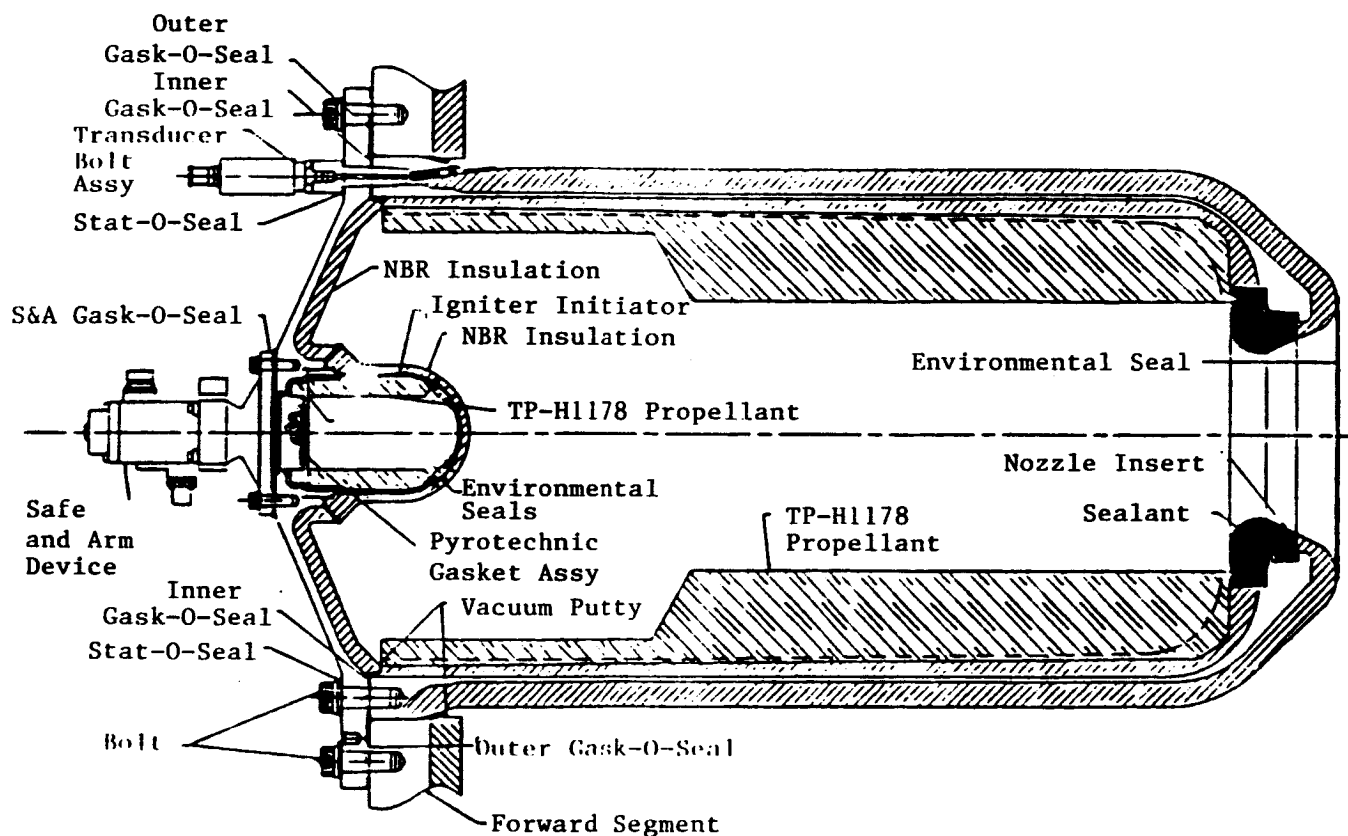


Figure 4
Igniter Cross Section

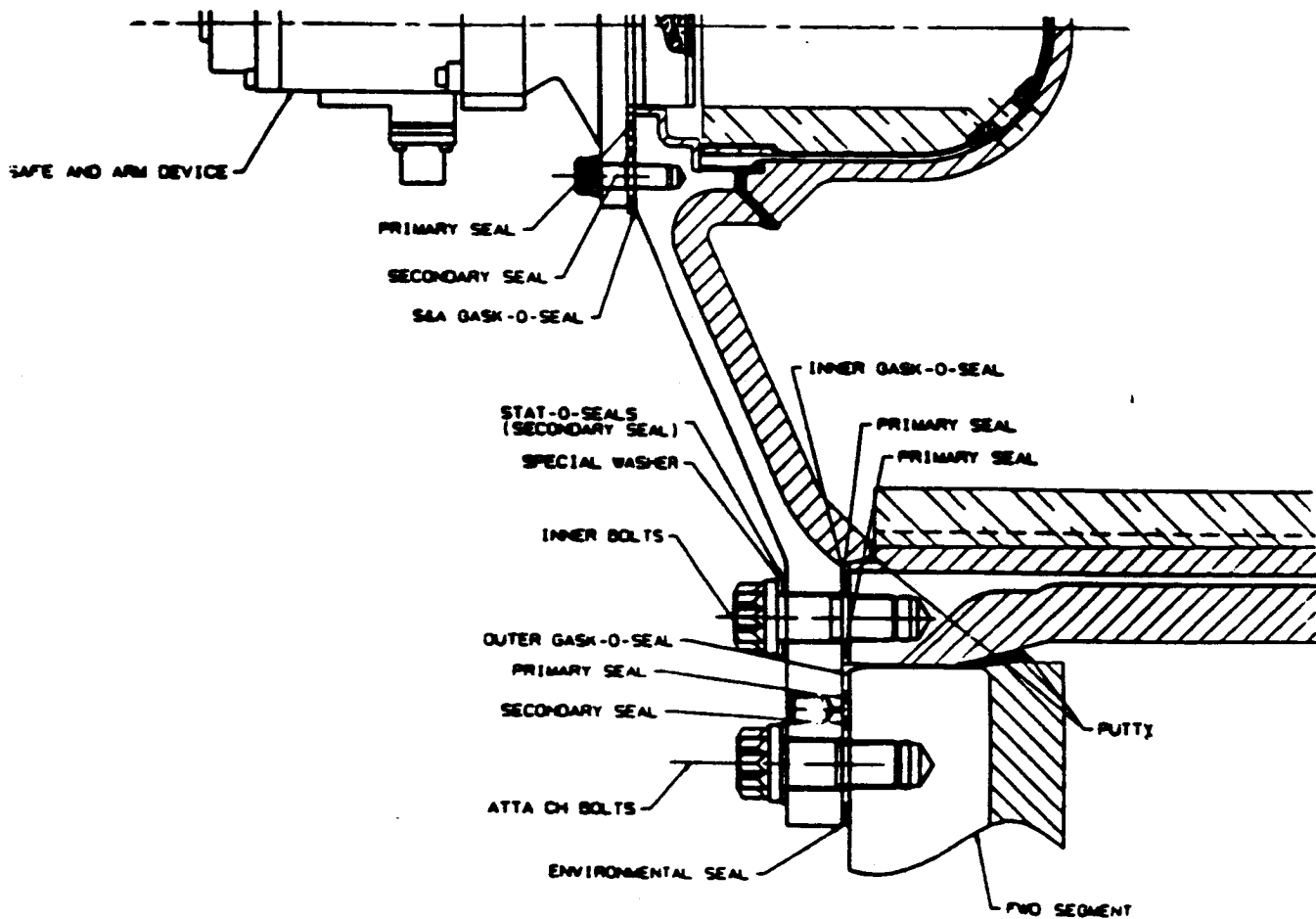


Figure 5
Ignition System Seals

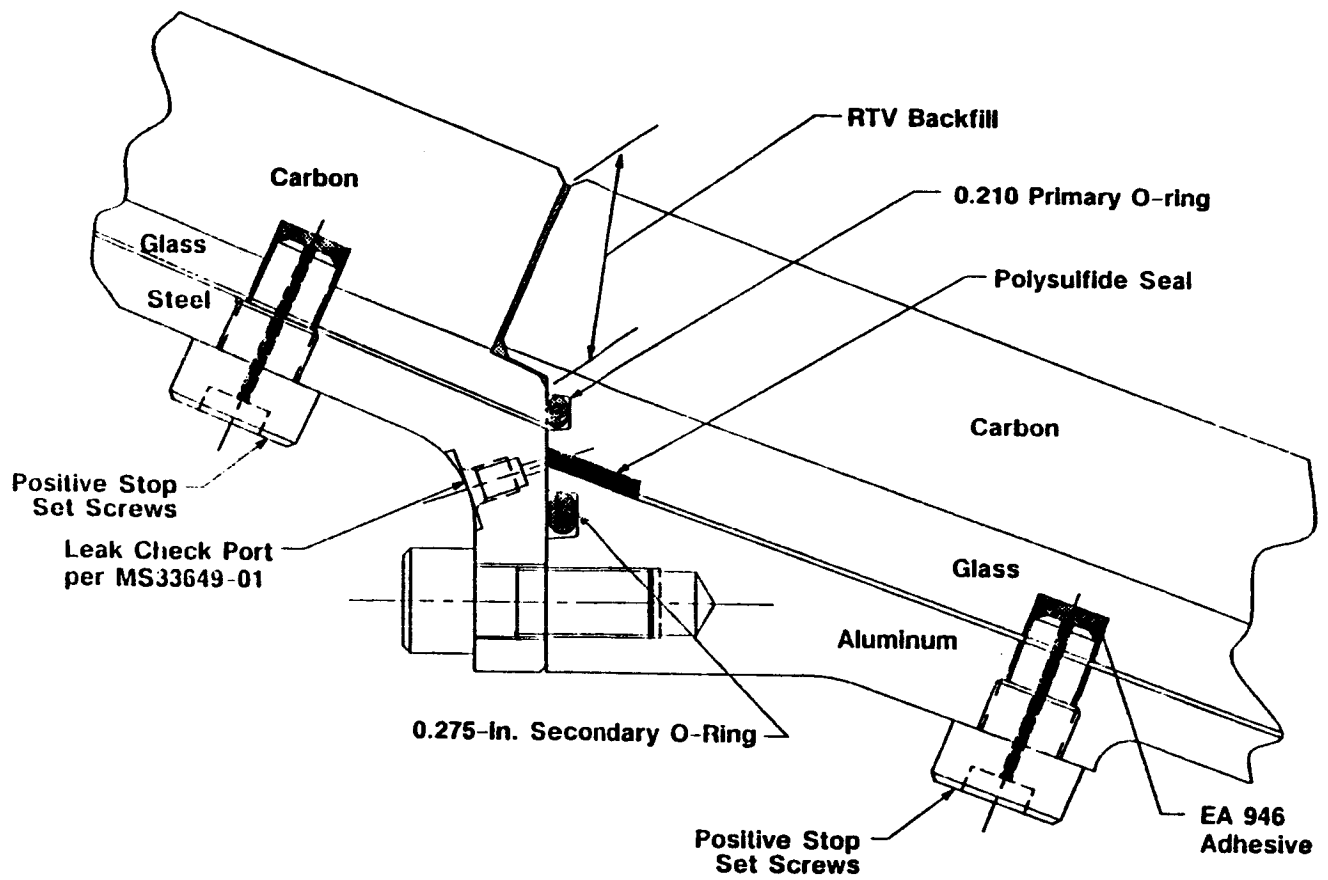


Figure 6
Forward Exit Cone-to-Aft Exit Cone Joint

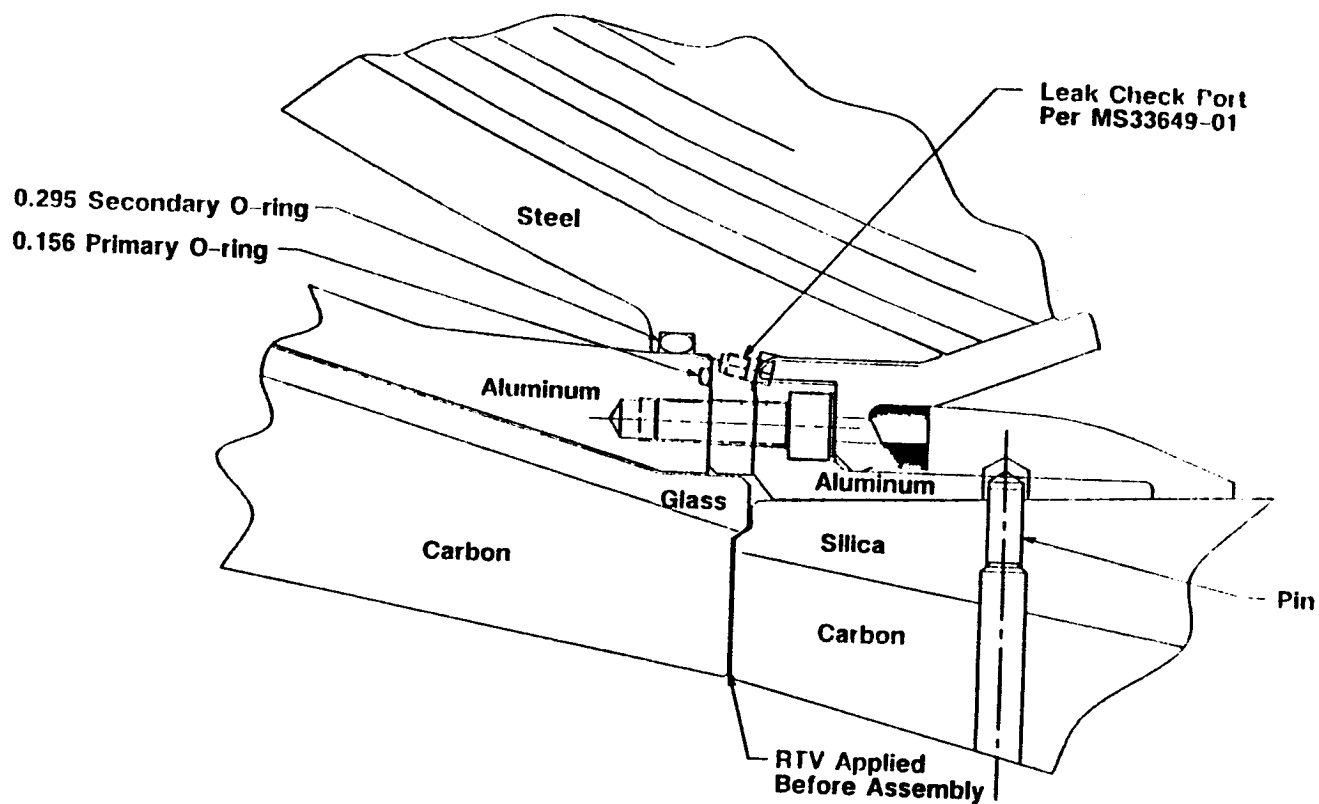


Figure 7
Nose Inlet Housing-to-Throat Support Housing Joint

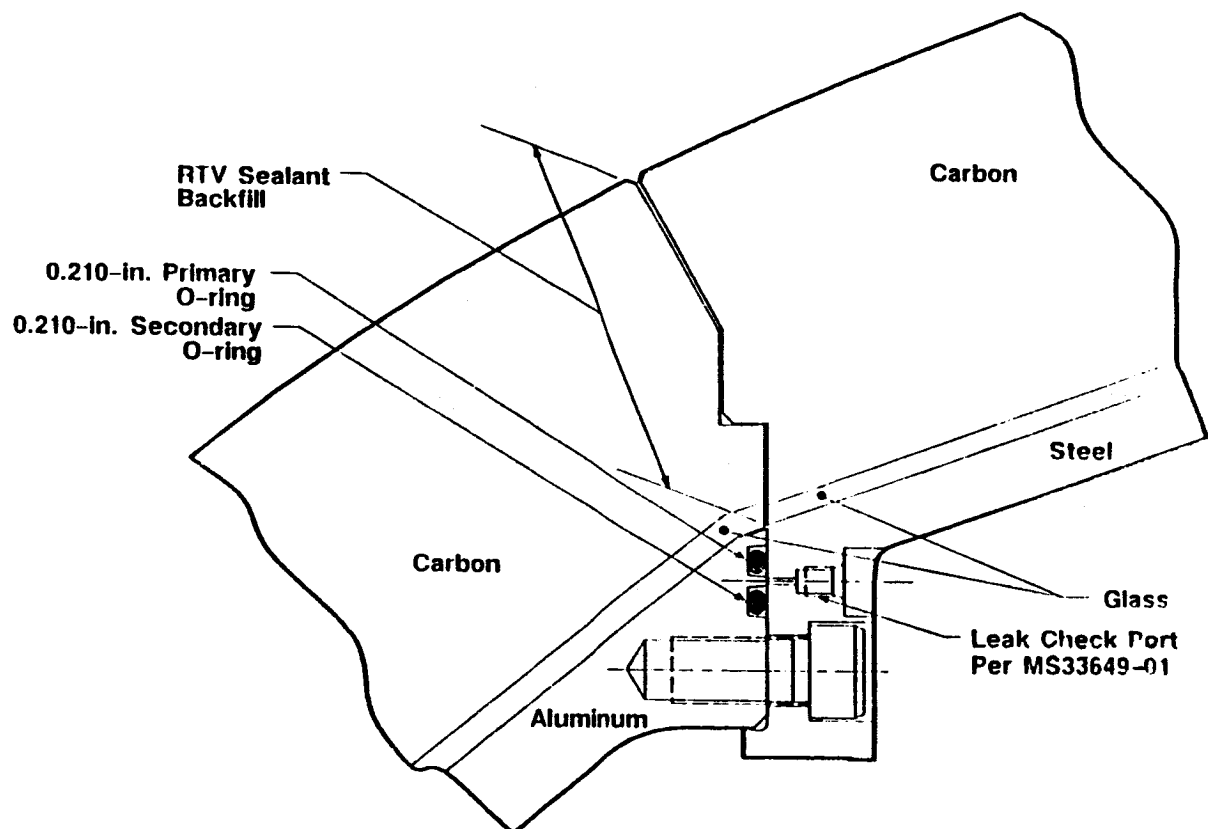


Figure 8
Nose Inlet Housing-to-Throat Support Housing Joint

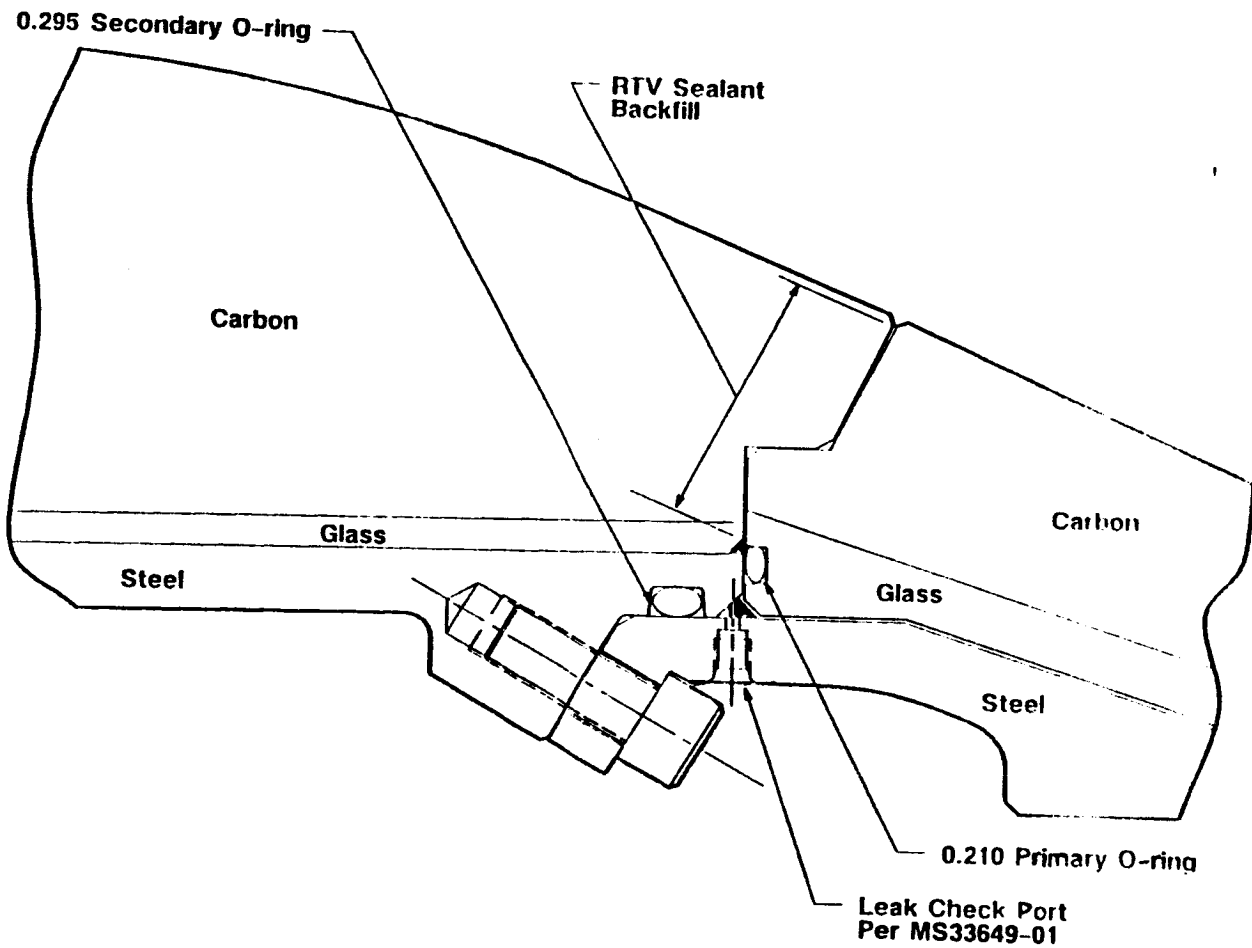


Figure 9
Throat Support Housing-to-Forward Exit Cone Joint

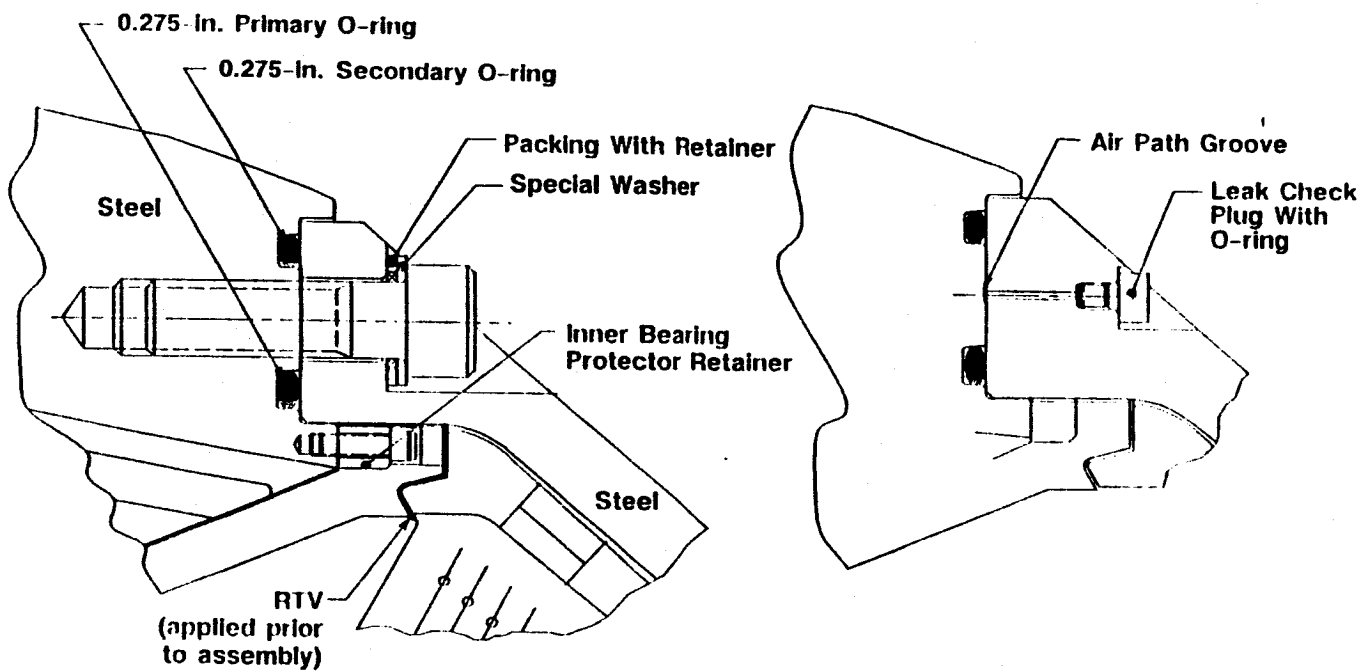


Figure 10
Aft End Ring-to-Fixed Housing Joint

2.0 SUMMARY

2.1 Structural Performance Summary

The girth gage measurements from the field and nozzle-to-case joints compare closely to corresponding gages on static tests and to pretest predictions. The predictions used a typical load case rather than actual loads, so they were only expected to predict the order of magnitude. The highest percentage difference with the predictions was 19.3 percent on the field joint girth gages (left SRB, center field joint), 41.0 percent on the nozzle-to-case joint girth gages (left SRB), and 13.3 percent on the case membrane (right SRB). The forward field joint girth gages on the left SRB, and a few others down the motor contained a spike in the data during the ignition transient. This spiking is similar to that seen on flights 360L001 and 360L002. Girth gage data on the forward field joint, and several on the center field joint of the right SRB, show a delay before movement occurs. This phenomena has been determined to be an electrical instrumentation problem, and was not caused by physical loading.

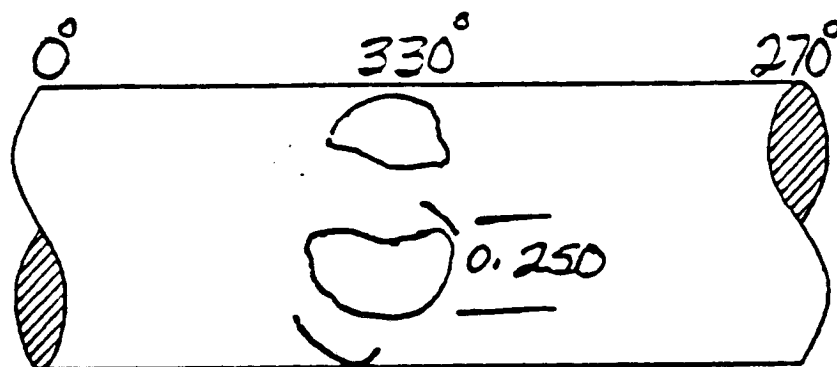
The biaxial gage line load measurements compared well with predicted values. The biaxial strain gage data for each station was used to calculate a stress distribution, and this information was used to calculate bending moments and axial force as a function of time. These data were plotted, and the results show the maximum bending moment occurred on the left SRB (station 1797) during SSME build-up, reaching a maximum value of

-264×10^6 in-lb. The axial force reached a maximum of -13.41 kips at Station 556 on the right motor, and occurred at lift-off. The maximum line load was -28 kips/inch and occurred at Station 556 on the right motor. Flight data were also plotted with the flight envelopes and revealed a close correlation. Data were also plotted with previous flights, and the correlation was good.

2.2 Post Fire Inspection Summary

The post fire inspection of both motors showed the seals component to be in excellent condition except for the wiper O-ring from the right hand motor which suffered a gouge (see Figure 11) from a radial bolt hole plug during disassembly of the nozzle-to-case joint. Details of inspections performed at A-2 by the O-ring Inspection Team can be found in Section 5.0 of this report.

There was no evidence of hot gas or soot past the J-seal on the six field joints or past the polysulfide on the two nozzle-to-case joints. The igniter joints showed no hot gas or soot past the primary seals. There was no soot to the aft exit cone primaries and there was no evidence of soot or hot gas past the primary seals on any of the internal nozzle joints. The left aft exit cone joint showed severe damage from splashdown; the phenolic was stripped to bare metal and both the primary and secondary O-rings suffered extensive damage.



$$\begin{aligned} L &= 0.250 \\ W &= 0.180 \\ D &= 0.040 \end{aligned}$$

Figure 11
Wiper O-ring Damage From Left Nozzle-to-Case Joint

REVISION A

There was light surface corrosion on the outer clevis leg on all the field joints, no corrosion was found on any sealing surfaces. Intermittent aluminum corrosion (Al_2O_3) was found between the primary and secondary seals on the right aft exit cone joint. Overall the grease application to all field and nozzle-to-case joints was nominal.

The factory joint disassembly inspections for this flight set; except for both aft segments, left forward segment, and the left aft center segment were omitted. The decision was based on the rationale that there is sufficient information in the present data base, and this would give H-7 refurbishment operations a faster turn around time. The factory joint disassembly inspections will resume for 360H005 (fifth flight) through 360L007 (seventh flight) due to a new grease application being used during the assembly process.

The Seals Component Post Fire Assessment Team has identified two observations, made during disassembly inspections, as "potential anomalies." The two potential anomalies were further classified as "minor anomalies". They are:

1. O.D. extrusion damage on secondary O-ring from the right aft field joint custom vent port plug.
2. Radial scratches across the sealing surface of MS9902-01 leak test port plugs that are used in the barrier-booster and safe and arm devices.

No major or critical anomalies were found in the joint sealing system of 360L002.

3.0 POST FIRE INSPECTION OBJECTIVES, O-RING SQUEEZE AND LEAK CHECK RESULTS

Post-fire inspection objectives are addressed in Reference 1. Calculations for Flight 360L003 O-ring squeeze are given in Reference 2. The results of the leak check of Flight 360L003 boosters are addressed in detail in Reference 3.

4.0 STRUCTURAL ASSESSMENT

The Redesigned Solid Rocket Motors (RSRM) of Flight 360L003 were fully instrumented to evaluate motor performance during hold-down, liftoff, and ascent through separation. This section details the structural assessment of the case field joints, nozzle-to-case joints and case metal components. Comparisons to flight envelopes and previous flights will also be presented.

In most cases, actual test data are compared to predicted values for each location and are shown in the Tables. A detailed global model of the RSRM was used to predict joint and case structural responses. This finite element model uses super element techniques to model all components of the RSRM in detail (except for the nozzle-to-case joint, which will be discussed in Section 4.5). Rockwell load case L02044R was chosen to represent typical loading parameters which are imposed upon the RSRM during liftoff.

This load case includes a time span from zero to ten seconds, with SRB ignition occurring at approximately 6.5 seconds, and was expected to predict displacement and strain values within an order of magnitude only. A detailed description of the model and analysis techniques used in predicting the structural response of the motor is found in Reference 4.

The predictions included in the Tables are ratioed to the Flight 360L003 pressure. The ratios were determined by multiplying the original prediction by the ratio of the estimated Flight 360L003 pressure to the prediction pressure. This is done because these predictions were calculated assuming a joint pressure, which is somewhat different than the actual pressure for a specific location. Therefore, by using the ratio of the predictions to Flight 360L003 values, a comparison can be made.

The calculation of the pressure ratio works as follows: Maximum radial growth, e.g., girth strain, for a particular location is found from test data, and the time at which it occurred. The head-end pressure at this time is next determined. Also, a predicted pressure drop at this time is found. For Flight 360L003, the predicted pressure drops are given in Reference 5. Therefore, the pressure ratio is:

$$\left[\frac{\text{Head End Pressure} - \text{Predicted Pressure Drop}}{\text{Predicted Pressure}} \right] = \text{Pressure Ratio}$$

The percent difference between analysis and measured data is given by:

$$\left[\frac{(\text{Pressure Ratio} \times \text{Prediction}) - \text{Measured}}{\text{Measured}} \right] \times 100$$

Biaxial strain gages were placed in the aft field joint and ETA ring regions and also around the nozzle-to-case joints and used to calculate the corresponding hoop and axial stresses. These stresses illustrate the effects of the ETA ring on the aft field joint and vectoring on the nozzle-to-case joint. The local stresses are then compared to the predicted values. Each table shows the maximum experienced hoop stress and its corresponding axial stress. Since the hoop stress is much larger than axial stress, this represents the maximum stress for each of the areas, and a safety factor can be determined.

The predictions included in the tables (not including the nozzle-to-case joint) are the maximum expected values for the first three seconds of flight. Tables are also included to show the maximum experienced axial and hoop strain for the duration of the flight.

The strain gages were zeroed after SRB stacking, but before mating with the orbiter and external tank, so the strain gages report some initial strain before launch, which is caused by the weight and induced bending of the orbiter and external tank. Because of when they were zeroed, the strain gages do not show any strain resulting from the weight of the segments above them. It would be ideal to know the actual strain experienced by the case at every instrumented location for every flight event. After separation, and before chute deployment, the SRBs are essentially in a free state

(free fall), with very little, if any motor pressure, and very small external loads. For this reason, all strain gages were adjusted to end at zero strain at this point in time. This shifting of the data show, as near as possible, the actual strain level at any point during flight. Because the data is shifted at every time, it also shows the strain caused by the weight of the case segments prior to SSME build-up. It should be noted, however, when comparing strain values with predicted values, the data has been adjusted to start at zero rather than end at zero. The reason is because the predictions represent a delta change from the state before SSME ignition to the state after full SRB motor pressure has been achieved. This is necessary to show a true comparison with predictions.

Once this adjustment has been made, the strain values are input into Program SLB01 which calculates the stress distribution around the case. The output from this program is put into Program SLB06 which calculates bending moment and axial force. The results of this program are presented as a function of time. The results of this program were also plotted with previous flight data as a function of time, and with the envelopes for specific flight events as a function of station. The average line load for each is calculated using the bending moment in each direction (MY and MZ), and the axial force (VX). The results are plotted as a function of time for Stations 556.6, 876.5, 1196, 1466, 1501, and 1797 (see appendix A).

4.1 Instrumentation

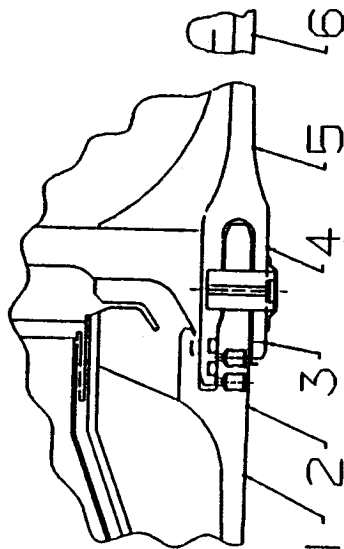
Instrumentation (girth and biaxial strain gages) was placed on, and close to, the field and nozzle-to-case joints to characterize joint performance. Following is a list of gages used and their function.

- Joint Girth Gages - Measures the average hoop strain for the entire 360 degree circumference. From the hoop strain, radial deflections are determined from the product of measured (average) girth strain and the nominal hardware radii at the corresponding gage location.
- Biaxial Gages - Measures local axial and hoop strain, rather than average, incurred in the case during flight. From these strains, stress can be calculated.
- Pressure Transducer - Installed in the igniter to measure head end chamber pressure.
- Thermocouple - Monitors temperature.

4.2 Field Joint Girth Gage Performance

Flight 360L003 instrumentation on both the left and right RSRM consisted of six girth gages per field joint. Tables 1 through 6 list the girth gage response from zero to three seconds and the maximum strain for -10 to 120 seconds for the forward, center and aft field joints for both the left and right motors. These tables compare the maximum measured strain and corresponding radial growth with the predicted values for the forward, center and aft field joints. The results show good correlation between analysis and test data. All field joint predictions are within 19.3 percent of measured values. The maximum experienced radial growth was 0.172 inch, which occurred on the forward field joint at Location 1 on the left SRB.

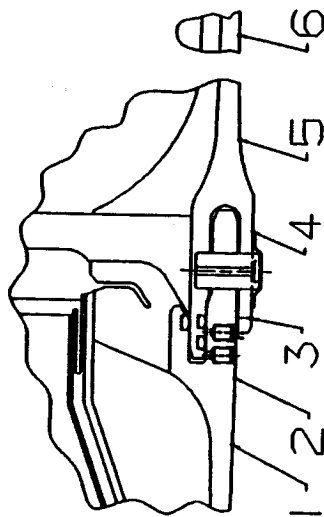
Table 1 Left SRM Forward Field Joint Girth Gages



TEST NAME: 360L003
JOINT: LEFT SRM FWD FIELD JOINT
DESCRIPTION: JOINT GIRTH GAGES
THE TIME RANGE IS 0.0 TO 3.0 SECONDS

GIRTH GAGE LOCATION	GAGE NUMBER	STATION	RADIUS (IN)	RADIAL GROWTH (IN)	TEST STRAIN (UIN/IN)	ADJUSTED ANALYSIS STRAIN (UIN/IN)	ADJUSTED ANALYSIS RADIAL GROWTH (IN)	DIFF IN RADIAL GROWTH (% DIFF)	MAXIMUM RADIAL GROWTH -10 TO 120 SECONDS
1	B08G7273	847.0	73.1	0.172	2349	2212	0.162	-5.8	0.178
2	B08G7274	848.5	73.1	0.159	2168	1940	0.142	-10.5	0.164
3	B08G7275	850.2	73.5	0.140	1903	1874	0.138	-1.5	0.145
4	B08G7276	852.6	73.5	0.158	2148	1808	0.133	-15.8	0.164
5	B08G7277	855.0	73.1	0.168	2303	2075	0.152	-9.9	0.177
6	B08G7278	857.5	73.1	ND	ND	ND	ND	ND	ND

Table 2 Left SRM Center Field Joint Girth Gages

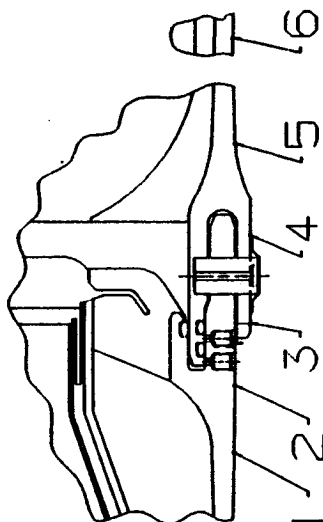


TEST NAME: 360L003
JOINT: LEFT SRM CTR FIELD JOINT
DESCRIPTION: JOINT GIRTH GAGES
THE TIME RANGE IS 0.0 TO 3.0 SECONDS

GIRTH GAGE LOCATION	GAGE NUMBER	STATION	RADIUS (IN)	RADIAL GROWTH (IN)	TEST STRAIN (UTN/IN)	ADJUSTED ANALYSIS STRAIN (UTN/IN)	ADJUSTED ANALYSIS RADIAL GROWTH (IN)	DIFF IN RADIAL GROWTH (% DIFF)	MAXIMUM RADIAL GROWTH -10 TO 120 SECONDS
1	B08G7283	1168.8	73.1	0.169	2308	2079	0.152	-9.9	0.177
2	B08G7284	1168.5	73.1	ND	ND	ND	ND	ND	ND
3	B08G7285	1170.2	73.5	0.138	1876	1768	0.130	-5.8	0.147
4	B08G7286	1172.6	73.5	0.155	2111	1705	0.125	-19.3	0.165
5	B08G7287	1175.0	73.1	ND	ND	ND	ND	ND	ND
6	B08G7288	1177.3	73.1	ND	ND	ND	ND	ND	ND

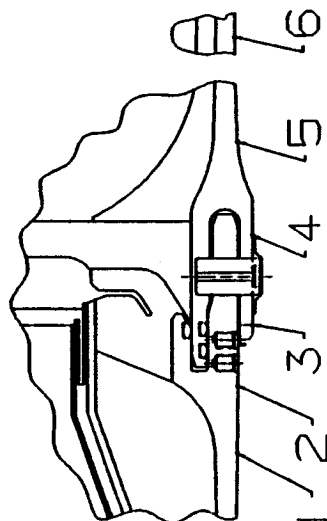
Table 3 Left SRM Aft Field Joint Girth Gages

TEST NAME: 360L003
JOINT: LEFT SRM AFT FIELD JOINT
DESCRIPTION: JOINT GIRTH GAGES
THE TIME RANGE IS 0.0 TO 3.0 SECONDS



GIRTH GAGE LOCATION	GAGE NUMBER	STATION	RADIUS (IN)	RADIAL GROWTH (IN)	TEST STRAIN (UTN/IN)	ADJUSTED ANALYSIS STRAIN (UTN/IN)	ADJUSTED ANALYSIS RADIAL GROWTH (IN)	DIFF IN RADIAL GROWTH (% DIFF)	MAXIMUM RADIAL GROWTH -10 TO 120 SECONDS
1	B08G7293	1487.0	73.1	0.157	2144	2050	0.150	-4.4	0.178
2	B08G7294	1488.5	73.1	ND	ND	1818	0.133	ND	ND
3	B08G7295	1490.2	73.5	ND	ND	1726	0.127	ND	ND
4	B08G7296	1492.6	73.5	ND	ND	1659	0.122	ND	ND
5	B08G7297	1495.0	73.1	0.139	1897	1833	0.134	-3.4	0.157
6	B08G7298	1497.5	73.1	0.143	1955	1994	0.146	2.0	0.164

Table 4 Right SRM Forward Field Joint Girth Gages

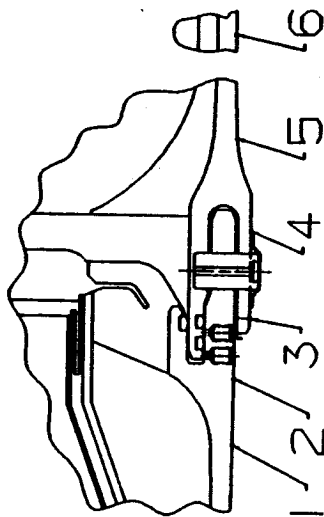


TEST NAME: 360L003
JOINT: RIGHT SRM FWD FIELD JOINT
DESCRIPTION: JOINT GIRTH GAGES
THE TIME RANGE IS 0.0 TO 3.0 SECONDS

GIRTH GAGE LOCATION	GAGE NUMBER	STATION	RADIUS (IN)	RADIAL GROWTH (IN)	TEST STRAIN (UIN/IN)	ADJUSTED ANALYSIS STRAIN (UIN/IN)	ADJUSTED ANALYSIS RADIAL GROWTH (IN)	DIFF IN RADIAL GROWTH (% DIFF)	MAXIMUM RADIAL GROWTH -10 TO 120 SECONDS
1	B08G8273	847.0	73.1	0.170	2319	2211	0.162	-4.6	0.177
2	B08G8274	848.5	73.1	ND	ND	ND	ND	ND	ND
3	B08G8275	850.2	73.5	0.141	1921	1875	0.138	-2.4	0.145
4	B08G8276	852.6	73.5	0.158	2147	1811	0.133	-15.6	0.164
5	B08G8277	855.0	73.1	0.169	2316	2078	0.152	-10.3	0.178
6	B08G8278	857.5	73.1	ND	ND	ND	ND	ND	ND

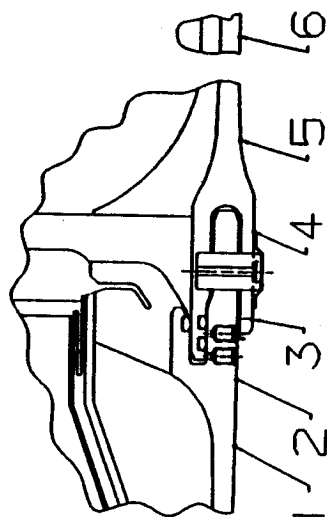
Table 5 Right SRM Center Field Joint Girth Gages

TEST NAME: 360L003
JOINT: RIGHT SRM CTR FIELD JOINT
DESCRIPTION: JOINT GIRTH GAGES
THE TIME RANGE IS 0.6 TO 3.0 SECONDS



GIRTH GAGE LOCATION	GAGE NUMBER	STATION	RADIUS (IN)	RADIAL GROWTH (IN)	TEST STRAIN (UIN/IN)	ADJUSTED ANALYSIS STRAIN (UIN/IN)	ADJUSTED ANALYSIS RADIAL GROWTH (IN)	DIFF IN RADIAL GROWTH (% DIFF)	MAXIMUM RADIAL GROWTH -10 TO 120 SECONDS
1	B08G8283	1168.8	73.1	0.167	2278	2049	0.150	-10.0	0.176
2	B08G8284	1168.5	73.1	ND	ND	ND	ND	ND	ND
3	B08G8285	1170.2	73.5	0.134	1828	1747	0.128	-4.4	0.140
4	B08G8286	1172.6	73.5	0.151	2051	1680	0.123	-18.1	0.158
5	B08G8287	1175.0	73.1	0.163	2231	1917	0.140	-14.1	0.183
6	B08G8288	1177.3	73.1	0.181	2472	2277	0.166	-7.9	0.196

Table 6 Right SRM Aft Field Joint Girth Gages



TEST NAME: 360L003
JOINT: RIGHT SRM AFT FIELD JOINT
DESCRIPTION: JOINT GIRTH GAGES
THE TIME RANGE IS 0.6 TO 3.0 SECONDS

GIRTH GAGE LOCATION	GAGE NUMBER	STATION	RADIUS (IN)	RADIAL GROWTH (IN)	TEST STRAIN (UTIN/IN)	ADJUSTED ANALYSIS STRAIN (UTIN/IN)	ADJUSTED ANALYSIS RADIAL GROWTH (IN)	DIFF IN RADIAL GROWTH (% DIFF)	MAXIMUM RADIAL GROWTH -10 TO 120 SECONDS
1	B08G8293	1487.0	73.1	ND	ND	ND	ND	ND	ND
2	B08G8294	1488.5	73.1	ND	ND	ND	ND	ND	ND
3	B08G8295	1490.2	73.5	0.126	1718	1712	0.126	-0.3	0.139
4	B08G8296	1492.6	73.5	0.139	1888	1619	0.119	-14.3	0.154
5	B08G8297	1495.0	73.1	0.146	2002	1789	0.131	-10.7	0.163
6	B08G8298	1497.5	73.1	0.154	2111	1948	0.142	-7.7	0.173

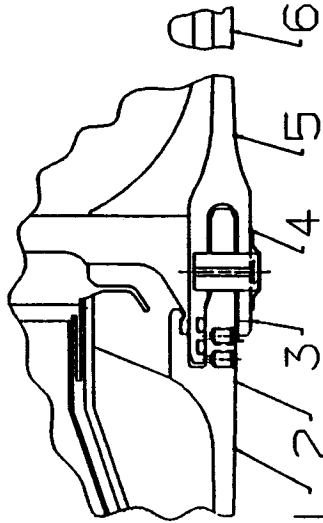
Tables 7 through 9 compare Flight 360L003 with several static motors, Flights 360L002, 360L001, and predictions. It can be seen from these tables that the correlation is good. Close study of the field joint growth behavior show the joint is rotating outward. This is evidenced by the higher radial growth values at the forward and aft ends of each joint, and the lower values closer to the pin centerline.

The center and aft field joint girth gages of the right SRB had spikes in the data during the ignition transient. There are a few other gages on both the left and right motor that illustrate some degree of spiking. The values in Tables 5 and 6 (Center and Aft field joints respectively) contain the maximum values found after the spiking in the data occurred (Time range of 0.6 to 3.0 seconds), and the maximum value found for the full time duration (Time range of -10 to 120 seconds). It has been determined that the spiking phenomena is not pressure related because:

1. Head end pressure gages are smooth with no spiking.
2. Spiking occurs at 0.25 second which is before peak head end pressure at approximately 0.6 second.
3. All spiking occurs at exactly the same time (0.25 second). If it were pressure related, there would be some finite delay as the pressure went down the motor.
4. Hoop strain biaxials located in the same areas do not exhibit spiking.

It is difficult to attribute any external physical loading to this phenomena because all spiking occurs at exactly the same time in a distance of over 13 feet. Some time delay would be expected if physical loading were present.

Table 7 Forward Field Joint Radial Growth Comparisons to 360L003 (STS-29)

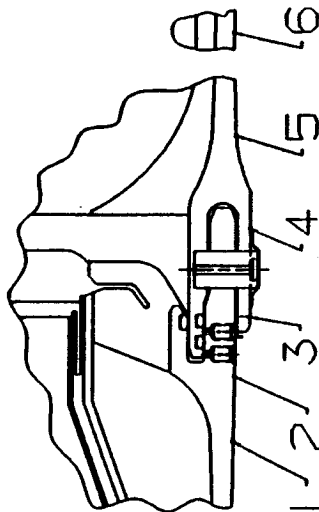


Fwd Field Girths

LOC.	STS-29		STS-29		STS-27		STS-26		RADIAL GROWTH (Inches)				NOMINAL RADIUS	
	GAGE	RIGHT	LEFT	RIGHT	LEFT	RIGHT	LEFT	PV-1	QM-7	QM-6	DM-9	DM-8	PRED	(INCHES)
1	B08GX273	0.170	0.172	0.170	0.174	ND	ND	ND	ND	0.162	0.167	0.170	0.162	73.1
2	B08GX274	ND	0.159	ND	ND	ND	ND	ND	0.186	0.152	0.155	0.158	0.142	73.1
3	B08GX275	0.141	0.140	ND	0.147	ND	0.187	ND	0.143	0.132	0.148	0.142	0.138	73.5
4*	B08GX276	0.158	0.158	ND	0.163	ND	0.164	ND	0.161	0.155	ND	0.155	0.133	73.5
5	B08GX277	0.169	0.168	0.179	0.175	ND	0.180	ND	0.178	0.174	0.169	0.177	0.152	73.1
6	B08GX278	ND	ND	0.198	0.194	ND	ND	ND	ND	0.200	ND	0.202	ND	73.1

* QM-7, QM-6, and DM-9 Locations are 1/3 Inch Aft of DM-8 Location.
Note: All Test Radial Growths Are Ratios of STS-29 Test Pressure

Table 8 Center Field Joint Radial Growth Comparisons to 360L003 (STS-29)



Center Field Girths

LOC.	STS-29 GAGE	STS-29 RIGHT	STS-29 LEFT	STS-27 RIGHT	STS-27 LEFT	STS-26 RIGHT	STS-26 LEFT	FV-1	QM-7	QM-6	DM-9	DM-8	FRED	NOMINAL RADIUS (INCHES)
1	B08GX283	0.167	0.169	0.166	0.167	ND	ND	ND	ND	0.160	ND	0.172	0.151	73.1
2	B08GX284	ND	ND	ND	ND	ND	ND	ND	ND	ND	0.153	0.158	ND	73.1
3	B08GX285	0.134	0.138	0.136	0.139	ND	0.138	ND	0.141	0.131	0.149	0.140	0.129	73.5
4*	B08GX286	0.151	0.155	ND	0.154	0.156	ND	0.152	0.156	0.148	0.134	0.155	0.124	73.5
5	B08GX287	0.163	ND	0.166	0.165	ND	ND	0.170	0.172	0.165	0.164	0.176	0.140	73.1
6	B08GX288	0.181	ND	ND	0.187	ND	ND	ND	ND	0.186	ND	0.211	0.166	73.1

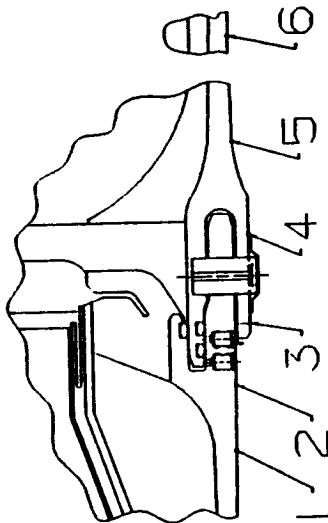
* QM-7, QM-6, and DM-9 Locations are 1/3 Inch Aft of DM-8 Location.

Note: All Test Radial Growths Are Ratios of STS-29 Test Pressure

Note: Locations 1, 3, and 4 on the right SRB contain negative spikes at 0.225 seconds

Note: Locations 5 and 6 on the right SRB contain spikes at 0.275 seconds

Table 9 Aft Joint Radial Growth Comparisons to 360L003 (STS-29)



Aft Field Girths

LOC.	STS-29 GAGE	STS-29		STS-27		STS-26		PV-1	RADIAL GROWTH (Inches)				NOMINAL RADIUS	
		RIGHT	LEFT	RIGHT	LEFT	RIGHT	LEFT		QM-7	QM-6	DM-9	DM-8	FRED	(INCHES)
1	B08GX293	ND	0.157	0.155	0.160	ND	ND	ND	ND	0.153	0.156	0.159	0.150	73.1
2	B08GX294	ND	ND	ND	0.146	ND	ND	ND	0.168	0.141	0.144	0.150	0.133	73.1
3	B08GX295	0.126	ND	ND	0.131	0.132	0.142	ND	0.133	0.118	0.125	0.132	0.126	73.5
4*	B08GX296	0.139	ND	ND	0.138	0.141	0.139	0.137	0.140	0.134	0.133	0.140	0.121	73.5
5	B08GX297	0.146	0.139	0.148	0.140	ND	0.151	0.143	0.140	0.141	0.138	0.148	0.133	73.1
6	B08GX298	0.154	0.143	0.140	0.146	ND	ND	ND	ND	ND	0.145	0.157	0.144	73.1

* QM-7, QM-6, and DM-9 Locations are 1/3 Inch Aft of DM-8 Location.
Note: All Test Radial Growths Are Ratios of STS-29 Test Pressure
Note: All Right SRB Gages Spike at 0.2875 seconds

An investigation indicates no reason to disbelieve the gages because:

1. The spiking gages were independent from each other; i.e., they were connected to different cables which lead to the data acquisition system.
2. The gage factors showed nothing out of the ordinary.
3. After the spiking occurs, the gages track normally giving acceptable (and believable) readings.
4. Post-flight inspection of the gages is not possible since when the protective cork covering is removed the gage is essentially destroyed.

Additional investigation into these phenomena indicate the spiking is an electrical/instrumentation problem associated with the girth gage, and is not caused by physical loading on the case. This conclusion was reached after instrumentation on Flight 360L003 showed conflicting data between adjacent girth and biaxial gages. Multiple biaxial gages showed normal case behavior, while the girth gages contained spiking data similar to that seen on Flight 360L002.

To further verify the conclusion stated above, the recommended course of action is to carefully inspect, during refurbishment, the cases which had the gages showing spiking. The cases should be inspected for out-of-roundness, case thickness, and any other abnormalities. It is also recommended that during the hydrotest, a series of girth and biaxial gages be installed to measure case strain. Since these phenomena is not fully understood, it is also recommended to continue DFI instrumentation of future flights to help determine if this is a real event.

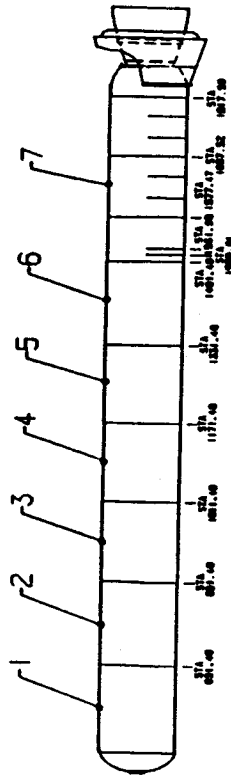
Another interesting event occurred on the forward (all gages) and center (three most forward gages) of the right SRB. In these gages, there was a time delay (approximately 0.25 seconds) before these gages showed an increase in magnitude. A girth gage is normally linear with pressure, but these show no response until the head end pressure is approximately 600 PSI. It is also interesting to note that biaxial gages in the membrane just aft of each of these joints respond normally, with no delay. The center field joint is the most interesting of all since three of the girth gages show the delay, two gages show spiking, and one gage is bad. All of these gages felt the same motor pressure, but responded differently. For these reasons it is believed that the gages that showed the delay are faulty gages.

4.3 Case Membrane Girth Gage Response

Instrumentation on both the left and right RSRM consisted of seven girth gages on the case membrane. Tables 10 and 11 list the girth gage response from zero to three seconds and compares the measured strain and calculated radial growth with predicted values (these predicted values are for the first three seconds only). Also listed is the maximum radial growth for -10 to 120 seconds. Every prediction is within 13.3 percent of measured test data. Table 12 shows the comparison of Flight 360L003 with several static tests, Flights 360L002, 360L001, and predictions (from zero to 120 seconds). This table shows a good correlation with these tests. The value for Station 1637.5 excludes the spiking event at 0.25 second (Section 4.2).

Table 10 Left SRM Case Radial Deflection Girth Gages

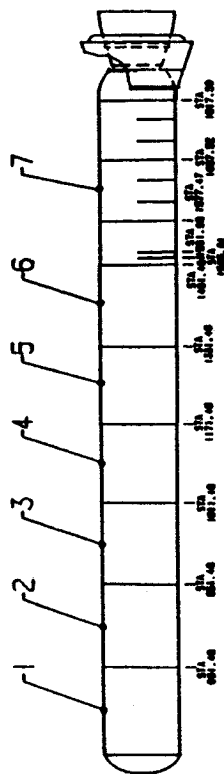
TEST NAME: 360L003
JOINT: LEFT SRM CASE RADIAL DEFLECTION
DESCRIPTION: CASE GIRTH GAGES
THE TIME RANGE IS 0.0 TO 3.0 SECONDS



GIRTH GAGE LOCATION	GAGE NUMBER	STATION	RADIUS (IN)	RADIAL GROWTH (IN)	TEST STRAIN (UTN/IN)	ADJUSTED ANALYSIS STRAIN (UTN/IN)	ADJUSTED ANALYSIS RADIAL GROWTH (IN)	DIFF IN RADIAL GROWTH (% DIFF)	MAXIMUM RADIAL GROWTH -10 TO 120 SECONDS
1	B08G7269	611.5	73.0	0.279	3816	3294	0.241	-13.3	0.279
2	B08G7272	771.5	73.0	0.261	3567	3225	0.236	-9.6	0.264
3	B08G7279	931.5	73.0	0.267	3651	3319	0.242	-9.1	0.275
4	B08G7282	1091.5	73.0	0.264	3618	3235	0.236	-10.6	0.274
5	B08G7289	1251.5	73.0	0.258	3534	ND	ND	ND	0.271
6	B08G7292	1411.5	73.0	0.227	3112	3077	0.225	-1.1	0.241
7	B08G7301	1637.5	73.0	0.230	3143	3152	0.230	0.3	0.260

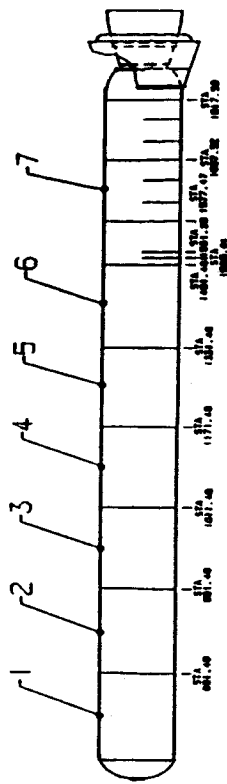
Table 11 Right SRM Case Radial Deflection Girth Gages

TEST NAME: 360L003
JOINT: RIGHT SRM CASE RADIAL DEFLECTION
DESCRIPTION: CASE GIRTH GAGES
THE TIME RANGE IS 0.0 TO 3.0 SECONDS



GIRTH GAGE LOCATION	GAGE NUMBER	STATION	RADIUS (IN)	RADIAL GROWTH (IN)	TEST STRAIN (UIN/IN)	ADJUSTED ANALYSIS STRAIN (UIN/IN)	ADJUSTED ANALYSIS RADIAL GROWTH (IN)	DIFF IN RADIAL GROWTH (% DIFF)	MAXIMUM RADIAL GROWTH -10 TO 120 SECONDS
1	B08G8269	611.5	73.0	0.275	3764	3302	0.241	-12.3	0.277
2	B08G8272	771.5	73.0	0.258	3532	3172	0.232	-10.2	0.263
3	B08G8279	931.5	73.0	0.264	3620	3327	0.243	-8.1	0.276
4	B08G8282	1091.5	73.0	0.265	3634	3242	0.237	-10.8	0.278
5	B08G8289	1251.5	73.0	0.258	3531	ND	ND	ND	0.267
6	B08G8292	1411.5	73.0	0.251	3433	3086	0.225	-10.1	0.266
7	B08G8301	1637.5	73.0	0.260	3558	3084	0.225	-2.8	0.265

Table 12 Case Membrane Radial Growth Comparisons to 360L003 (STS-29)



Case Membrane Girths

LOC.	STS-29		STS-27		STS-26		RADIAL GROWTH (Inches)					NOMINAL RADIUS (INCHES)		
	GAGE	RIGHT	LEFT	RIGHT	LEFT	RIGHT	LEFT	FV-1	QM-7	QM-6	DM-9	DM-8	PRED	
1	B08GX269	0.275	0.279	0.280	0.279	ND	ND	ND	0.289	0.275	0.268	0.284	0.241	73.04
2	B08GX272	0.258	0.261	0.265	0.270	ND	0.275	ND	0.275	0.262	0.271	0.282	0.234	73.04
3	B08GX279	0.264	0.267	0.273	ND	ND	ND	ND	0.287	0.279	0.283	0.291	0.243	73.04
4	B08GX282	0.265	0.264	0.270	ND	0.281	0.279	ND	0.288	0.273	0.279	0.292	0.237	73.04
5	B08GX289	0.258	0.258	0.268	0.268	ND	ND	ND	0.279	0.264	ND	0.285	ND	73.04
6	B08GX292	0.251	0.227	0.265	0.258	0.276	ND	ND	0.278	0.268	ND	ND	0.225	73.04
7	B08GX301	0.260	0.230	0.244	ND	0.261	0.260	ND	0.266	0.253	0.253	0.260	0.227	73.04

* QM-7, QM-6, and DM-9 Locations are 1/3 Inch Aft of DM-8 Location.

Note: Only the Predicted Radial Growths Are Ratios of STS-29 Test Pressure

Note: Location 1 contains small spike on the way up at 0.2625 seconds

Note: Location 7 contains a double spike at 0.2875 and 0.3125 seconds which exceeds overall maximum

The maximum girth strain for the duration of the flight is slightly larger than that found from zero to three seconds. The maximum radial growth occurred at station 611.5 on the left SRB, and has a value of 0.279 inch.

4.4 Case Biaxial Stresses

4.4.1 Case Line Loads, Aft Field-to-ET Attach Joint

Flight 360L003 instrumentation consisted of biaxial gages at seven locations along the case (4 pair on Stations 556.50, 876.50, 1196.50, 1466.00, and 1797.00 and 9 pair on Stations 1497.0 and 1501.00). Tables 13 and 14 illustrate the hoop and axial strain values with corresponding predictions for the first three seconds of flight. A good correlation between measured and predicted values is shown, with the exception of Station 1330 in the axial direction. The strain gages are located on the outer leg of the clevis, and forward of the pins. This location is not as constrained as other areas on the joint, so the behavior is different, and less predictable - especially in the axial direction.

Table 15 lists the maximum hoop and axial stresses measured from biaxial gages for the total 120 second burn time. These tables do not provide a comparison between test data and analysis. Analysis was performed for the initial 3 second burn time only, which does not necessarily correspond with maximum stress occurrence. The maximum measured hoop stress occurred at station 1466 at 98 degrees on the Right SRB, measuring a local stress of 133.2 ksi. The ultimate strength of D6AC steel is 214 ksi with biaxial

Table 13 360L003 (STS-29) Comparison of Maximum Predicated vs. Measured
Biaxial Strain Values (Zero to 3 Seconds) Left SRM

Station	Deg.	Maximum Hoop Strain (μ in/in)			Maximum Axial Strain (μ in/in)		
		Gage Name	Predicted	Measured	Gage Name	Predicted	Measured
556.5	0.	B08G7319A	3563.	3696.	B08G7318A	791.	821.
"	98.	B08G7321A	3583.	3409.	B08G7320A	731.	828.
"	180.	B08G7323A	3579.	3561.	B08G7322A	734.	774.
"	270.	B08G7325A	3577.	3570.	B08G7324A	765.	997.
876.5	0.	B08G7327A	3502.	3362.	B08G7326A	1371.	1058.
"	98.	B08G7329A	3472.	3430.	B08G7328A	1141.	872.
"	180.	B08G7331A	3555.	3460.	B08G7330A	1114.	828.
"	270.	B08G7333A	3513.	3526.	B08G7332A	957.	792.
1196.5	0.	B08G7335A	3165.	ND	B08G7334A	1580.	996.
"	98.	B08G7337A	3289.	3449.	B08G7336A	1266.	921.
"	180.	B08G7339A	3435.	3393.	B08G7338A	1129.	788.
"	270.	B08G7341A	3356.	3186.	B08G7340A	893.	803.
1330.0	0.	B08G7260A	2552.	861.	B08G7259A	1579.	-201.
"	95.	B08G7266A	2533.	1696.	B08G7265A	1313.	-432.
"	180.	B08G7264A	2652.	2398.	B08G7263A	1100.	-1035.
"	270.	B08G7262A	2041.	1943.	B08G7261A	864.	-1267.
1466.0	0.	B08G7343A	3172.	3006.	B08G7342A	1837.	941.
"	98.	B08G7345A	3199.	3497.	B08G7344A	1519.	957.
"	180.	B08G7347A	3383.	3346.	B08G7346A	1264.	690.
"	270.	B08G7349A	3239.	ND	B08G7348A	1029.	ND

Table 13 (Continued)

Station	Deg.	Maximum Hoop Strain (μ in/in)			Maximum Axial Strain (μ in/in)		
		Gage Name	Predicted	Measured	Gage Name	Predicted	Measured
1497.0	0:	B08G7373A	1919.	1926.	B08G7372A	2672.	1282.
"	98:	B08G7371A	1926.	1859.	B08G7370A	2284.	996.
"	180:	B08G7369A	2106.	1869.	B08G7368A	2223.	1139.
"	225:	B08G7385A	2070.	1883.	B08G7384A	2132.	945.
"	227:	B08G7383A	2030.	1817.	B08G7382A	2086.	1063.
"	235:	B08G7381A	1989.	1869.	B08G7380A	2034.	1012.
"	280:	B08G7379A	1943.	1823.	B08G7378A	1980.	1096.
"	300:	B08G7377A	1971.	1799.	B08G7376A	2059.	1229.
"	320:	B08G7375A	1933.	1763.	B08G7374A	2239.	1185.
1501.0	0:	B08G7391A	1864.	1737.	B08G7390A	1553.	1073.
"	98:	B08G7389A	1855.	1865.	B08G7388A	1273.	976.
"	180:	B08G7387A	2107.	1793.	B08G7386A	1191.	936.
"	220:	B08G7403A	1914.	1894.	B08G7402A	1140.	837.
"	225:	B08G7401A	1905.	ND	B08G7400A	1049.	ND
"	235:	B08G7399A	1907.	ND	B08G7398A	1041.	ND
"	280:	B08G7397A	1819.	1788.	B08G7396A	1005.	ND
"	300:	B08G7395A	1888.	1697.	B08G7394A	1075.	1037.
"	320:	B08G7393A	1733.	1697.	B08G7392A	1239.	1010.
1797.0	0:	B08G7405A	3574.	ND	B08G7404A	2907.	1030.
"	98:	B08G7407A	3580.	3097.	B08G7406A	1171.	545.
"	180:	B08G7409A	3557.	3015.	B08G7408A	1960.	737.
"	270:	B08G7411A	3631.	2986.	B08G7410A	904.	449.

Table 14 360L003 (STS-29) Comparison of Maximum Predicated vs. Measured
Biaxial Strain Values (Zero to 3 Seconds) Right SRM

Station	Deg.	Maximum Hoop Strain (μ in/in)			Maximum Axial Strain (μ in/in)		
		Gage Name	Predicted	Measured	Gage Name	Predicted	Measured
556.5	0:	B08G8323A	3586.	3490.	B08G8322A	736.	788.
"	82:	B08G8321A	3583.	3573.	B08G8320A	731.	821.
"	180:	B08G8319A	3568.	3486.	B08G8318A	791.	850.
"	270:	B08G8325A	3580.	3596.	B08G8324A	765.	885.
670.0	0:	B08G8252A	2680.	3690.	B08G8251A	985.	1102.
"	85:	B08G8254A	2691.	3827.	B08G8253A	1059.	1041.
"	180:	B08G8256A	2670.	3277.	B08G8255A	1111.	885.
"	270:	B08G8258A	2668.	3481.	B08G8257A	971.	867.
876.5	0:	B08G8331A	3688.	3680.	B08G8330A	1114.	787.
"	82:	B08G8329A	3685.	3552.	B08G8328A	1139.	898.
"	180:	B08G8327A	3688.	3609.	B08G8326A	1371.	1006.
"	270:	B08G8333A	3685.	3576.	B08G8332A	955.	806.
1196.5	0:	B08G8339A	3408.	3281.	B08G8338A	1567.	791.
"	82:	B08G8337A	3286.	3415.	B08G8336A	1266.	896.
"	180:	B08G8335A	3302.	3148.	B08G8334A	1130.	1076.
"	270:	B08G8341A	3353.	3378.	B08G8340A	888.	618.
1330.0	0:	B08G8264A	2654.	1136.	B08G8263A	1084.	-223.
"	85:	B08G8266A	2516.	1532.	B08G8265A	1303.	-405.
"	180:	B08G8260A	2553.	2699.	B08G8259A	1574.	-1086.
"	270:	B08G8262A	2590.	2581.	B08G8261A	886.	ND
1466.0	0:	B08G8347A	3381.	3244.	B08G8346A	1264.	646.
"	82:	B08G8345A	3199.	3147.	B08G8344A	1516.	902.
"	180:	B08G8343A	3216.	3180.	B08G8342A	1829.	1128.
"	270:	B08G8349A	3267.	3205.	B08G8348A	1029.	654.

TWR-17542

Station	Deg.	Maximum Hoop Strain (μ in/in)		Maximum Axial Strain (μ in/in)	
		Gage Name	Predicted	Gage Name	Predicted
1497.0	0.	B08G8369A	2104.	B08G8368A	2234.
"	80.	B08G8371A	1925.	B08G8370A	2284.
"	180.	B08G8373A	1934.	B08G8372A	2265.
"	2240.	B08G8377A	1973.	B08G8377A	2258.
"	2250.	B08G8379A	1987.	B08G8378A	2078.
"	2270.	B08G8381A	2032.	B08G8380A	2039.
"	2285.	B08G8383A	2071.	B08G8382A	2083.
"	2320.	B08G8385A		B08G8384A	2132.
					1266.
					1178.
					1175.
					1132.
					1103.
					1122.
					1175.
					1141.
1501.0	0.	B08G8387A	2104.	B08G8386A	190.
"	80.	B08G8389A	1851.	B08G8390A	1127.
"	180.	B08G8391A	1729.	B08G8392A	1135.
"	2240.	B08G8393A	1881.	B08G8394A	1123.
"	2255.	B08G8397A	1840.	B08G8396A	1107.
"	2270.	B08G8399A	1930.	B08G8398A	1100.
"	2285.	B08G8401A	1933.	B08G8399A	1104.
"	2320.	B08G8403A	1917.	B08G8400A	1106.
				B08G8402A	1145.
					598.
					981.
					1034.
					911.
					800.
					ND.
					819.
					732.
					842.
1797.0	0.	B08G8409A	3548.	B08G8408A	1960.
"	80.	B08G8407A	3385.	B08G8406A	1161.
"	180.	B08G8405A	3383.	B08G8404A	2921.
"	2270.	B08G8411A	3628.	B08G8410A	906.
					634.
					1533.
					1054.
					1440.

Table 15 Maximum Measured Biaxial Stress Values (Zero to 120 Seconds)

Station	Degree	Left SRB		Right SRB	
		Max Hoop	Stress (KSI)	Max Hoop	Stress (KSI)
		Measured	Corr. Axial	Measured	Corr. Axial
		Measured	Measured	Measured	Measured
556.5	0.	129.9	61.6	123.2	59.6
"	98.	120.4	62.3	125.7	64.5
"	180.	124.8	59.2	123.5	61.4
"	270.	126.0	47.2	125.8	45.8
670.0	0.	-	-	ND	ND
"	98.	-	-	137.4	74.5
"	180.	-	-	119.0	60.7
"	270.	-	-	124.3	48.3
876.5	0.	124.7	59.6	132.8	58.2
"	98.	124.5	64.8	128.1	63.9
"	180.	125.7	57.4	133.1	60.5
"	270.	127.3	49.6	128.8	50.9
1196.5	0.	ND	ND	121.6	54.1
"	98.	127.7	57.9	126.9	58.4
"	180.	125.1	55.4	120.7	56.4
"	270.	119.7	49.3	125.5	46.2
1330.0	0.	-64.8	-21.1	34.4	1.3
"	98.	54.6	4.2	48.0	4.2
"	180.	73.4	-9.3	74.9	-19.5
"	270.	55.7	-10.1	ND	ND
1466.0	0.	115.0	57.2	121.6	51.5
"	98.	133.2	58.9	122.0	53.9
"	180.	124.6	52.4	124.2	54.2
"	270.	ND	ND	120.8	49.8

Table 15 (Continued)

Station	Degree	Left SRB		Right SRB	
		Stress (KSI)	Max Hoop Corr. Axial	Stress (KSI)	Max Hoop Corr. Axial
		Measured	Measured	Measured	Measured
1497.0	0.	80.8	54.8	89.1	63.4
"	98.	78.2	51.4	87.9	74.0
"	180.	78.4	54.6	83.9	63.4
"	220.	78.3	52.4	82.1	58.4
"	255.	77.6	55.6	84.4	54.8
"	270.	78.5	52.5	81.1	60.4
"	285.	77.3	53.7	81.5	59.9
"	300.	78.8	57.6	83.3	59.9
"	320.	78.4	55.2	86.9	69.9
1501.0	0.	73.5	45.4	74.6	38.7
"	98.	75.7	46.9	76.3	47.7
"	180.	74.4	47.6	73.1	44.2
"	220.	76.9	48.5	75.3	46.1
"	255.	ND	ND	76.2	43.3
"	270.	ND	ND	ND	ND
"	285.	ND	ND	72.5	44.1
"	300.	75.8	49.7	74.5	43.1
"	320.	75.3	49.7	78.5	50.6
1797.0	0.	ND	ND	114.5	45.4
"	98.	117.7	50.0	120.3	51.3
"	180.	117.1	48.3	112.9	43.3
"	270.	117.5	40.9	121.0	41.3

improvement. The maximum measured hoop stress results in a safety factor (SF) of 1.61 with the ultimate strength. The yield strength of D6AC is 180 ksi. Therefore, no local yielding occurred in this area.

4.5 Nozzle-to-Case Joint Performance

Flight 360L003 instrumentation on the nozzle-to-case joint consisted of six girth gages, and two stations of biaxial gages. Results at these locations are compared to analytical results acquired from a three-dimensional finite element analysis. The analysis was performed with the finite element code ANSYS using a 1.8-degree model of the nozzle-to-case joint. Near the joint region, the model was three-dimensional, transitioning into two dimensional away from the joint.

The following assumptions and parameters were included in the model:

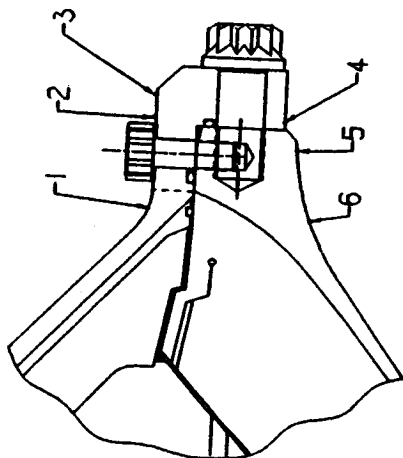
- o Nominal values for material properties and hardware dimensions
- o Preload of 140 kips in the axial bolts and 47 kips in the radial bolts
- o Internal pressure of 920 psig applied up to the backside of the primary O-ring groove
- o Frictionless joint behavior
- o Zero vectoring nozzle condition
- o Propellant and insulation was not modeled

Because the model is cyclic-symmetric, any circumferential variation indicated by test data will not be taken into account. The analysis was performed at 920 psig which was linearly scaled to the estimated nozzle stagnation pressure, which involves approximately five percent error because of the nonlinear analysis.

4.5.1 Nozzle-to-Case Girth Gages

Radial deflection is an important parameter to characterize, since it is proportional to joint hoop stress. Tables 16 and 17 list the girth gage response during the flight and compare it to analysis. These tables show a good correlation with predicted values with the exception of gage B08G8314 (the percent difference for this gage is 41%). The percent difference ranges from 8.3 to 26.1, excluding the above mentioned gage. These tables also show the maximum experienced strain and radial growth for the duration of the flight. As expected, calculated radial growths indicated a "prying open" action and outward rotation of the joint. The maximum radial growth was 0.101 in. and occurred at Location 4 on the left SRB. Table 18 is a comparison between Flight 360L003, several static test motors, Flights 360L0002, 360L001, and predictions. The correlation is very good with Flights 360L002, 360L001, and slightly lower with static motors.

Table 16 Left SRM Aft Dome, Fixed Housing Nozzle-to-Case Girth Gages

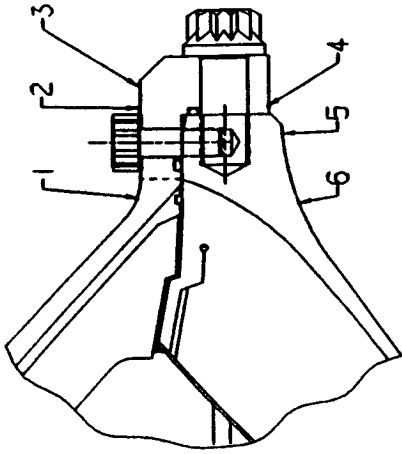


TEST NAME: 360L003
JOINT: LEFT SRM AFT DOME, FIXED HOUSING
DESCRIPTION: NOZZLE CASE GIRTH GAGES
THE TIME RANGE IS -10.0 TO 120.0 SECONDS

GIRTH GAGE LOCATION	GAGE NUMBER	STATION	RADIUS (IN)	RADIAL GROWTH (IN)	TEST STRAIN (UTN/IN)	ADJUSTED ANALYSIS STRAIN (UTN/IN)	ADJUSTED ANALYSIS RADIAL GROWTH (IN)	DIFF IN RADIAL GROWTH (% DIFF)
1	B08G7312	1873.0	50.4	0.059	1181	1476	0.074	25.0
2	B08G7310	1875.7	50.5	0.094	1868	2022	0.102	8.3
3	B08G7315	1876.0	50.5	0.100	1987	2440	0.123	22.8
4	B08G7314	1875.5	54.4	0.101	1859	2344	0.128	26.1
5	B08G7313	1874.0	54.8	0.085	1547	1860	0.102	20.2
6	B08G7311	1872.5	55.2	0.062	1118	1392	0.077	24.5

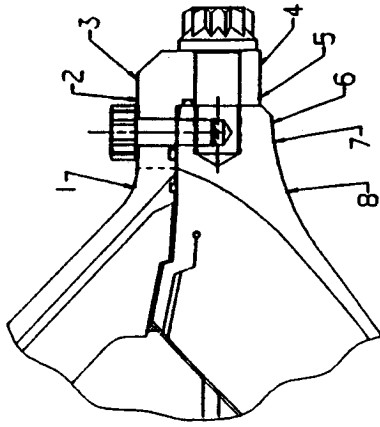
Table 17 Right SRM Aft Dome, Fixed Housing Nozzle-to-Case Girth Gages

TEST NAME: 360L003
JOINT: RIGHT SRM AFT DOME, FIXED HOUSING
DESCRIPTION: NOZZLE CASE GIRTH GAGES
THE TIME RANGE IS -10.0 TO 120.0 SECONDS



GIRTH GAGE LOCATION	GAGE NUMBER	STATION	RADIUS (IN)	RADIAL GROWTH (IN)	TEST STRAIN (UIN/IN)	ADJUSTED ANALYSIS STRAIN (UIN/IN)	ADJUSTED ANALYSIS RADIAL GROWTH (IN)	DIFF IN RADIAL GROWTH (% DIFF)
1	B08G8312	1873.0	50.4	0.059	1174	1460	0.074	24.4
2	B08G8310	1875.7	50.5	0.092	1820	2014	0.102	10.7
3	B08G8315	1876.0	50.5	0.098	1934	2420	0.122	25.1
4	B08G8314	1875.5	54.4	0.091	1665	2348	0.128	41.0
5	B08G8313	1874.0	54.8	0.083	1515	1845	0.101	21.8
6	B08G8311	1872.5	55.2	0.066	1198	1383	0.076	15.4

Table 18 Nozzle-to-Case Joint Radial Growth Comparisons to 360L003 (STS-29)



Nozzle to Case Girths

LOC.	STS-29		STS-27		STS-26		RADIAL GROWTH (Inches)				NOMINAL RADIUS (INCHES)				
	GAGE	RIGHT	LEFT	RIGHT	LEFT	RIGHT	LEFT	FV-1	QM-7	QM-6	DM-9	DM-8	FRED		
1	B08GX312	0.059	0.059	0.057	0.059	ND	0.049	0.087	0.068	0.081	0.072	ND	0.074	50.4	
2	B08GX310		0.092	0.094	0.090	ND	ND	ND	ND	ND	ND	ND	0.102	50.5	
3	B08GX315		0.098	0.100	0.095	0.094	0.093	0.127	0.128	0.130	0.115	ND	0.122	50.5	
4	NO GAGE		ND	ND	ND	ND	ND	0.118	0.126	0.126	ND	0.124	ND	54.4	
5	B08GX314		0.091	0.101	0.088	0.088	0.097	0.097	0.124	0.120	0.119	0.114	ND	0.128	54.4
6	B08GX313		0.083	0.085	0.081	0.080	ND	ND	0.107	0.109	0.106	0.087	0.110	0.101	54.8
7	NO GAGE		ND	ND	ND	ND	0.087	0.084	0.100	0.101	0.102	0.103	ND	54.8	
8	B08GX311		0.066	0.062	0.063	0.062	0.070	0.067	0.084	0.087	0.086	0.086	0.090	0.076	55.2

Note: All Test Radial Growths Are Ratios of STS-29 Test Pressure

4.5.2 Nozzle-to-Case Biaxial Strain Gages

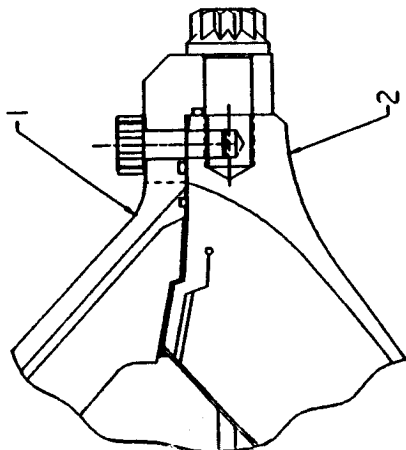
The nozzle-to-case biaxials measure local rather than average strains. Tables 19 through 20 show the maximum hoop stress values for the duration of the flight (-10 to 120 seconds). The maximum stress occurred in the hoop direction at Location 1, 180 degrees on the left SRB, and had a value of 39.9 ksi. This gives a safety factor of 5.4 with the ultimate strength.

Tables 21 and 22 show a comparison with predicted values between -10 and 120 seconds. The hoop direction compares very closely, but the axial direction is somewhat different. Previous static-fire tests have shown that the nozzle-to-case joint gages do not compare as well to analytical data in the meridional direction as in the hoop direction. Some possible reasons for discrepancies with predicted values are discussed below:

- o Some gages are located in the neck of the fixed housing, the 3-D model grid may not be fine enough to accurately predict circumferential strain
- o Analytical data was linearly scaled to the test data
- o Nozzle stagnation pressure was estimated to be 824 psig at 20 seconds, but not measured.
- o Nominal materials were used for the finite element model.

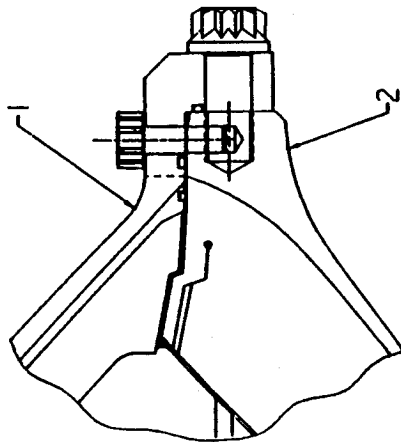
Table 19 Left SRM Fixed Housing, Aft Dome Nozzle-to-Case Girth Gages

TEST NAME: 360L003
JOINT: LEFT SRM FIXED HOUSING, AFT DOME
DESCRIPTION: NOZZLE / CASE BIAXIAL GAGES
CORRECTED LOCAL PRESS:
THE TIME RANGE IS -10.0 TO 120.0 SECONDS



LOCAT	ANGULAR LOCATION	HOOP GAGE	MERID GAGE	MAX HOOP STRESS (KSI)	MERID STRESS (KSI)	TEST DATA	
						HOOP STRAIN (UIN/IN)	MERID STRAIN (UIN/IN)
1	0.0	B08G7415	B08G7416	38.9	-17.6	1503	-1014
	90.0	B08G7420	B08G7421	32.2	-38.4	1504	-1646
	180.0	B08G7425	B08G7426	35.9	-16.9	1529	-1001
	270.0	B08G7430	B08G7431	35.2	-16.5	1504	-981
			AVERAGE:	37.6	-22.3	1510	-1161
2	0.0	B08G7413	B08G7412	ND	ND	ND	ND
	90.0	B08G7418	B08G7417	27.3	-32.7	1277	-1401
	180.0	B08G7423	B08G7422	ND	ND	ND	ND
	270.0	B08G7428	B08G7427	37.2	-18.4	1287	-969
			AVERAGE:	27.8	-25.5	1282	-1185

Table 20 Right SRM Fixed Housing, Aft Dome Nozzle-to-Case Girth Gages

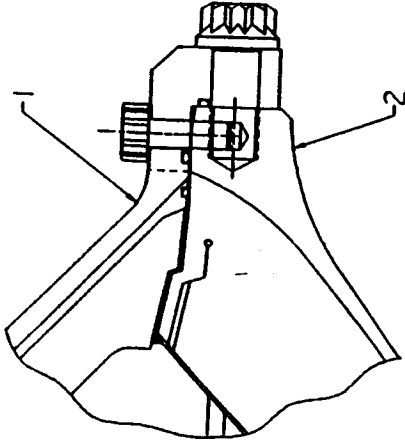


TEST NAME: 360L003
JOINT: RIGHT SRM FIXED HOUSING, AFT DOME
DESCRIPTION: NOZZLE / CASE BIAXIAL GAGES
THE TIME RANGE IS -10.0 TO 120.0 SECONDS

LOCAT	ANGULAR LOCATION	HOOP GAGE	MERID GAGE	MAX HOOP STRESS (KSI)	MERID STRESS (KSI)	TEST DATA	
						HOOP STRAIN (UIN/IN)	MERID STRAIN (UIN/IN)
1	0.0	B08G8425	B08G8426	25.3	-22.3	1094	-1026
	90.0	B08G8420	B08G8421	66.6	-27.6	2547	-1651
	180.0	B08G8415	B08G8416	39.0	-20.8	1540	-1123
	270.0	B08G8430	B08G8431	38.3	-15.3	1459	-932
		AVERAGE:		42.3	-21.5	1660	-1183
2	0.0	B08G8423	B08G8422	30.8	-20.5	1263	-1027
	90.0	B08G8418	B08G8417	27.0	-29.6	1233	-1291
	180.0	B08G8413	B08G8412	25.4	-19.6	1068	-935
	270.0	B08G8428	B08G8427	31.4	-18.2	1257	-953
		AVERAGE:		28.6	-22.0	1205	-1052

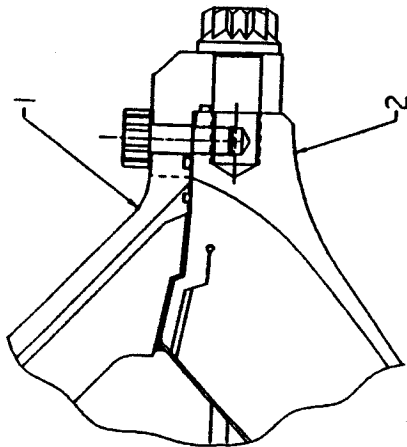
Table 21 Left SRM Fixed Housing, Aft Dome Nozzle-to-Case Girth Gages Compared to Predictions

TEST NAME: 360L003
JOINT: LEFT SRM FIXED HOUSING, AFT DOME
DESCRIPTION: NOZZLE / CASE BIAXIAL GAGES
THE TIME RANGE IS -10.0 TO 120.0 SECONDS



LOCAT	ANGULAR LOCATION	TEST DATA		ADJUSTED ANALYSIS				%DIFF HOOP	%DIFF MERID
		HOOP GAGE	HOOP STRAIN (UIN/IN)	HOOP STRAIN (UIN/IN)	HOOP STRAIN (UIN/IN)	HOOP STRAIN (UIN/IN)	HOOP STRAIN (UIN/IN)		
1	0.0	B08G7415	B08G7416	1503	-1038	1363	-1336	-9.3	28.6
	90.0	B08G7420	B08G7421	1504	-1666	1371	-1337	-8.9	-19.7
	180.0	B08G7425	B08G7426	1529	-1013	1365	-1334	-10.7	31.6
	270.0	B08G7430	B08G7431	1504	-1001	1366	-1331	-9.2	32.9
		AVERAGE:		1510	-1180				
2	0.0	B08G7413	B08G7412	ND	-1054	ND	-659	ND	-37.5
	90.0	B08G7418	B08G7417	1277	-1477	1066	-659	-16.5	-55.4
	180.0	B08G7423	B08G7422	ND	-2142	ND	-657	ND	-69.3
	270.0	B08G7428	B08G7427	1295	-1013	1071	-659	-17.3	-34.9
		AVERAGE:		1286	-1422				

Table 22 Right SRM Fixed Housing, Aft Dome Nozzle-to-Case Girth Gages
Compared to Predictions



TEST NAME: 360L003
JOINT: RIGHT SRM FIXED HOUSING, AFT DOME
DESCRIPTION: NOZZLE / CASE BIAXIAL GAGES
THE TIME RANGE IS -10.0 TO 120.0 SECONDS

LOCAT	ANGULAR LOCATION	HOOP GAGE	MERID GAGE	TEST DATA		ADJUSTED ANALYSIS			
				HOOP STRAIN (UIN/TN)	MERID STRAIN (UIN/TN)	HOOP STRAIN (UIN/TN)	MERID STRAIN (UIN/TN)	%DIFF HOOP	%DIFF MERID
1	0.0	B08G8425	B08G8426	1094	-1050	1359	-1328	24.2	26.5
	90.0	B08G8420	B08G8421	2563	-2563	1309	-1292	-48.9	-49.6
	180.0	B08G8415	B08G8416	1540	-1131	1362	-1327	-11.6	17.3
	270.0	B08G8430	B08G8431	1459	-960	1362	-1328	-6.7	38.3
		AVERAGE:		1664	-1426				
2	0.0	B08G8423	B08G8422	1263	-1079	1062	-657	-15.9	-39.1
	90.0	B08G8418	B08G8417	1257	-1404	1066	-656	-15.2	-53.3
	180.0	B08G8413	B08G8412	1261	-1715	1064	-655	-15.6	-61.8
	270.0	B08G8428	B08G8427	1257	-1017	1058	-656	-15.8	-35.5
		AVERAGE:		1260	-1304				

4.6 Moment, Shear and Strut Forces

Six stations along the full length of the SRM contained biaxial strain gages at four locations around the circumference (approximately 90 degrees apart). From these, a stress plane at each station is generated. From the stress plane, the Y and Z axis bending moments and axial loads are computed. These results are compared to both previous flights and predicted loads at all significant operational periods including: prelaunch, build-up, liftoff, shuttle roll maneuver, maximum acceleration, maximum dynamic pressure, and separation.

4.6.1 Bending About The Y Axis (MY)

Figure 12 shows a typical case of bending about the Y axis (see pages A-1 through A-23, Appendix A). Initially, the case is seen to be bending in the +Y direction which is caused by the orbiter weight. The magnitude increases more or less linearly going down the case toward the hold down point. There is an abrupt shift at Station 1501 which is caused by the struts giving added support, and the fact that the case thickness at this station is slightly greater (0.58 inch at Station 1501, 0.479 at other stations). During SSME build-up, every station experiences a change from positive to negative bending as the assembly bends over. The maximum value was -264×10^6 in.-lb at Station 1797 on the left SRB (see page A-6, Appendix A). This value compares well with the design maximum of

-304 x 10⁶ in.-lb. Upon lift-off, the values reduce significantly, coming back to nearly zero for every station. During the shuttle roll maneuver, the left SRB experiences an increase in bending, while the right SRB experiences a decrease. This is because the nozzles are vectoring to cause the roll, and the SRBs are essentially pivoting about the struts. At the end of the roll, the change for the left and right SRBs is opposite for the same reason. From this point on, the data are not very interesting, and reduces to zero. The large spike seen at approximately 124 seconds occurs at separation, and is typical of other flights.

Pages A-7 through A-23 of Appendix A are plots of the first three flights, Flight 360L001, Flight 360L002, and Flight 360L003. Stations were chosen on Flights 360L001, 360L002, and Flight 360L003 that were as near as possible to the stations used on these previous flights. As shown in the figures, the correlation is very good. From these plots, the difference in the roll maneuver between Flights 360L001, 360L002, and 360L003 can be noted. The roll maneuver of Flight 360L003 is most similar to 360L001. The only notable difference is at Station 556 on the left SRB. Flight 360L001 is significantly higher, and follows a different path than Flights 360L002, and 360L003. Comparison between Flight 360L001 and Flights 360L002, and 360L003 could not be made for Station 556 and 876 on the right motor because these stations have bad data for Flight 360L001. Also, there was no instrumentation on the left SRB of the first three flights near Station 556, so no comparison can be made there.

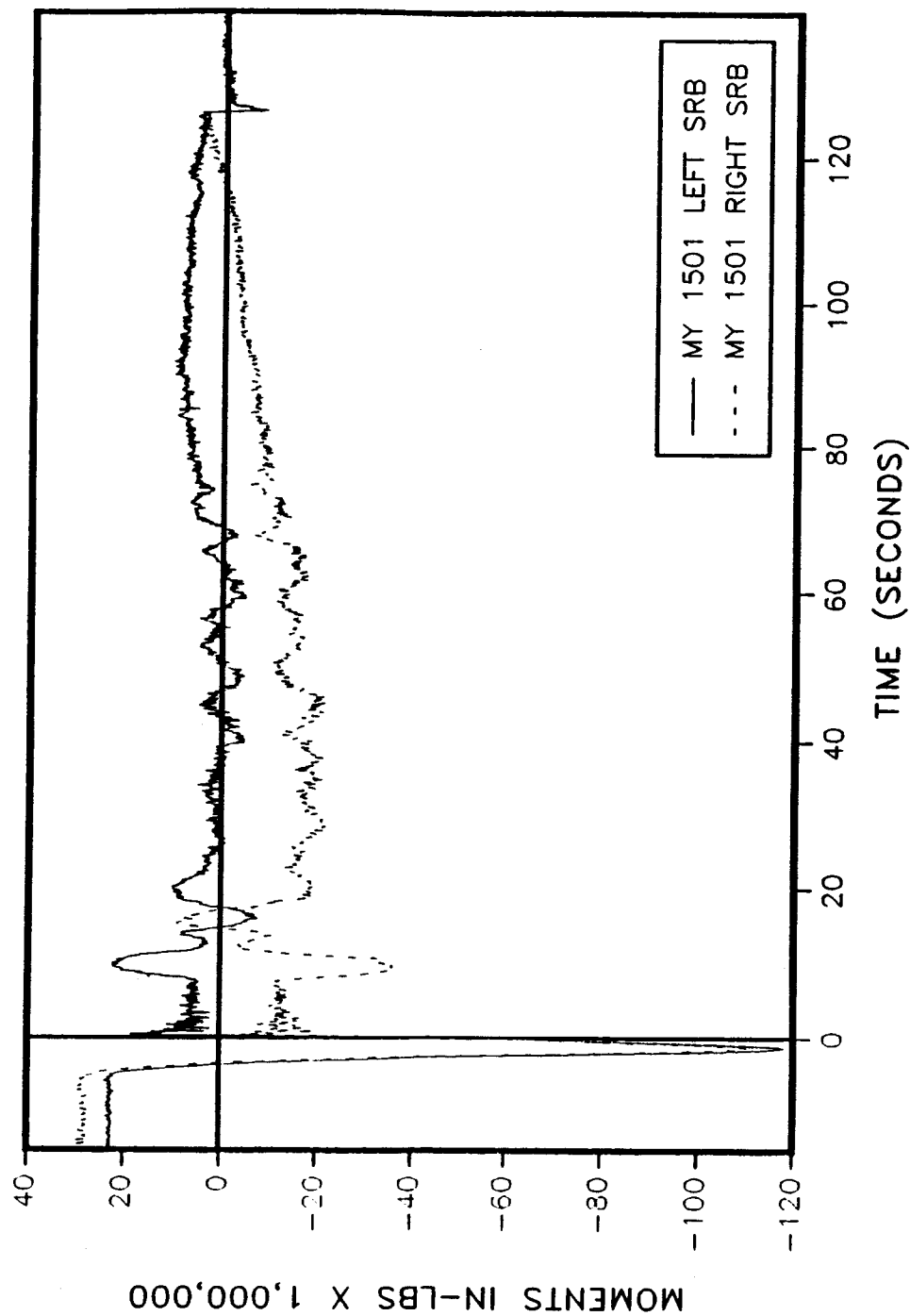


Figure 12 Bending About the Y Axis, Station 1501

4.6.2 Bending About The Z Axis (MZ)

Figure 13 shows a typical case of bending about the Z axis (see pages A-24 through A-46, Appendix A). Initially, the top of the motors are seen to be bending toward the external tank, which is caused by the weight of the external tank and orbiter. Moving down the motor, the bending becomes less then changes sign between Stations 1196 and 1466 as expected. At Station 1797, it changes back to the same sign as at the top of the motor, as expected. Upon liftoff, these same effects are seen with a larger magnitude because the SRBs are firing, and the motor is essentially pivoting about the attach points.

During the roll maneuver, Stations 1196 and 1466 show the same peaks as bending about the Y axis with the exception that both the left and right motors move in the same direction. This is caused by the sign convention.

During the first phase of the roll, the left motor is pushing away from the external tank, and the right motor is pushing toward the external tank. The opposite is true of the second part of the roll maneuver. Station 1797 is different from the other stations because after liftoff, it follows a more or less linear path back to zero during the flight.

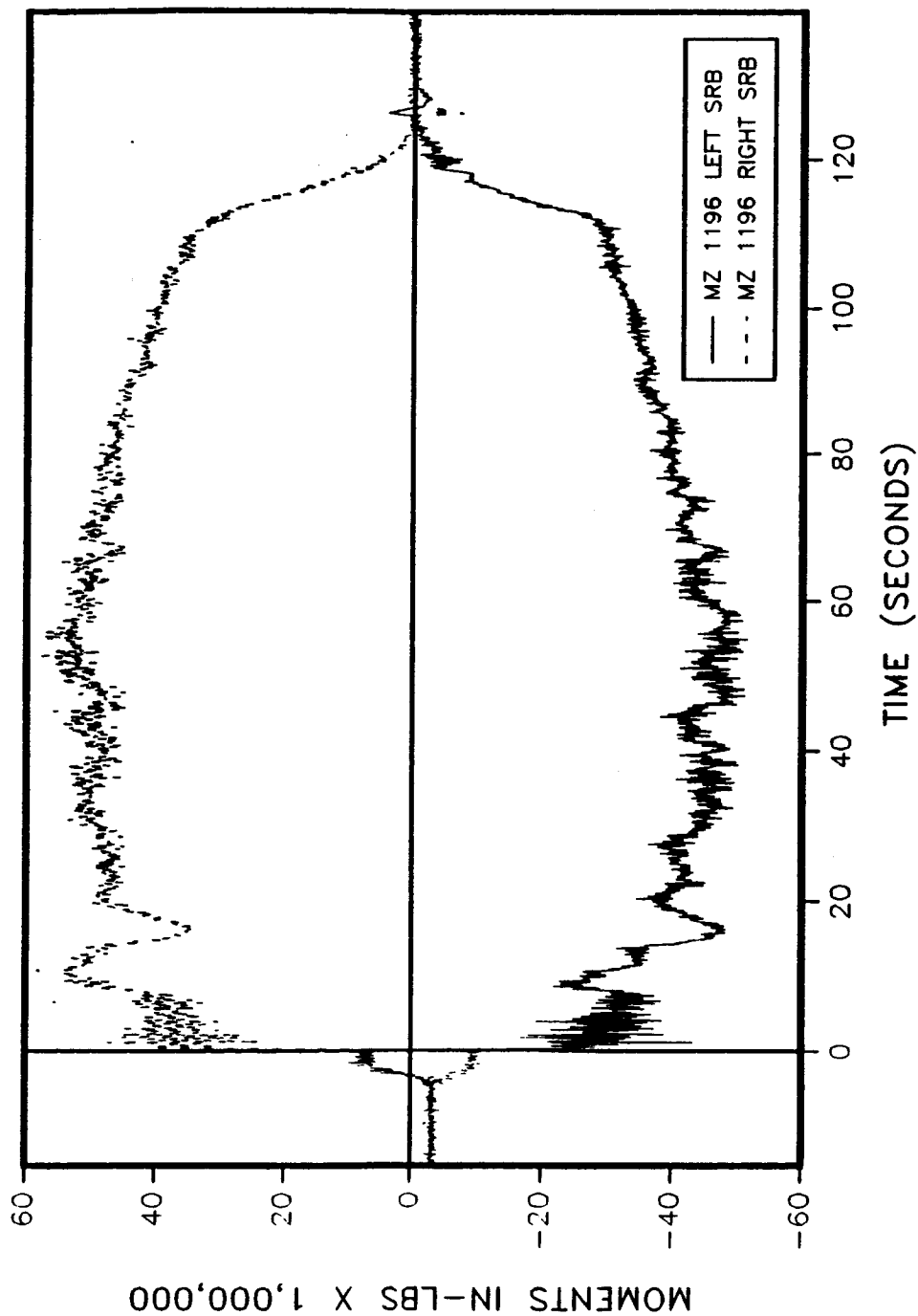


Figure 13 Bending About the Z Axis, Station 1196

Pages A-30 through A-46 are plots of the first three flights, Flights 360L003, 360L002 and 360L001 as a function of time. Station 556 of Flight 360L001 shows a much lower magnitude than Flights 360L002 and 360L001. Station 1466 shows a higher magnitude than the other flights. Comparisions at the other stations show good correlation between Flight 360L003 and previous flights.

4.6.3 Axial Force, X Axis (VX)

Figure 14 shows a typical plot of axial force (see pages A-47 through A-69, Appendix A). In this figure, a positive value represents a compressive force, and a negative value represents a tensile force. Initially the SRBs are subjected to the weight of the external tank, orbiter, and the weight of the segments above the particular station. Since these are the only forces acting axially, the result should increase linearly proceeding down the case. Station 1501 shows a marked decrease in measured strain as seen with bending about the Y and Z axis, and is caused by the increased case thickness in this region. Upon SRB ignition, the cases immediately go into tension as the motors pressurize and liftoff. The maximum value was 13,408 kips and occurred at Station 556.5 of the right motor. After this point, the shape of the plot looks like the motor pressure plots. There is good agreement between left and right motors. Some of the difference can be attributed to the fact that the gages were zeroed at the end of the flight, and the actual strain values experienced by the left and right motors, and each station, were probably not exactly zero.

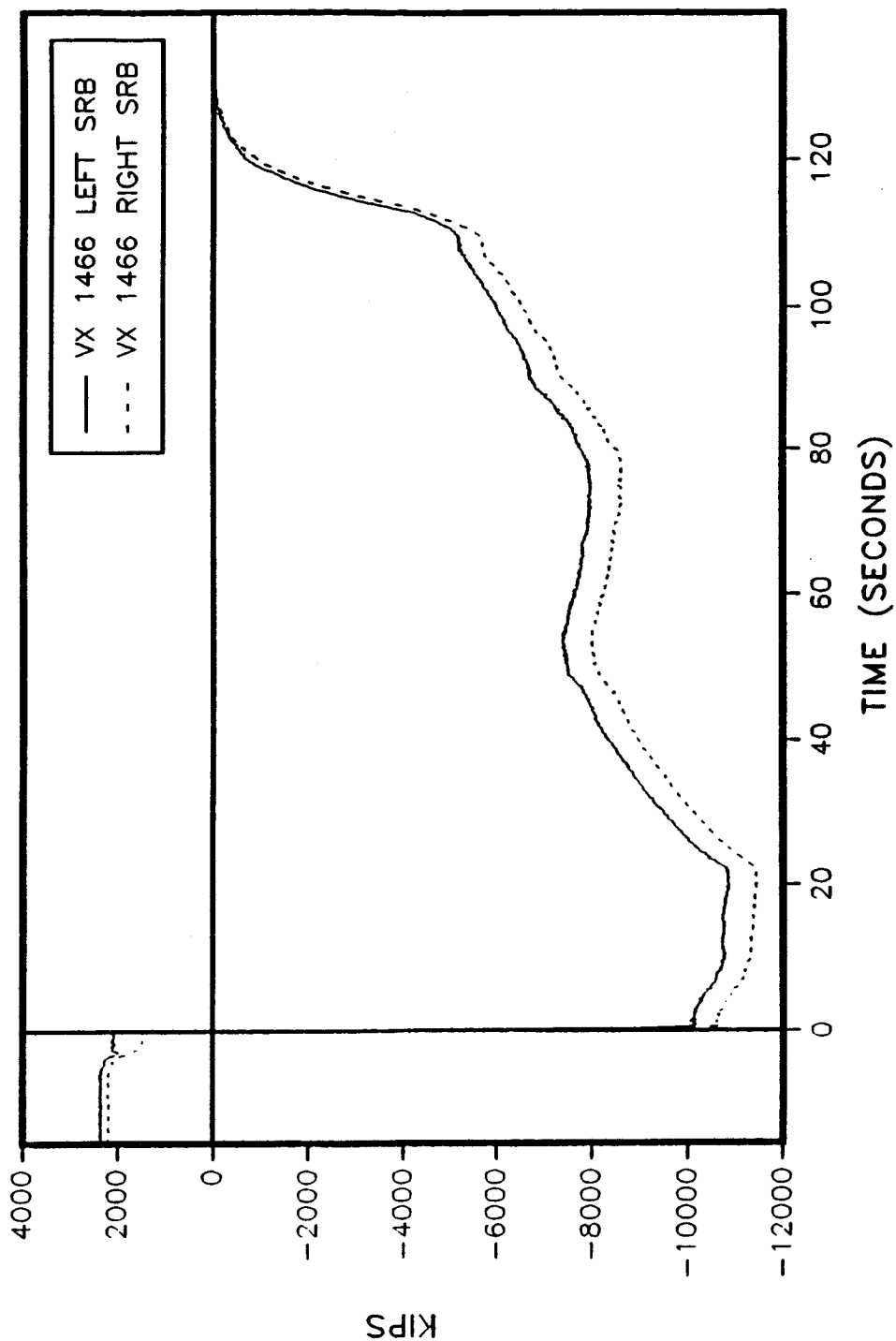


Figure 14 Axial Force, Station 1466

Pages A-53 through A-69 are plots of the first three flights, Flights 360L003, 360L002, and 360L001. As shown in the figures, the shape of the curves are very similar. The higher magnitude of Flights 360L003, 360L002, and 360L001 can be explained by the fact that the redesigned boosters are high performance motors, and obtain a higher operating pressure than the older motors. The comparisons between Flights 360L003, 360L002, and 360L001 are very good.

4.6.4 Line Loads

Using the bending moment, and axial force data, the average line loads were calculated. Pages A-70 through A-75 of Appendix A show the line load as a function of time. These figures show a similar curve shape as axial force, only with a different magnitude. The method of calculation of this line load produces only an average value around the case, so it is not directly comparable to maximum design line loads.

4.6.5 Strut Forces

Figures 15 and 16 show the resultant strut force in the Y and Z directions respectively. The left and right motors are mirror images of each other in the resultant Y force direction. The left SRB shows a positive value while the right SRB shows a negative value.

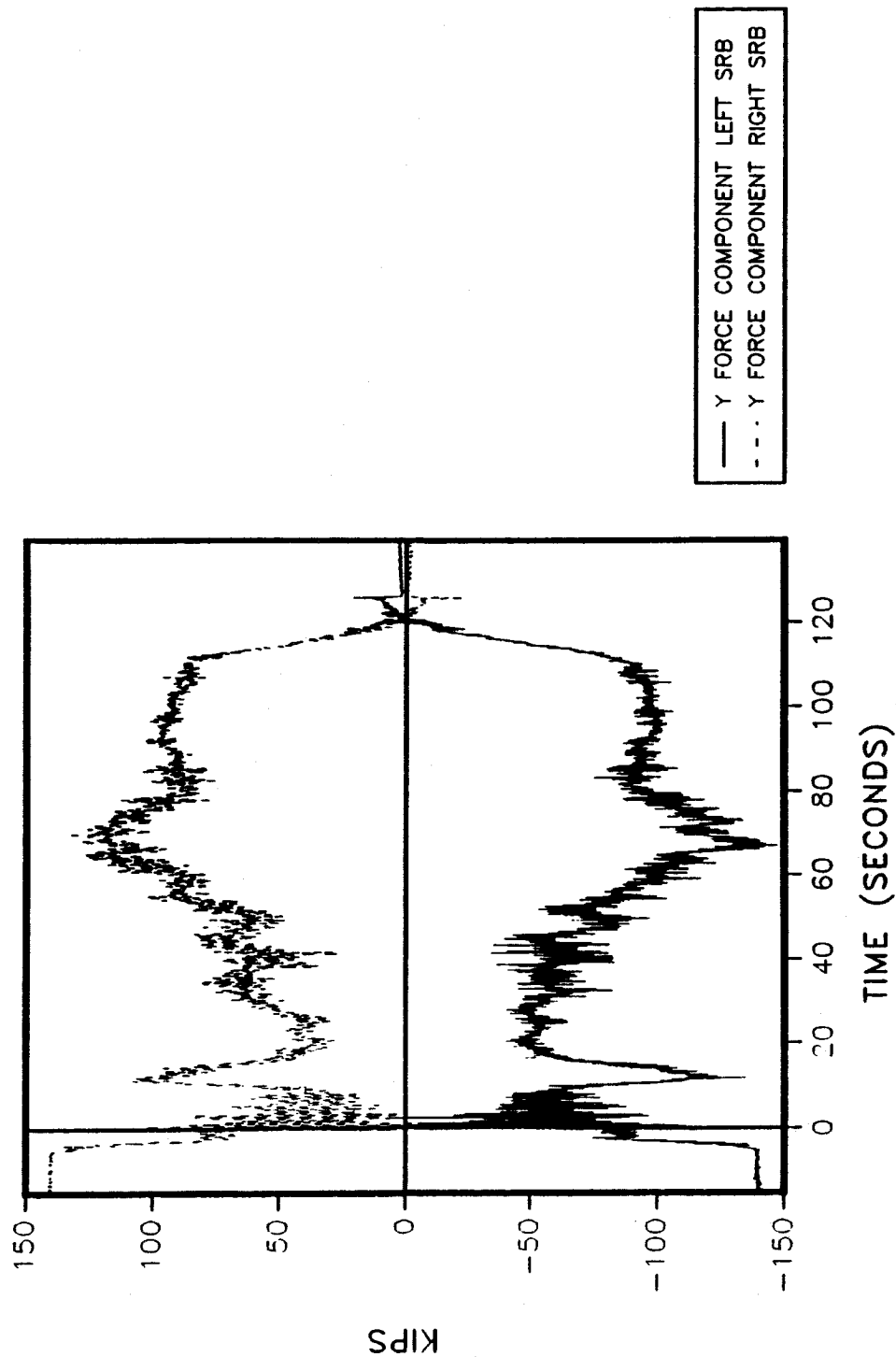


Figure 15 Strut Forces, Y Axis

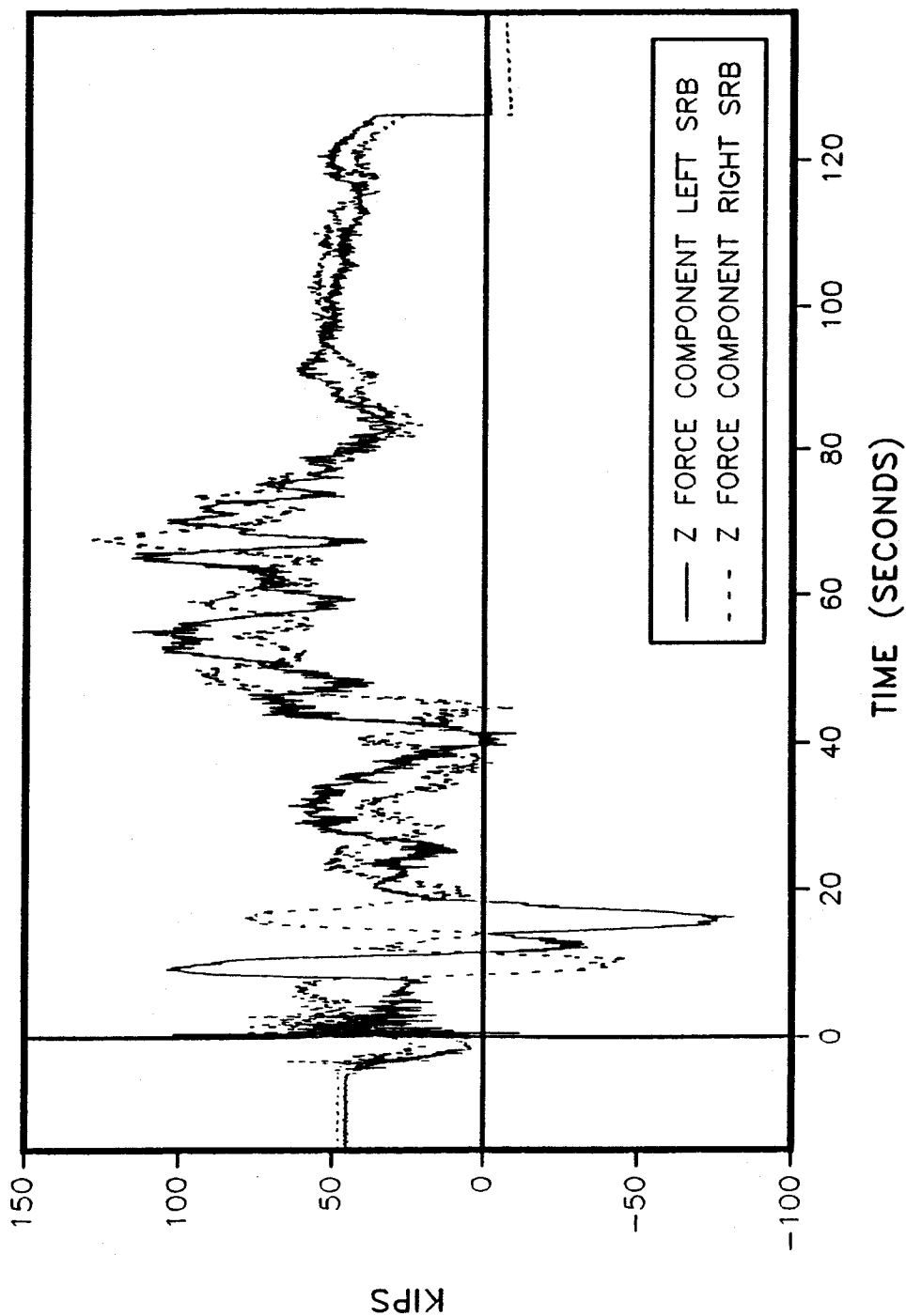


Figure 16 Strut Forces, Z Axis

4.7 Flight Envelopes

In general, the bending moments and axial force experienced by Flight 360L003 were either within the envelopes, or slightly out. The following are some possible reasons all the loading did not fall within the envelopes:

1. Several strain gages went into the calculation of each load, and every gage has an uncertainty associated with the gage itself, plus some drift might occur in each gage during the flight.
2. Adjusting the strain data to end at zero adds some uncertainty, since the exact strain experienced during free fall is not known.
3. The program calculates a linear stress distribution from strain data, and the case does not necessarily behave linearly during flight.

It should be noted that the data compare favorably with previous flight data, as expected. The time ranges used to find the maximum and minimum values for each event are defined in Table 23.

4.7.1 Bending About The Y Axis

Pages A-76 through A-89 of Appendix A are plots of the maximum and minimum values for Flight 360L003 and the envelopes for specific flight events. These plots show the data fits the envelopes quite well. Those stations that do fall outside the envelope are of a relatively small magnitude.

4.7.2 Bending About The Z Axis

Pages A-90 through A-103 of Appendix A are plots of the maximum and minimum values for Flight 360L003 and the envelopes for specific flight events. These plots show that the data follows the correct trend, and is quite close to the envelopes.

Table 23
Flight Event Time Ranges

Flight Event	Time range (in seconds)
Pre-launch	-15.0 to -7.0
Build-up	-1.6 to -0.8
Lift-off	0.5 to 4.0
Roll maneuver	5.0 to 22.0
Max Q	27.0 to 76.0
Max G	72.0 to 90.0
Preseparation	119.0 to 124.0

4.7.3 Axial Force

Pages A-102 through A-114 of Appendix A are the axial force envelopes and the Flight 360L003 data plotted as a function of station. These data are very near the envelopes.

5.0 POST FIRE INSPECTION RESULTS

Structural Applications Design Engineering performed a post-fire evaluation of the Flight 360L003 forward, center, and aft field joints, aft exit cone field joints, nozzle-to-case joints, the igniter, and safe and arm joints at Hangar AF. The internal nozzles and some of the factory joints were disassembled and inspected at the refurbishment facilities in Clearfield, Utah. The factory joint disassembly inspections were omitted except for both aft segments, left forward segment, and the left aft center segment. This section documents the post-fire condition of Flight 360L003 sealing surfaces and seals as noted during disassembly, and discusses all observations assessed by the Seals Component Team.

In an attempt to standardize and document the evaluation of flight motors, a standard evaluation plan has been written (see References 6 and 7). Appropriate procedures contained in this plan were used to evaluate the sealing system of all joints in the RSRM. The intent of this plan is to ensure that all pertinent evaluation points of Flight 360L003 were examined and documented in a consistent and complete manner. Also, to accurately

document the magnitude of the types of damage that are seen, definitions are presented in Table 24. The left motor will be discussed first, then the right motor. The evaluation will start at the igniter and proceed down the motors to the aft exit cones.

5.1 Left Motor Disassembly Evaluation

5.1.1 External Walk Around

The external walk around inspection revealed no signs of hot gas leakage past any joints.

5.1.2 Safe and Arm Joint

There was no soot up to the primary seal on the S&A gasket. There was no corrosion or damage found to the joint or gasket seals at the time of disassembly.

5.1.3 Outer Igniter Joint (Adapter-to-Forward Dome)

No blow paths through the zinc chromate putty were present and there was no evidence of hot gas leakage past the primary seal or damage observed on the joint or gasket seals.

Table 24 Post Fire Inspection Definitions

O-RINGS AND STAT-O-SEALS

<u>Cut:</u>	Width, essentially zero (have to open up to find the damage), and depth greater than 0.005 inch.
<u>Scratch:</u>	Width less than 0.005 inch and depth less than 0.005 inch.
<u>Nick:</u>	Width less than 0.020 inch, but greater than 0.005 inch; and depth less than 0.010 inch, but greater than 0.005 inch.
<u>Gouge:</u>	Width greater than 0.020 inch and depth greater than 0.010 inch.
<u>Circumferential or Radial Flowline:</u>	Visible evidence of incomplete flow or knit of the material.
(i) Closed:	Tightly adhered, not separable, does not open when lightly probed.
(ii) Separable:	Visually appears closed. Separates when lightly probed.
(iii) Open:	Obvious separation or gap.
<u>Hard Inclusion:</u>	Foreign material enclosed in the seal material.
<u>Porosity/Soft Inclusion:</u>	An air pocket enclosed in the seal material.
<u>Extrusion Damage:</u>	Seal material pinched and/or cut due to extrusion under pressure or an overfill condition.
<u>Heat Effect:</u>	Glossy and/or hardened seal surface due to hot gas impingement.
<u>Erosion:</u>	Seal material missing due to hot gas impingement or blow-by.

CORROSION

<u>Light Corrosion:</u>	Can be wiped off by hand. Surface discoloration.
<u>Medium Corrosion:</u>	Cannot be wiped off by hand without the use of a Scotch-Brite material, methyl chloroform, or grease soaked rag.
<u>Heavy Corrosion:</u>	Starting to penetrate into the metal surface such that pitting and/or metal material is significantly eroded.

5.1.4 Inner Igniter Joint (Adapter-to-Chamber)

No blow paths through the zinc chromate putty were present and there was no evidence of hot gas leakage past the primary seal, or damage observed on the joint or gasket seals. All stat-o-seals from the inner joint bolts were damaged during disassembly.

There was corrosion, from the forward dome, on the tips of the transducer bolts at 40, 100, and 180 degrees and in the bottom of all transducer bolt holes located at 40, 100, 180 and 270 degrees.

5.1.5 Forward Field Joint

There was no sign of hot gas or soot past the J-leg. The grease coverage was per design and no corrosion was found on any of the sealing surfaces. Intermittent pin hole and shim area corrosion was found on the tang and clevis. The O.D. of the outer clevis leg showed moderate to light corrosion from zero to 360 degrees. The joint was slightly contaminated with debris and water from hydrolase operations which remove the joint protection system.

No seal damage was observed at the time of disassembly, and the V2 filler was properly installed with no visible damage. Detailed inspection of the O-rings revealed no damage.

hydrolaze operations which remove the joint protection system.

No seal damage was observed at the time of disassembly and the V2 filler was properly installed with no visible damage. No damage was observed on the three O-rings during detailed inspection.

5.1.8 Nozzle-to-Case Joint

There was no evidence of hot gas or soot past the polysulfide. The grease application was per specification. There was no corrosion found on either the fixed housing or the aft dome. No polysulfide extruded past the wiper O-ring. Ten radial bolt hole disassembly plugs were damaged during the disassembly process.

There were no signs of O-ring damage at the time of disassembly on the primary, secondary, or wiper O-rings. Detailed inspection of the O-rings found no damage to the primary or secondary O-rings. The wiper has a radial gouge at 158 degrees that is 0.080 inch long by 0.025 inch wide by 0.010 inch deep. Inspection of the Stat-O-Seals found three that had open flow lines, the longest being 0.4 inch long. Fifteen stat-o-seals were found with closed flow lines, two that had excessive grinding on the I.D. of the seal, and one that had a blister on the I.D. of the seal.

5.1.9 Aft Exit Cone Joint (Joint 1)

This joint suffered extensive damage caused by splashdown. All the phenolic on the aft exit cone was gone, as was all but 3 inches of the primary O-ring, which was stuck between the glass phenolic and the metal housing of the forward exit cone at 306 degrees. The secondary O-ring also was cut and the portion of the O-ring between 71 and 197 degrees was missing. From the remaining RTV on the aft end on the forward exit cone it was determined that no pressure paths were formed through the RTV, so no pressure or soot reached the primary O-ring. Medium corrosion was found on the aft face of the forward exit cone flange from 71 to 197 degrees. It appears that because the secondary O-ring was missing at this location, sea water flowing through the joint caused degradation of the grease which allowed the D6AC to rust. The aft exit cone shell sustained two radial stamp marks that originate at the 146 and 157 degree bolt holes and progress inward into the O.D. wall of the secondary O-ring groove. The stamp mark came from damaged heli-coils at those bolt holes.

5.1.10 Forward End Ring-To-Nose Inlet Housing (Joint 2)

Inspection of the joint did not revealed any obvious pressure paths through the RTV/adhesive of the joint interface. Soot was found in the high pressure side of the primary O-ring groove from 342 degrees to 27 degrees. Scalloped shaped sooting of the grease was found about half way between the edge of the aluminum housing and the primary O-ring groove situated between

bolt holes. No soot or evidence of blow-by was present past the primary O-ring. No apparent damage to the primary or secondary O-rings was found during preliminary inspection, and the sealing surfaces suffered no assembly or disassembly damage.

Detailed inspection of the primary and secondary O-rings discovered no damage to either O-ring. Also, inspection of the sealing surface revealed no signs of heat-effect, corrosion, or disassembly damage.

5.1.11 Nose Inlet Housing-To-Throat Support Housing (Joint 3)

Detailed inspection revealed no pressure reached the primary O-ring and no anomalies to the joint. Inspection of the primary and secondary O-rings showed no damage. Inspection of the sealing surface found no disassembly damage, heat effect or appreciable corrosion.

5.1.12 Forward Exit Cone-To-Throat Support Housing (Joint 4)

Pressure did not reach the primary O-ring, and inspection of the joint interface revealed no anomalous conditions. Inspection of the sealing surfaces showed no signs of damage. The leak test port had heavy corrosion in the bottom, no corrosion was on the sealing surfaces of the port plug O-ring. Detailed inspection of the O-rings found no damage. Inspection of the sealing surface found no disassembly damage, heat effect or appreciable corrosion.

5.1.13 Fixed Housing-To-Aft End Ring (Joint 5)

This joint showed no signs of pressure past the RTV; i.e., no heat-effected grease, soot, or RTV voids. RTV completely filled the gaps between the inner boot ring and the aft end of the bearing protector. Inspection of the sealing surface revealed no signs of damage. Detailed inspection of the 0-rings found no damage on the primary 0-ring, and a 0.065 inch long by 0.010 inch wide by 0.005 inch deep nick on the secondary 0-ring that was caused during disassembly operations.

Inspection of all Stat-0-Seals showed extensive damage of the fluorocarbon portion of the seal from disassembly operations, which is expected.

5.1.14 Factory Joints

The center forward cylinder-to-cylinder factory joint was not inspected for the reasons stated in section 2.2.

5.1.14.1 Forward Dome-to-Cylinder Factory Joint. The outer clevis leg had intermittent areas of light corrosion around the joint. Insulation and Chemlok were found on the land forward of the primary 0-ring groove intermittently throughout the circumference of the joint.

Inspection of the port plug and port threads found no damage. Inspection of the 0-rings found no damage on the primary or secondary 0-rings.

5.1.14.2 Forward Cylinder-to-Cylinder Factory Joint. The clevis and tang exhibited ten areas where pitting occurred. This pitting is believed to be fretting marks, reference 8 examines these fretting marks in depth. Insulation and Chemlok were on the land forward of the primary O-ring groove intermittently throughout the circumference of the joint.

The port plug and port threads were not damaged, but they had no grease on them. Inspection of the O-rings found no damage to the primary or secondary O-rings.

5.1.14.3 Center Forward Cylinder-to-Cylinder Factory Joint. Omitted.

5.1.14.4 Center Aft Cylinder-to-Cylinder Factory Joint. The outer clevis leg outside diameter, the end of the outer clevis leg, the inside diameter of the outer clevis leg, and the outside diameter of the inner clevis leg all had medium to heavy corrosion with black areas on top of the heavy corrosion areas intermittently around the circumference of the joint. The inside and outside of the tang also had medium to heavy corrosion intermittently around the circumference of the joint. The tang had two areas where the corrosion was heaviest. These areas were zero to 104 and 310 to 328 degrees. The joint area had minute quantities of debris inside the area between the outer clevis inside diameter and the secondary O-ring. This area probably was introduced to moisture because of the joint protection system leakage. Chemlok and insulation were found up to the primary O-ring groove intermittently around the circumference of the

clevis.

The leak check port had nominal grease application on the threads, but the conical portion was unlubricated. Inspection of the primary and secondary O-rings found no damage to the primary O-ring, the secondary O-ring suffered a nick 0.040 inch long by 0.020 inch wide by 0.005 inch deep during disassembly of the joint.

5.1.14.5 ET-to-Stiffener Factory Joint. The outer clevis leg and the tang outside diameter had light to medium corrosion intermittently around the circumference of the joint. Insulation and Chemlok were on the land forward of the primary O-ring groove intermittently throughout the circumference of the joint.

Initial inspection of the port plug hole showed no damage. Inspection of the primary and secondary O-rings found no damage to either O-ring.

5.1.14.6 Stiffener-to-Stiffener Factory Joint. Spotty areas of light to medium corrosion were found on the outer clevis leg. A small area of medium corrosion was found at zero degrees on the inside of the clevis. The tang outside diameter had light to medium corrosion intermittently around the entire circumference of the joint. Insulation and Chemlok were on the land forward of the primary O-ring groove intermittently throughout the circumference of the joint.

Initial inspection of the port plug hole showed no damage. Inspection of the primary and secondary O-rings found no damage to either O-ring.

5.1.14.7 Aft Dome-to-Stiffener Factory Joint. The outside of the outer clevis leg had light to medium corrosion intermittently around the circumference of the joint. No corrosion was observed in any other areas of the joint. Insulation and Chemlok were on the land forward of the primary O-ring groove intermittently throughout the circumference of the joint. Scratches were found on the outside diameter of the tang from 204 to 214 degrees.

Initial inspection of the port plug hole showed no damage. Inspection of the primary and secondary O-rings found no damage to either O-ring.

5.2 Right Motor Disassembly Evaluation

5.2.1 External Walk Around

The external walk around inspection revealed no signs of hot gas leakage past any of the joints.

5.2.2 Safe and Arm Joint (Adapter-to-Barrier Booster)

There was no soot up to the primary seal on the S&A gasket. There was no corrosion or damage found to the joint or gasket seals at the time of disassembly.

5.2.3 Outer Igniter Joint (Adapter-to-Forward Dome)

There was no evidence of hot gas leakage past the primary seal and no seal damage observed on the gasket. A putty blow hole was observed at 220 degrees. Soot was found on the outer diameter of the igniter chamber next to the igniter boss from 140 degrees to 280 degrees. Soot was found intermittently on the forward face of the gasket from zero to 280 degrees. On the aft face of the gasket, there was soot from 18 to 360 degrees, and no soot reached the primary seal. Intermittent corrosion was found on the inside edge of the forward dome boss. No gasket seal damage was observed.

5.2.4 Inner Igniter Joint (Adapter-to-Chamber)

No blow holes were found in the putty, therefore no soot reached the inner primary seal. There was some light soot on the outboard edge of the retainer at 220 degrees from the blow hole on the outer joint. All stat-o-seals from the inner joint bolts were damaged during disassembly. No gasket seal damage was observed at the time of disassembly.

There was corrosion on the tip of the transducer bolt at 100 degrees. All other bolts only had soot on the bottom end of the bolt.

5.2.5 Forward Field Joint

There was no sign of hot gas or soot past the J-leg. The grease coverage was per design and no corrosion was found on any of the sealing surfaces.

Intermittent pin hole corrosion was found on the tang and clevis. The O.D. of the outer clevis leg showed moderate to light surface corrosion from zero to 360 degrees. The joint was slightly contaminated with debris from hydrolaze operations which remove the joint protection system.

No seal damage was observed at the time of disassembly and the V2 filler was properly installed with no visible damage. Detailed inspection of the O-rings revealed no damage.

5.2.6 Center Field Joint

There was no sign of hot gas or soot past the J-leg. The grease coverage was per design and no corrosion was found on any of the sealing surfaces. Intermittent pin hole corrosion was found on the tang and clevis. The O.D. of the outer clevis leg showed moderate to light surface corrosion from zero to 360 degrees. The joint was slightly contaminated with debris from hydrolaze operations which remove the joint protection system.

No seal damage was observed at the time of disassembly and the V2 filler was properly installed with no visible damage. Detailed inspection of the O-rings revealed no damage.

5.2.7 Aft Field Joint

There was no sign of hot gas or soot past the J-leg. The grease coverage

was per design and no corrosion was found on any sealing surfaces. Intermittent shim area corrosion was found on the clevis and the O.D. of the outer clevis leg showed moderate to heavy corrosion from zero to 360 degrees. The tang showed intermittent pin hole corrosion and corrosion of the shim areas around 232, 226, 220, and 212 to 208 degrees. The joint was heavily contaminated with debris and water from hydrolase operations which remove the joint protection system.

No seal damage was observed at the time of disassembly and the V2 filler was properly installed with no visible damage. Inspection of the O-rings revealed no damage to the three O-rings.

5.2.8 Nozzle-to-Case Joint

There was no evidence of hot gas or soot past the polysulfide. The grease application was per specification. There was no corrosion found on either the fixed housing or the aft dome. No polysulfide extruded past the wiper O-ring except at the 122 degree vent slot, and the polysulfide did not reach the primary O-ring groove at this location. Thirteen radial bolt hole disassembly plugs suffered damage between 304 and 9 degrees.

There were no signs of O-ring damage at the time of disassembly on the primary or secondary O-rings. However, inspection of the wiper O-ring on disassembly revealed a scalloped shaped gouge (see Figure 11) at 334 degrees with dimensions of 0.250 inch in length by 0.180 inch in radial

width by 0.040 inch deep. The gouge was caused by the radial bolt hole plug at 333 degrees during the disassembly of the nozzle-to-case. Detailed inspection found no damage to the primary O-ring, the secondary had a small nick at 186 degrees. Inspection of the Stat-O-Seals found one that had 0.350 inch long open flow line, fifteen with closed flow lines, and two that had excessive grinding on the I.D. of the seal.

5.2.9 Aft Exit Cone Joint (Joint 1)

No pressure paths were found through the RTV, so no pressure or soot reached the primary O-ring. Intermittent corrosion was found at the polysulfide groove to aluminum housing interface on the aft exit cone.

No damage to the primary or secondary O-rings were observed at the time of disassembly except that the primary O-ring fell out of the groove during disassembly. Inspection of the O-rings conducted by the inspection team at A2 revealed that both the primary and secondary O-rings sustained no damage.

5.2.10 Forward End Ring-To-Nose Inlet Housing (Joint 2)

Inspection of the joint did not revealed any obvious pressure paths through the RTV/adhesive of the joint interface. Soot was found in the high pressure side of the primary O-ring groove from 272 degrees to 273 degrees. Scalloped shaped sooting of the grease was found about half way between the

edge of the aluminum housing and the primary O-ring groove situated between bolt holes, with the heaviest sooting occurring between 36 to 78 degrees and 270 to 342 degrees. No soot or evidence of blow-by was present past the primary O-ring. No apparent damage to the primary or secondary O-rings was found on in the groove inspection, and the sealing surfaces suffered no assembly or disassembly damage.

Detailed inspection of the primary and secondary O-rings discovered no damage to either O-ring. Inspection of the sealing surface revealed no signs of heat-effect, rust, or disassembly damage.

5.2.11 Nose Inlet Housing-To-Throat Support Housing (Joint 3)

Detailed inspection revealed no pressure reached the primary O-ring and no anomalies to the joint were found. No apparent damage was found during preliminary inspection of the primary or secondary O-rings. Inspection of the sealing surfaces revealed no signs of damage. Detailed inspection of both O-rings revealed no signs of damage.

5.2.12 Forward Exit Cone-To-Throat Support Housing (Joint 4)

Inspection of the joint revealed two pressure paths through the RTV backfill at 185 and 330 degrees. No apparent damage to the primary or secondary O-rings was found during preliminary inspection, and the sealing surfaces suffered no assembly/disassembly damage.

Inspection of the sealing surfaces showed no signs of damage. Detailed inspection of the O-rings showed no damage.

5.2.13 Housing-To-Aft End Ring (Joint 5)

This joint showed no signs of pressure past the RTV; i.e., no heat-effected grease, soot, or RTV voids. RTV completely filled the gaps between the inner boot ring and the aft end of the bearing protector. Detailed inspection of the O-rings found no damage. Inspection of the sealing surfaces revealed no apparent damage.

Inspection of all Stat-O-Seals showed damage of the fluorocarbon portion of the seal from disassembly operations, which is expected.

5.2.14 Factory Joints

All of the right hand motor factory joints except for the aft segment factory joints were not inspected for the reasons stated in section 2.2.

5.2.14.1 Forward Dome-to-Cylinder Factory Joint. Omitted.

5.2.14.2 Forward Cylinder-to-Cylinder Factory Joint. Omitted.

5.2.14.3 Center Forward Cylinder-to-Cylinder Factory Joint. Omitted.

5.2.14.4 Center Aft Cylinder-to-Cylinder Factory Joint. Omitted.

5.2.14.5 ET-to-Stiffener Factory Joint. No corrosion was observed on the outer clevis leg or in the joint areas. Scratches were observed on the land between the O-ring grooves at 74, 86, 90, 130, 170, 178, 180, and 266 degrees. Scratches were also observed on the land forward of the primary groove at 74, 86, 90, 130, 162, and 170 degrees and downstream of the secondary groove at 170 degrees. Pitting and raised metal was observed on the tang downstream of the sealing surface at 168 and 170 degrees. Insulation and Chemlok were on the land forward of the primary O-ring groove intermittently throughout the circumference of the joint.

Initial inspection of the port plug O-ring, threads, and port hole showed no damage. Inspection of the primary and secondary O-rings showed no damage.

5.2.14.6 Stiffener-to-Stiffener Factory Joint. Intermittent areas of light to heavy corrosion was observed on the outer clevis leg. No corrosion was observed in the internal joint areas. Scratches were observed on the land between the O-ring grooves at 122, 130, 132, 136, 138, 142, 146, 150, 152, 156, 158, 160, 162, 164, 166, 168, 170, and 182 degrees. Scratches were also observed on the land forward of the primary groove at 261 degrees. Insulation and Chemlok were on the land forward of the primary O-ring groove intermittently throughout the circumference of the joint.

Initial inspection of the port plug O-ring, threads, and port hole found no damage. Inspection of the primary and secondary O-rings found no damage.

5.2.14.7 Aft Dome-to-Stiffener Factory Joint. Intermittent areas of light to heavy corrosion were observed on the outer clevis leg. No corrosion was observed in the internal joint areas. Scratches were observed on the land between the O-ring grooves at 206 degrees. Insulation and Chemlok were on the land forward of the primary O-ring groove intermittently throughout the circumference of the joint.

Initial inspection of the port plug and port threads found no damage except that no grease was on them, including the conical transition area of the port. Inspection of the primary and secondary O-rings found no damage to either O-ring.

5.3 Leak Check and Vent Port Plug Post Flight Evaluations

The evaluation of the port plugs after flight use consisted of adding to the port plug torque database, visual inspection of the port plug for damage, and visual inspection of the port plug O-rings for anomalies.

Prior to removal, all port plugs had breakaway torques recorded. This exercise was done to add to the port plug torque database so evaluation of installation torque levels and locking devices can be made on each type of port plug.

A summary of the post flight inspection evaluations of the port plugs and port plug O-rings is contained in table 25. Port plugs in the field joints and nozzle to case joints were removed during disassembly operations at KSC. Port plugs in the factory joints, internal nozzle joints and igniter were removed at Clearfield. Factory joint inspections were waived in third flight and this carried over in the port plug inspections so most port plugs were not available for inspection. The initial inspection of the port plugs occurred at the time of removal. Closure plugs were removed from the custom vent port plugs by the MTI O-ring Inspection Team. All port plugs and O-rings were then inspected by the MTI O-ring Inspection Team as a final inspection.

Table 25
LEAK CHECK AND VENT PORT
PLUG POST FIRE INSPECTION RESULTS

JOINT LOCATION	PART INSPECTED	RIGHT HAND (3B)		LEFT HAND (3A)	
		INITIAL INSPECTION	FINAL INSPECTION	INITIAL INSPECTION	FINAL INSPECTION
Forward Field	Custom Vent Port Plug	No Damage	No Damage	No Damage	No Damage
	Primary O-ring	No Damage	I.D. Impression O.D. Circum. Cut	No Damage	I.D. Impression O.D. Circum. Cut
	Secondary O-ring	No Damage	No Damage	No Damage	No Damage
	Closure Plug	N/A	No Damage	N/A	No Damage
	O-ring	N/A	No Damage	N/A	No Damage
Center Field	Leak Check Plug	No Damage	No Damage	No Damage	No Damage
	O-ring	No Damage	Sep. Flow Lines (.090X.020)	No Damage	I.D. Cut (.60X.020)
	Custom Vent Port Plug	No Damage	No Damage	No Damage	No Damage
	Primary O-ring	No Damage	I.D. Impression O.D. Circum. Cut	No Damage	I.D. Impression O.D. Circum. Cut
	Secondary O-ring	No Damage	No Damage	No Damage	No Damage

Table 25 (Continued)
LEAK CHECK AND VENT PORT
PLUG POST FIRE INSPECTION RESULTS

JOINT LOCATION	PART INSPECTED	RIGHT HAND (3B)		LEFT HAND (3A)	
		INITIAL INSPECTION	FINAL INSPECTION	INITIAL INSPECTION	FINAL INSPECTION
	Closure Plug	N/A	No Damage	N/A	No Damage
	O-ring	N/A	No Damage	N/A	No Damage
	Leak Check Plug	No Damage	No Damage	No Damage	No Damage
	O-ring	No Damage	No Damage	No Damage	I.D. Cut (.45X.015)
Aft Field	Custom Vent Port Plug	No Damage	No Damage	No Damage	No Damage
	Primary O-ring	No Damage	No Damage	No Damage	I.D. Impression O.D. Circum. Cut
	Secondary O-ring	O.D. Extrusion Impression	O.D. & I.D. Extrusion Damage	No Damage	No Damage
	Closure Plug	N/A	No Damage	N/A	No Damage
	O-ring	N/A	No Damage	N/A	No Damage
	Leak Check Plug	No Damage	No Damage	Slight Corrosion on Spot Face	No Damage

Table 25 (Continued)
LEAK CHECK AND VENT PORT
PLUG POST FIRE INSPECTION RESULTS

JOINT LOCATION	PART INSPECTED	RIGHT HAND (3B)		LEFT HAND (3A)	
		INITIAL INSPECTION	FINAL INSPECTION	INITIAL INSPECTION	FINAL INSPECTION
Nozzle to Case	O-ring	No Damage	No Damage	No Damage	I.D. Cut (.38X.010)
	Custom Vent Port Plug	No Damage	No Damage	No Damage	No Damage
	Primary O-ring	No Damage	O.D. & I.D. Extrusion Damage	No Damage	I.D. Impression O.D. Circum. Cut
	Secondary O-ring	No Damage	No Damage	No Damage	I.D. Cut (.30X.020)
	Closure Plug	N/A	No Damage	N/A	No Damage
	O-ring	N/A	No Damage	N/A	No Damage
	Leak Check Plug	No Damage	No Damage	No Damage	No Damage
	O-ring	No Damage	No Damage	No Damage	No Damage

Table 25 (Continued)
LEAK CHECK AND VENT PORT
PLUG POST FIRE INSPECTION RESULTS

JOINT LOCATION	PART INSPECTED	RIGHT HAND (3B)		LEFT HAND (3A)	
		INITIAL INSPECTION	FINAL INSPECTION	INITIAL INSPECTION	FINAL INSPECTION
Internal Nozzle Joints					
No.1	Leak Check Plug	No Damage	No Damage	No Damage	No Damage
	O-ring	No Damage	No Damage	No Damage	No Damage
No.2	Leak Check Plug	No Damage	No Damage	No Damage	No Damage
	O-ring	No Damage	No Damage	No Damage	No Damage
No.3	Leak Check Plug	No Damage	No Damage	No Damage	No Damage
	O-ring	No Damage	No Damage	No Damage	No Damage
No.4	Leak Check Plug	No Damage	No Damage	Rust in Port Bottom	No Damage
	O-ring	No Damage	No Damage	No Damage	No Damage
No.5	Leak Check Plug	No Damage	No Damage	No Damage	No Damage
	O-ring	No Damage	No Damage	No Damage	No Damage
				No Damage	I.D. Scratch (.15X.001)

Table 25 (Continued)
LEAK CHECK AND VENT PORT
PLUG POST FIRE INSPECTION RESULTS

JOINT LOCATION	PART INSPECTED	RIGHT HAND (3B)		LEFT HAND (3A)	
		INITIAL INSPECTION	FINAL INSPECTION	INITIAL INSPECTION	FINAL INSPECTION
Factory Joints					
Forward Dome	Leak Check Plug	N/A	N/A	N/A	No Damage
	O-ring	N/A	N/A	N/A	I.D. Cut (.70X.001) Plug Head Gouged No Grease
Forward Segment	Leak Check Plug	N/A	N/A	N/A	I.D. Cut (.40X.015) N/A
	O-ring	N/A	N/A	N/A	N/A
Forward Center Segment	Leak Check Plug	N/A	N/A	N/A	N/A
	O-ring	N/A	N/A	N/A	N/A
Aft Center Segment	Leak Check Plug	N/A	N/A	No Damage	No Damage
	O-ring	N/A	N/A	No Damage	No Damage
Attach to Stiffener	Leak Check Plug	Plug Head Gouged	Plug Head Gouged No Grease	N/A	N/A
	O-ring	No Damage	No Damage	N/A	N/A

Table 25 (Continued)
LEAK CHECK AND VENT PORT
PLUG POST FIRE INSPECTION RESULTS

JOINT LOCATION	PART INSPECTED	RIGHT HAND (3B)		LEFT HAND (3A)	
		INITIAL INSPECTION	FINAL INSPECTION	INITIAL INSPECTION	FINAL INSPECTION
Stiffener to Leak Check Stiffener	Plug	Plug Head Gouged	Plug Head Gouged	N/A	N/A
	O-ring	No Damage	No Damage	N/A	N/A
Aft Dome	Leak Check Plug	Plug Head Gouged	Plug Head Gouged No Grease	N/A	N/A
	O-ring	No Damage	I.D. Cut (.78X.030)	N/A	N/A
Igniter					
Adapter to Case	Leak Check Plug	N/A	N/A	N/A	No Damage
	O-ring	N/A	N/A	N/A	I.D. Cuts (1.30X.050) No Damage
Adapter to Leak Check Chamber	Leak Check Plug	N/A	N/A	N/A	No Damage
	O-ring	N/A	N/A	N/A	No Damage
Safe and Arm 126 deg	Leak Check Plug	No Damage	No Damage	No Damage	Radial Scratch on Seal Surface
	O-ring	No Damage	No Damage	No Damage	No Damage

Table 25 (Continued)
LEAK CHECK AND VENT PORT
PLUG POST FIRE INSPECTION RESULTS

JOINT LOCATION	PART INSPECTED	RIGHT HAND (3B)		LEFT HAND (3A)	
		INITIAL INSPECTION	FINAL INSPECTION	INITIAL INSPECTION	FINAL INSPECTION
306 deg	Leak Check Plug	No Damage	Radial Scratch on Seal Surface	No Damage	No Damage
	O-ring	No Damage	I.D. Scratch (.070X.002)	No Damage	No Damage

N/A- Not Available

During the initial inspection at KSC several observations were reported. The most recurrent observation was the extrusion crease to the O.D. and I.D. of the primary O-ring on the custom vent port plug. The extrusion damage was caused during installation of the port plug in to the port. This damage is an acceptable condition due to the design of the primary seal. The primary O-ring is used as a packing seal. When the vent port plug (custom or adjustable) is fully installed in the vent port, the primary O-ring extrudes out of the gland area and is damaged. The damage is inherent to the design. The secondary O-ring taken from the right hand aft field joint custom vent port plug had extrusion damage documented. This damage was caused from an under sized port which was previously documented. The port will be reworked prior to reuse of the cylinder. Light corrosion on a port spotface was noted at one port. The planning to install the port plugs has been updated on subsequent flights to include a more thorough application of grease preservative to the port area to prevent this type of corrosion.

Initial inspection of the port plugs removed at Clearfield found light corrosion on one internal nozzle joint spotface. Port plug head gouges were reported on three factory joint leak check port plugs. The gouges are caused by pneumatic chisels used to remove the weather seal. The gouges do not affect the use or removal of the port plug but the breakaway torque readings taken for evaluation are invalidated.

The final inspection of the port plugs and O-rings by the MTI O-ring

Inspection Team documented the I.D. cut/ scratch observation on the shoulder O-ring from ten port plugs. This observation consists of a cut that extends circumferentially around the I.D. of the O-ring. The length and depth of the cut varies. A sharp last thread on the port plug is the cause of the cut. The cut occurs as the port plug is removed from the port and the O-ring is rubbed along the thread. O-ring installation aids were used to install many of the discrepant O-rings on the port plugs to prevent this type of damage during installation. O-ring installation aids are being incorporated in the planning to be used with all small O-rings. Separated flowlines were documented on the shoulder seal O-ring removed from the right hand forward field joint leak check plug. These flowlines are a result of the O-ring manufacturing process. They are not acceptable conditions and corrective actions are being incorporated to keep this type of anomaly off the RSRM. Small radial scratches were observed on the barrier booster port plug seal surfaces. An investigation revealed the scratches were caused by sharp instrument used to remove the O-ring from the port plugs during assembly. The assembly process has been changed and increased inspection has been implemented to alleviate this problem.

5.4 Post-Fire Team Assessments

The Seals Component Post-Fire Assessment Team has reviewed all observations presented in this document and has determined that the following two observations were potential anomalies, classified as critical, major, minor or remains observation, as defined under Table 26 criteria.

5.4.1 Remains Observation

There were no anomalies that were classified as "remains observation".

5.4.2 Minor Anomalies

Two "potential anomalies" were classified as minor anomalies.

These minor anomalies are:

1. O.D. extrusion damage on secondary O-ring from right aft field joint custom vent port plug.
2. Radial scratches across the sealing surface of MS9902-01 leak test port plugs that are used in the barrier-booster and safe and arm devices.

5.4.3 Major Anomalies

There were no major anomalies.

5.4.4 Critical Anomalies

There were no critical anomalies.

5.5 RPRB Position

The RPRB has excepted all the recommendations as presented (see Appendix B).

Table 26
Criteria for Classifying "Potential Anomalies"

Remains Observation	Anomaly		
	Minor	Major	Critical
Requires no Specific Action	<p>Requires correc- tive action, but has no impact on:</p> <ul style="list-style-type: none"> - Motor Performance - Program Schedule <p>Does not reduce usability of part for its intended function</p> <p>Could cause damage preventing reuse of hardware in combination with other anomaly</p> <p>Significant depar- ture from the his- torical database</p>	<p>Could cause failure in combination w/ other anomaly</p> <p>Could cause damage preventing reuse of hardware</p> <p>Program acceptance of cause, correc- tive action, and risk assessment re- quired before sub- sequent static test or flight</p>	<p>Violates CEI Spec. requirements</p> <p>Could cause failure and possible loss of mission/life</p> <p>Mandatory resolution before subsequent static test/flight</p>
<p>Note: These criteria to be applied to the specific observed "potential anomaly" as it relates to the observed article and as it relates to subsequent articles.</p>			

6.0 REFERENCES

1. G. A. Ricks, TWR-17542, Vol. I, "Flight Motor Set 360L003 (STS-29R) Final Report", Thiokol Corporation, July 1989.
2. R. Ash, TWR-18759, Rev. A, "O-Ring Squeeze Calculations and Temperature Requirements 360L003", Morton Thiokol, Inc., January 1989.
3. C. D. Rice, TWR-18796, "Redesigned Solid Rocket Motor 360L003 Seal Leak Test Results", Morton Thiokol, Inc., December 1988.
4. V. B. Call, TWR-19197, "Structural Pre-Flight Predictions for 360L003 (STS-29) DFI Instrumentation", Morton Thiokol Inc., 02 February 1989.
5. A. S. Drendel, TWR-19092, "Predicted Ballistic Performance Characteristics for RSRM-3", Morton Thiokol, Inc., 05 January 1989.
6. Performance and Advanced Design, et. al., TWR-16475, Book 1, Volumes 1-9, "KSC Post-Flight Engineering Evaluation Plan", Morton Thiokol, Inc., 24 February 1989 (Vol. 4, Rev. B, Seals Component)
7. Performance and Advanced Design, et. al., TWR-16475, Book 2, Volumes. 1-9, "Clearfield Post-Flight Engineering Evaluation Plan", Morton Thiokol, Inc., 7 October 1988 (Vol. 4, Seals Component)
8. R. A. Mackley, TWR-17542, Rev. A, "Flight Set 360L003 (STS-29) Case Component Final Report", Thiokol Corproation.

APPENDIX A

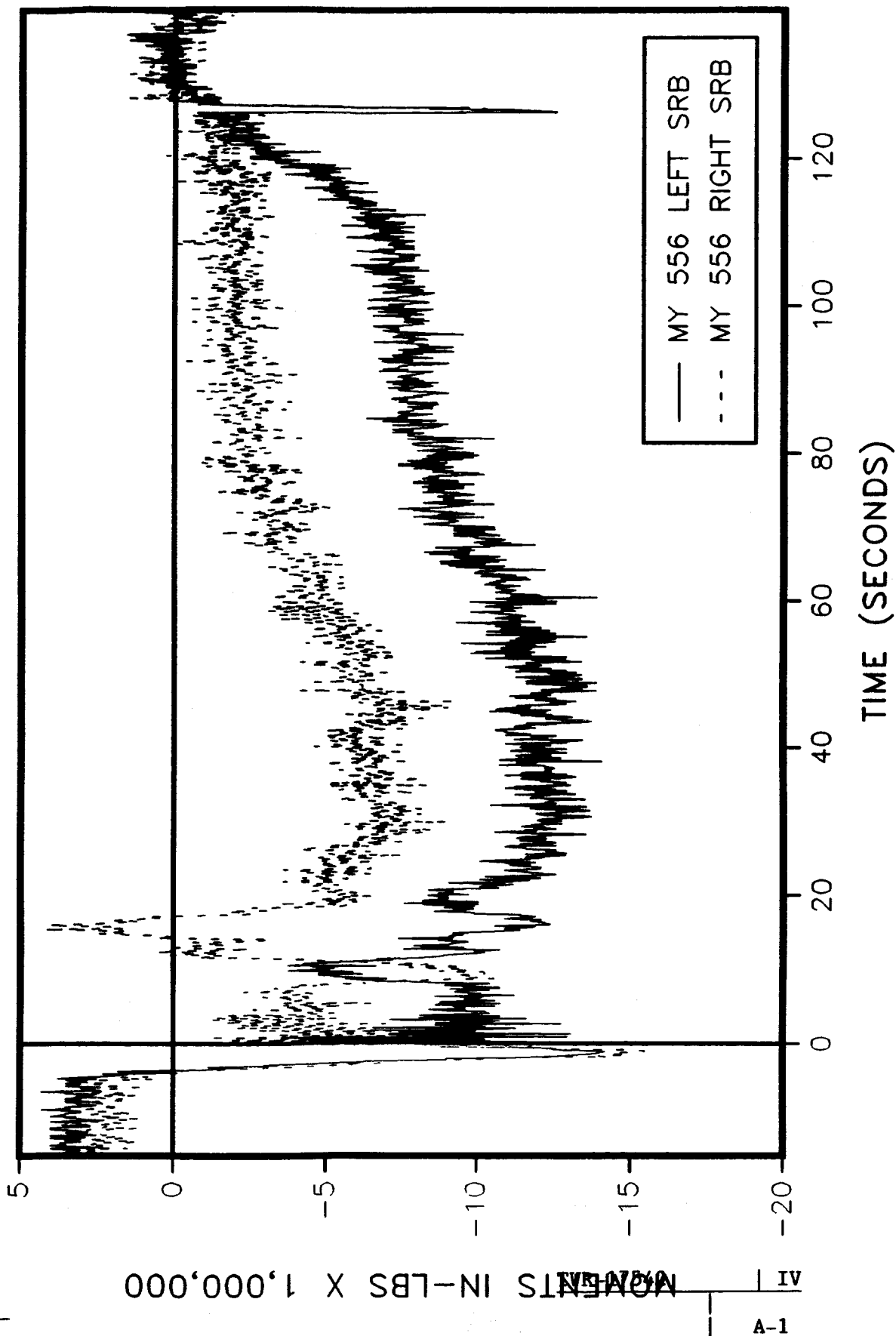
Developmental Flight Instrumentation Plots

REVISION A

DOC NO.	TWR-17541	VOL	IV
SEC	PAGE	A	

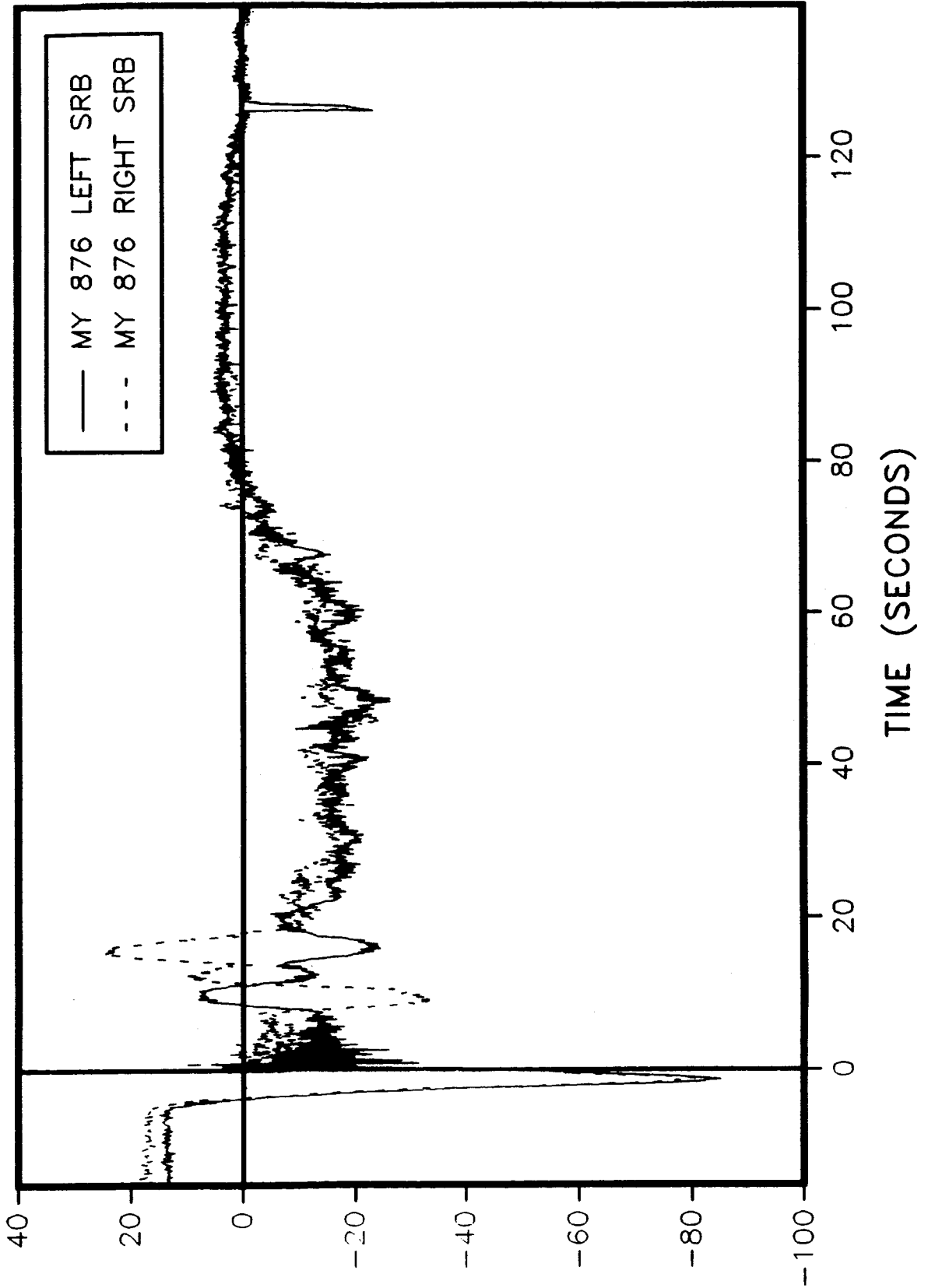
360L003 STATION 556

BENDING ABOUT THE Y AXIS



360L003 STATION 876

BENDING ABOUT THE Y AXIS

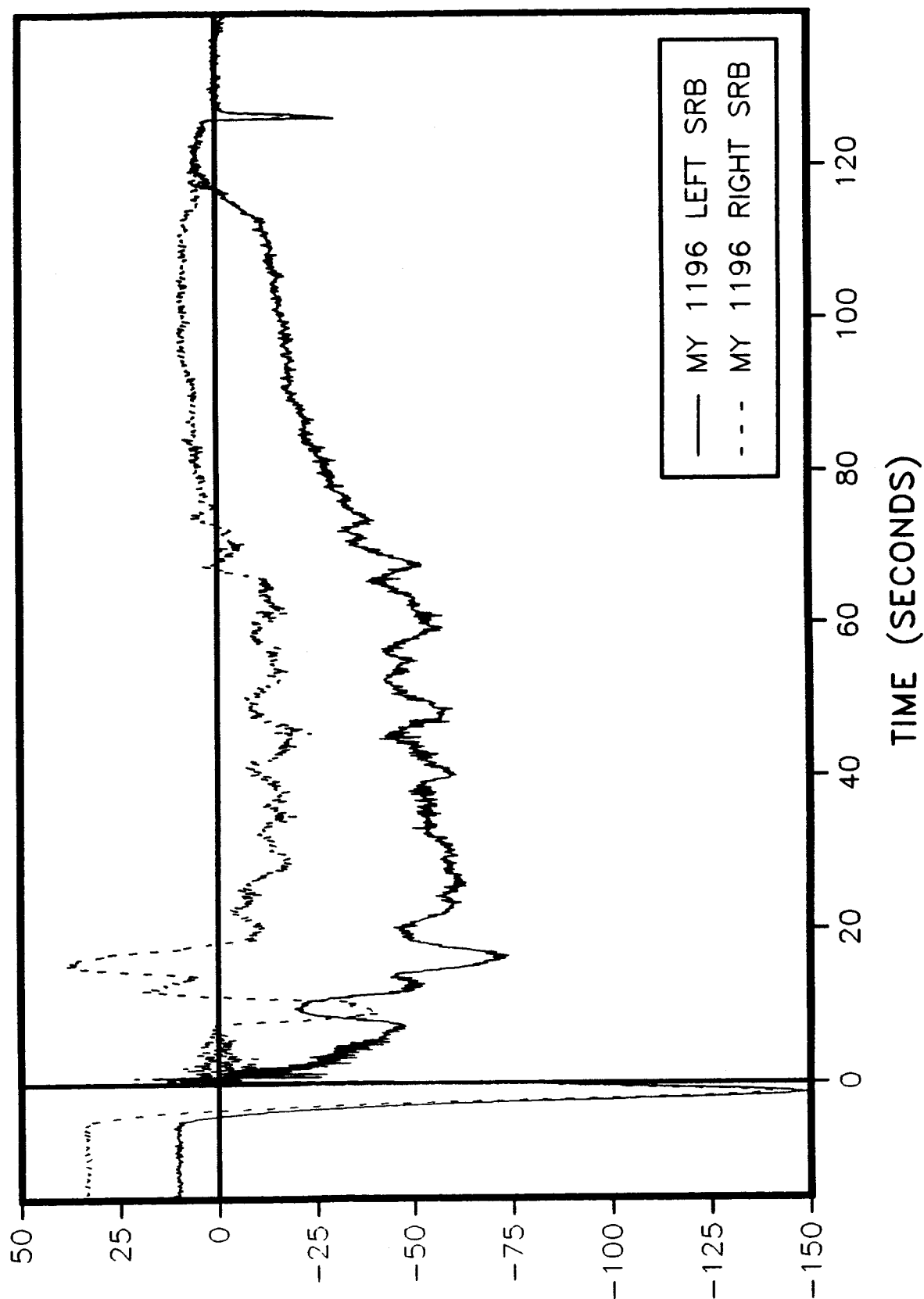


A-2 | TWR-17542 | IV
MOMENTS IN-LBS X 1,000,000

A

360L003 STATION 1196

BENDING ABOUT THE Y AXIS



A

MOMENTS IN-LBS X 1,000,000

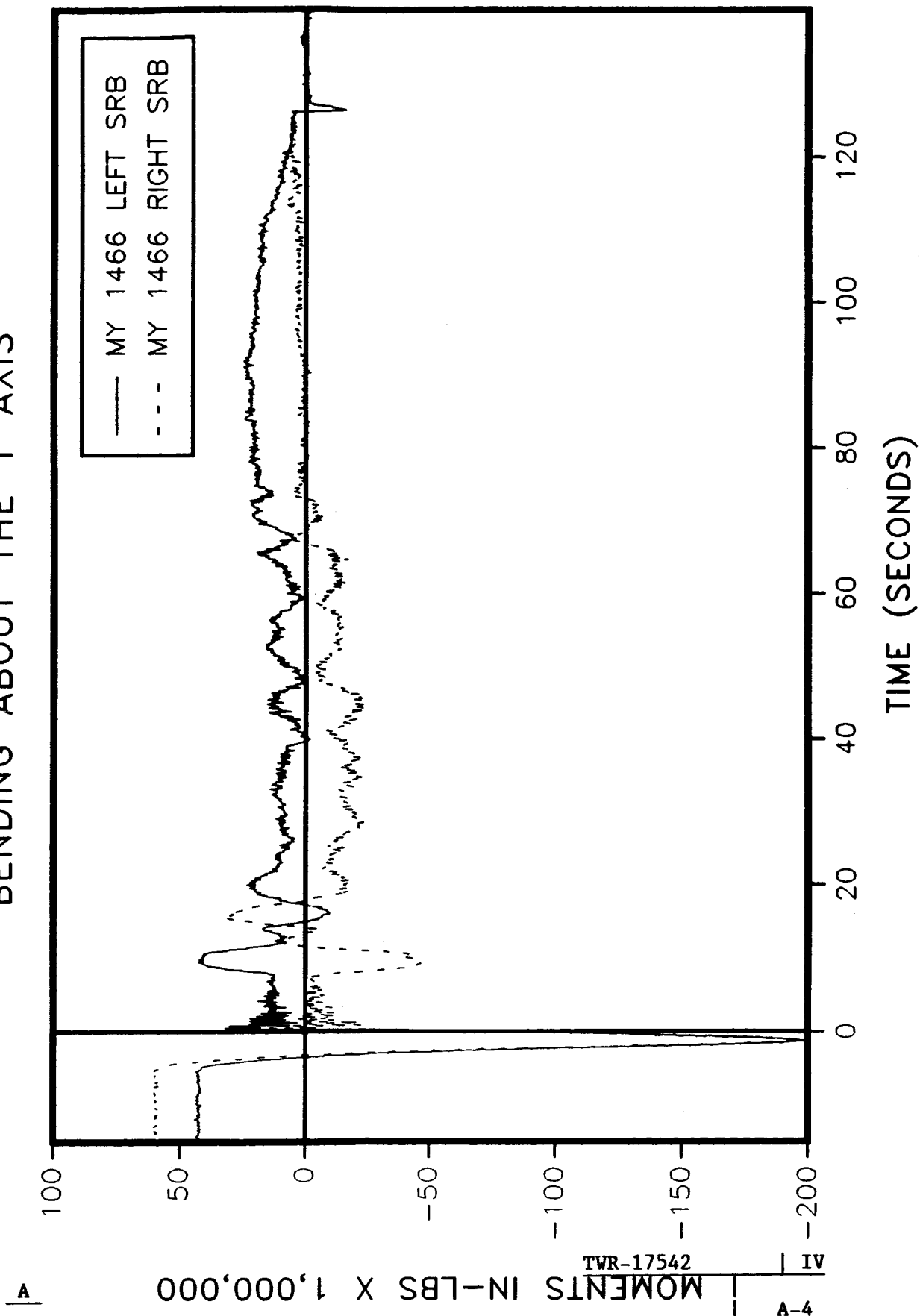
TWR-17542

A-3

IV

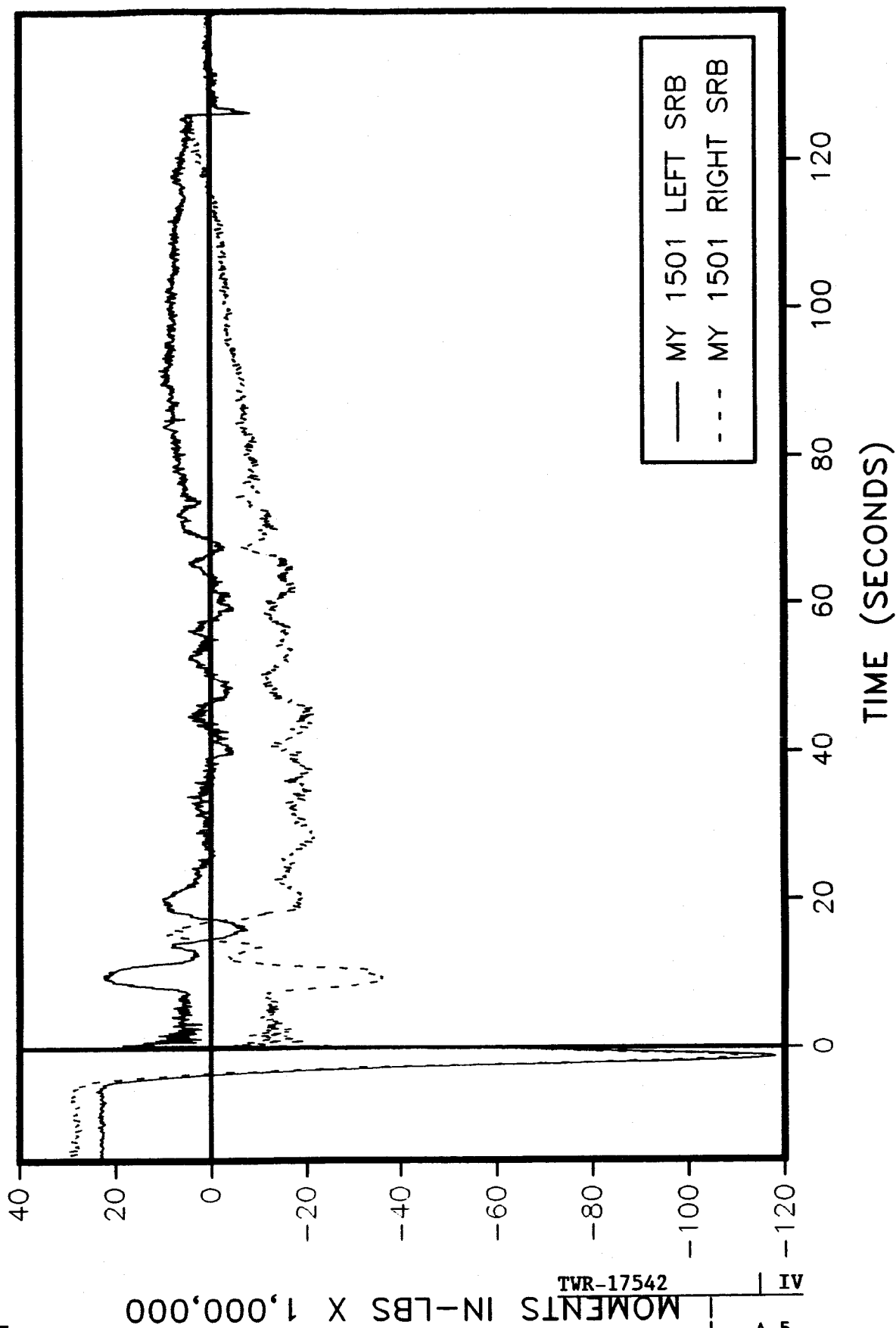
360L003 STATION 1466

BENDING ABOUT THE Y AXIS



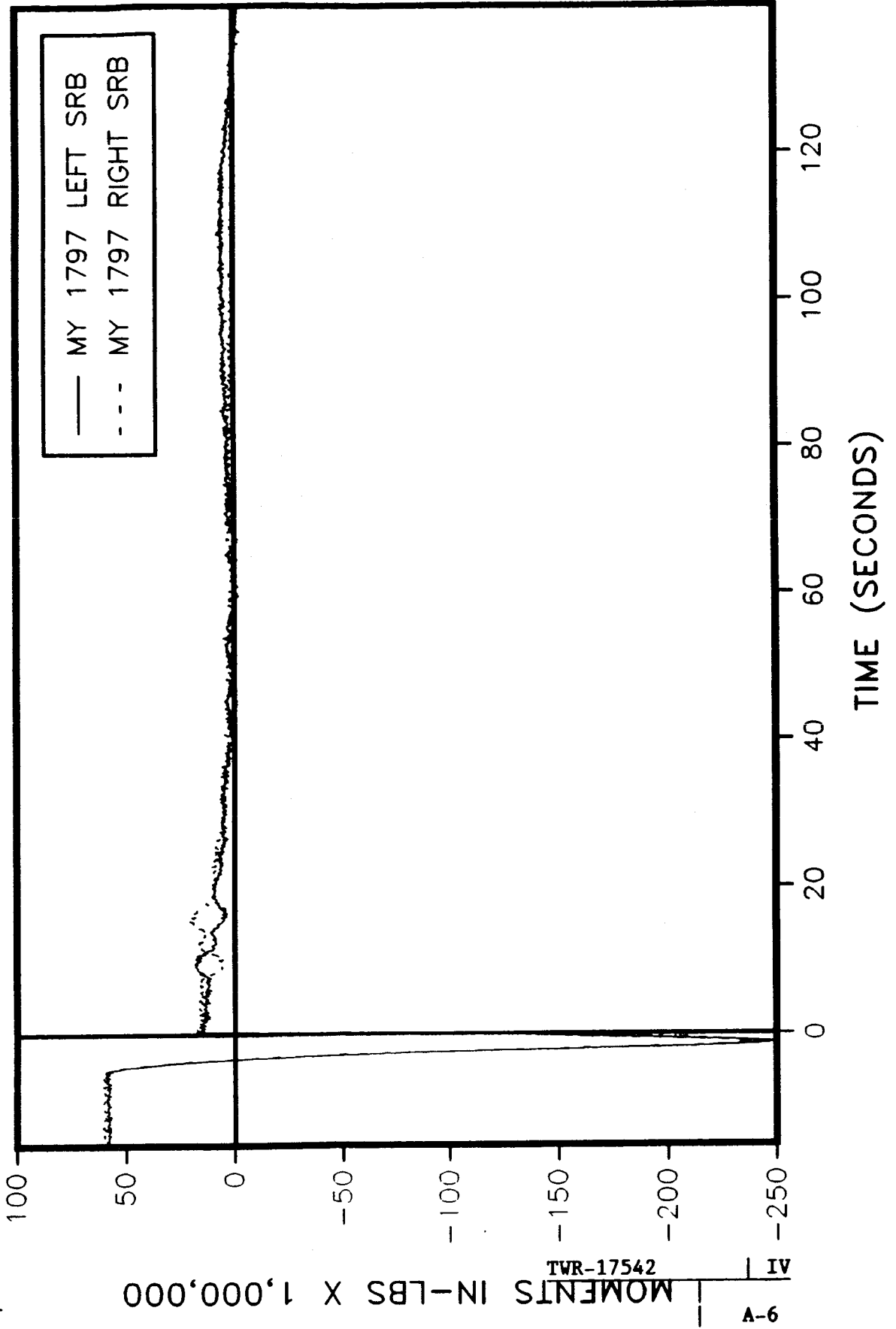
360L003 STATION 1501

BENDING ABOUT THE Y AXIS



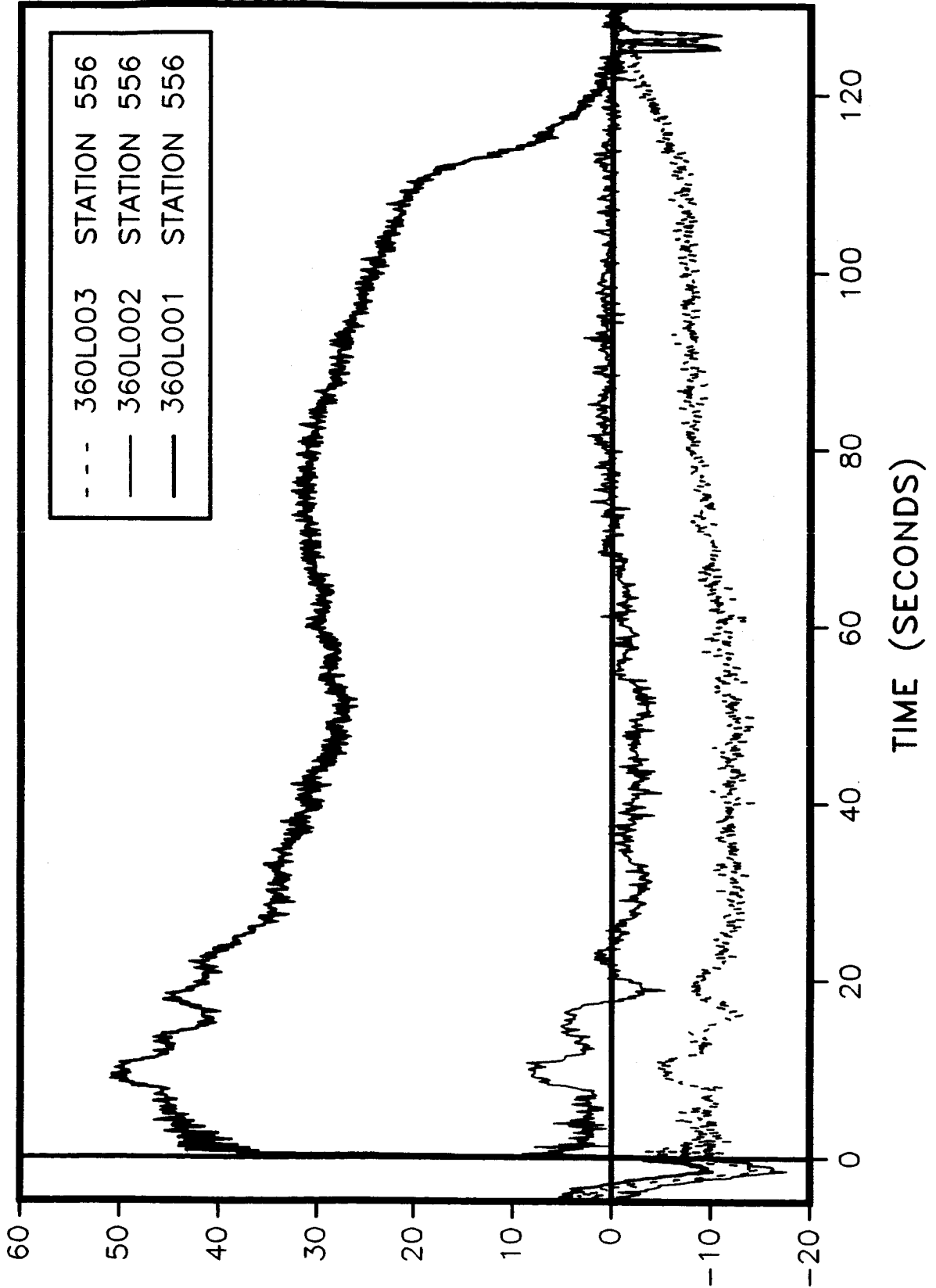
360L003 STATION 1797

BENDING ABOUT THE Y AXIS



360L003 VS PREVIOUS FLIGHTS

BENDING ABOUT THE Y AXIS LEFT SRB



MOMENTS IN-LBS X 1,000,000

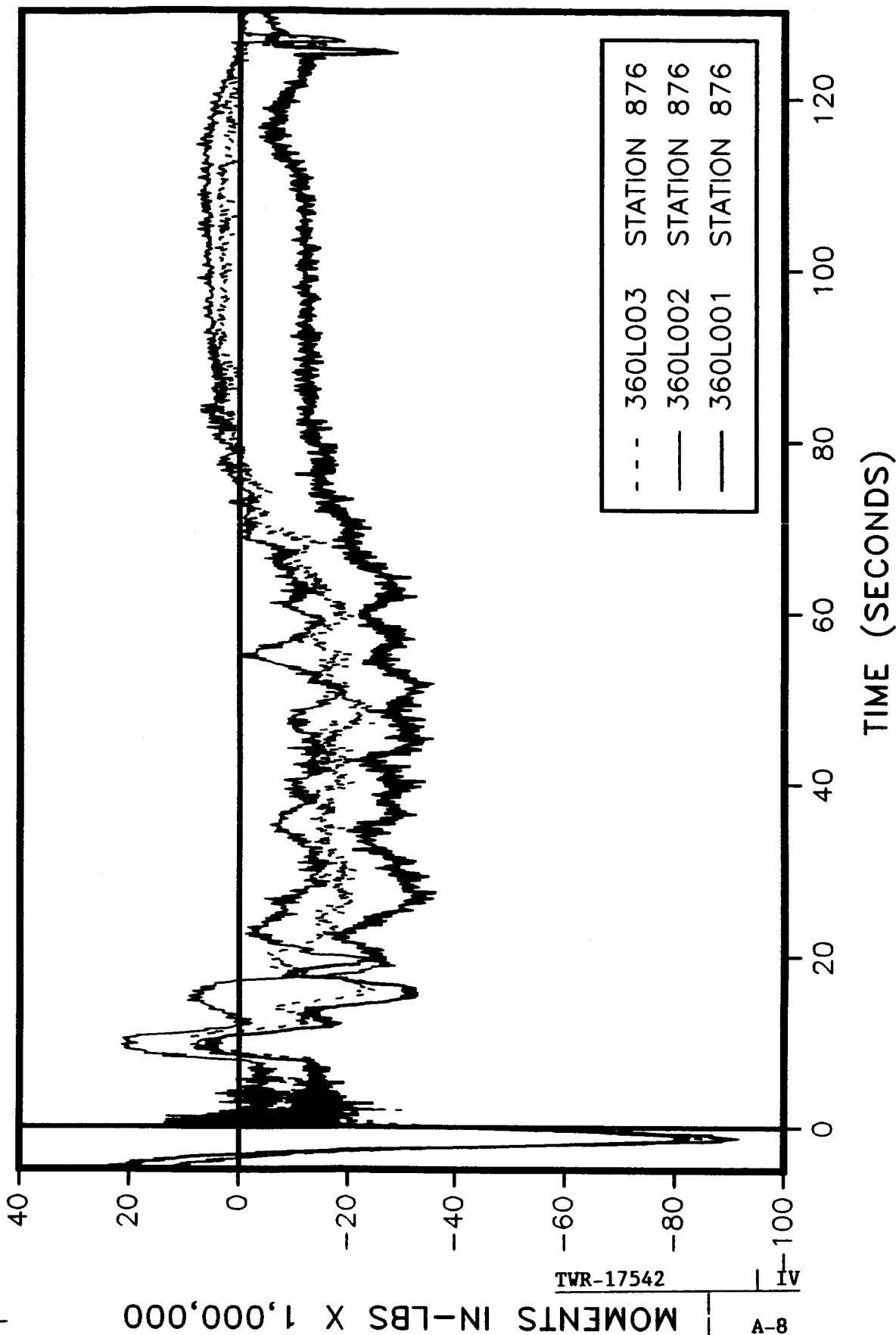
TVR-17542

A-7

A

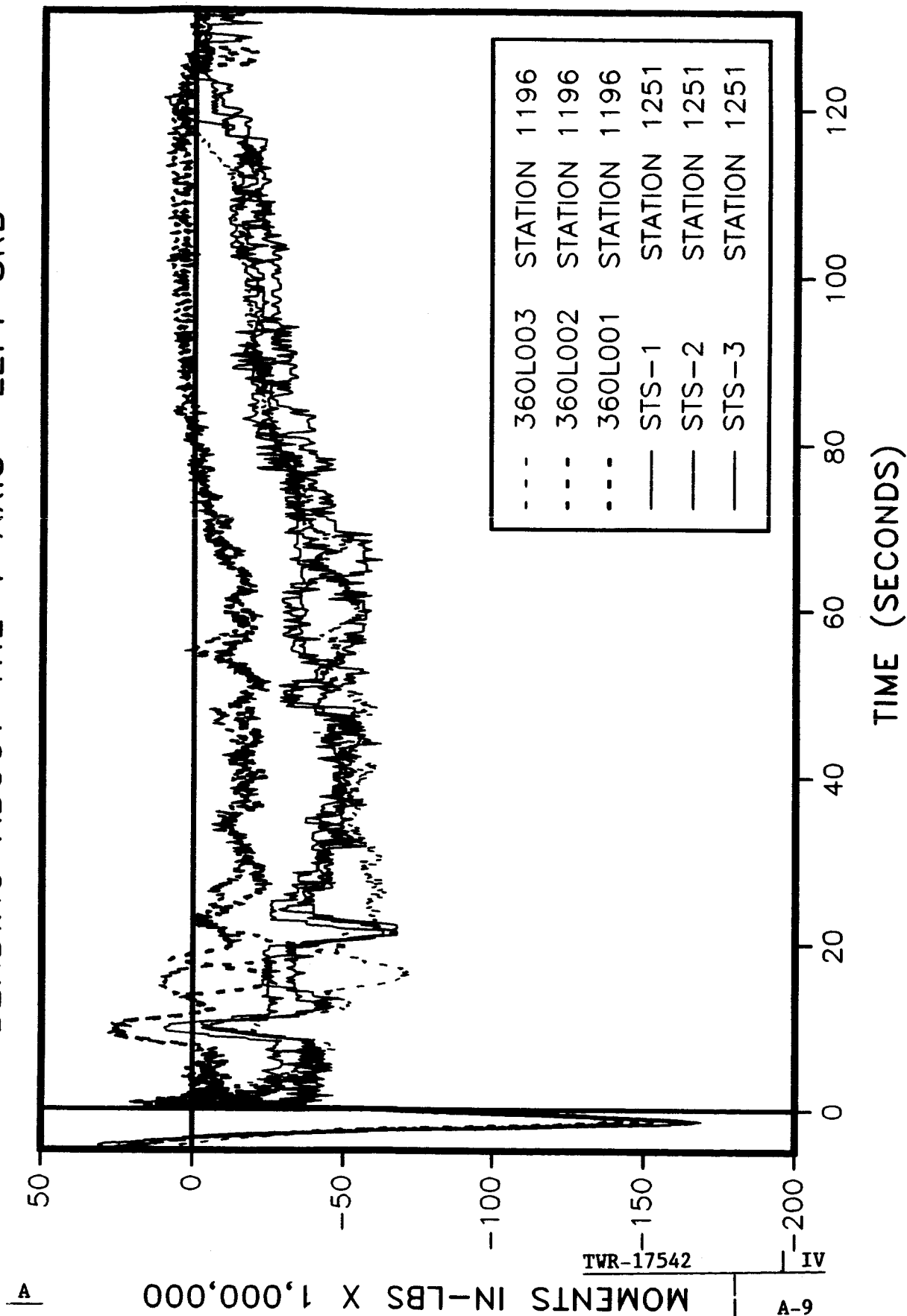
360L003 VS PREVIOUS FLIGHTS

BENDING ABOUT THE Y AXIS LEFT SRB



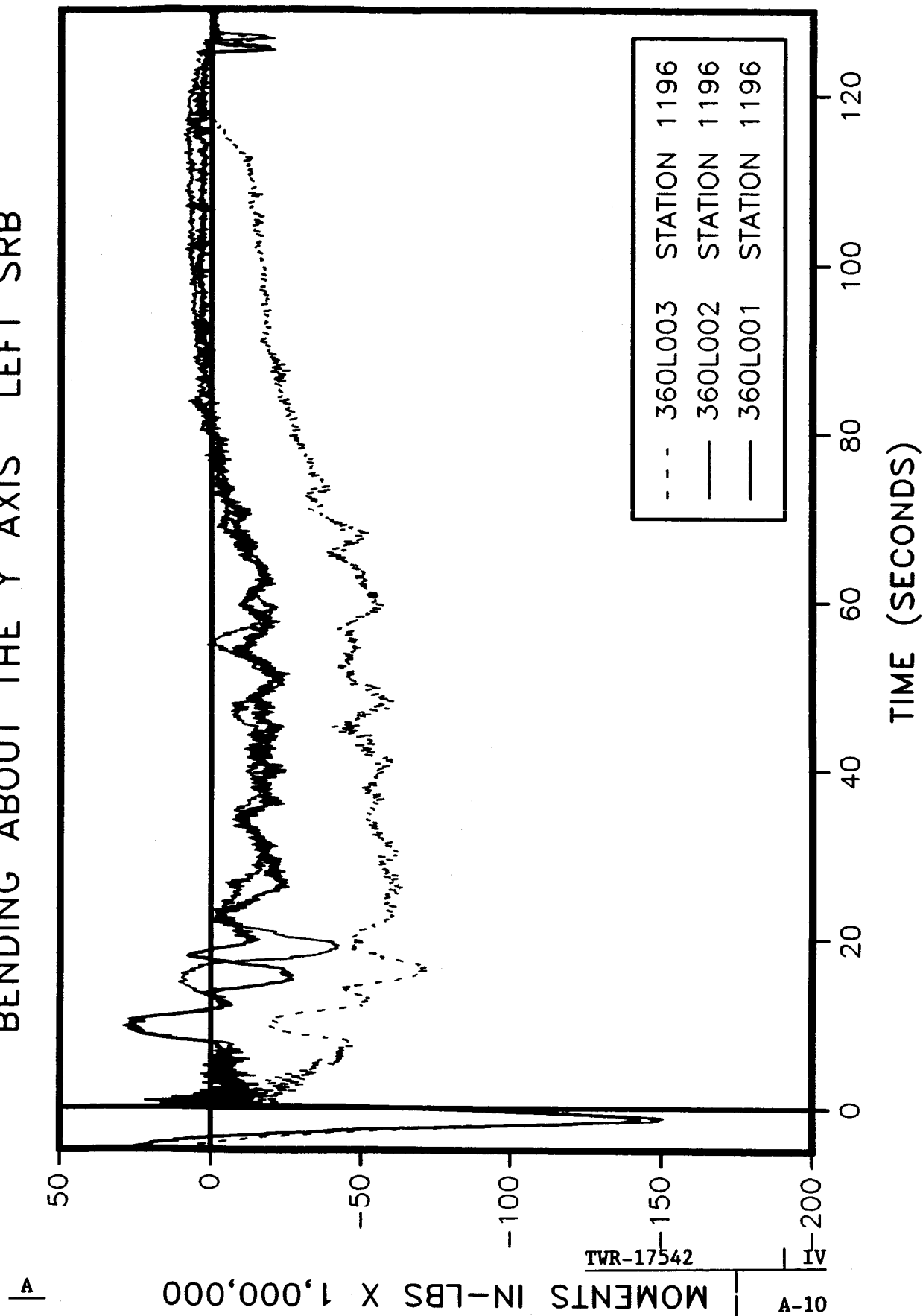
360L003 VS PREVIOUS FLIGHTS

BENDING ABOUT THE Y AXIS LEFT SRB



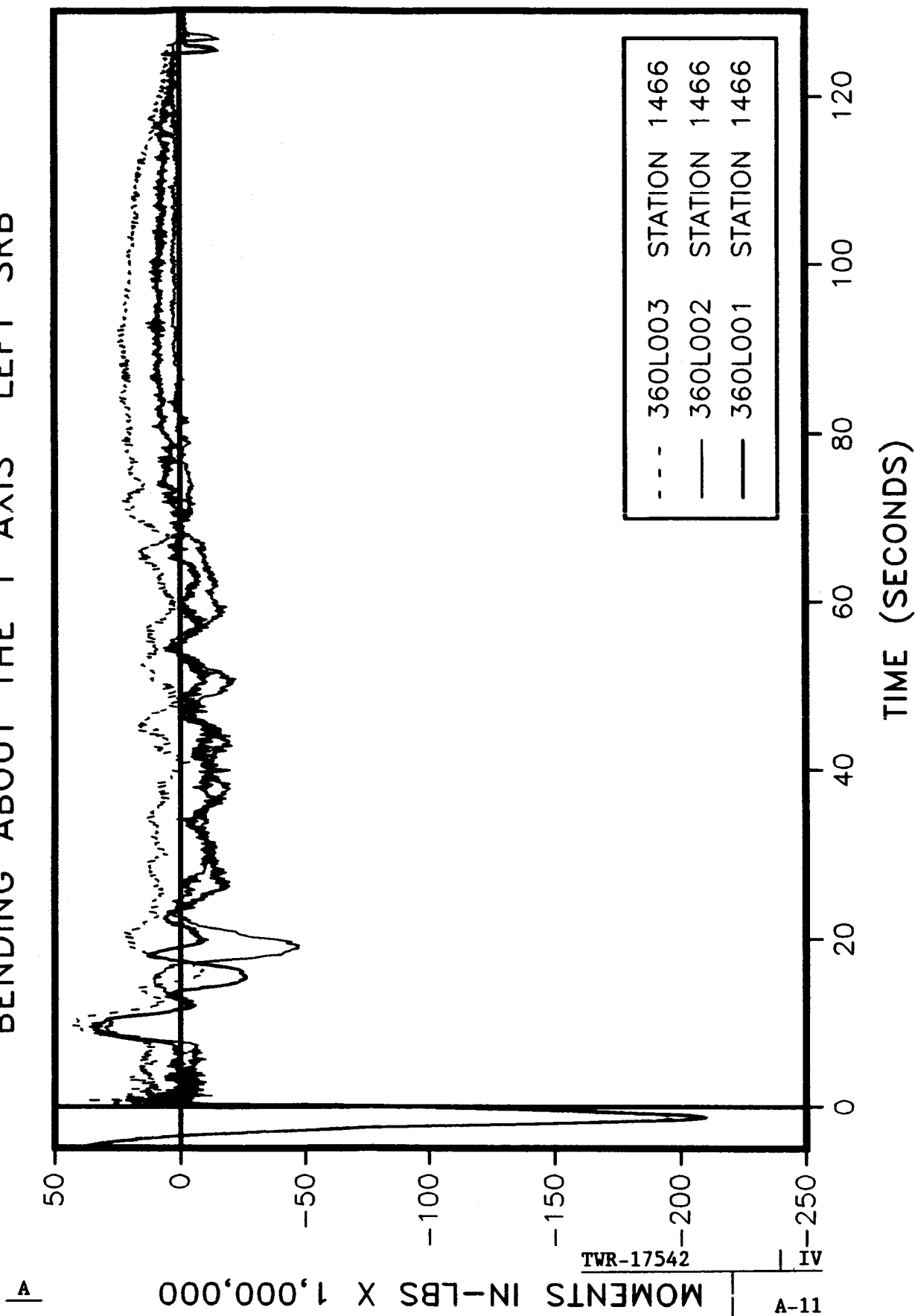
360L003 VS PREVIOUS FLIGHTS

BENDING ABOUT THE Y AXIS LEFT SRB



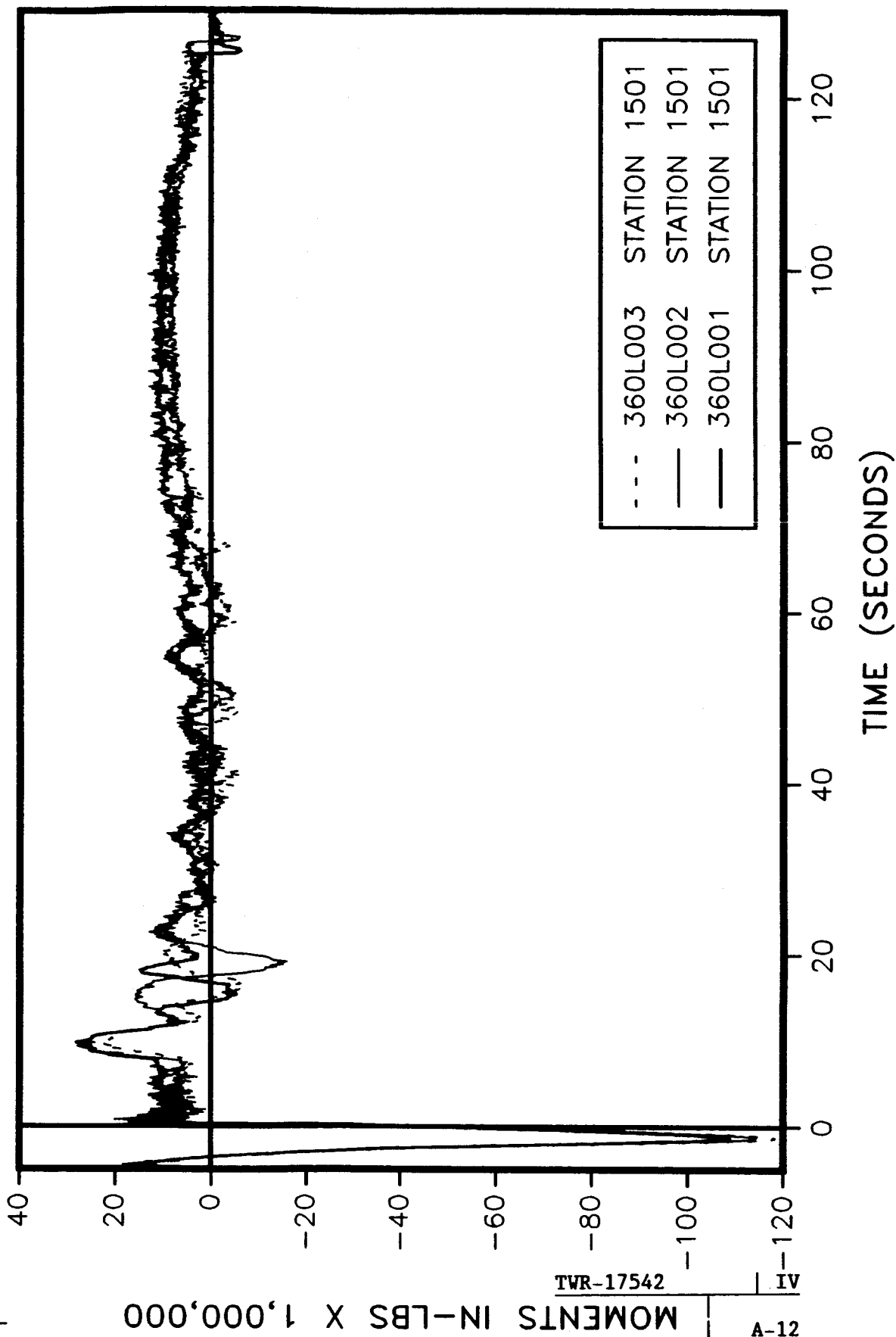
360L003 VS PREVIOUS FLIGHTS

BENDING ABOUT THE Y AXIS LEFT SRB



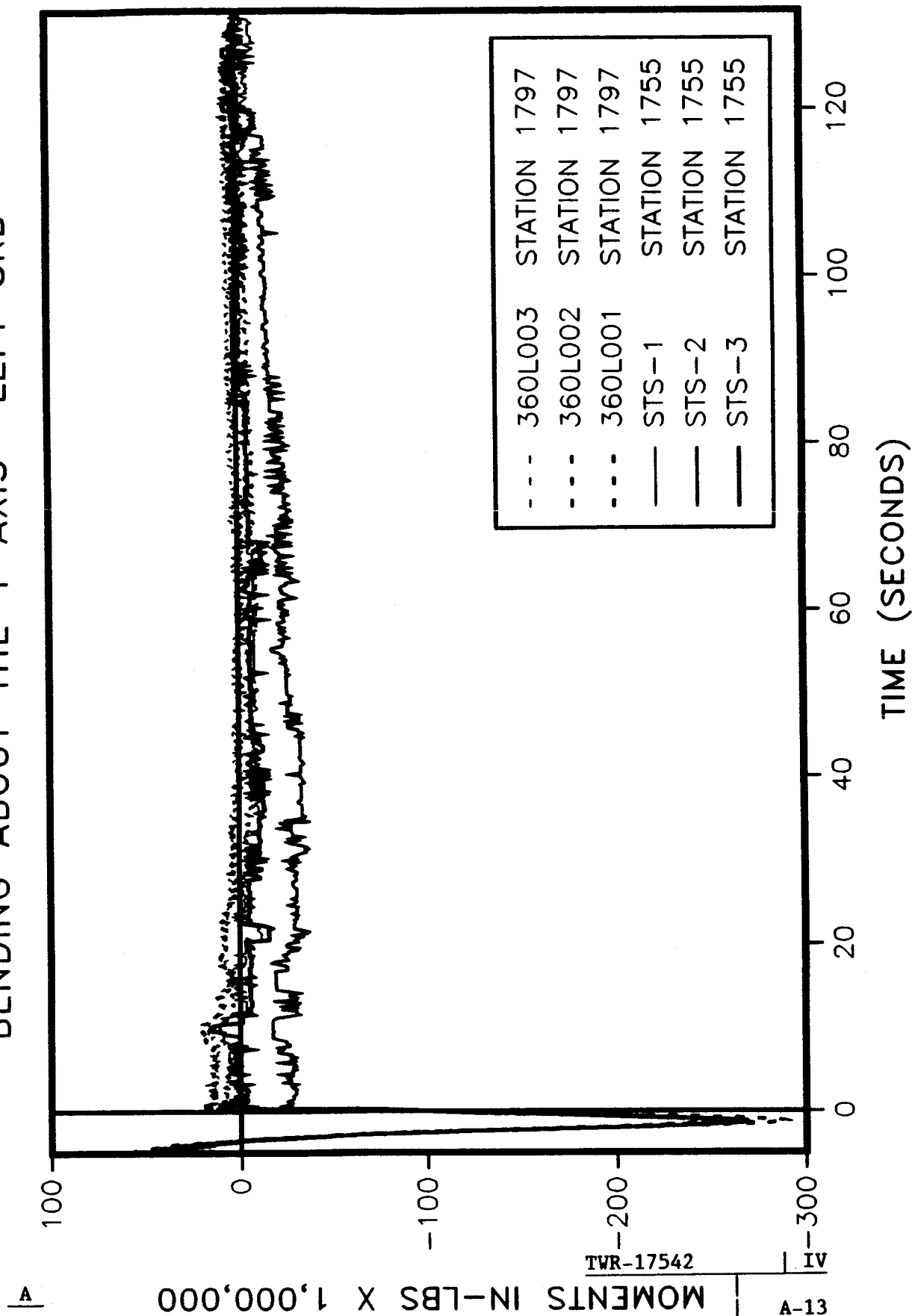
360L003 VS PREVIOUS FLIGHTS

BENDING ABOUT THE Y AXIS LEFT SRB



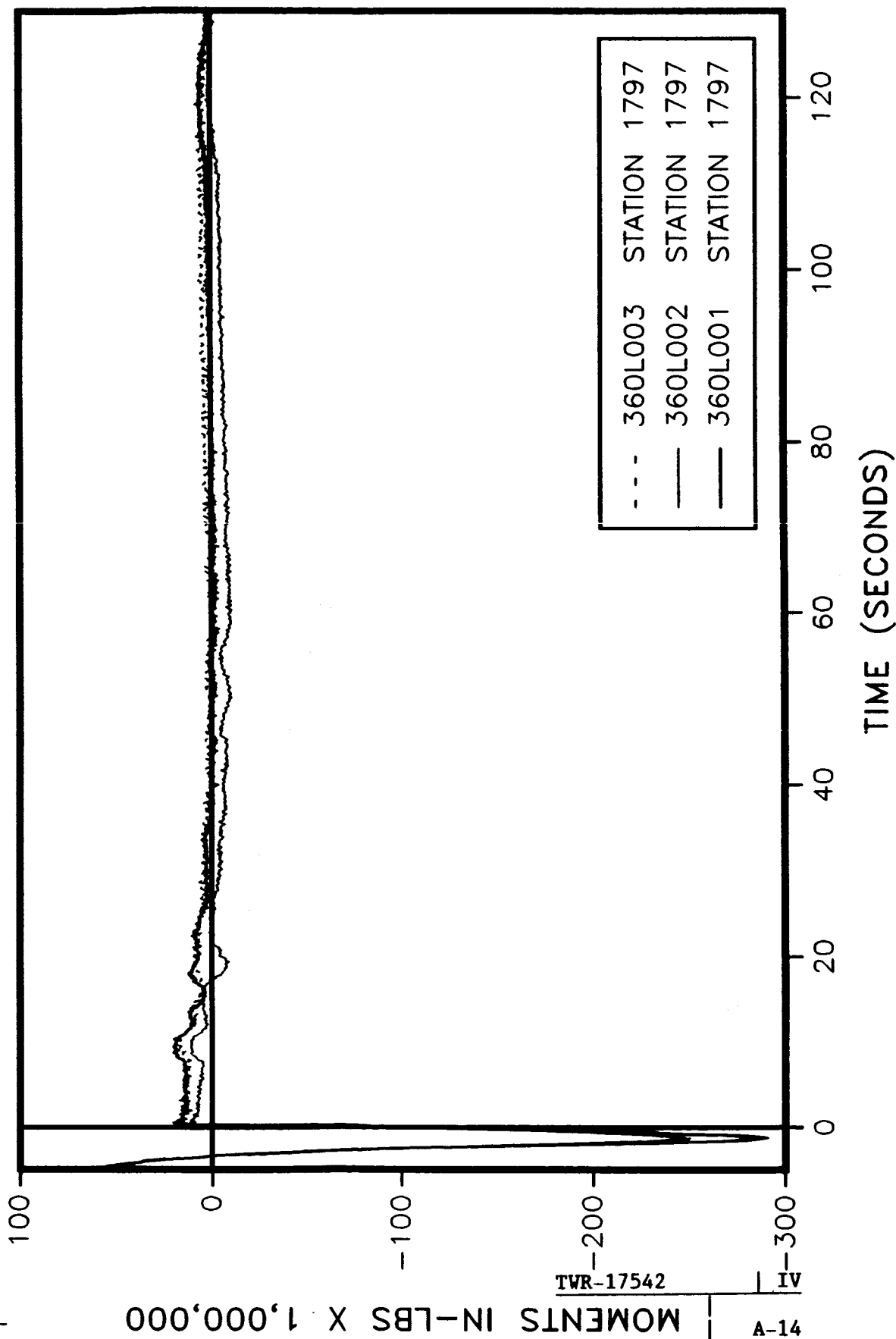
360L003 VS PREVIOUS FLIGHTS

BENDING ABOUT THE Y AXIS LEFT SRB



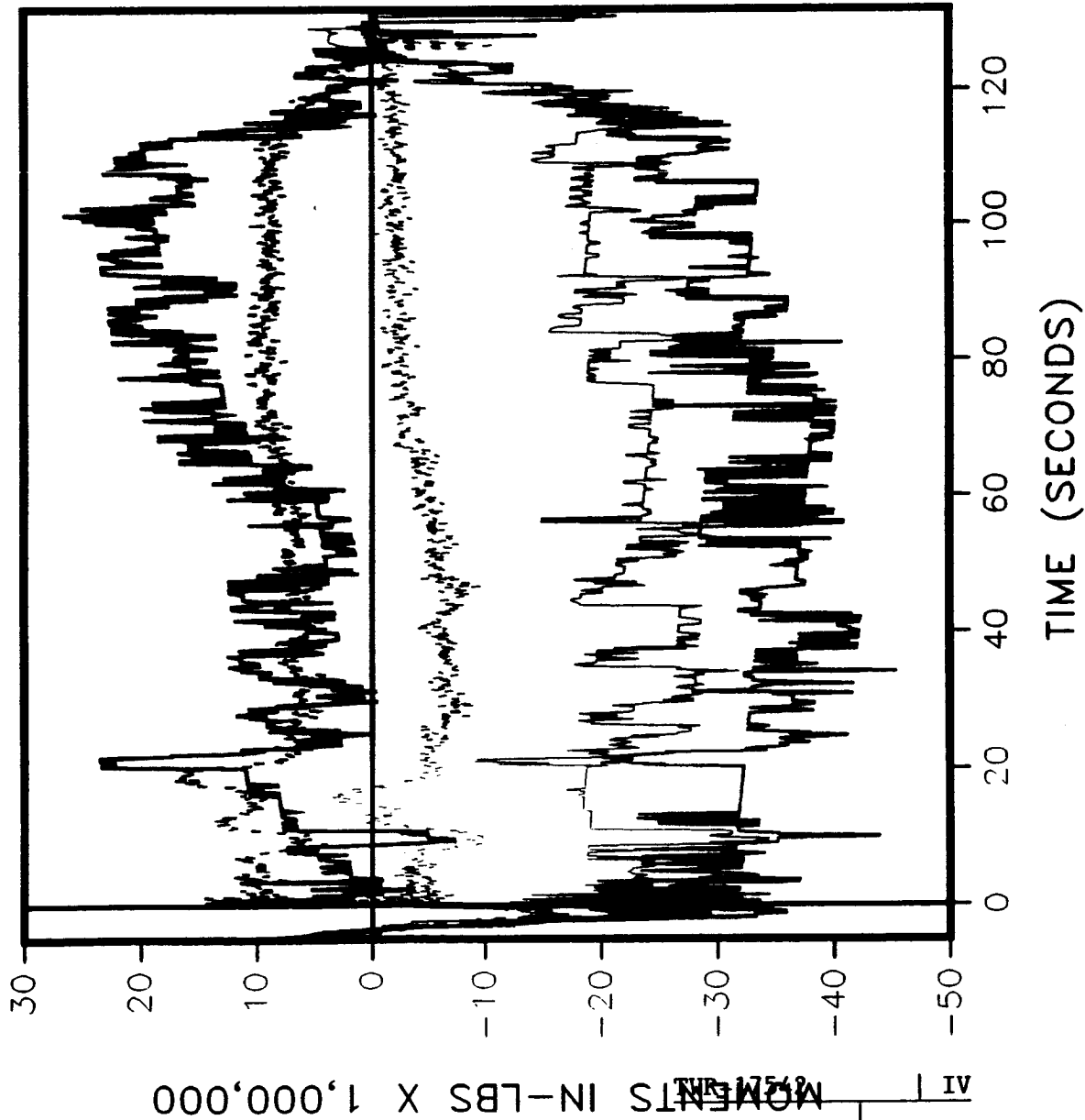
360L003 VS PREVIOUS FLIGHTS

BENDING ABOUT THE Y AXIS LEFT SRB



360L003 VS PREVIOUS FLIGHTS

BENDING ABOUT THE Y AXIS RIGHT SRB

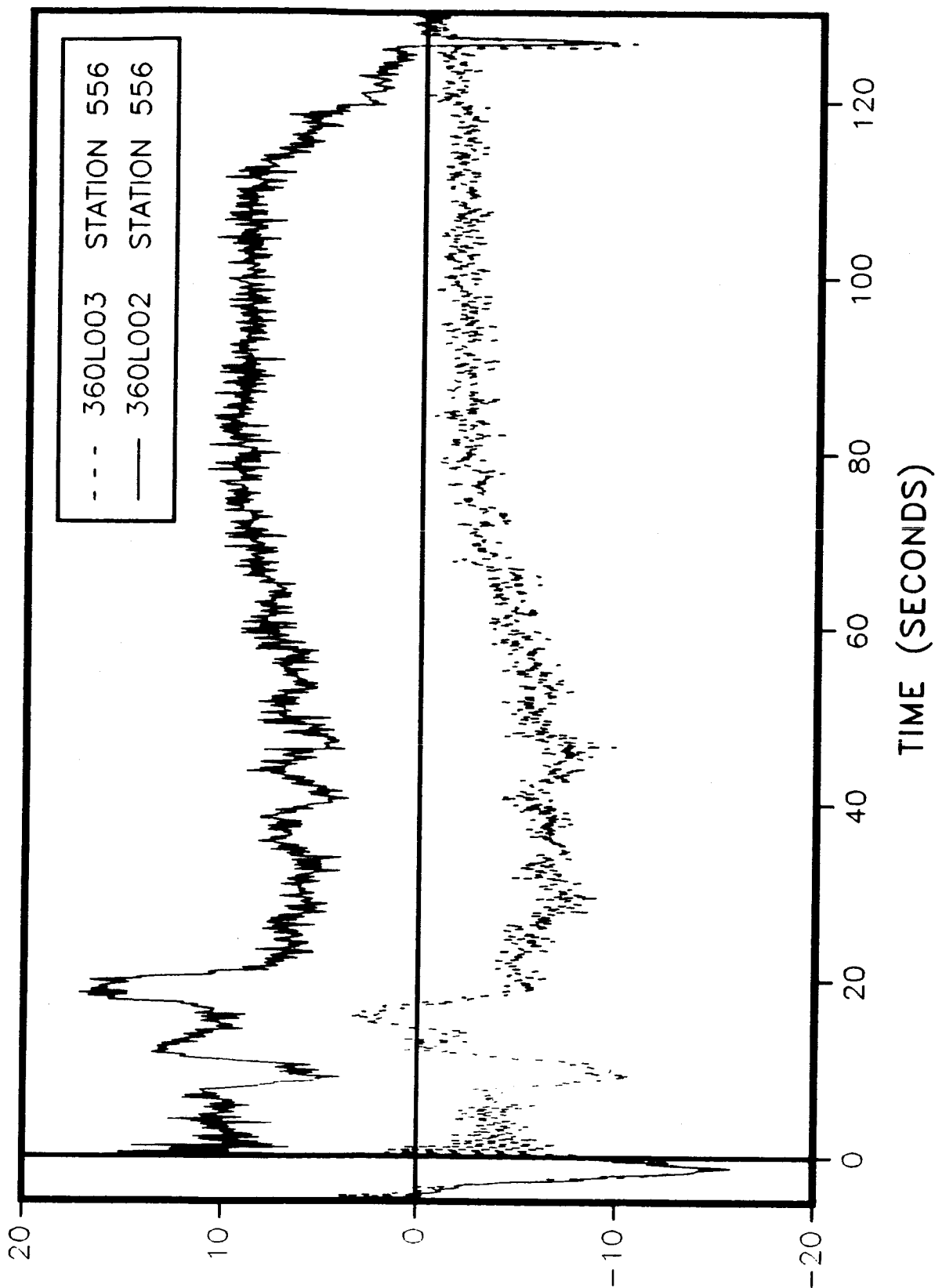


A

A-15

360L003 VS PREVIOUS FLIGHTS

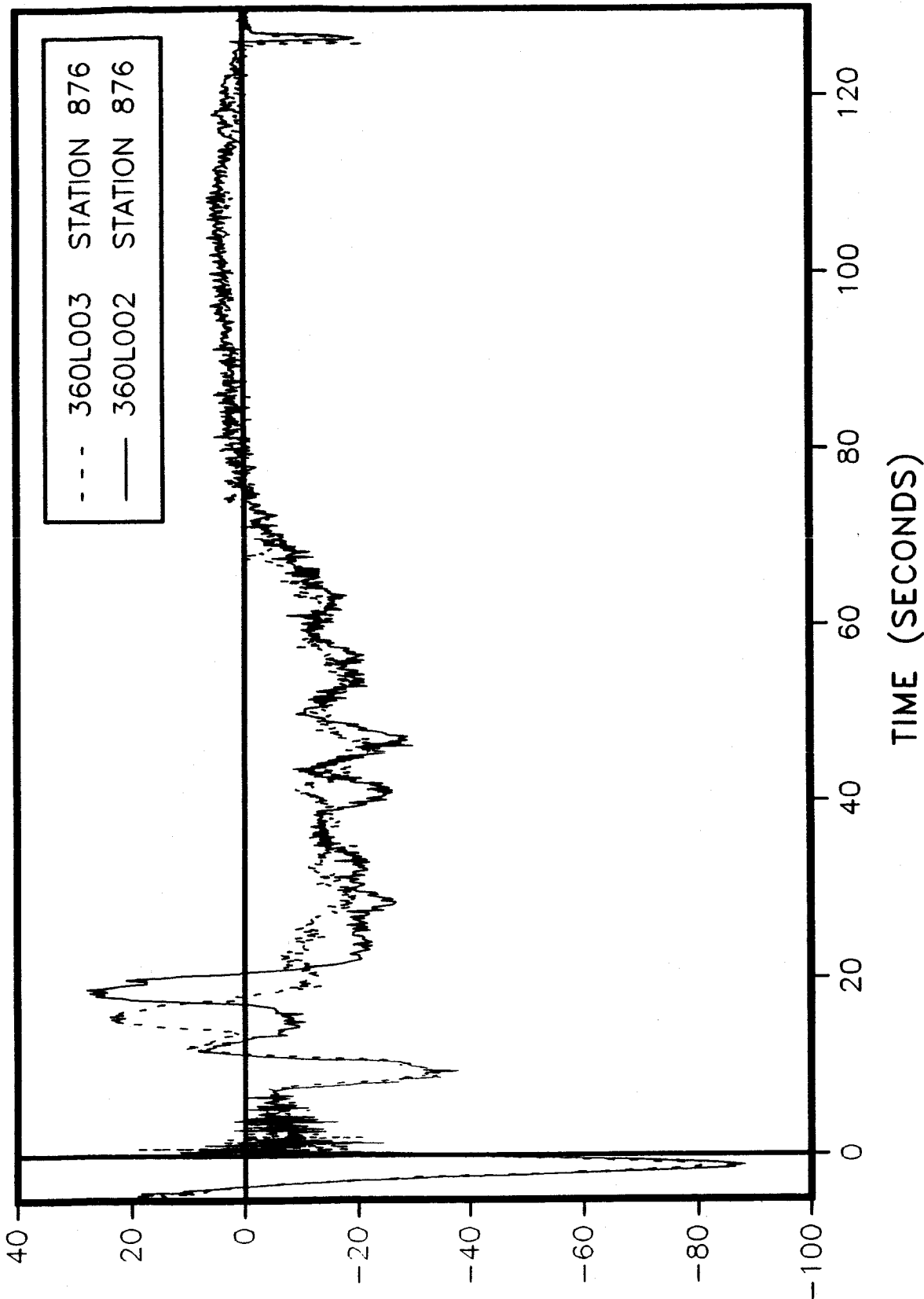
BENDING ABOUT THE Y AXIS RIGHT SRB



MOMENTS IN-LBS X 1,000,000

360L003 VS PREVIOUS FLIGHTS

BENDING ABOUT THE Y AXIS RIGHT SRB



A

MOMENTS IN-LBS X 1,000,000

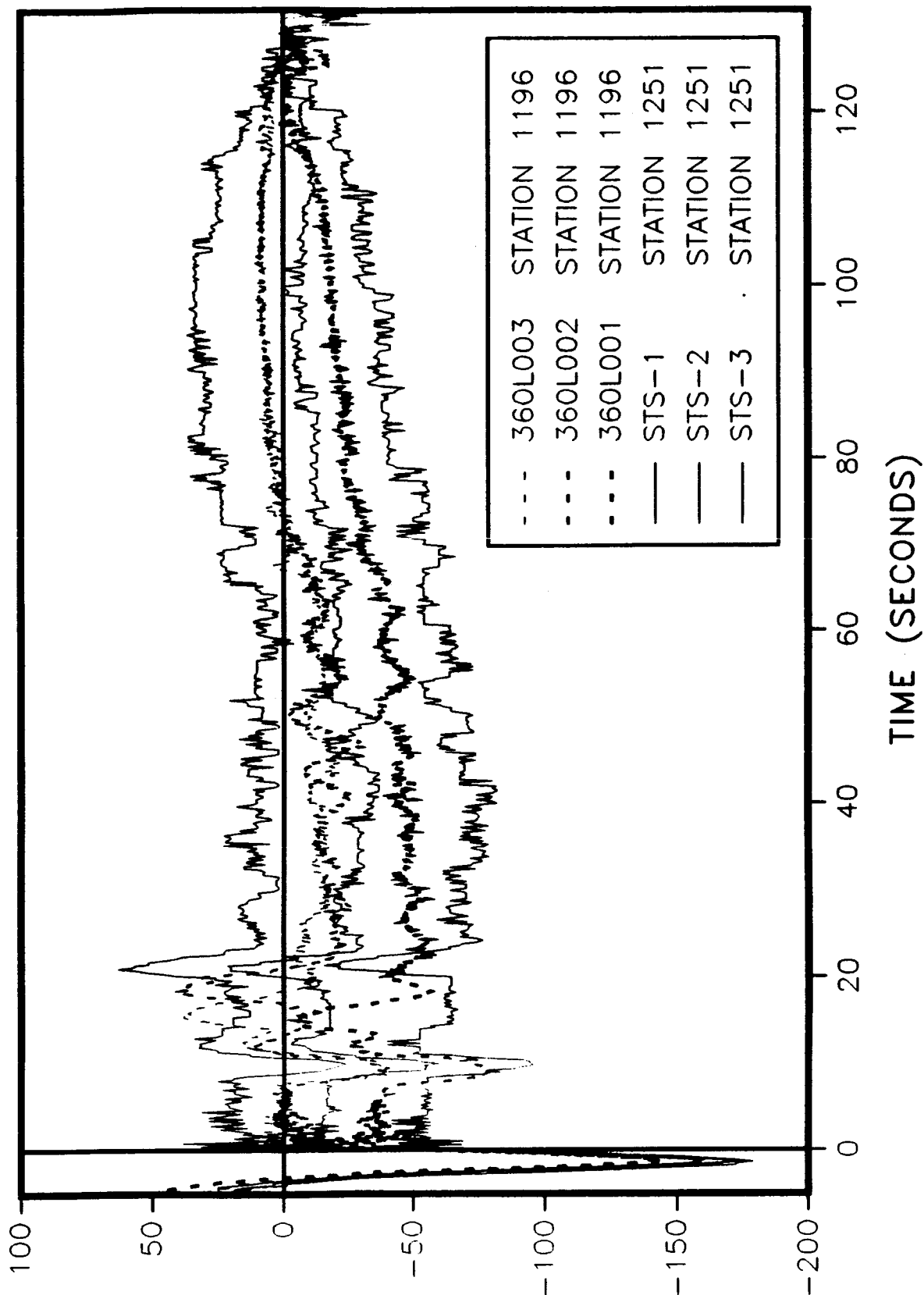
TWR-17542

A-17

IV

360L003 VS PREVIOUS FLIGHTS

BENDING ABOUT THE Y AXIS RIGHT SRB



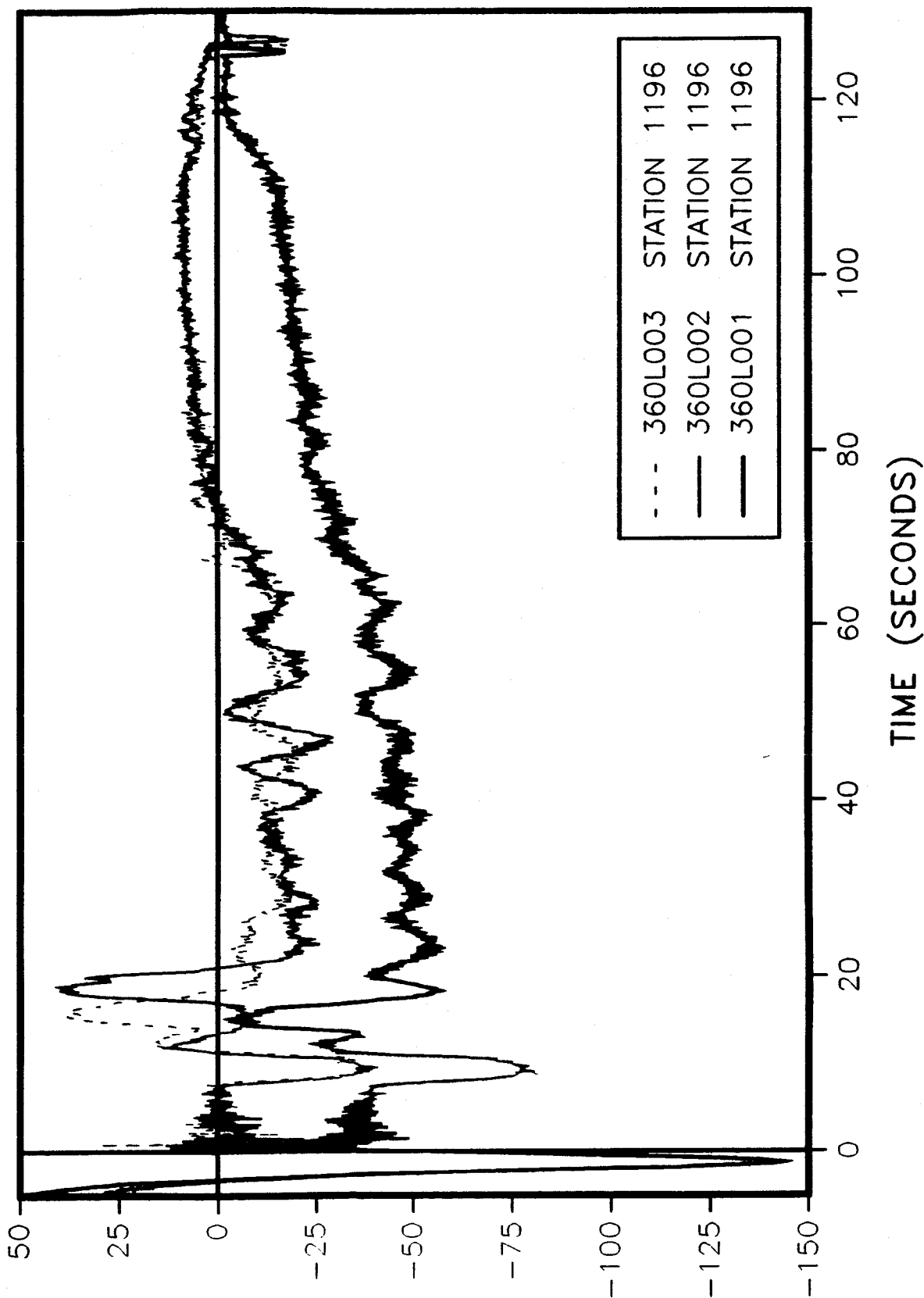
MOMENTS IN-LBS X 1,000,000

TWR-17542

A-18 IV

360L003 VS PREVIOUS FLIGHTS

BENDING ABOUT THE Y AXIS RIGHT SRB



A

MOMENTS IN-LBS X 1,000,000

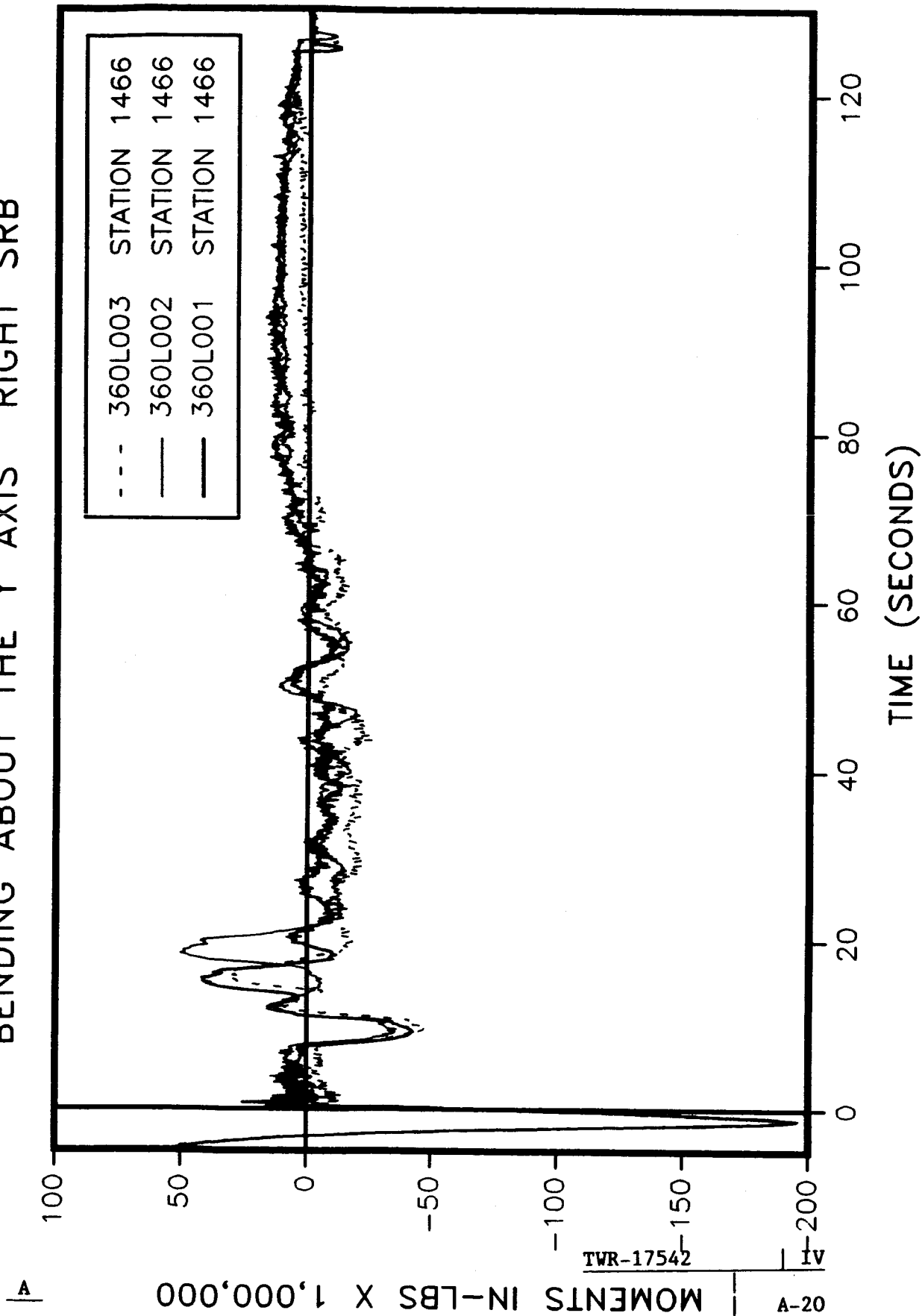
TWR-17542

A-19

IV

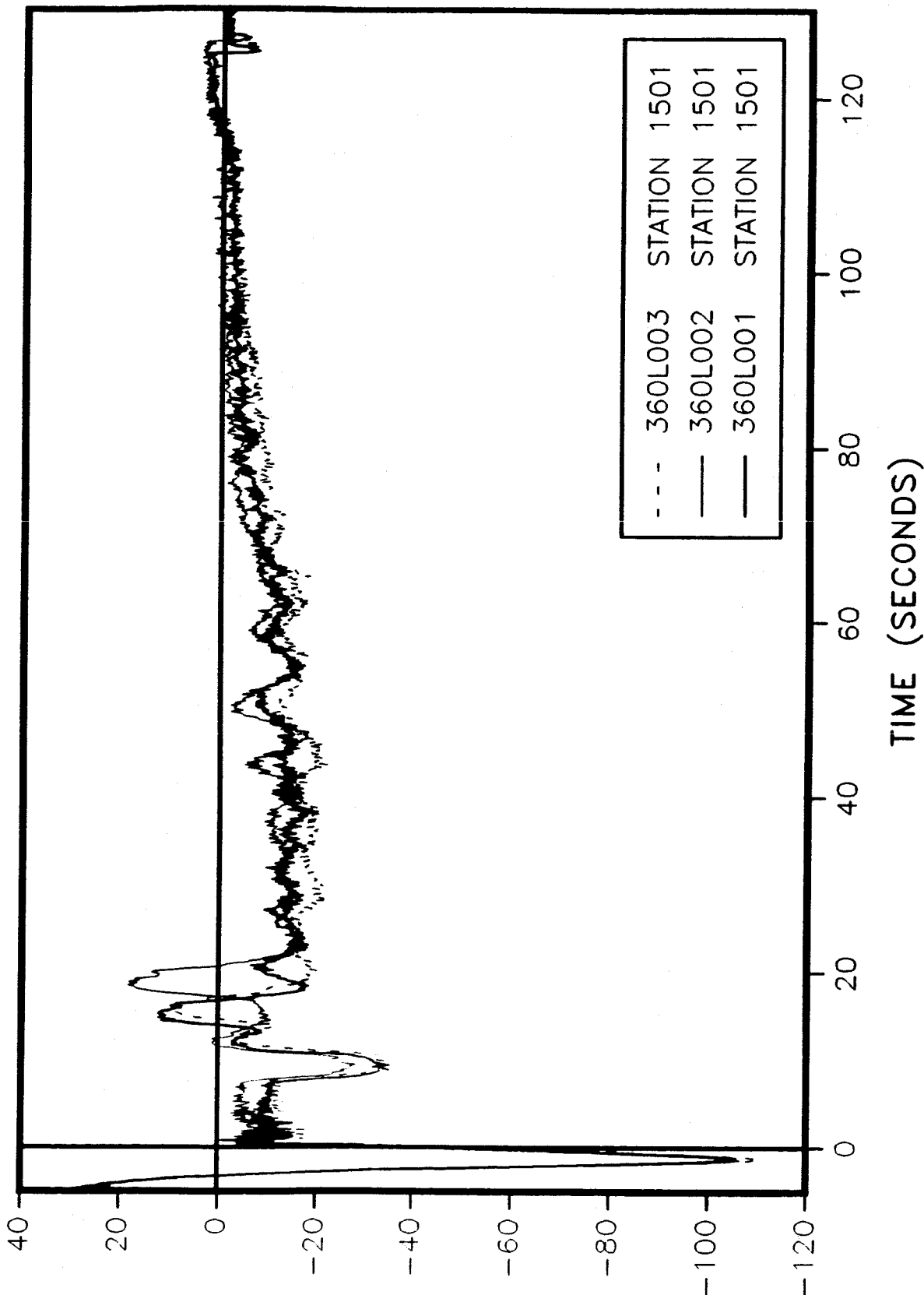
360L003 VS PREVIOUS FLIGHTS

BENDING ABOUT THE Y AXIS RIGHT SRB



360L003 VS PREVIOUS FLIGHTS

BENDING ABOUT THE Y AXIS RIGHT SRB



A

MOMENTS IN-LBS X 1,000,000

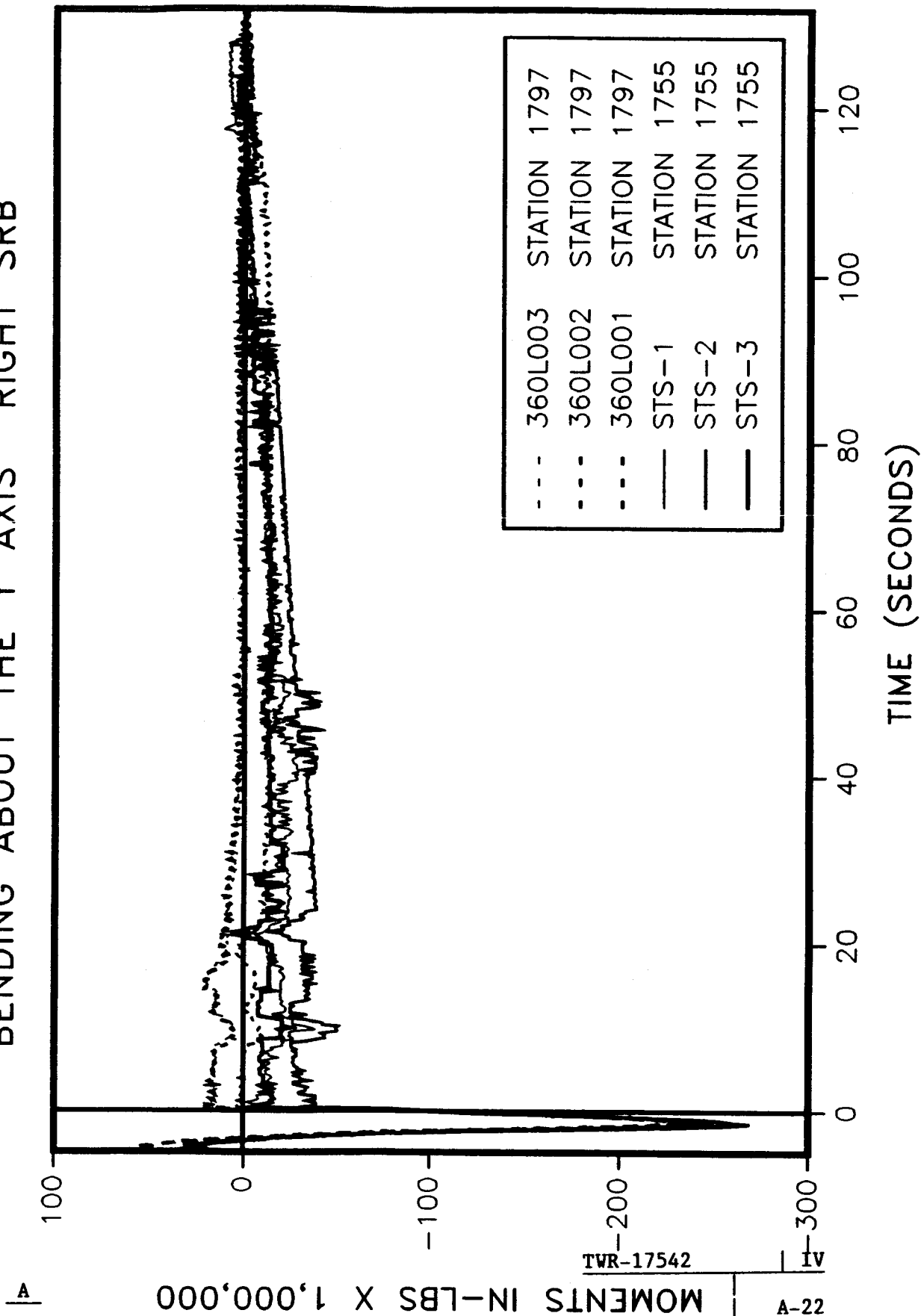
TWR-17542

A-21

IV

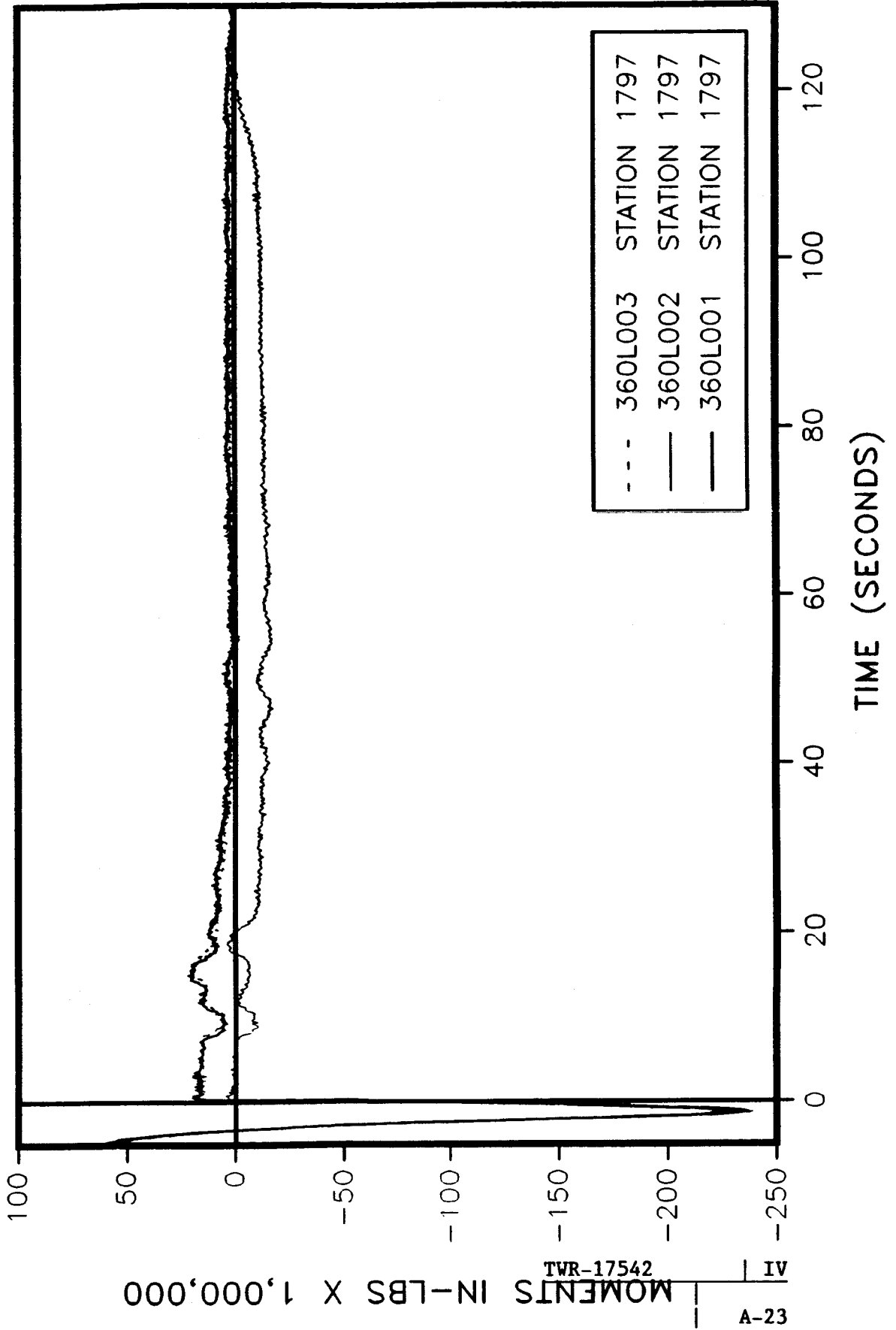
360L003 VS PREVIOUS FLIGHTS

BENDING ABOUT THE Y AXIS RIGHT SRB



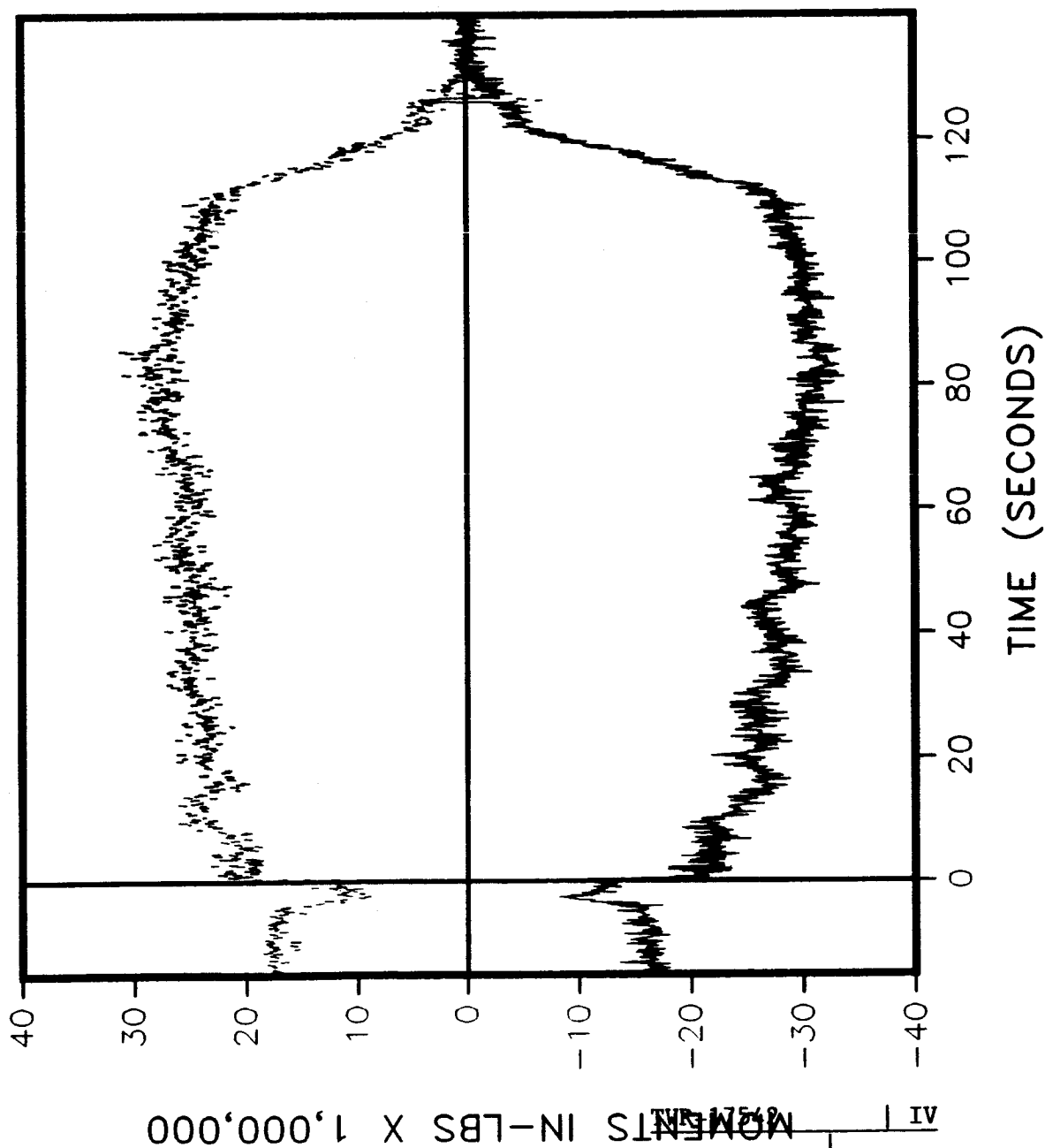
360L003 VS PREVIOUS FLIGHTS

BENDING ABOUT THE Y AXIS RIGHT SRB



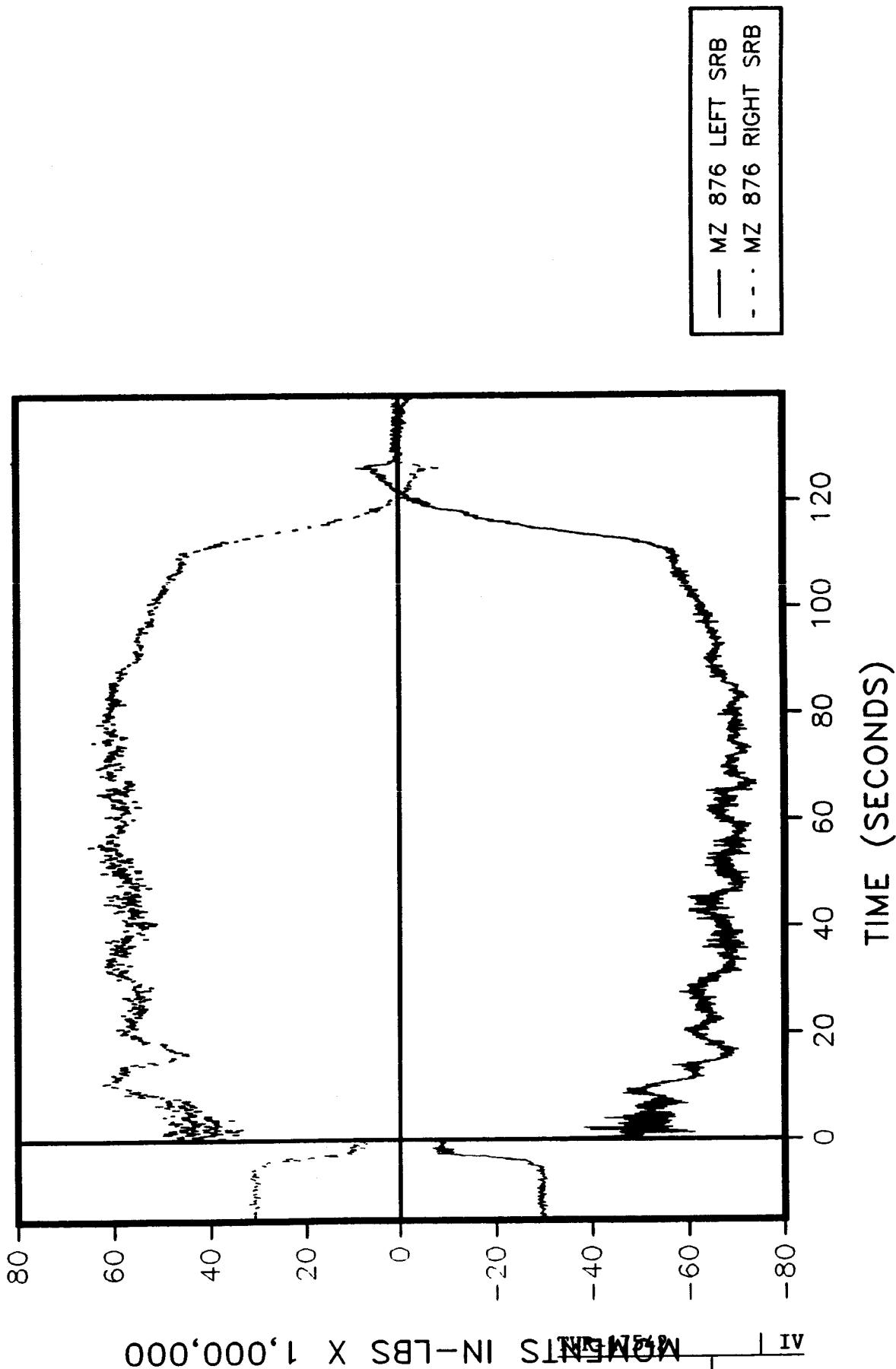
360L003 STATION 556

BENDING ABOUT THE Z AXIS



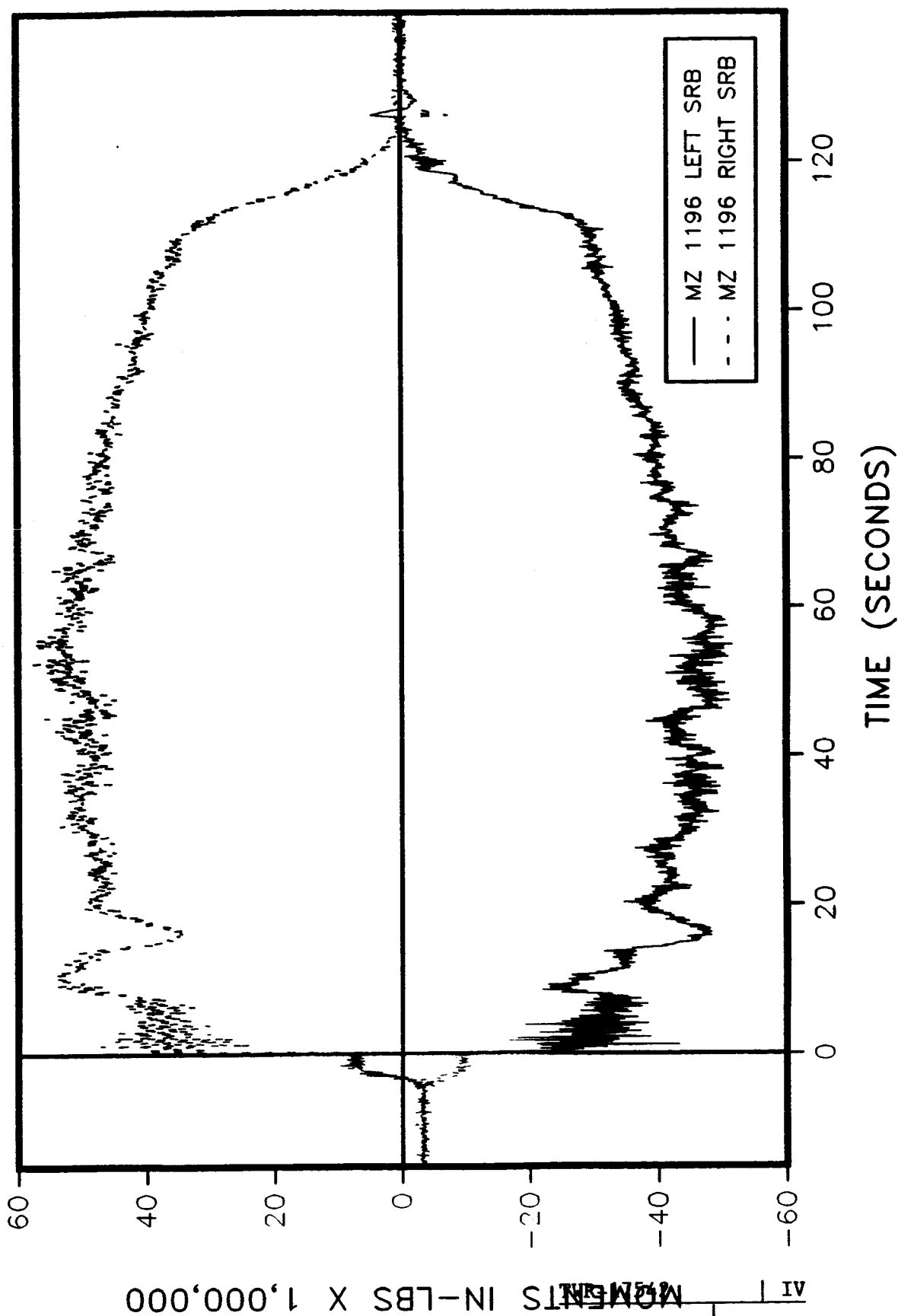
360L003 STATION 876

BENDING ABOUT THE Z AXIS



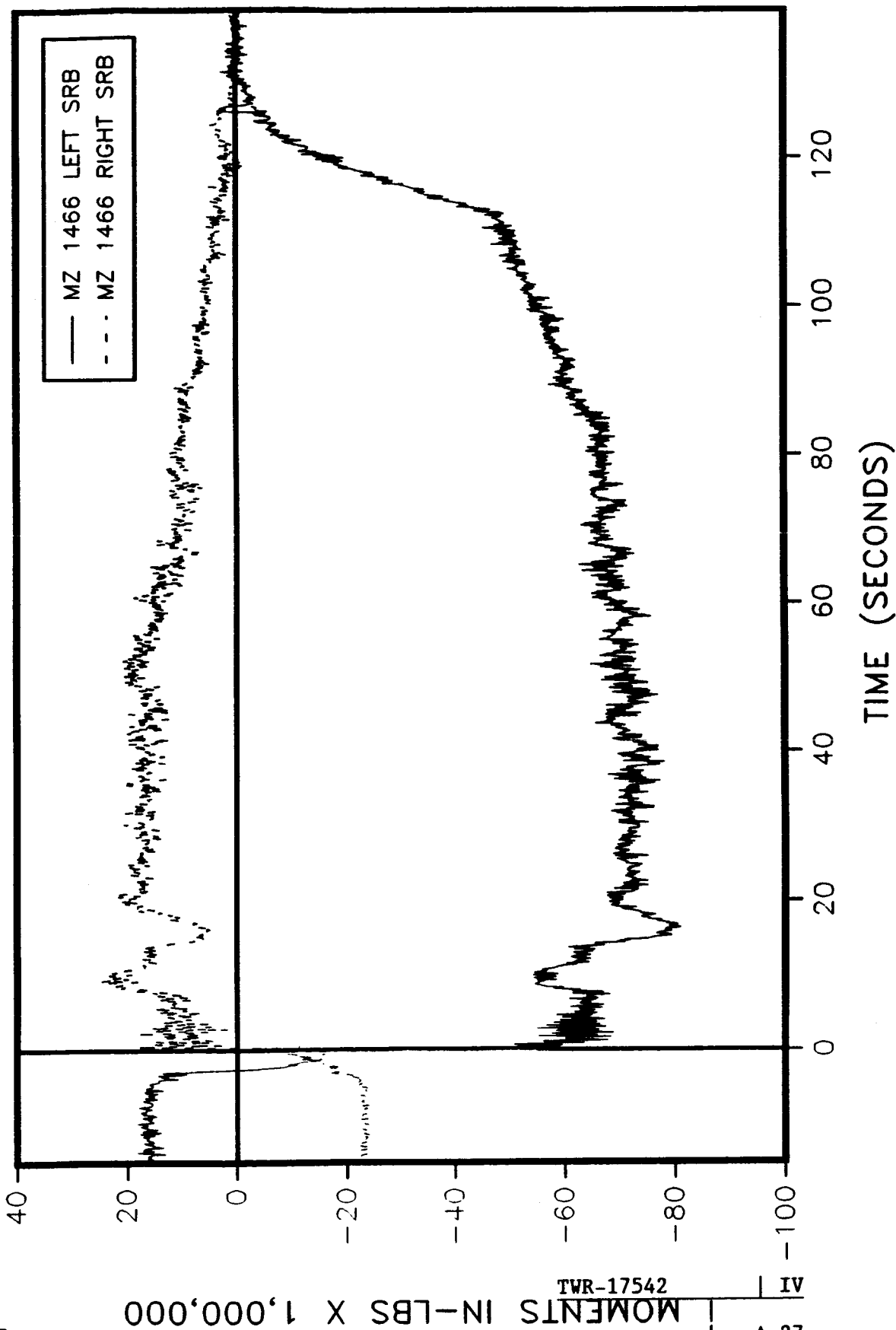
360L003 STATION 1196

BENDING ABOUT THE Z AXIS



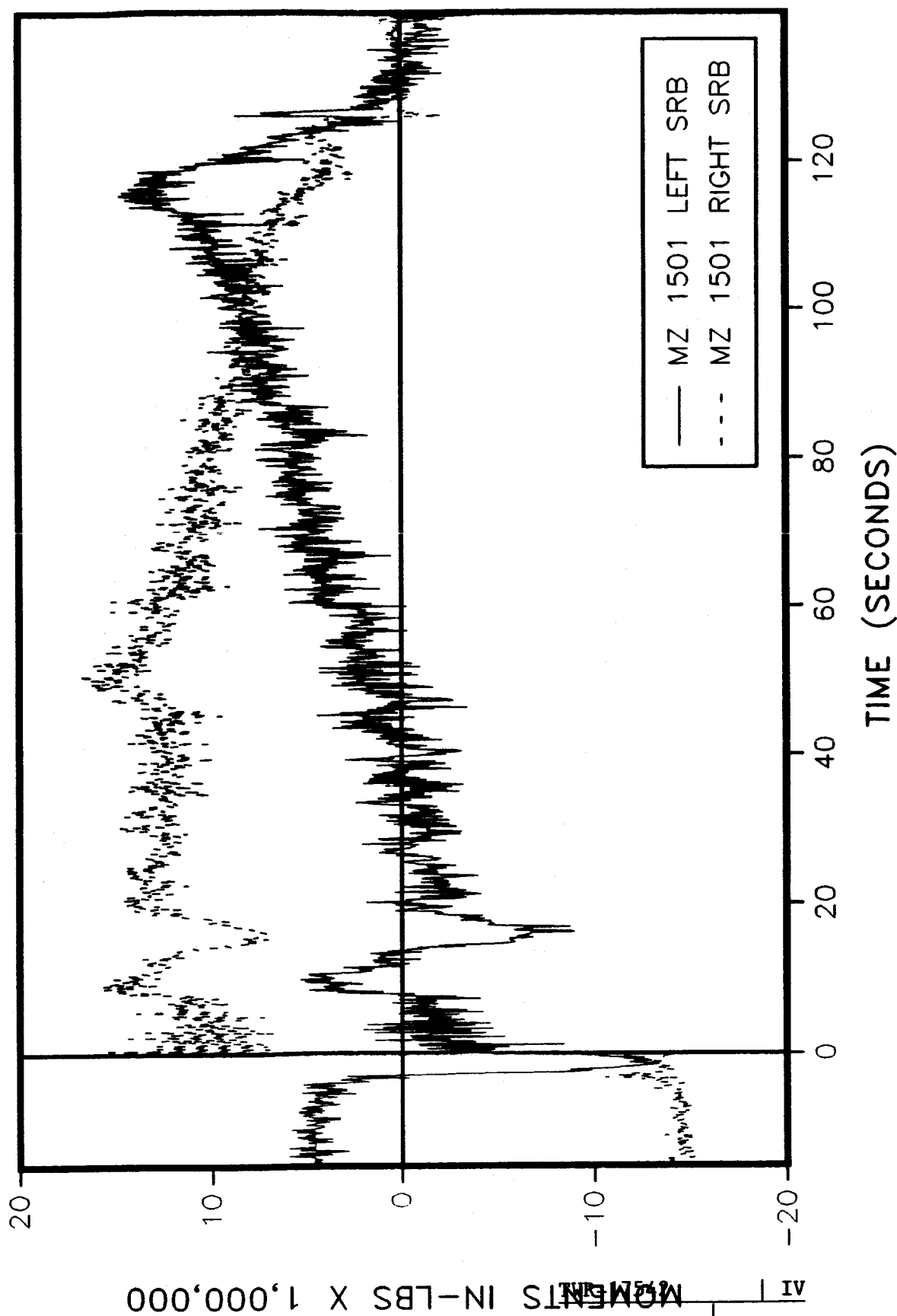
360L003 STATION 1466

BENDING ABOUT THE Z AXIS



360L003 STATION 1501

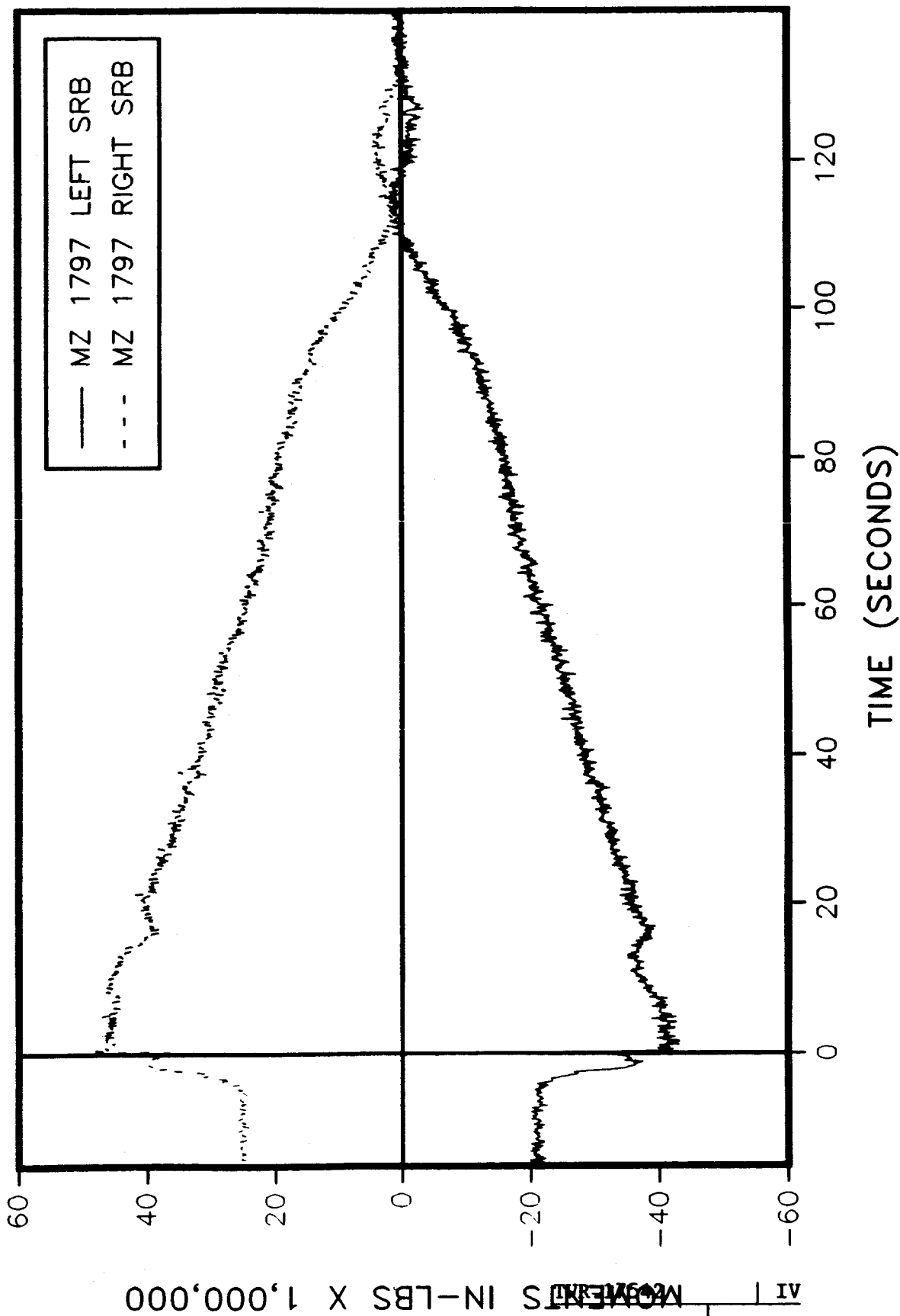
BENDING ABOUT THE Z AXIS



A

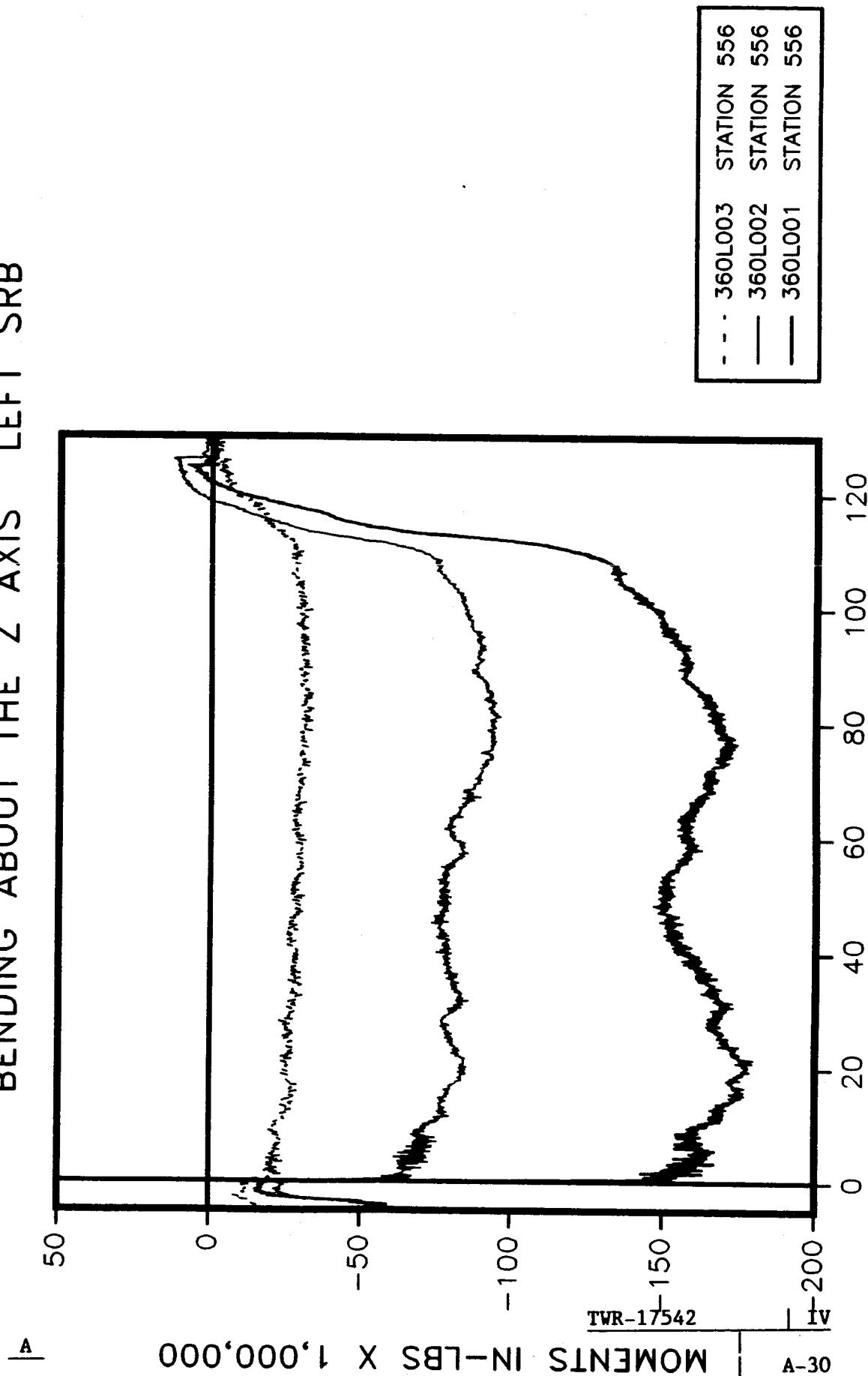
360L003 STATION 1797

BENDING ABOUT THE Z AXIS



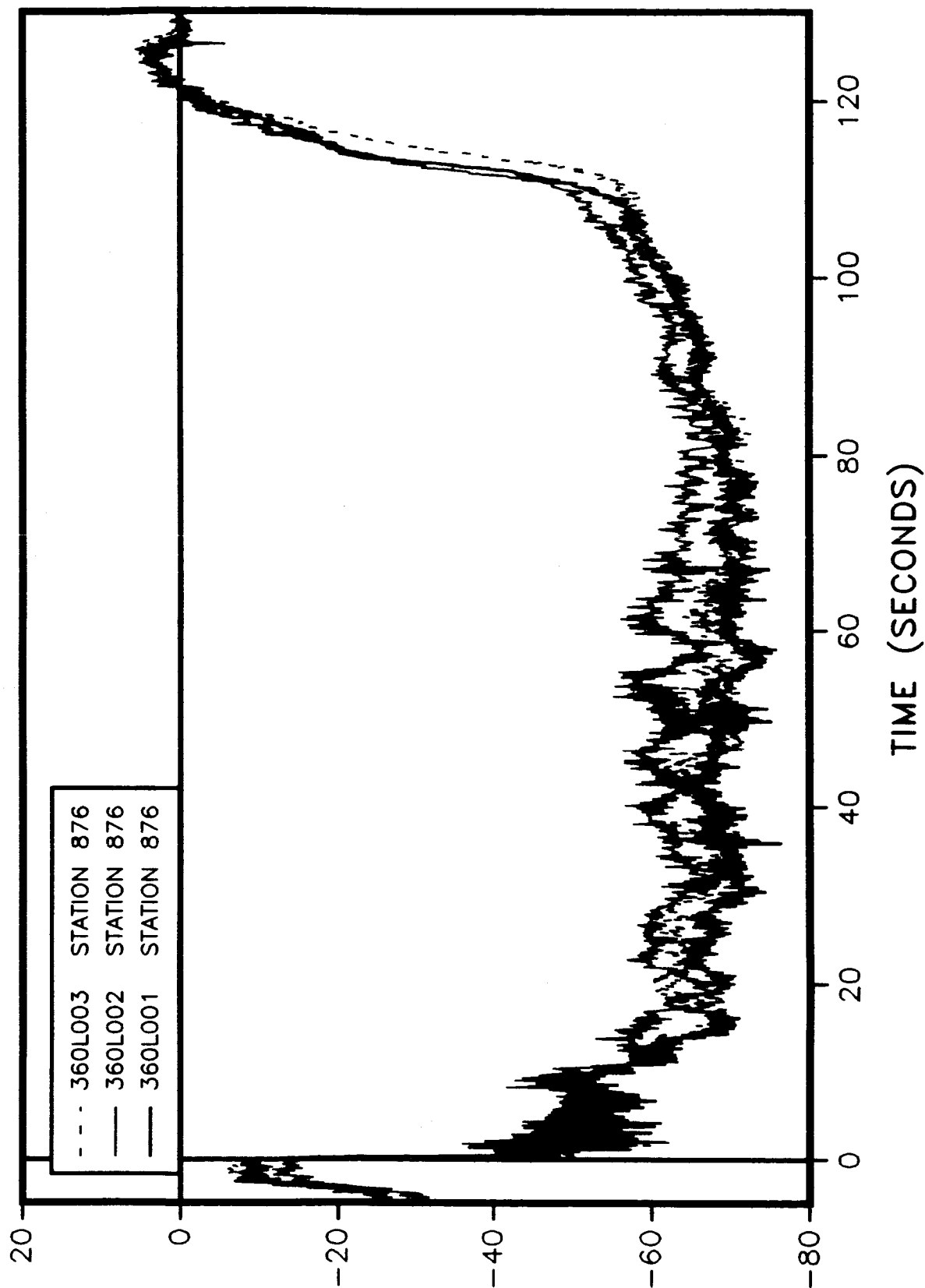
360L003 VS PREVIOUS FLIGHTS

BENDING ABOUT THE Z AXIS LEFT SRB



360L003 VS PREVIOUS FLIGHTS

BENDING ABOUT THE Z AXIS LEFT SRB



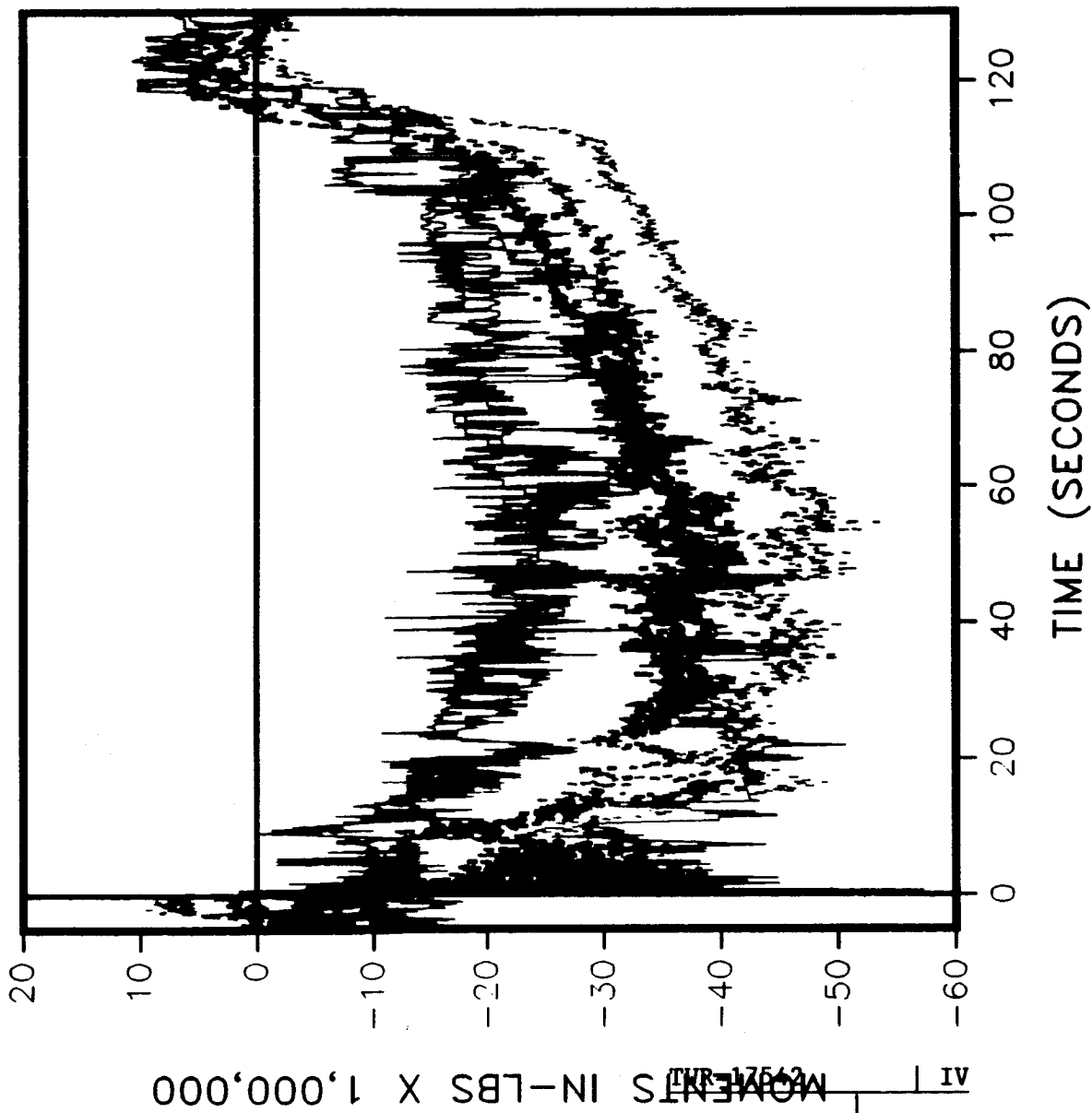
MOMENTS IN-LBS X 1,000,000

TVR-17542

IV
A-31

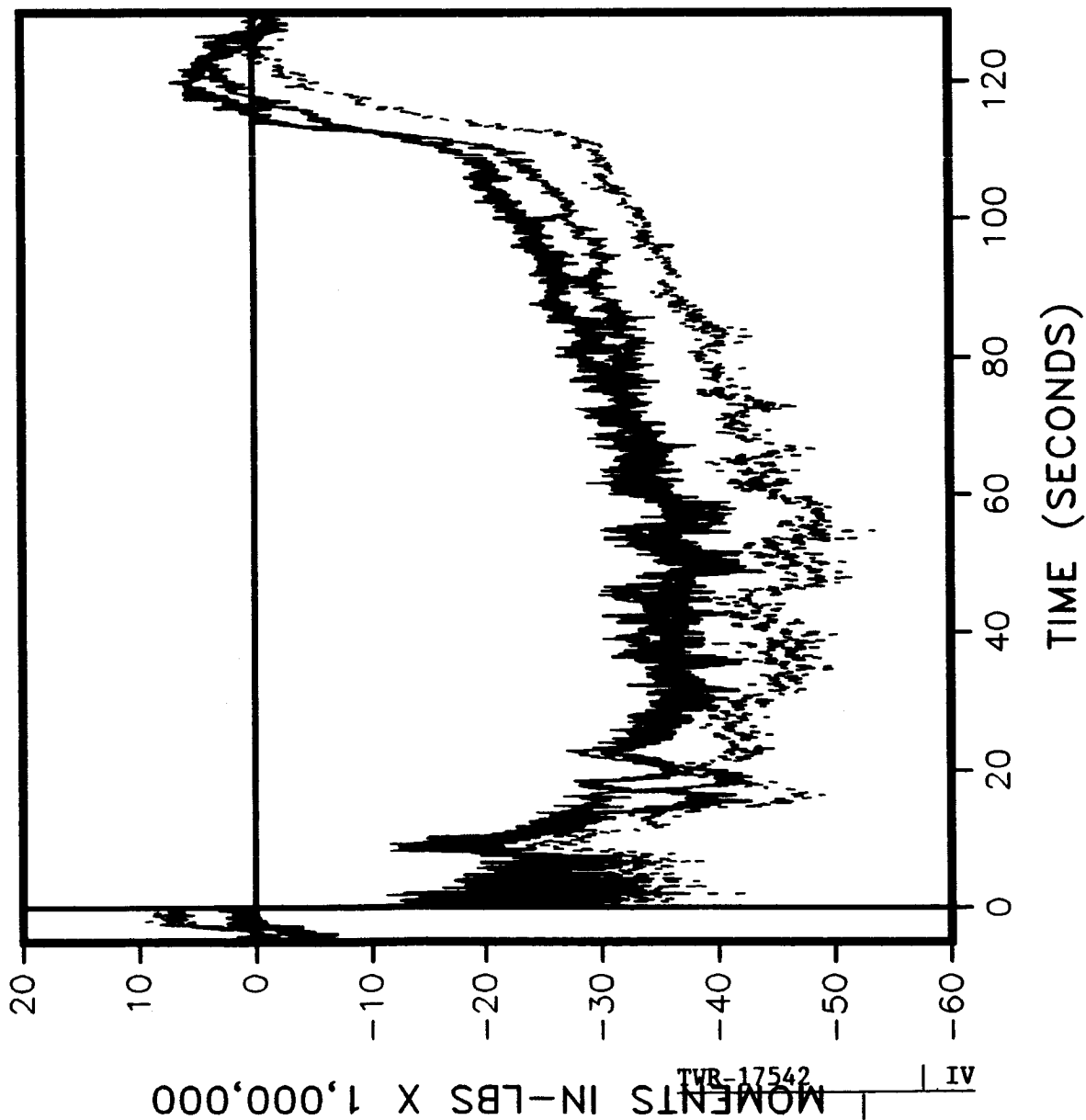
360L003 VS PREVIOUS FLIGHTS

BENDING ABOUT THE Z AXIS LEFT SRB



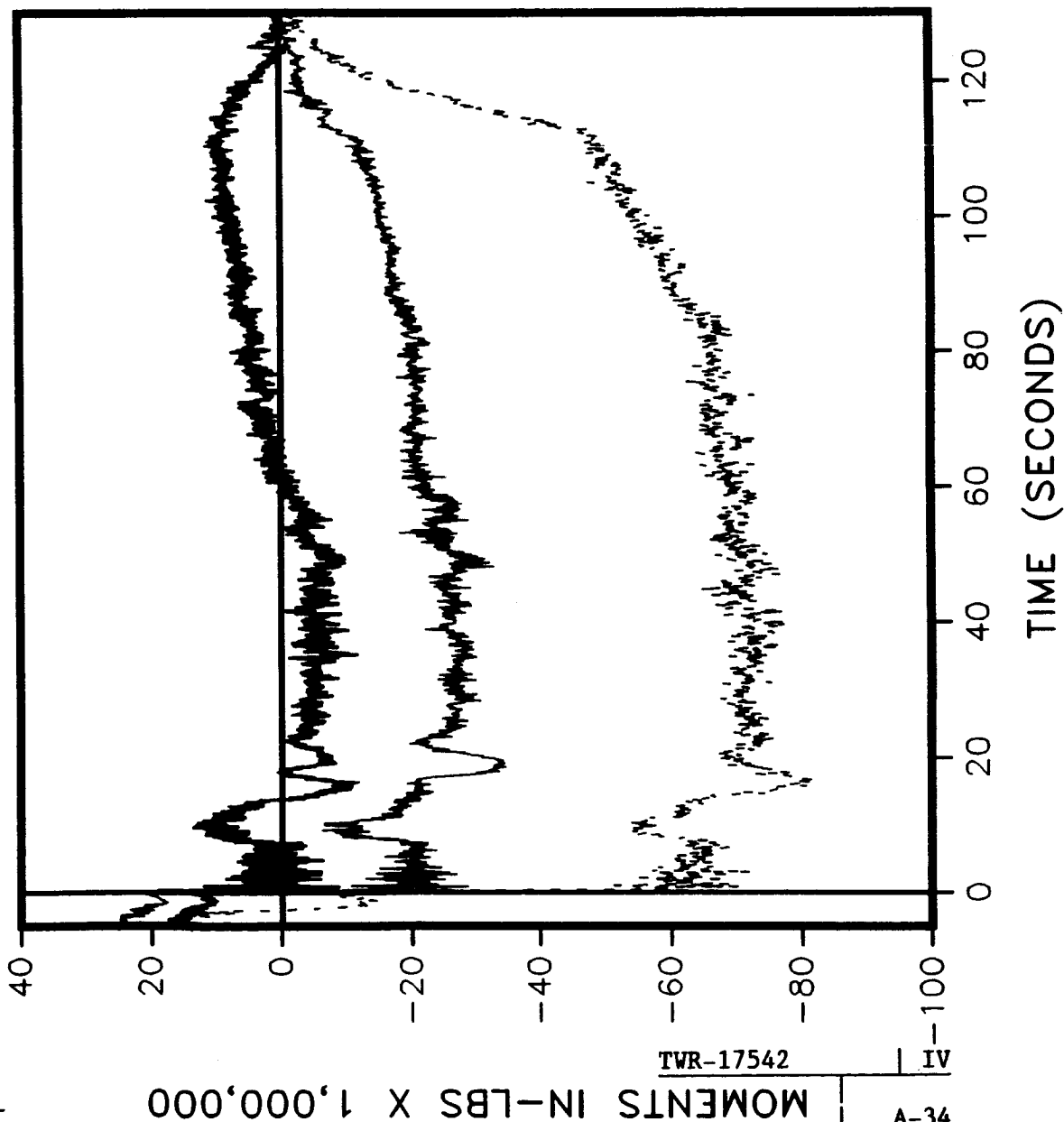
360L003 VS PREVIOUS FLIGHTS

BENDING ABOUT THE Z AXIS LEFT SRB



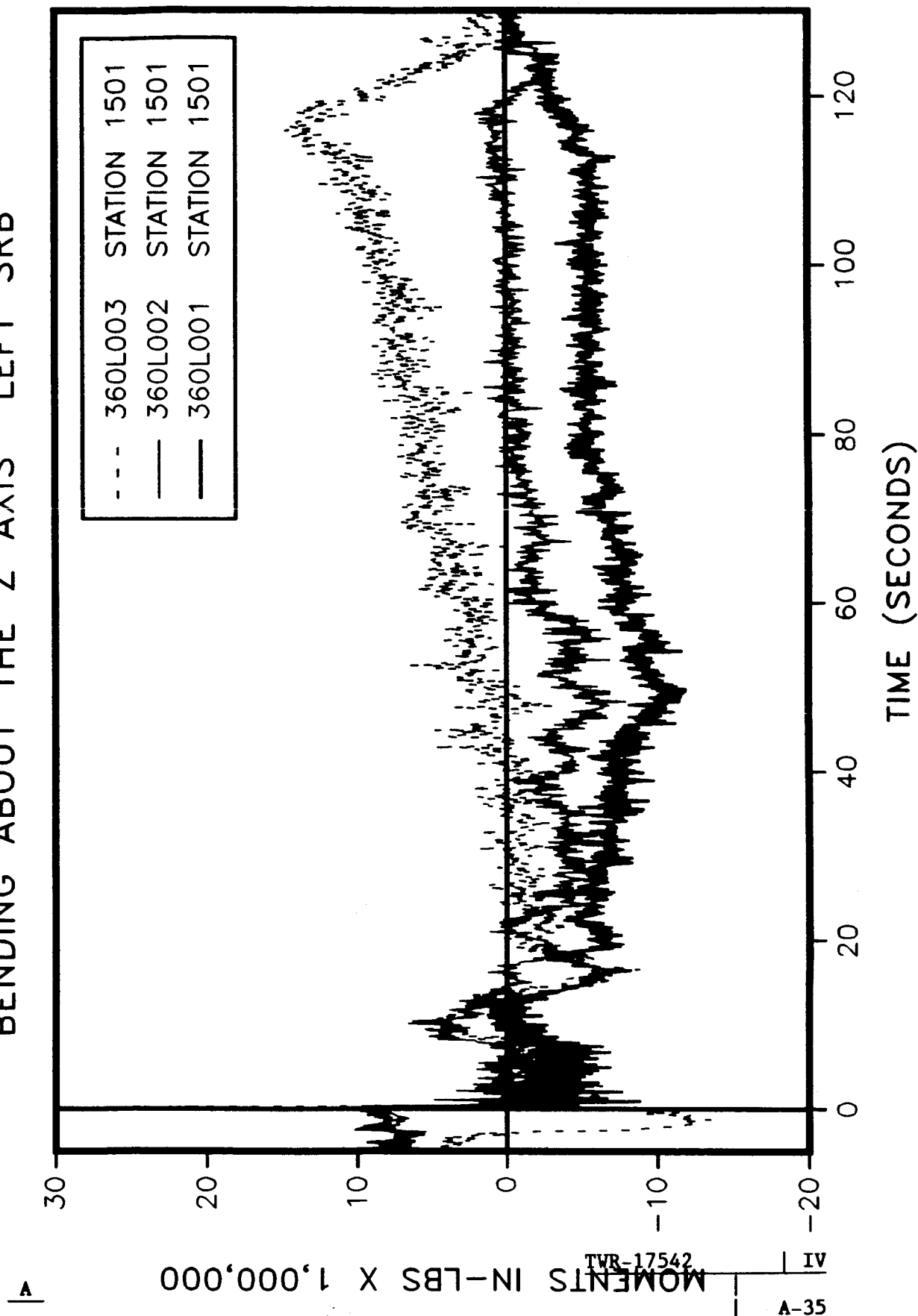
360L003 VS PREVIOUS FLIGHTS

BENDING ABOUT THE Z AXIS LEFT SRB



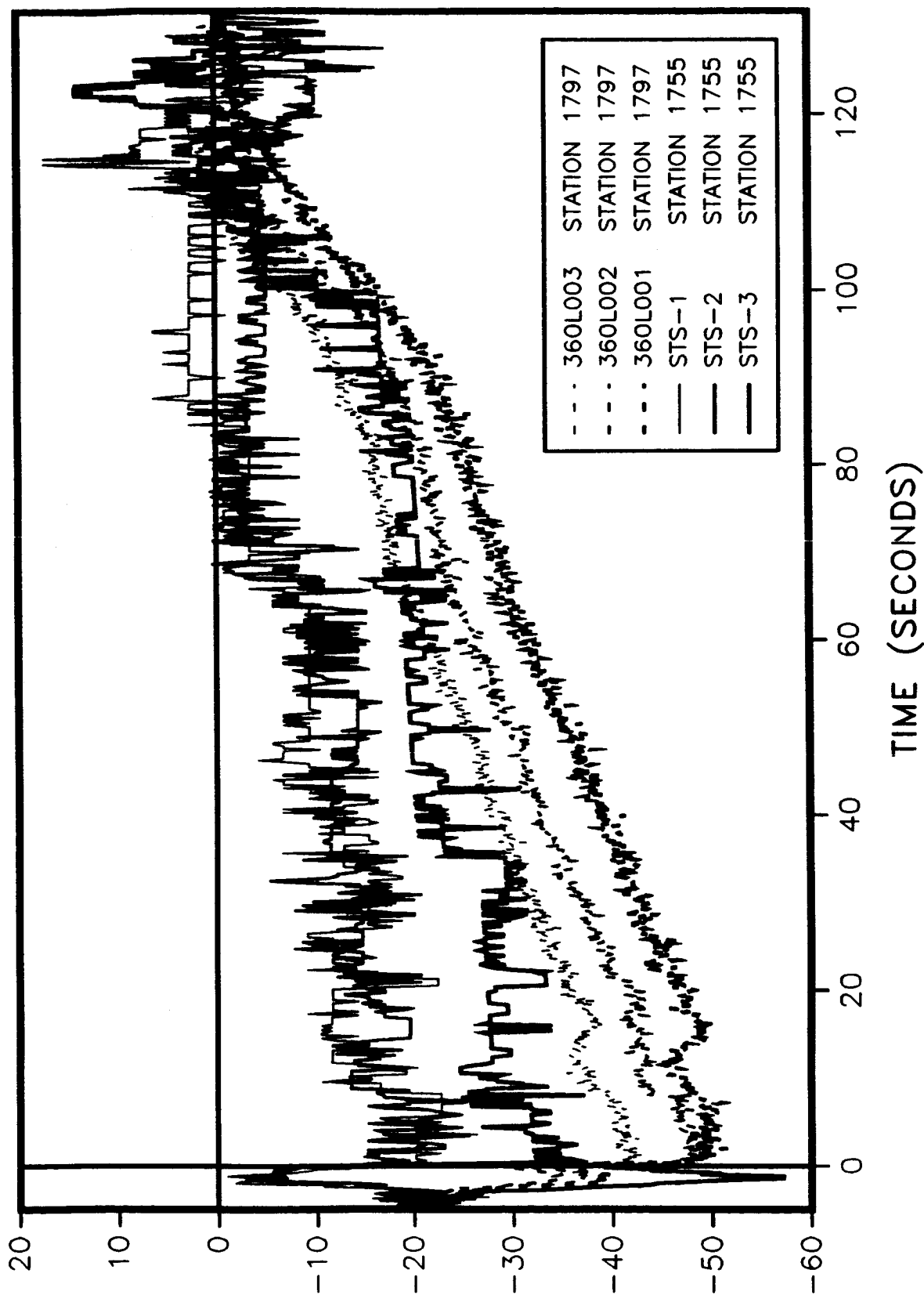
360L003 VS PREVIOUS FLIGHTS

BENDING ABOUT THE Z AXIS LEFT SRB



360L003 VS PREVIOUS FLIGHTS

BENDING ABOUT THE Z AXIS LEFT SRB



MOMENTS IN-LBS X 1,000,000

A-36

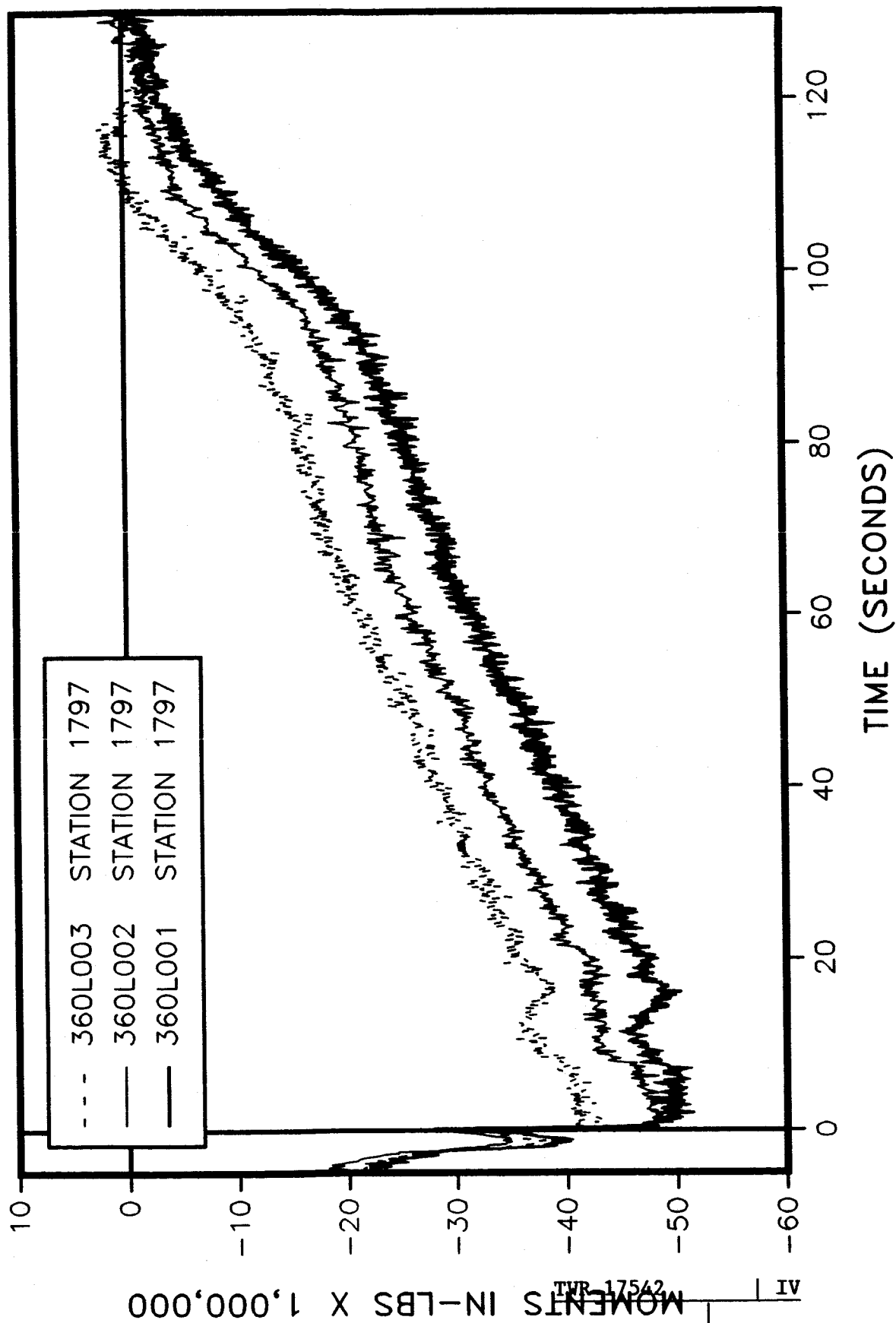
IV

TVR-17542

A

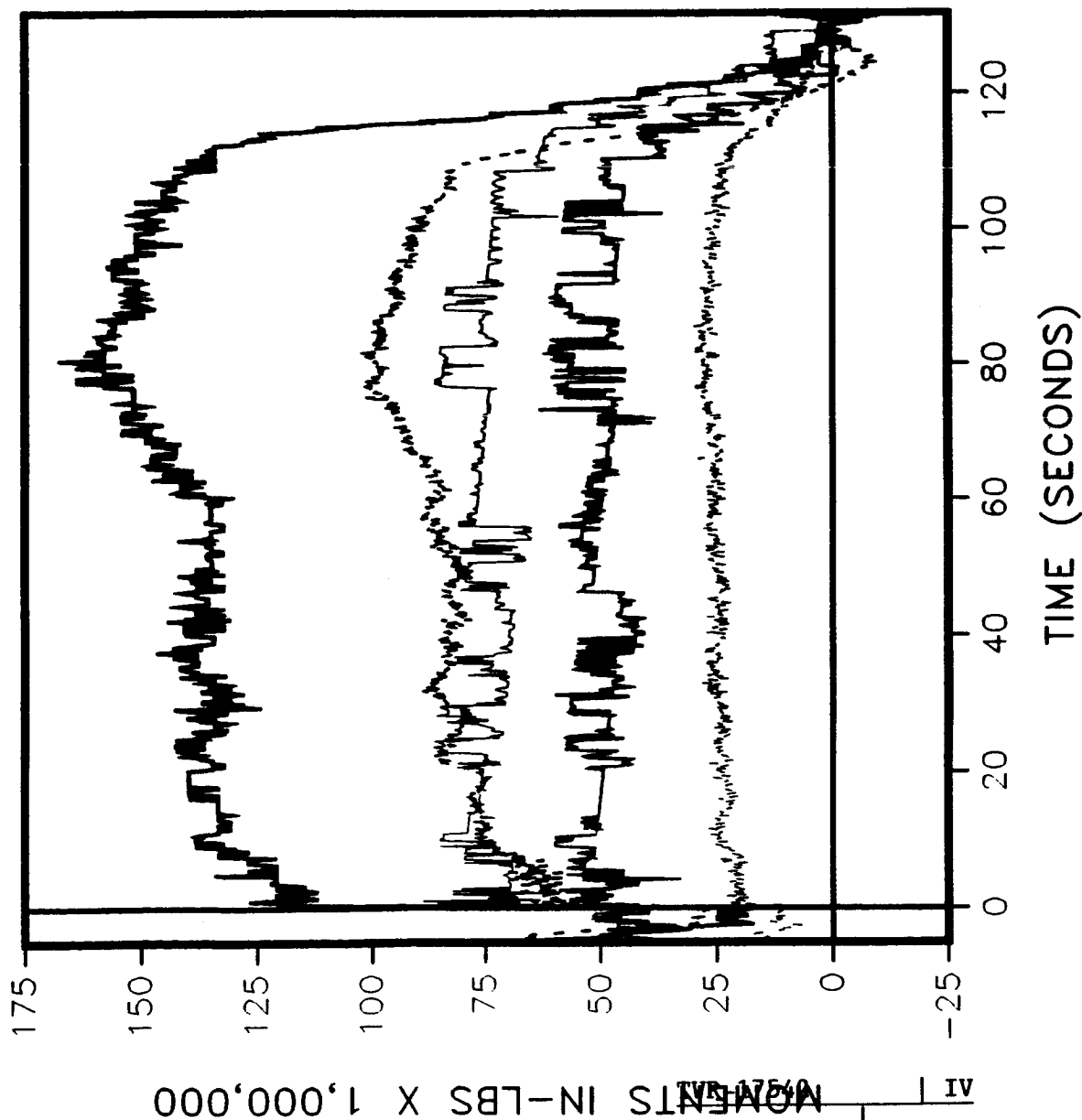
360L003 VS PREVIOUS FLIGHTS

BENDING ABOUT THE Z AXIS LEFT SRB



360L003 VS PREVIOUS FLIGHTS

BENDING ABOUT THE Z AXIS RIGHT SRB



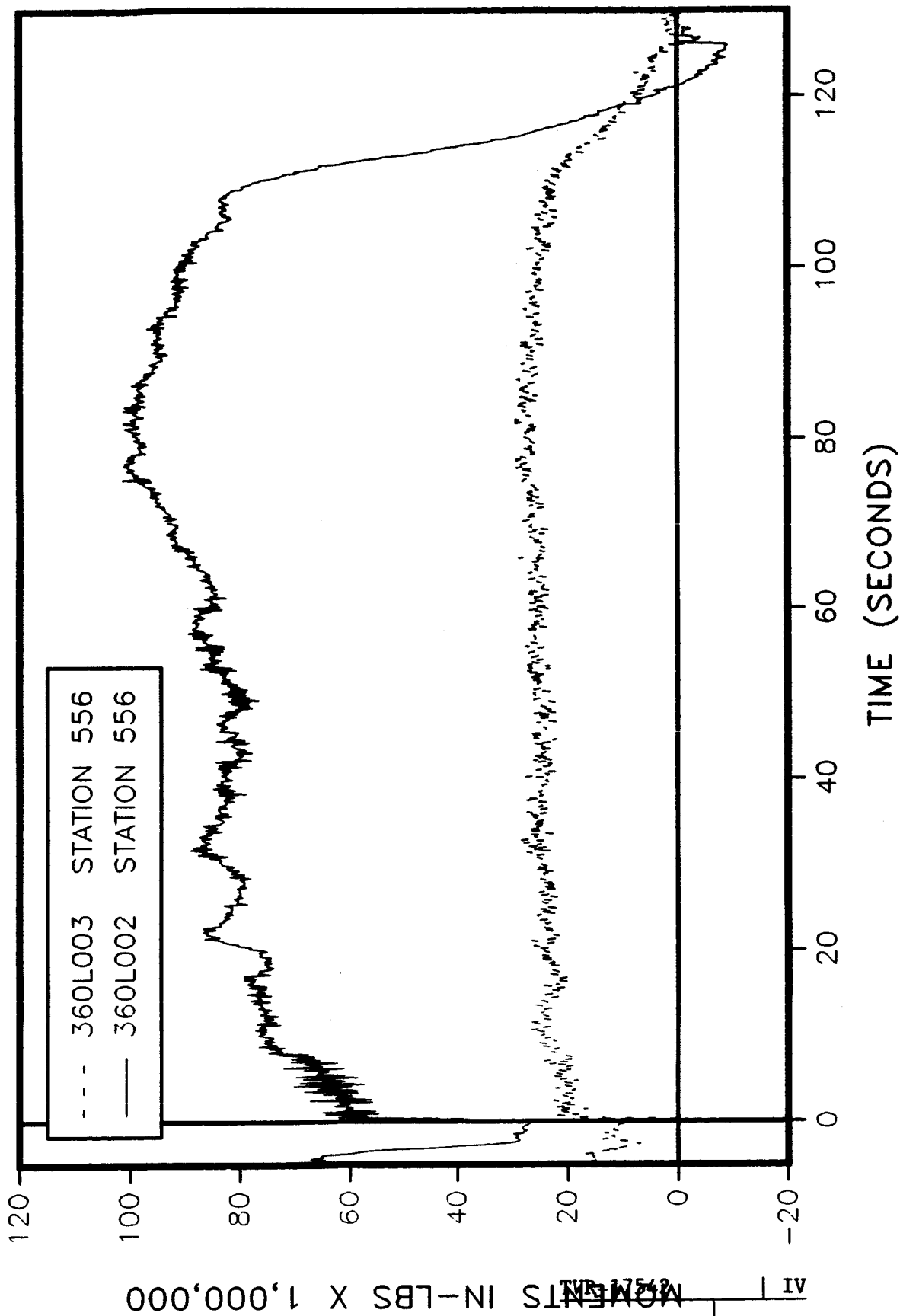
A

MOMENTS IN-LBS X 1,000,000

A-38

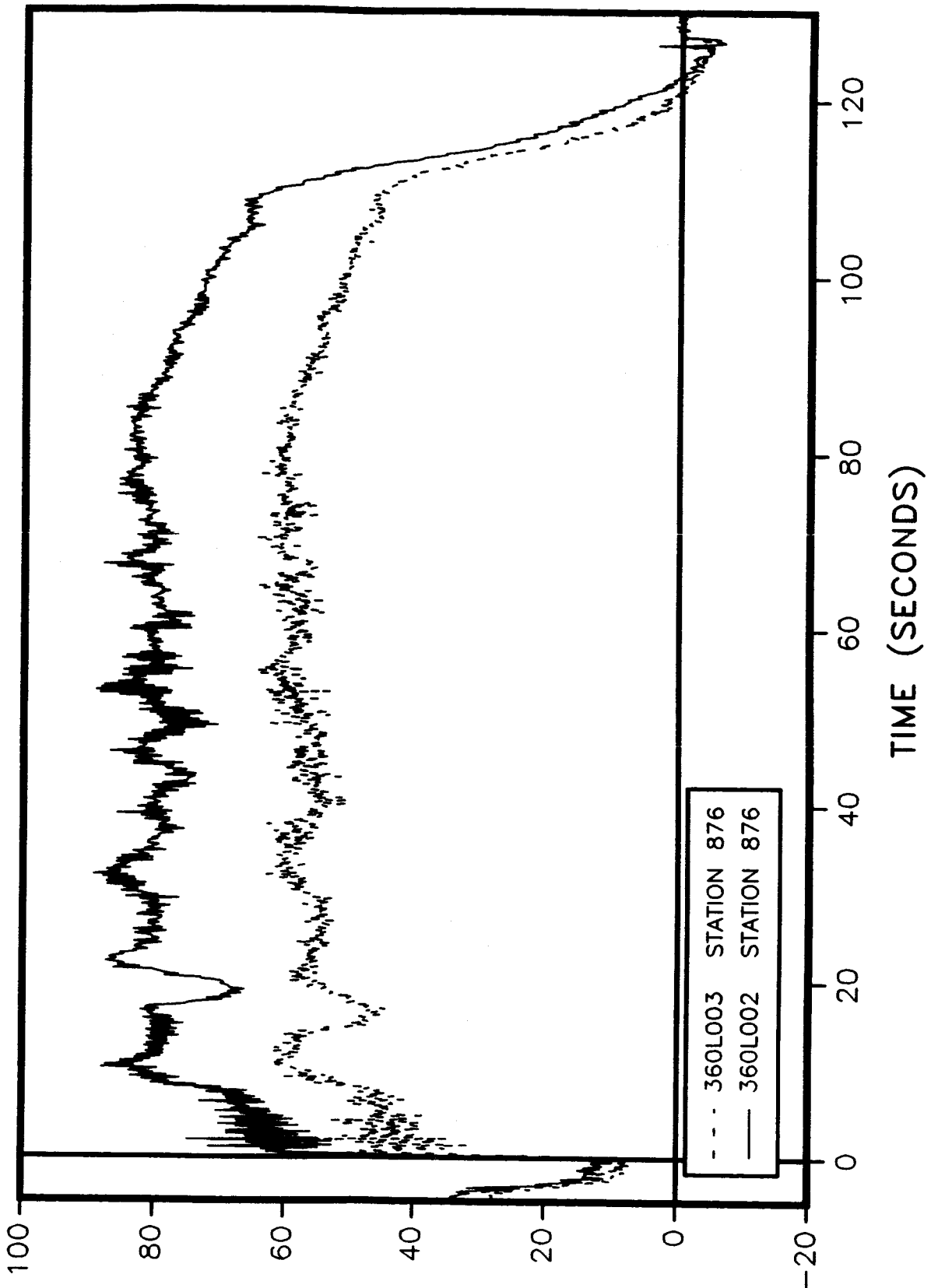
360L003 VS PREVIOUS FLIGHTS

BENDING ABOUT THE Z AXIS RIGHT SRB



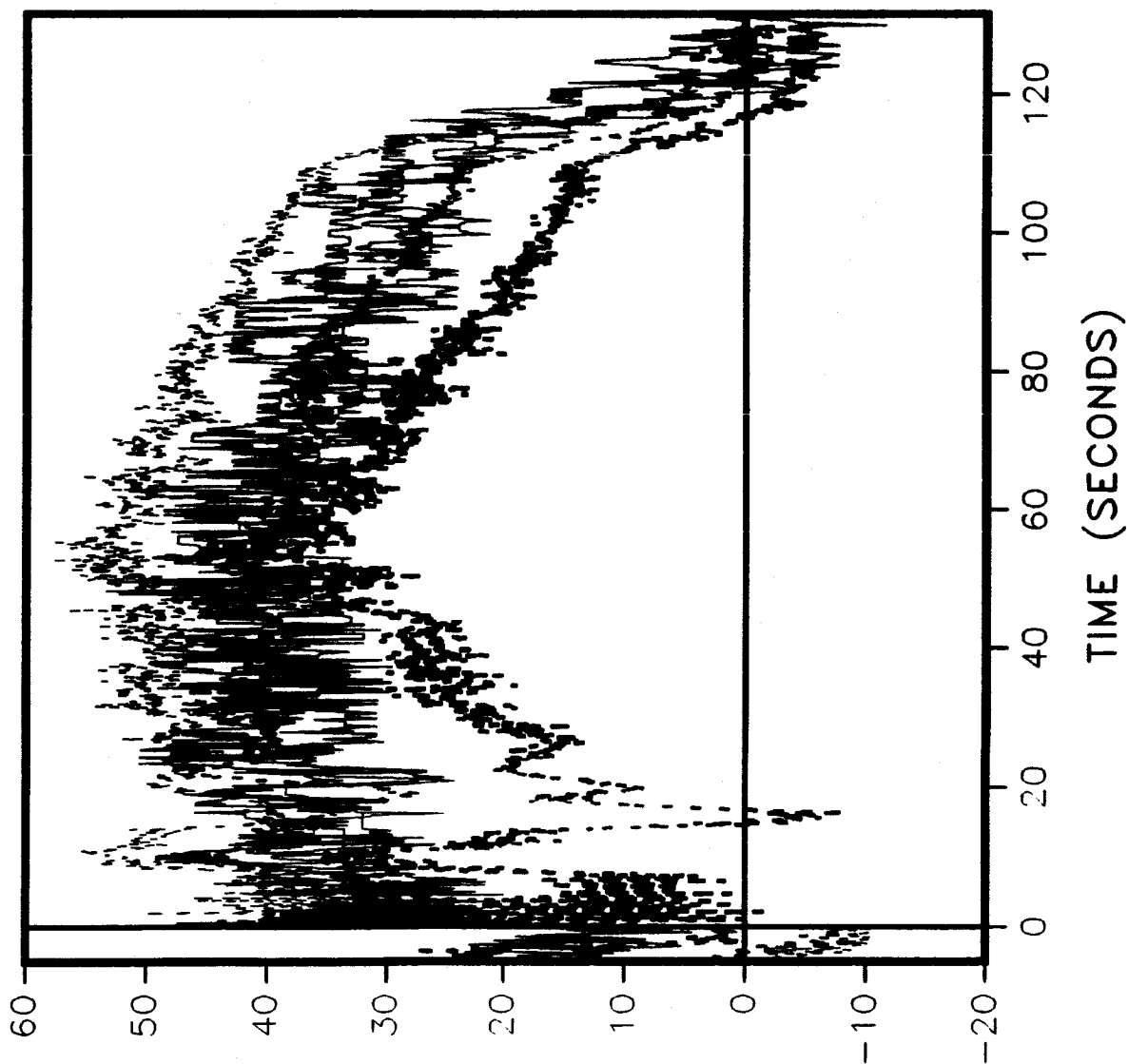
360L003 VS PREVIOUS FLIGHTS

BENDING ABOUT THE Z AXIS RIGHT SRB



360L003 VS PREVIOUS FLIGHTS

BENDING ABOUT THE Z AXIS RIGHT SRB



---	360L003	STATION 1196
---	360L002	STATION 1196
---	360L001	STATION 1196
---	STS-1	STATION 1251
---	STS-2	STATION 1251
---	STS-3	STATION 1251

MOMENTS IN-LBS X 1,000,000

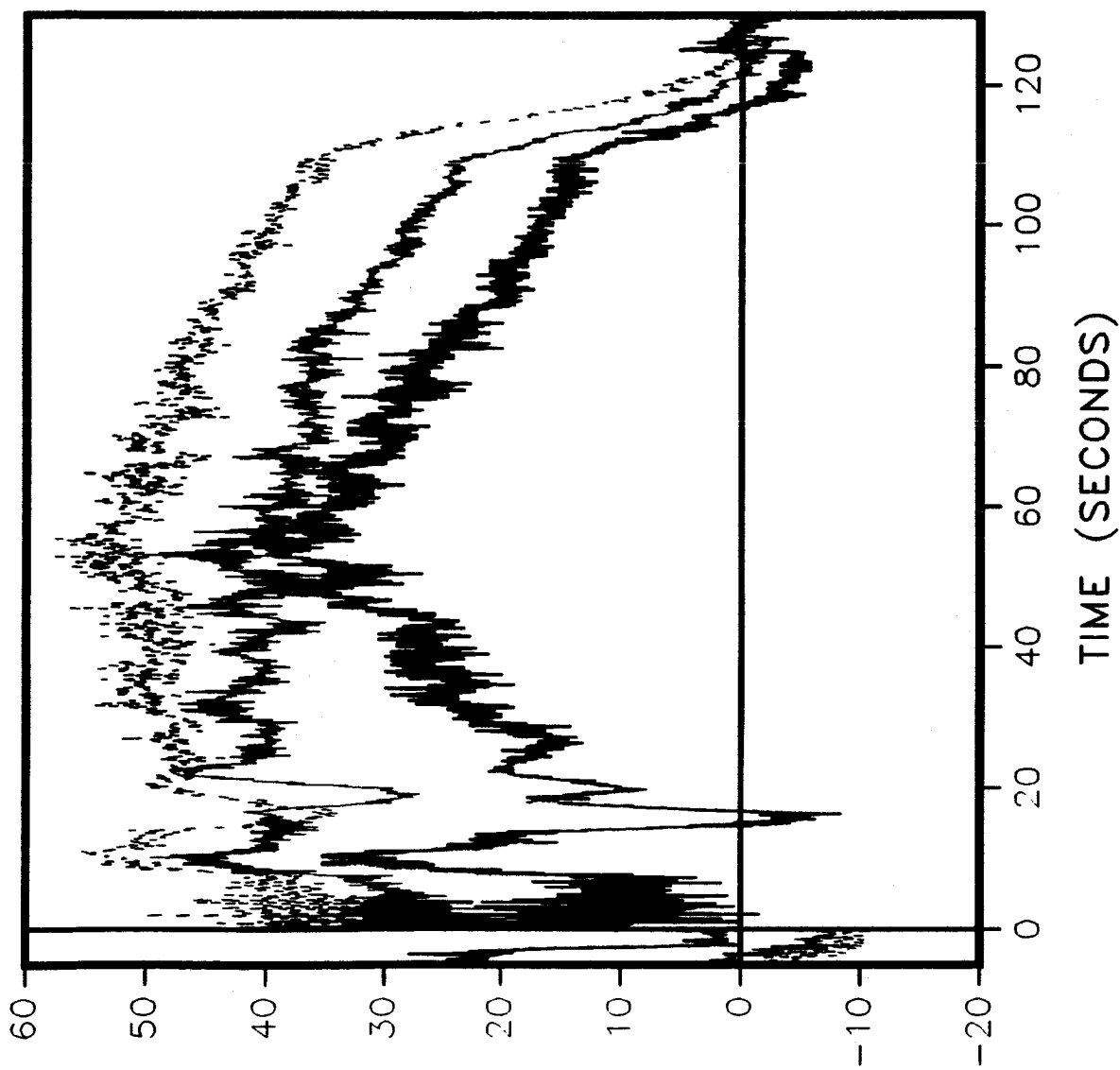
IV

A-41

A

360L003 VS PREVIOUS FLIGHTS

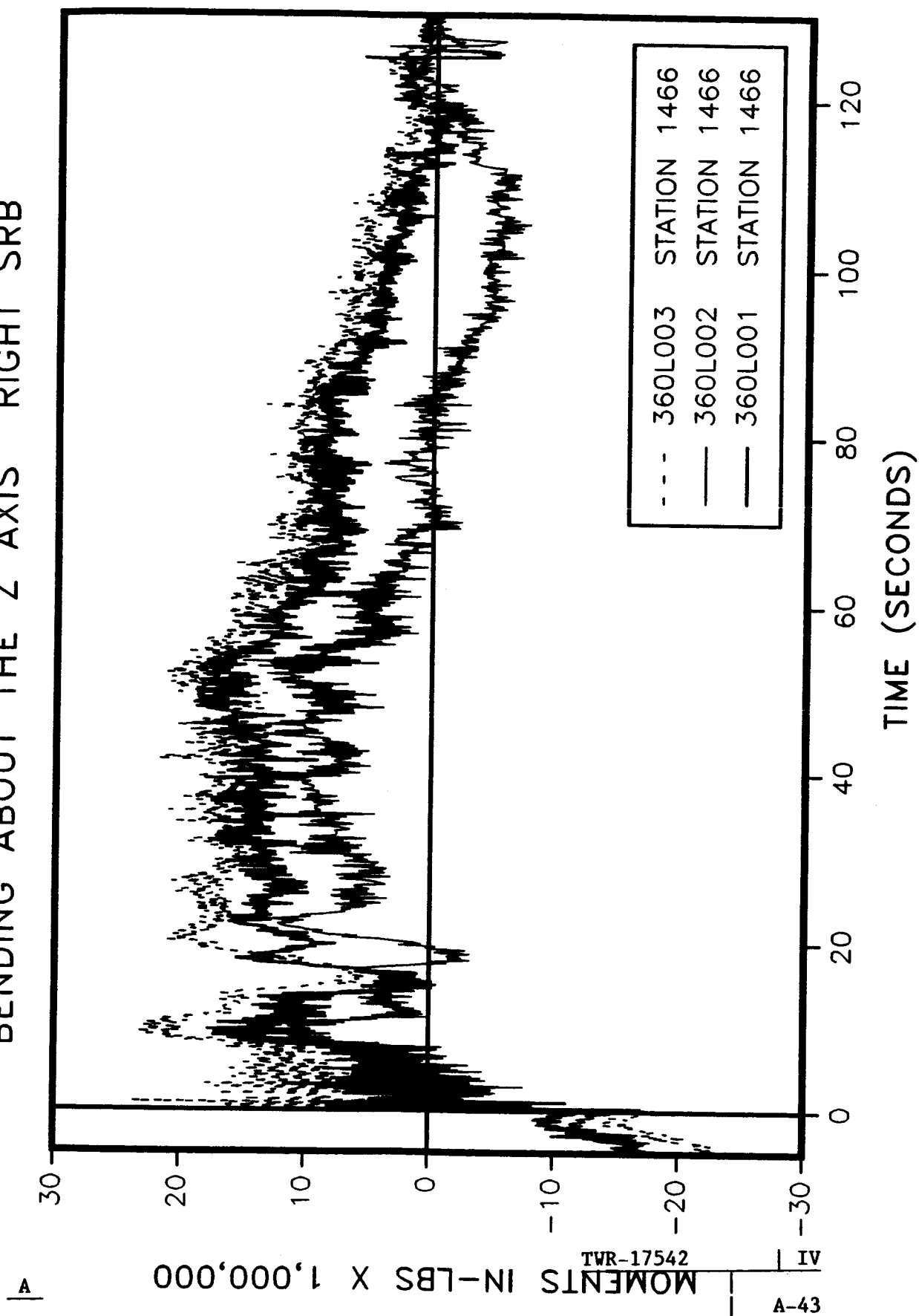
BENDING ABOUT THE Z AXIS RIGHT SRB



MOMENTS IN-LBS X 1,000,000

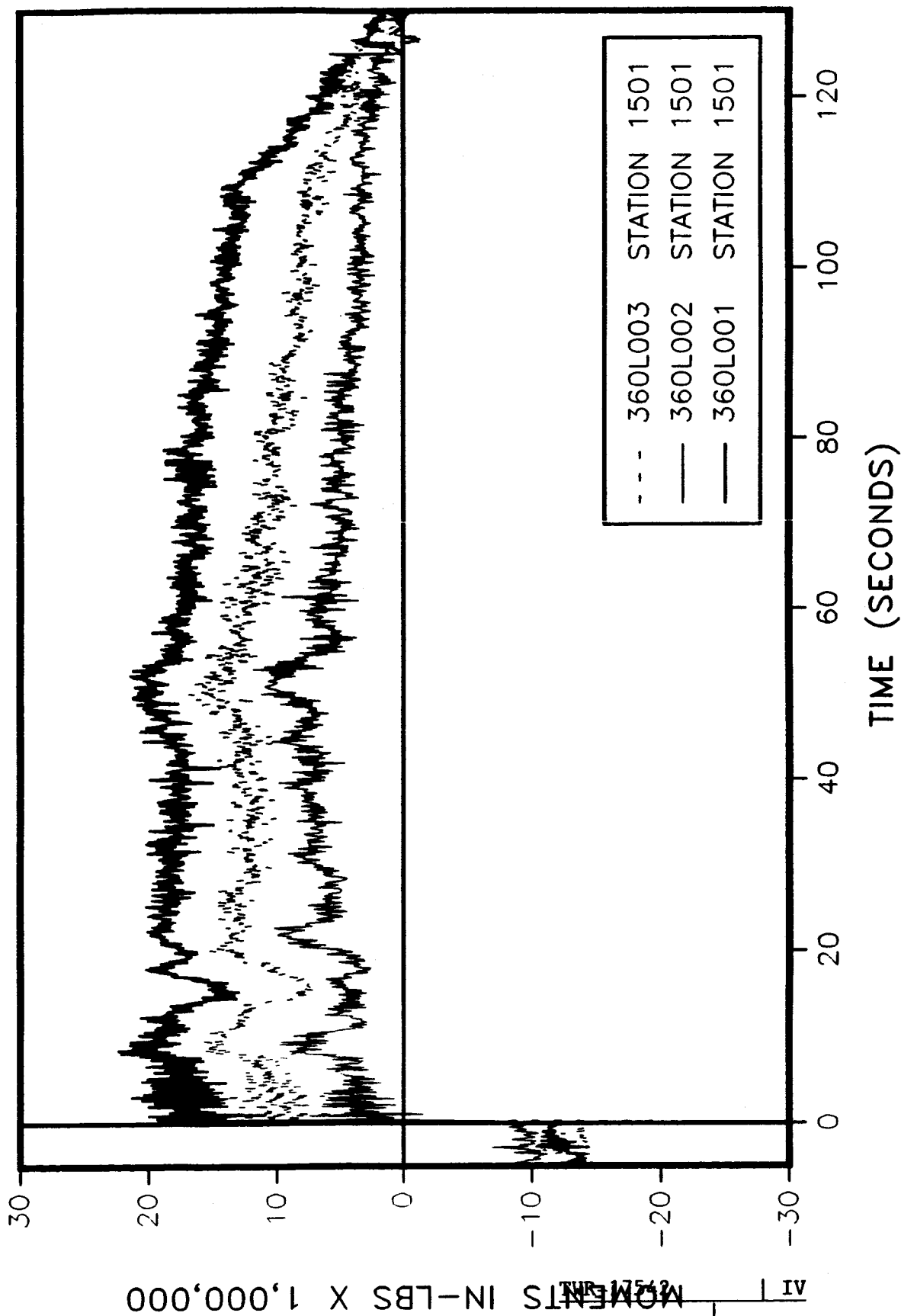
360L003 VS PREVIOUS FLIGHTS

BENDING ABOUT THE Z AXIS RIGHT SRB



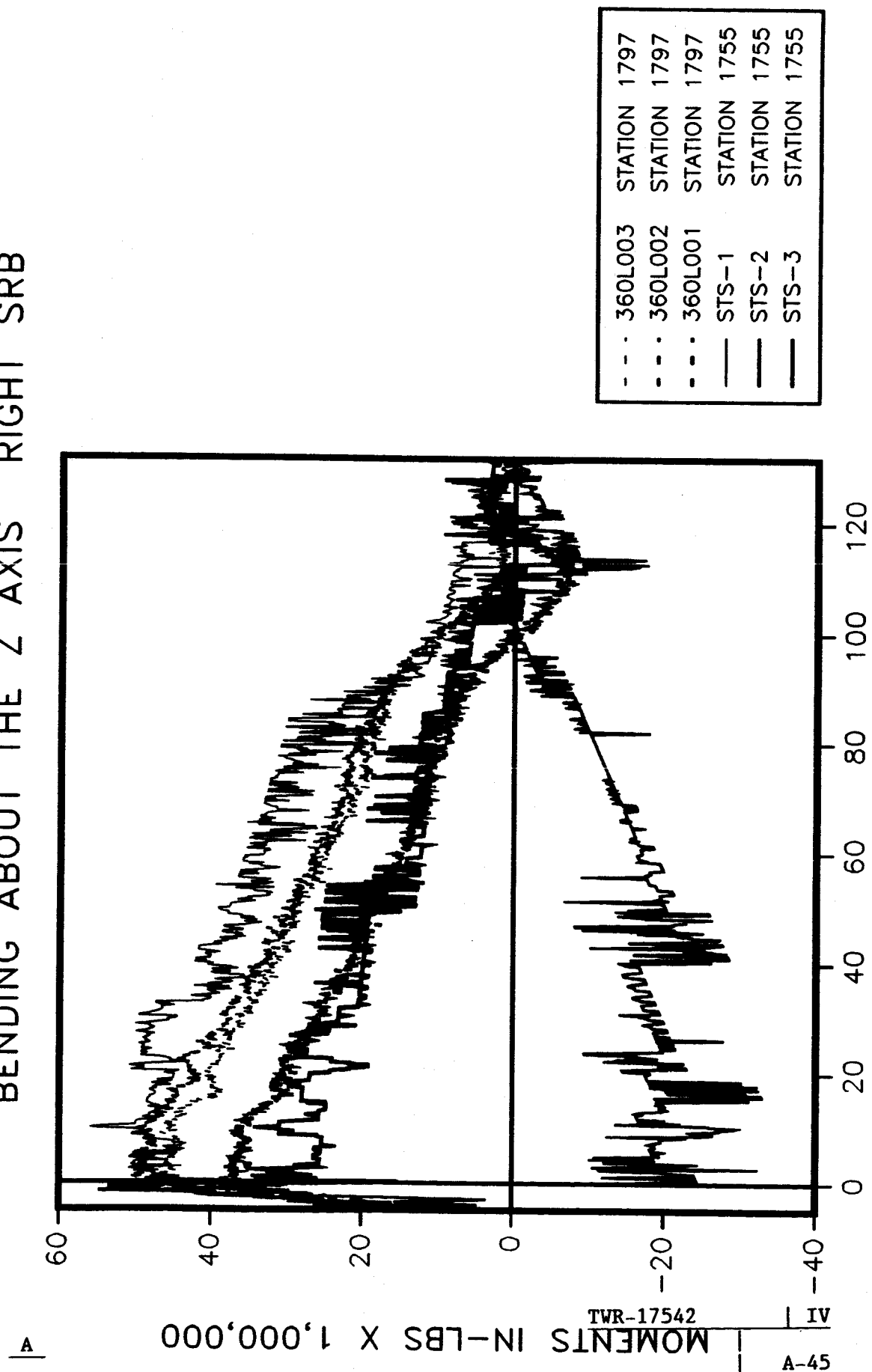
360L003 VS PREVIOUS FLIGHTS

BENDING ABOUT THE Z AXIS RIGHT SRB



360L003 VS PREVIOUS FLIGHTS

BENDING ABOUT THE Z AXIS RIGHT SRB



MOMENTS IN-LBS X 1,000,000

TWR-17542

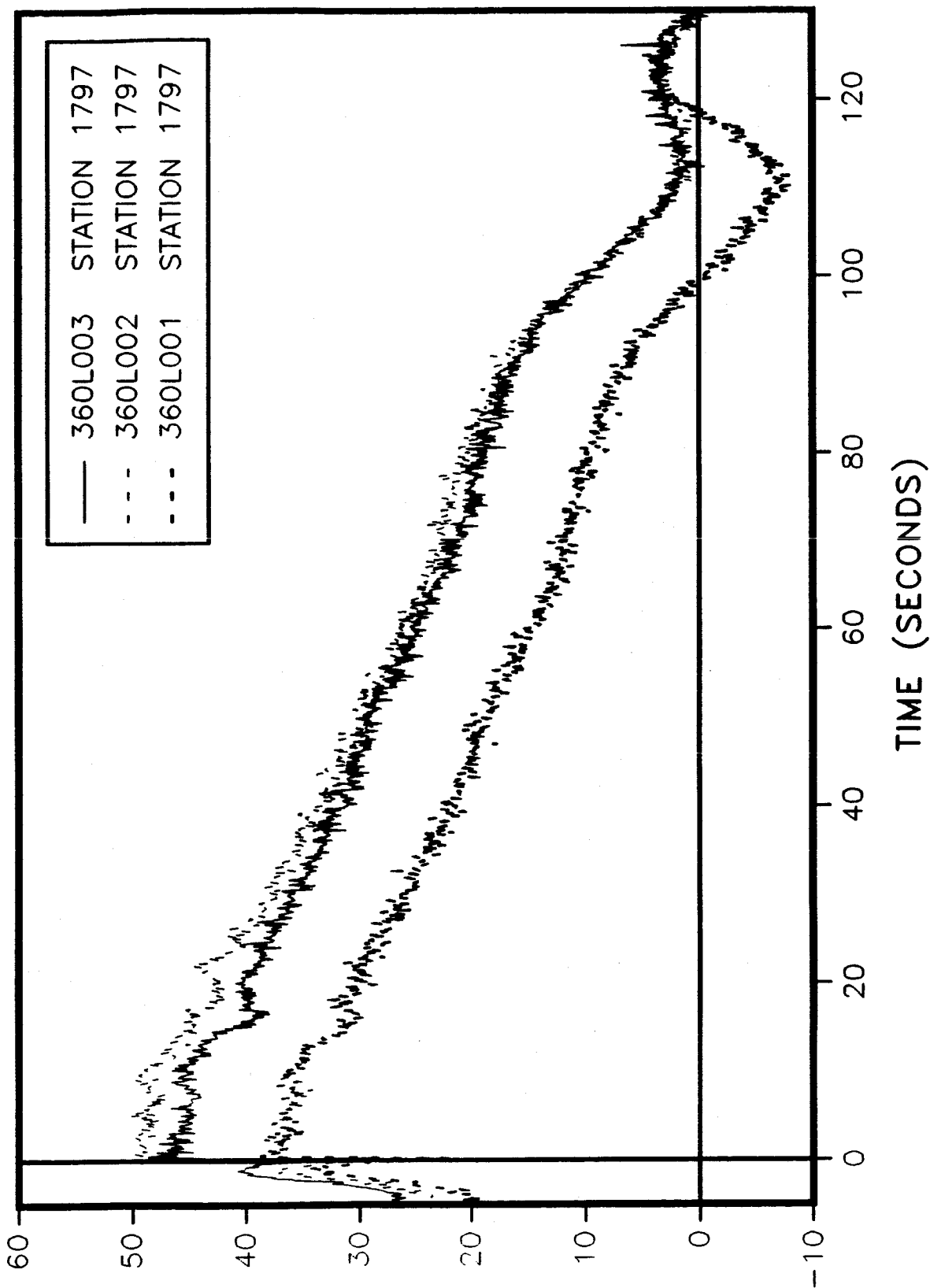
A-45

A

TIME (SECONDS)

360L003 VS PREVIOUS FLIGHTS

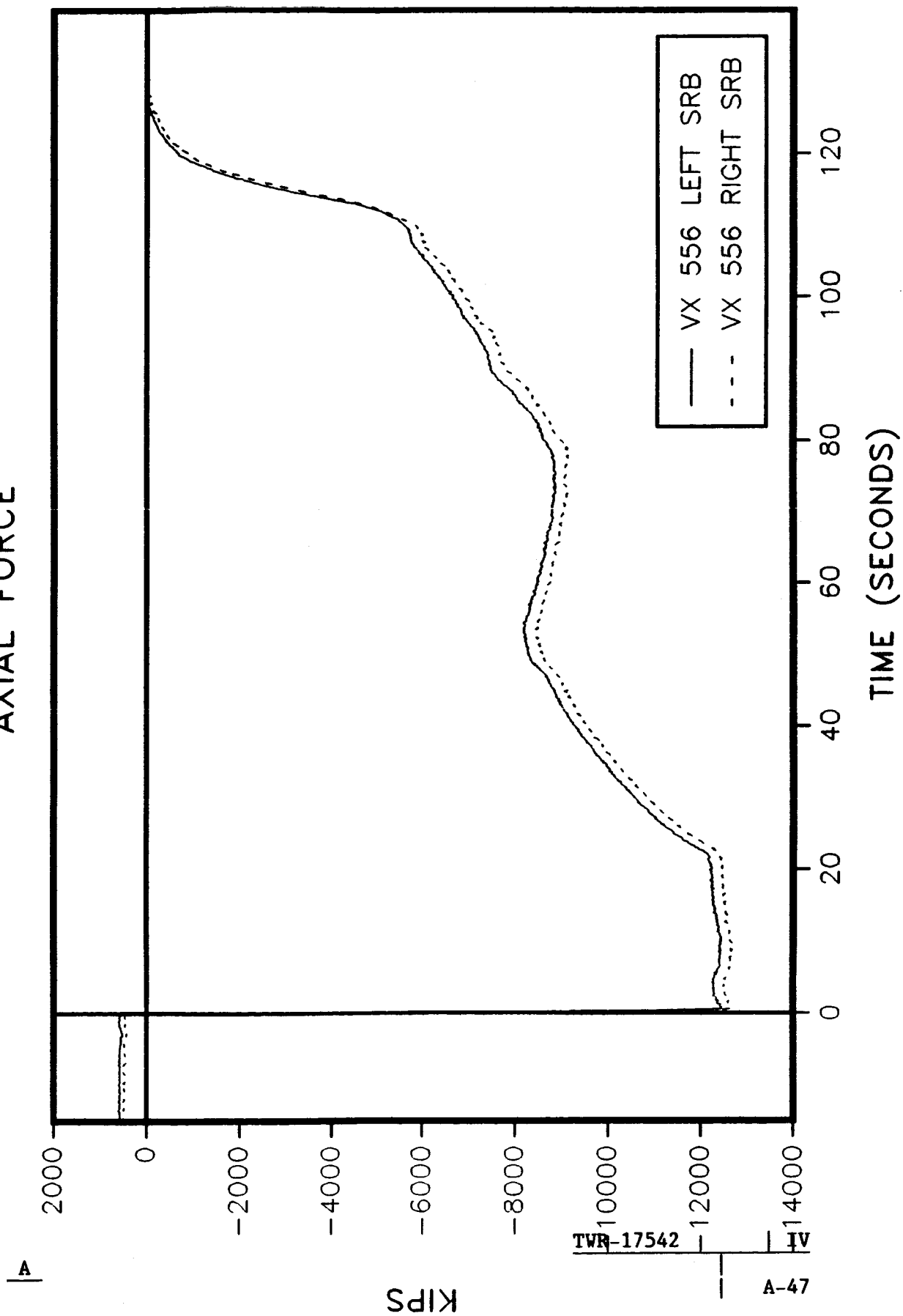
BENDING ABOUT THE Z AXIS RIGHT SRB



MOMENTS IN-LBS X 1,000,000

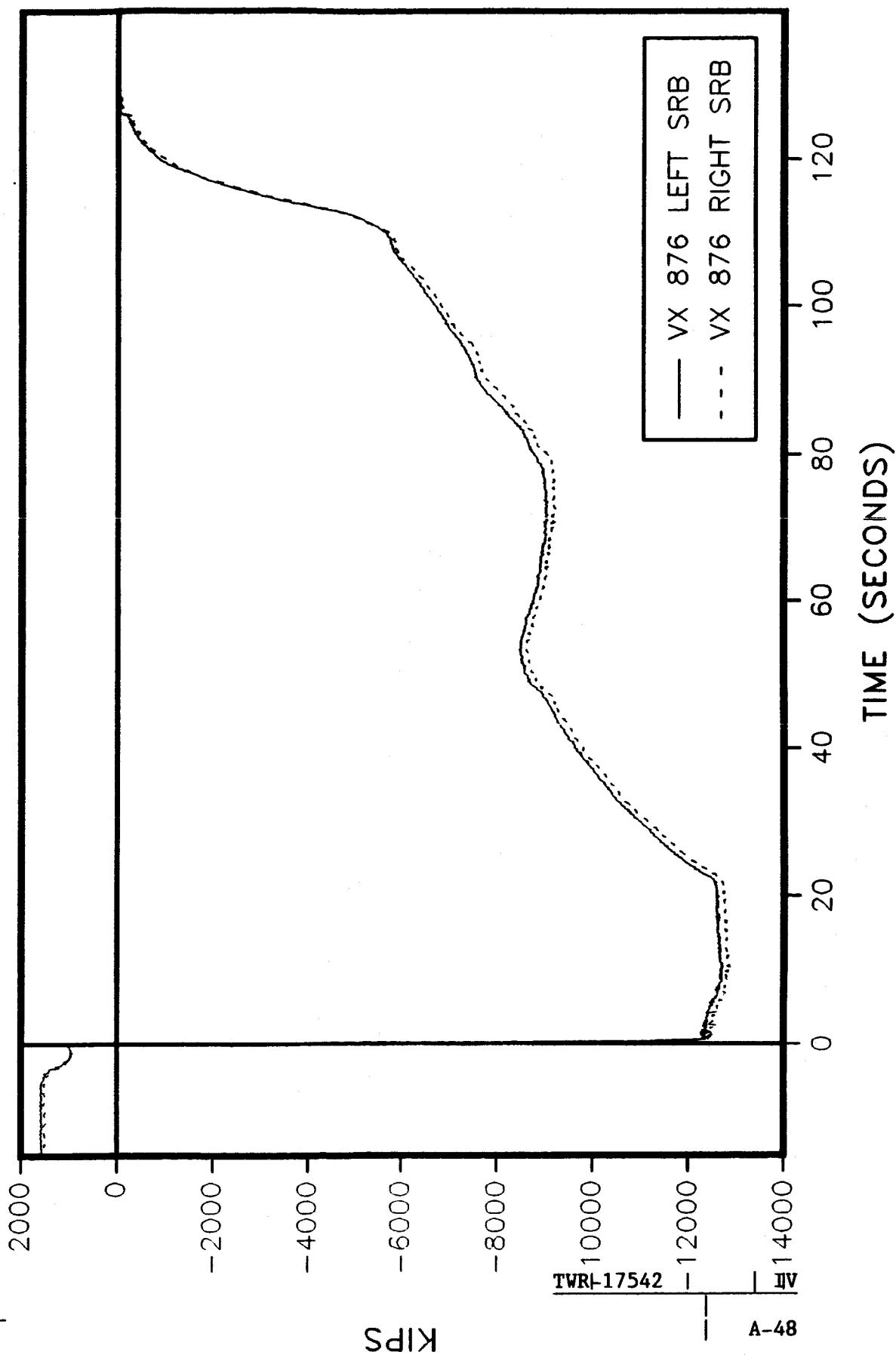
360L003 STATION 556

AXIAL FORCE



360L003 STATION 876

AXIAL FORCE



A

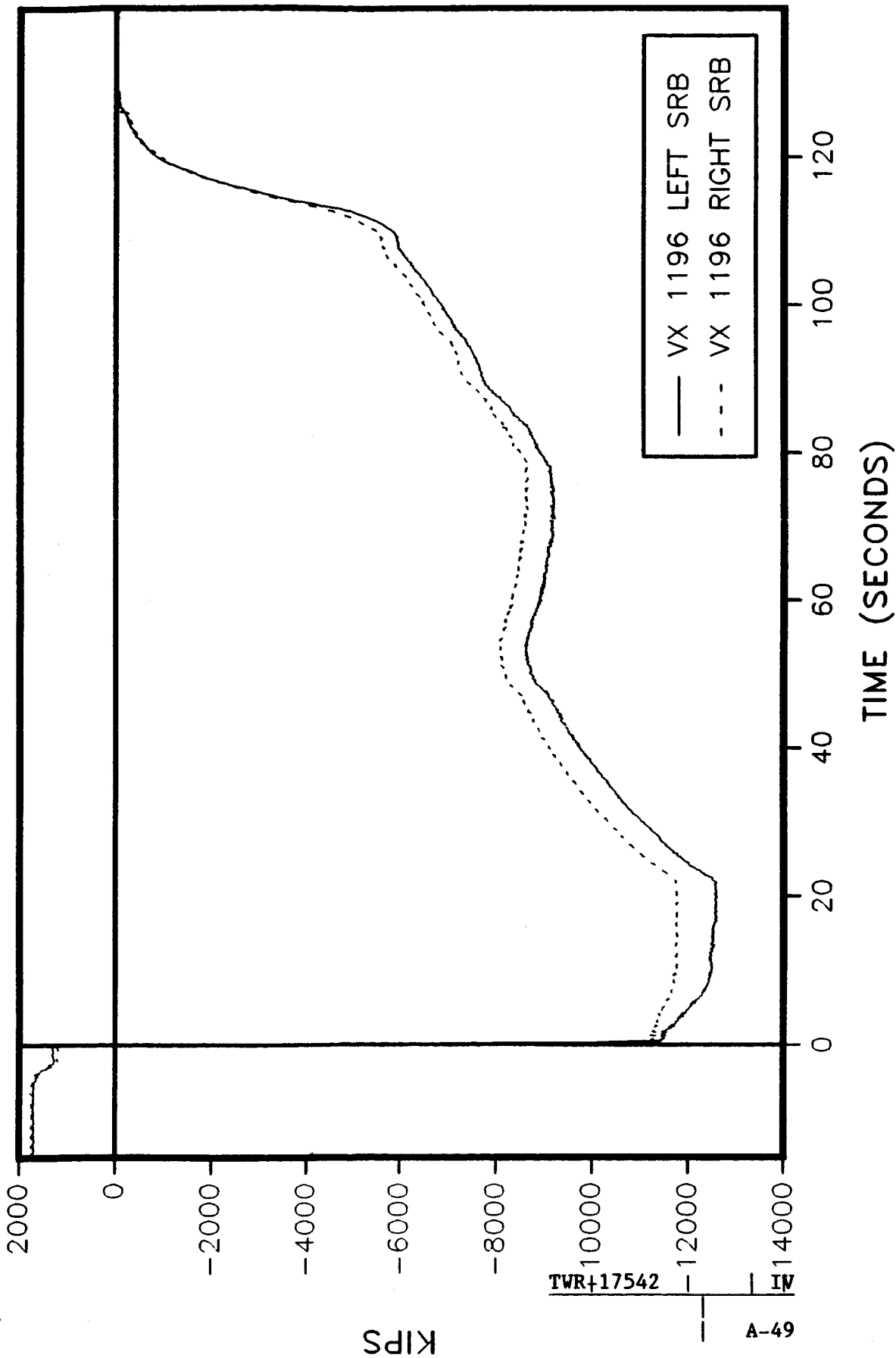
KIPS

TWR-17542

A-48

360L003 STATION 1196

AXIAL FORCE



A

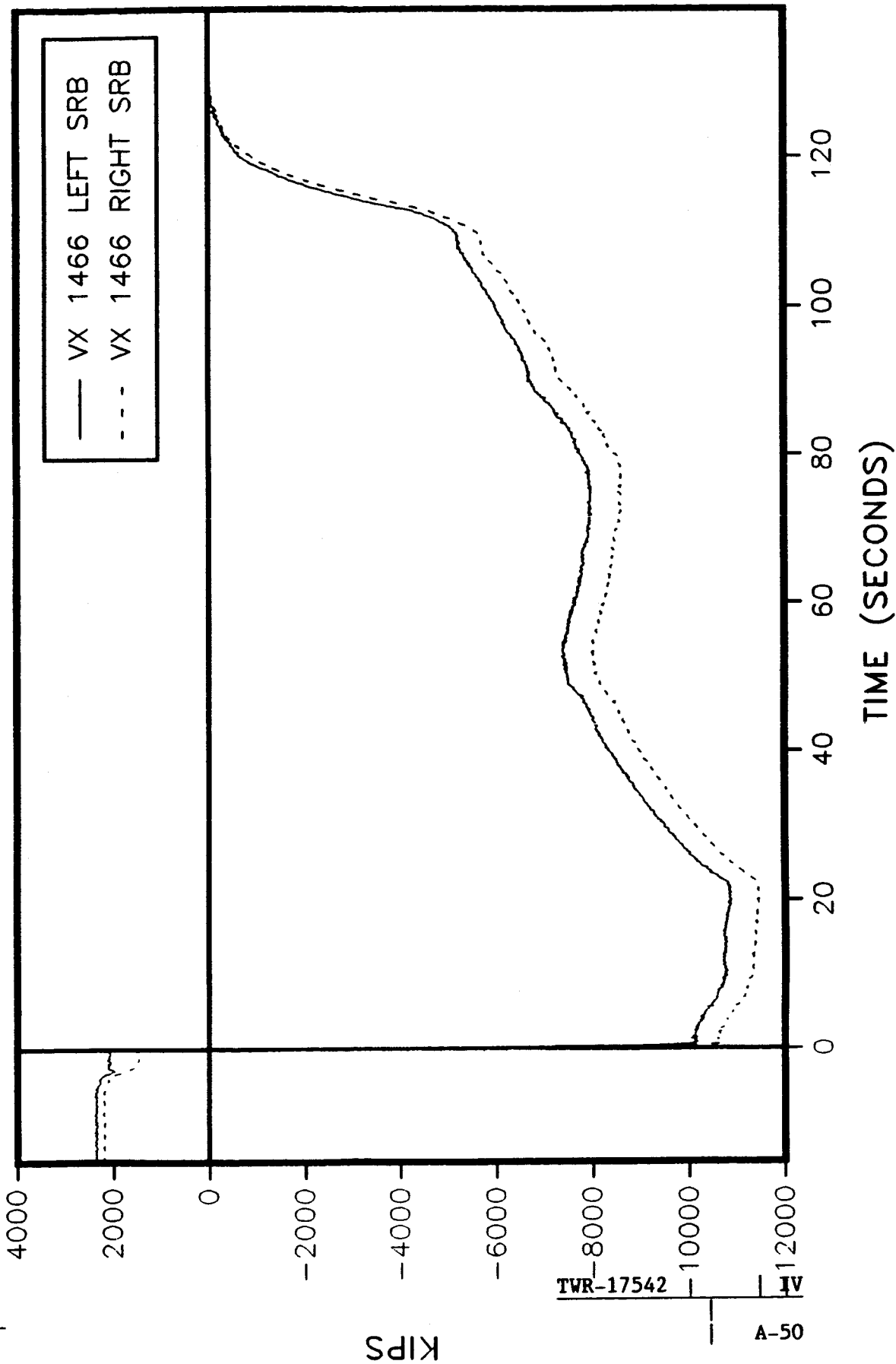
KIPS

TWR+17542

A-49

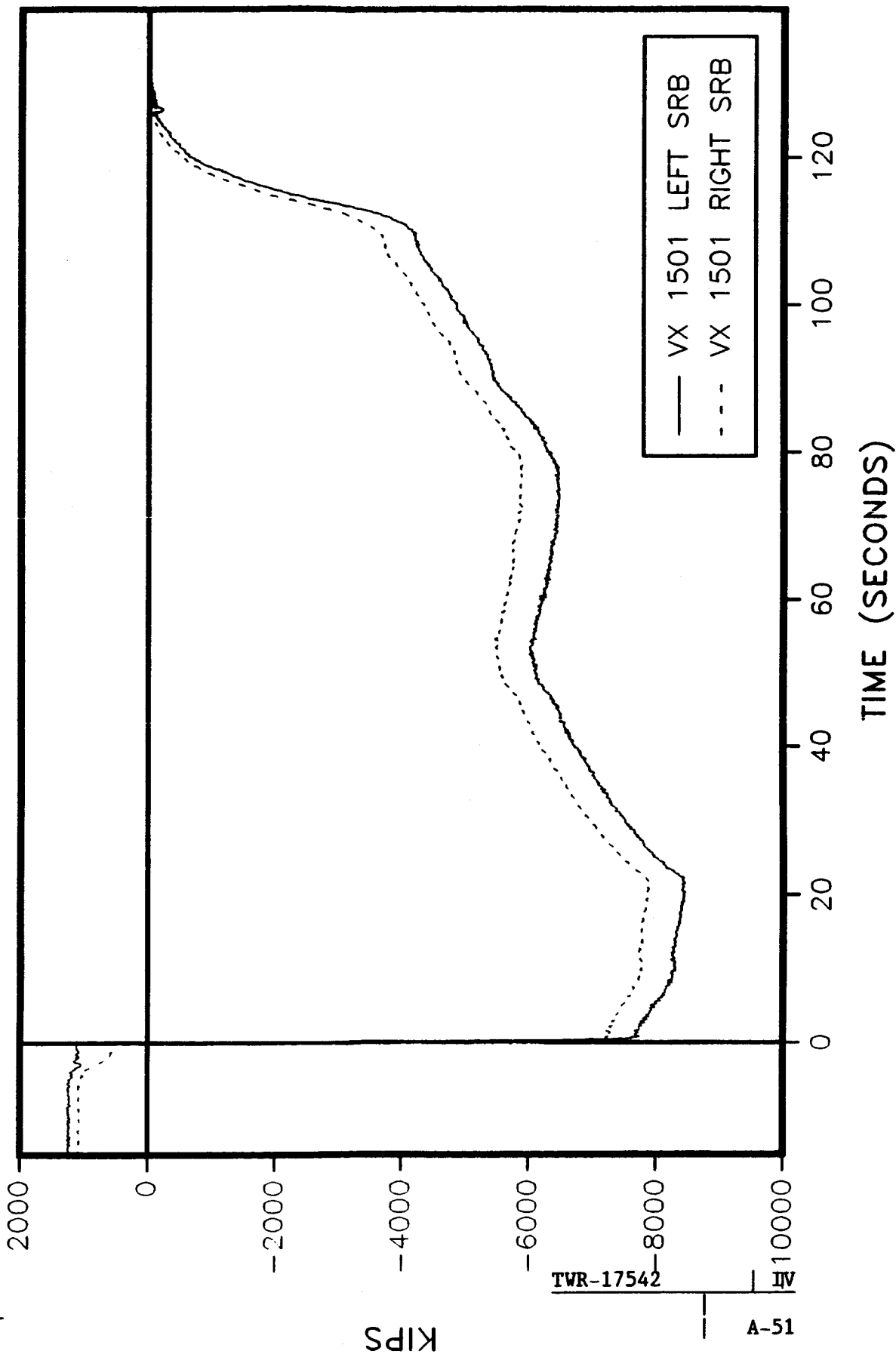
360L003 STATION 1466

AXIAL FORCE



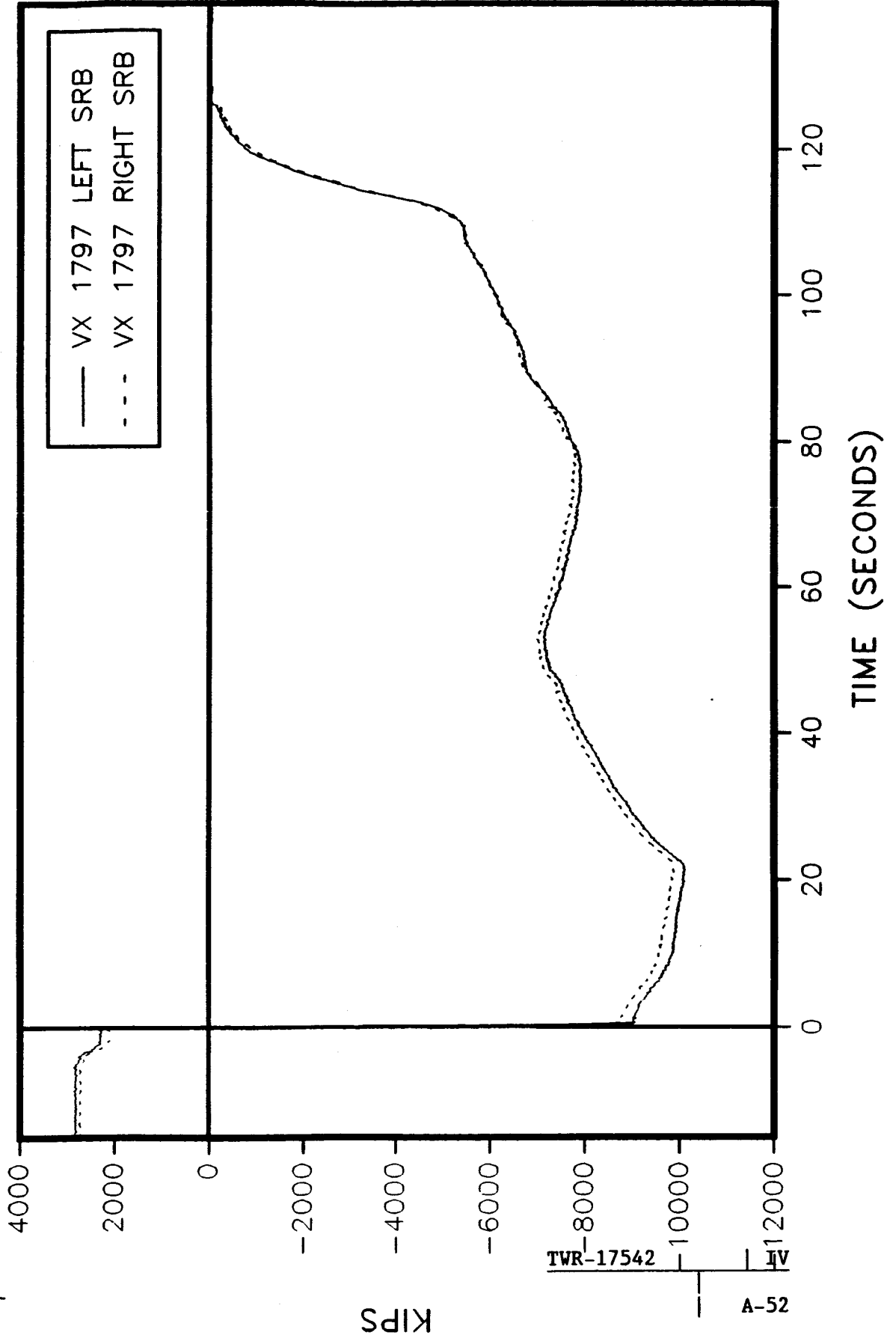
360L003 STATION 1501

AXIAL FORCE



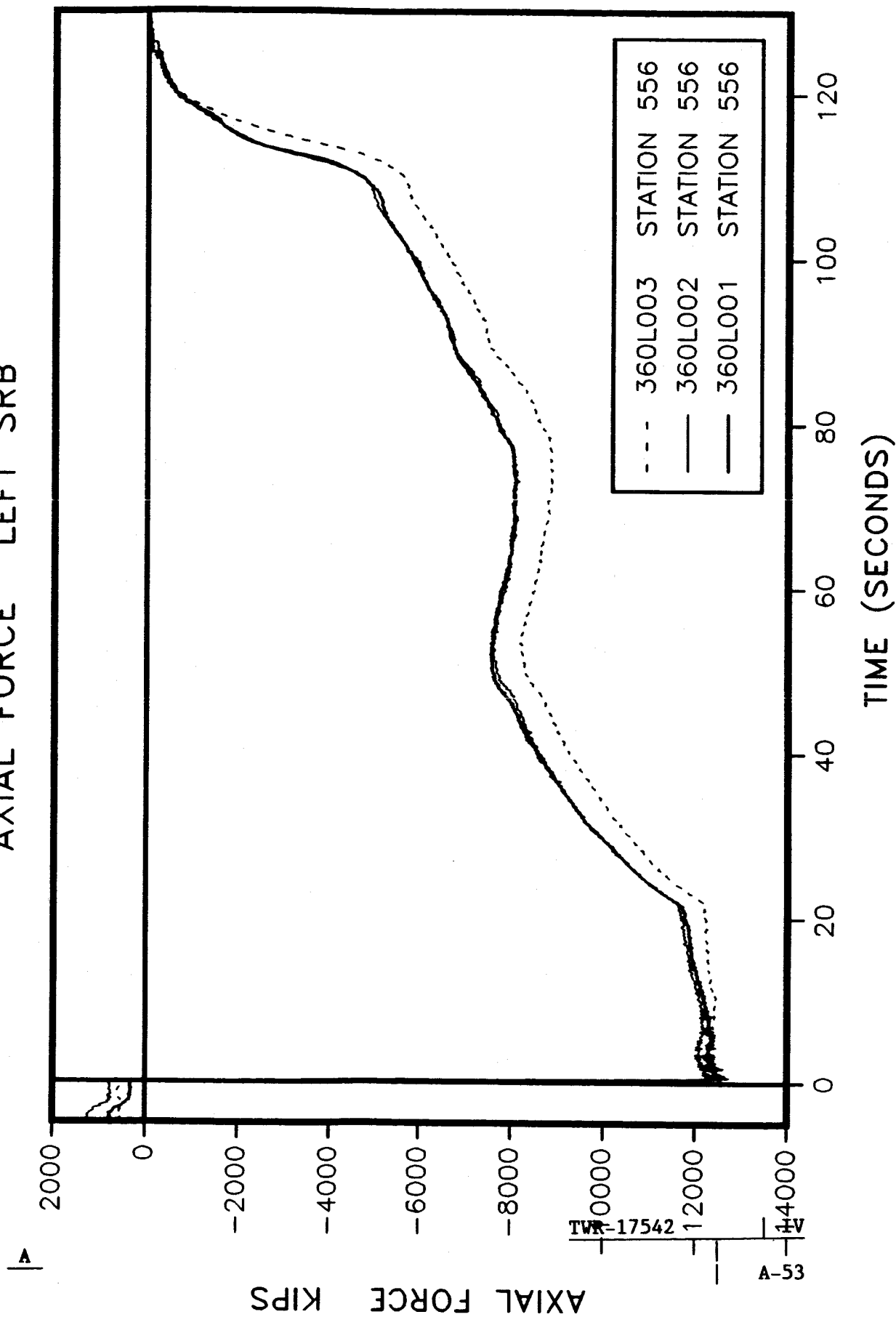
360L003 STATION 1797

AXIAL FORCE



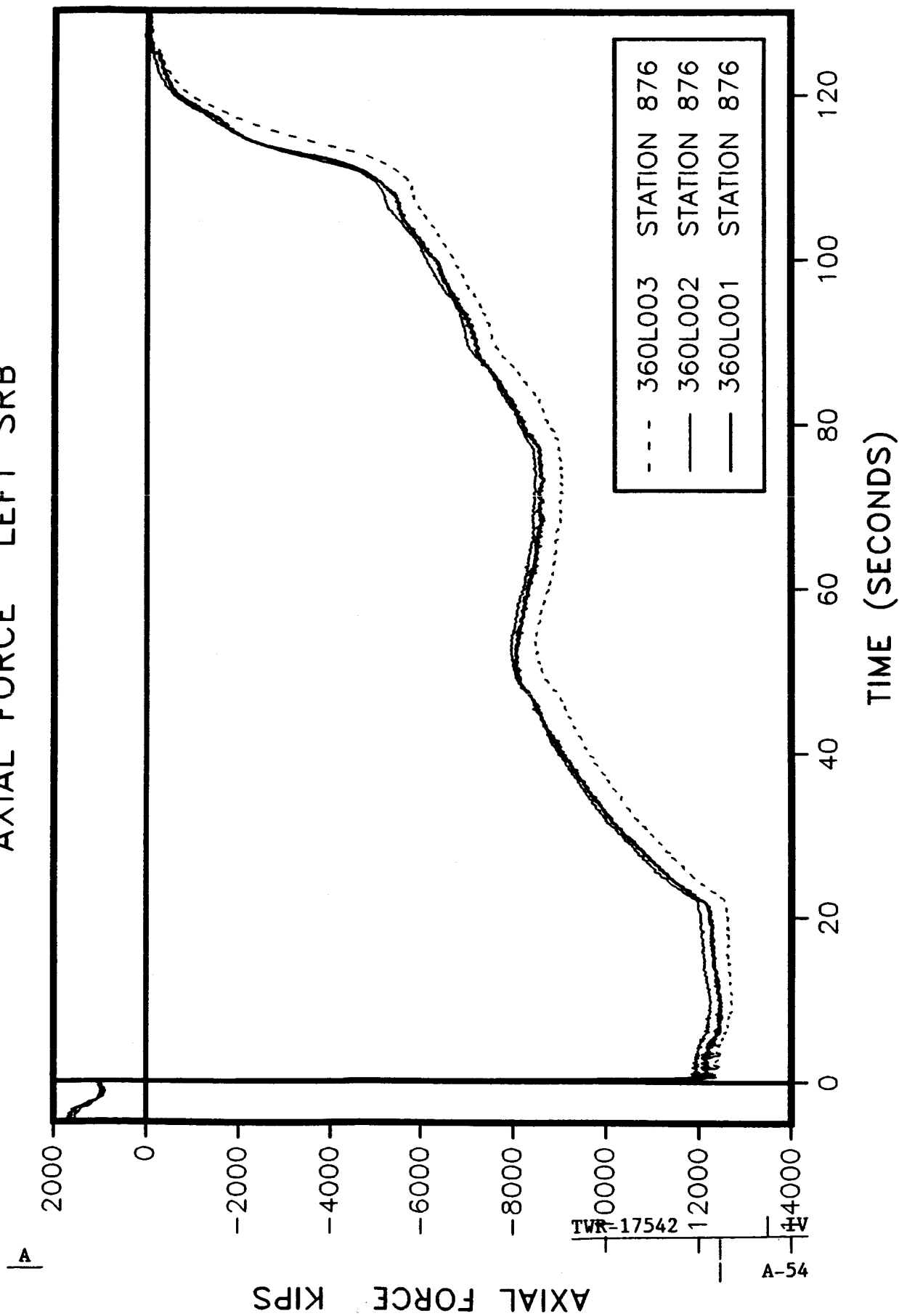
360L003 VS PREVIOUS FLIGHTS

AXIAL FORCE LEFT SRB



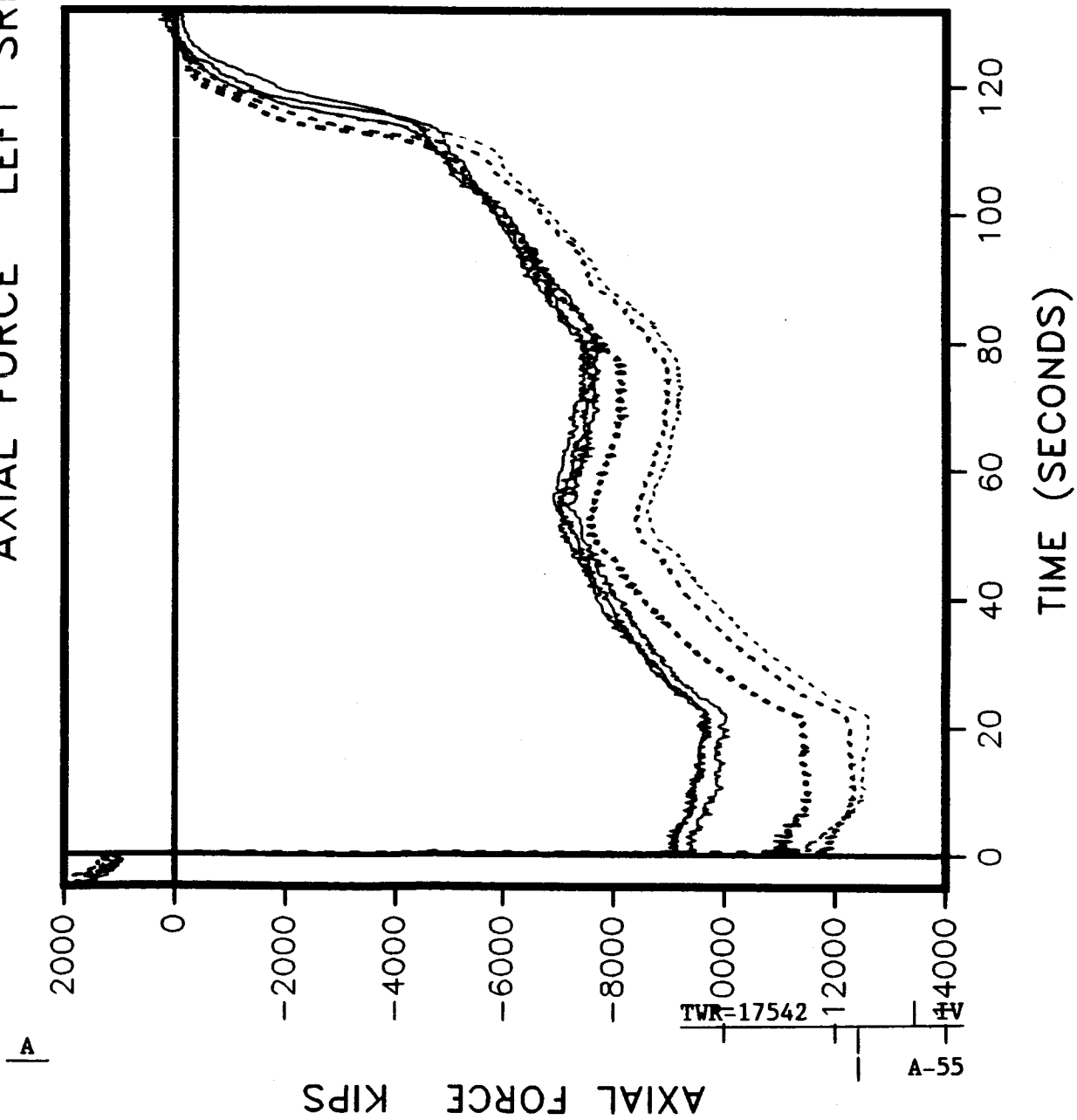
360L003 VS PREVIOUS FLIGHTS

AXIAL FORCE LEFT SRB



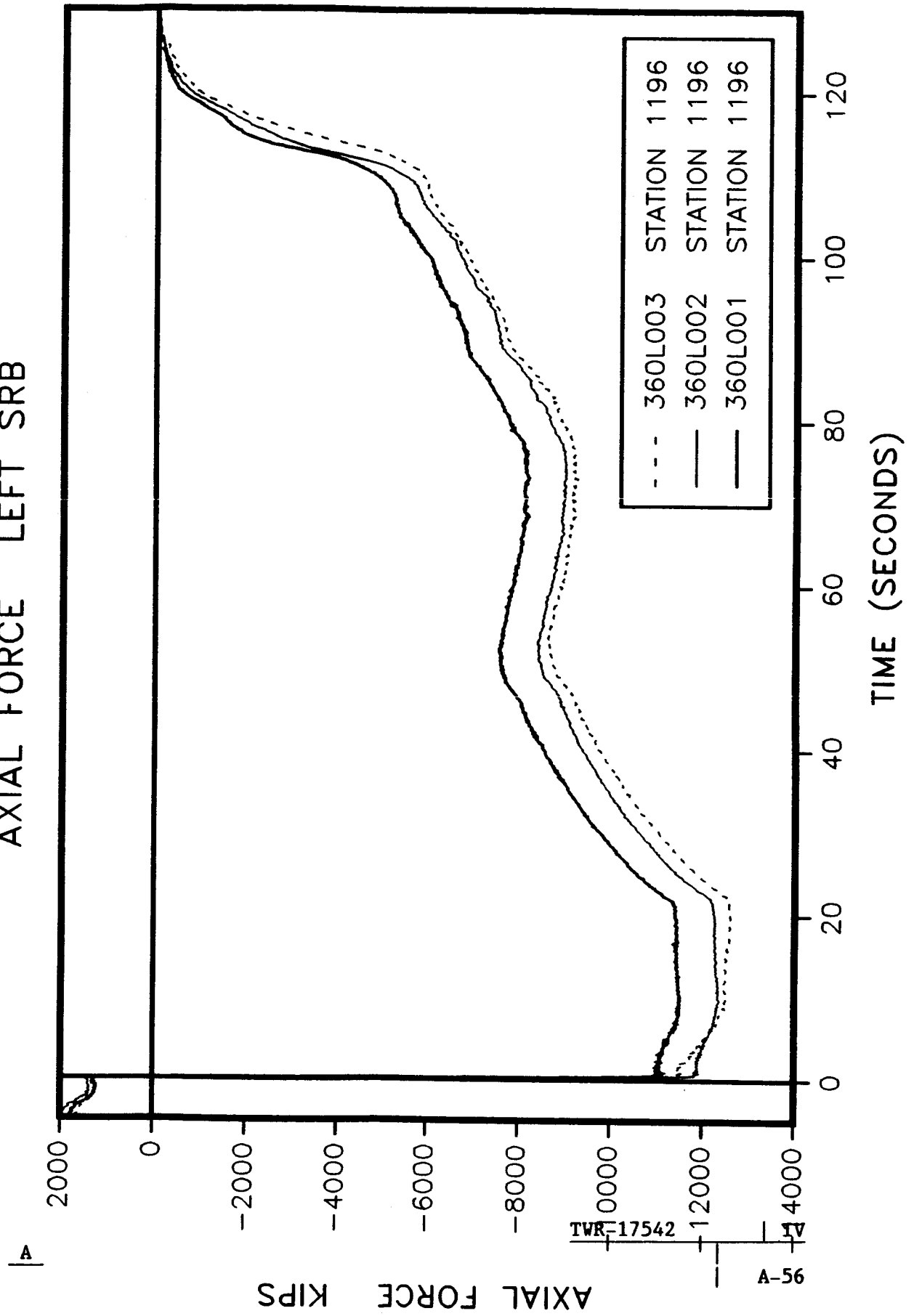
360L003 VS PREVIOUS FLIGHTS

AXIAL FORCE LEFT SRB



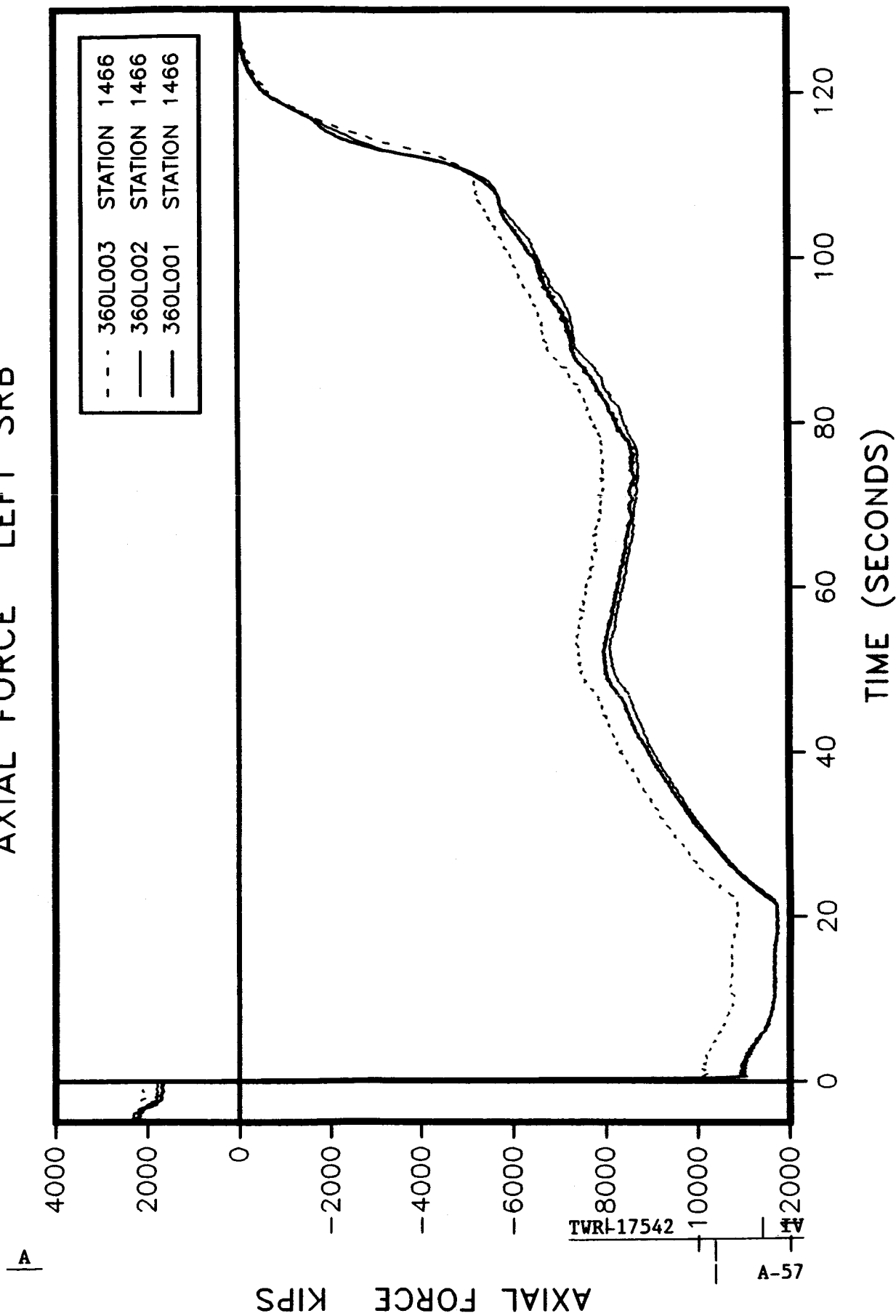
360L003 VS PREVIOUS FLIGHTS

AXIAL FORCE LEFT SRB



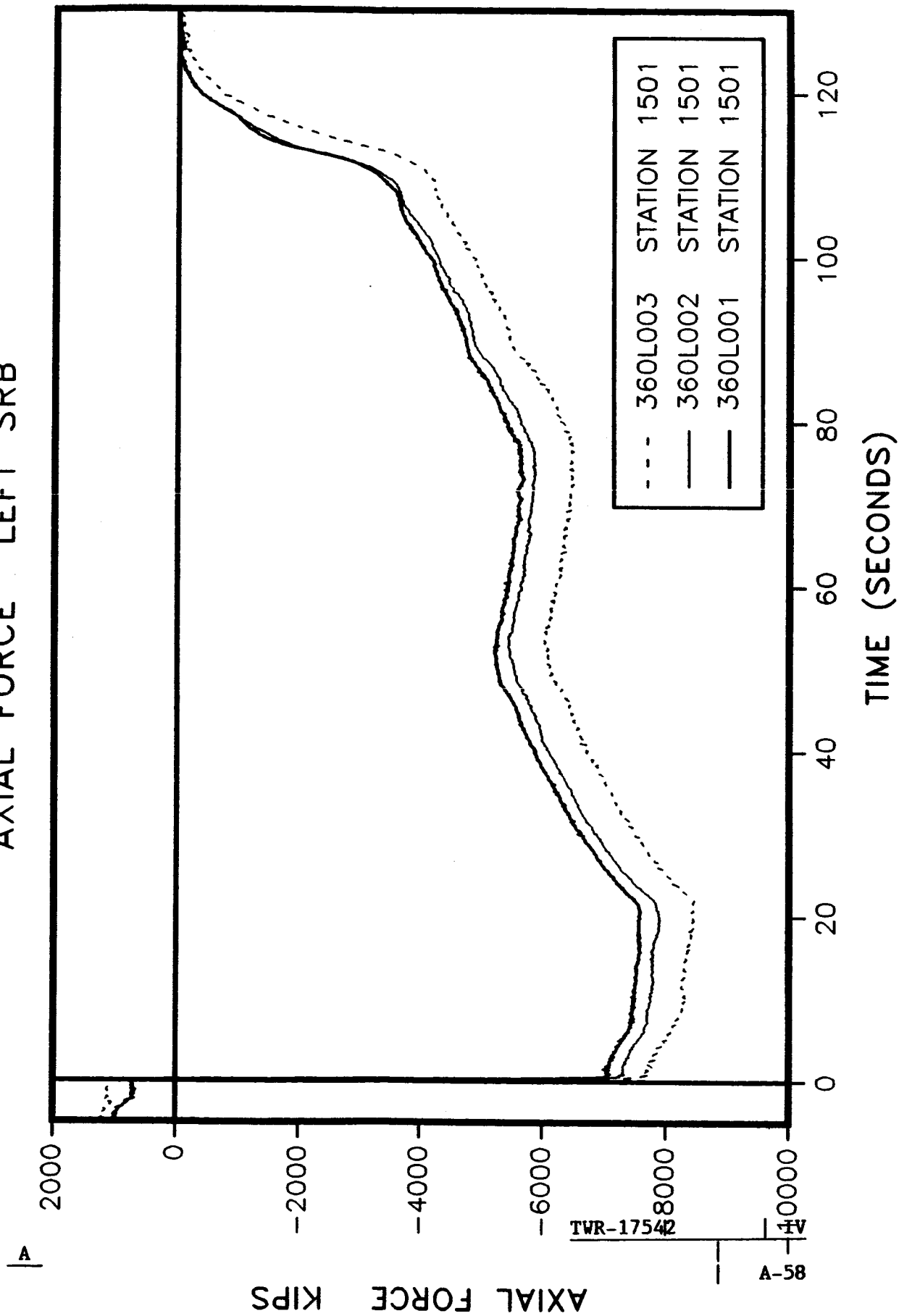
360L003 VS PREVIOUS FLIGHTS

AXIAL FORCE LEFT SRB



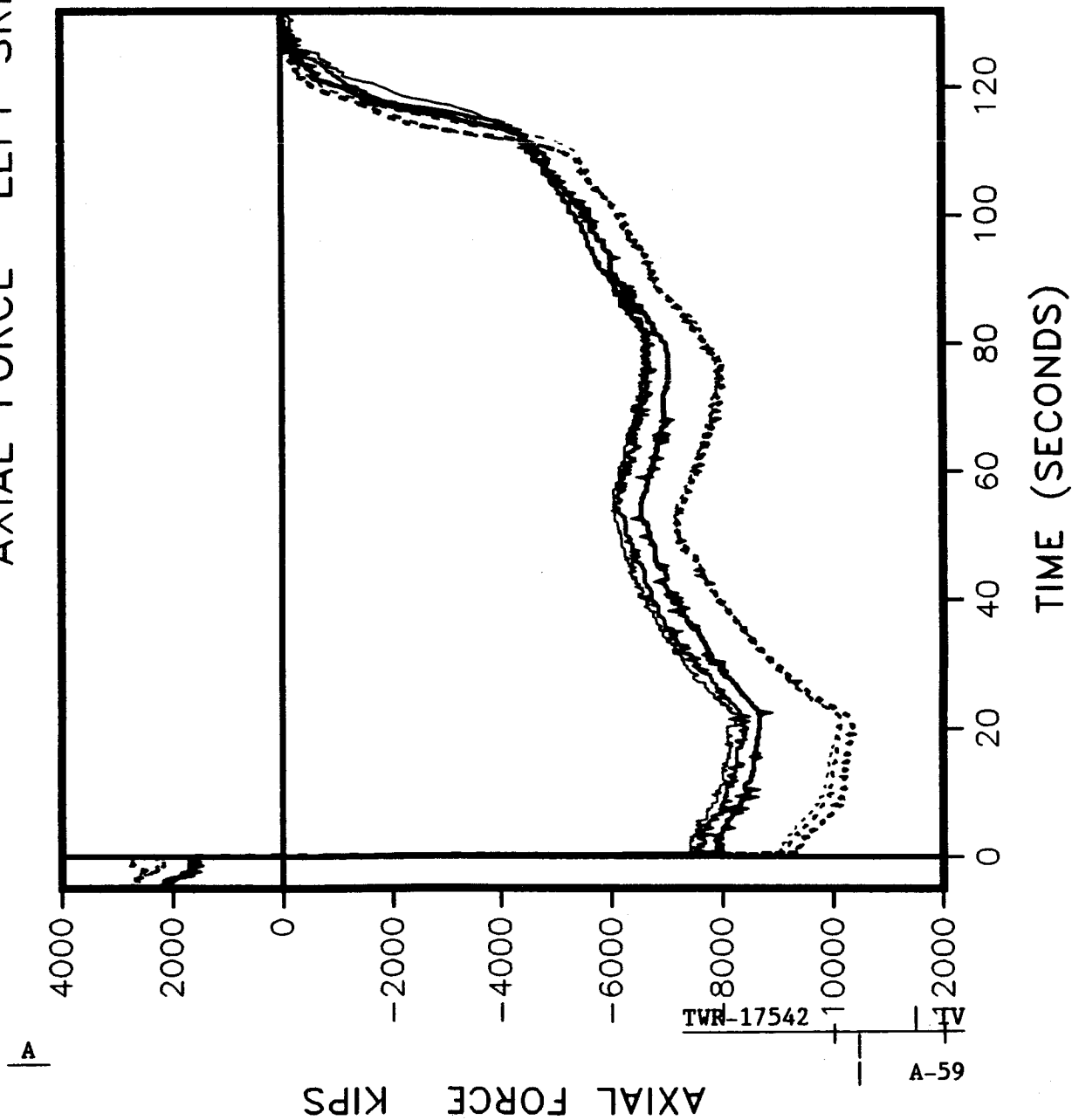
360L003 VS PREVIOUS FLIGHTS

AXIAL FORCE LEFT SRB



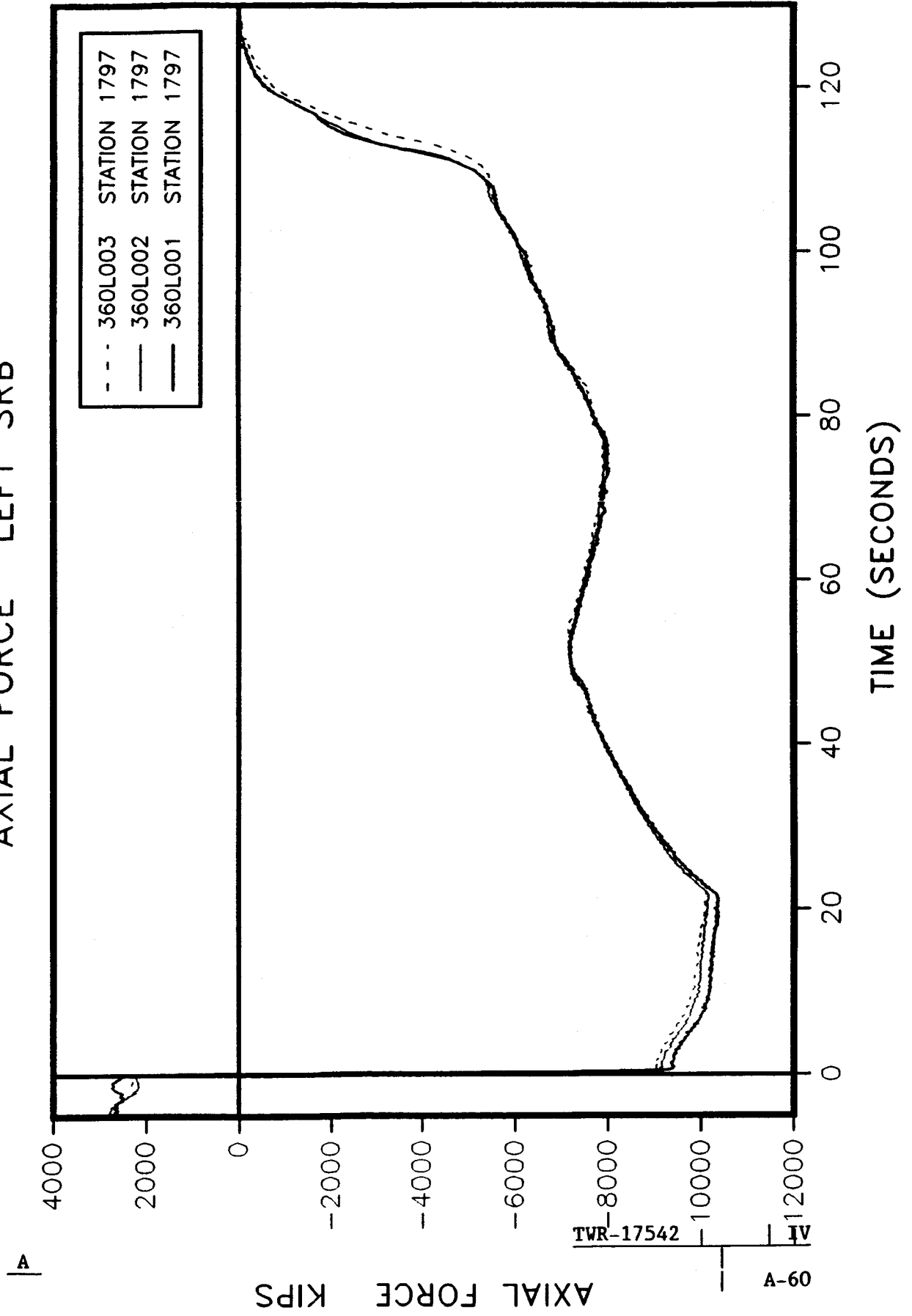
360L003 VS PREVIOUS FLIGHTS

AXIAL FORCE LEFT SRB



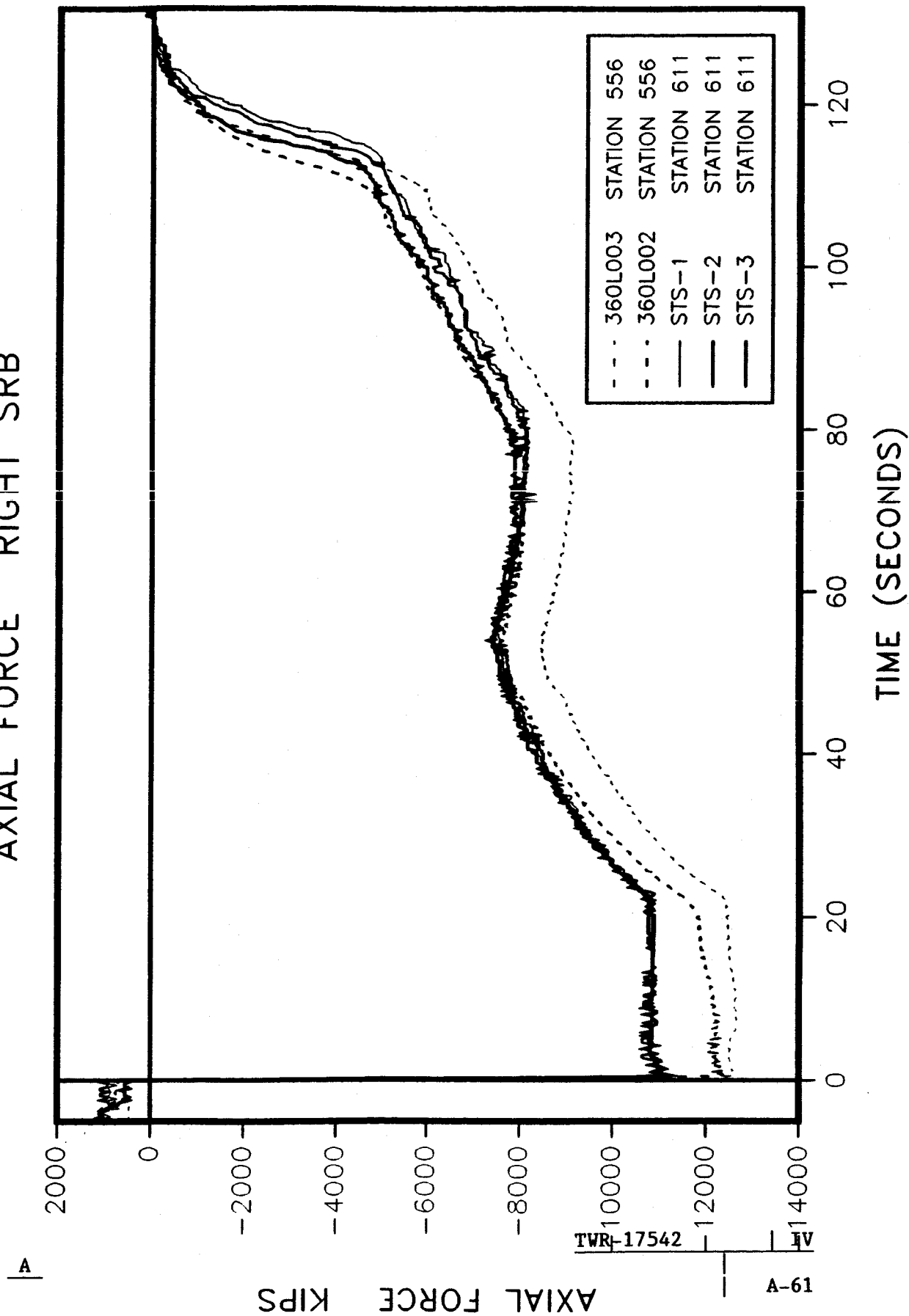
360L003 VS PREVIOUS FLIGHTS

AXIAL FORCE LEFT SRB



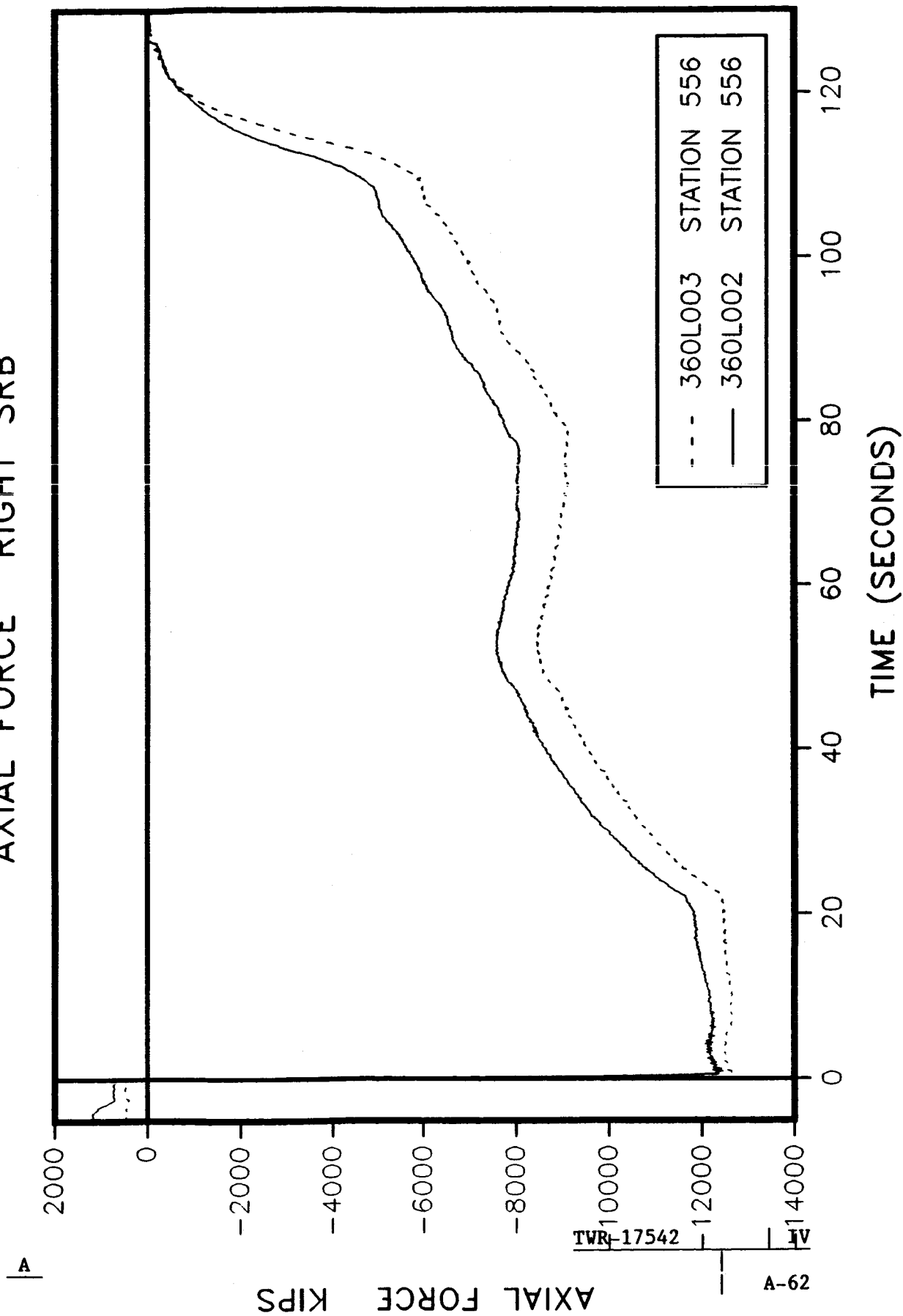
360L003 VS PREVIOUS FLIGHTS

AXIAL FORCE RIGHT SRB



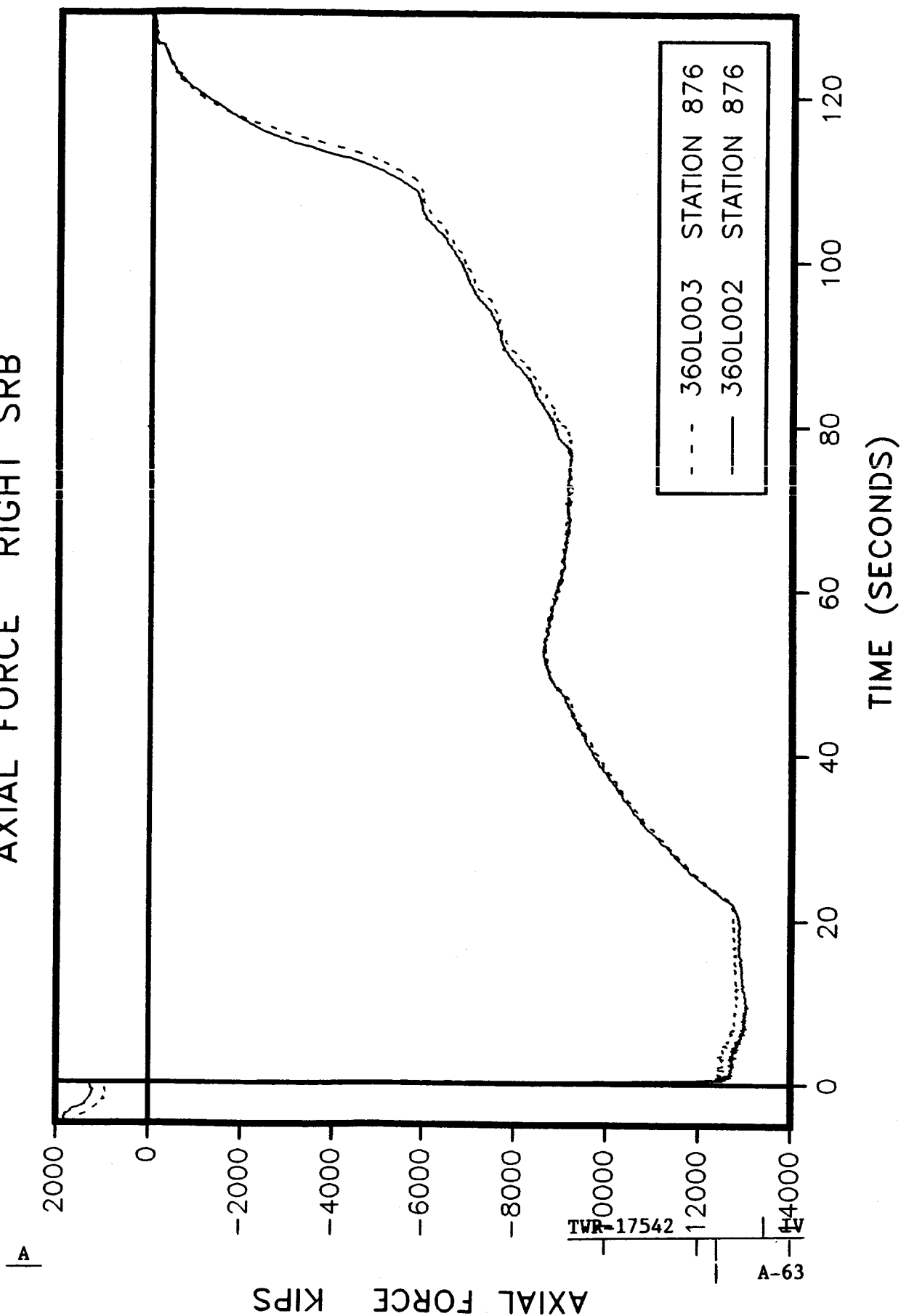
360L003 VS PREVIOUS FLIGHTS

AXIAL FORCE RIGHT SRB



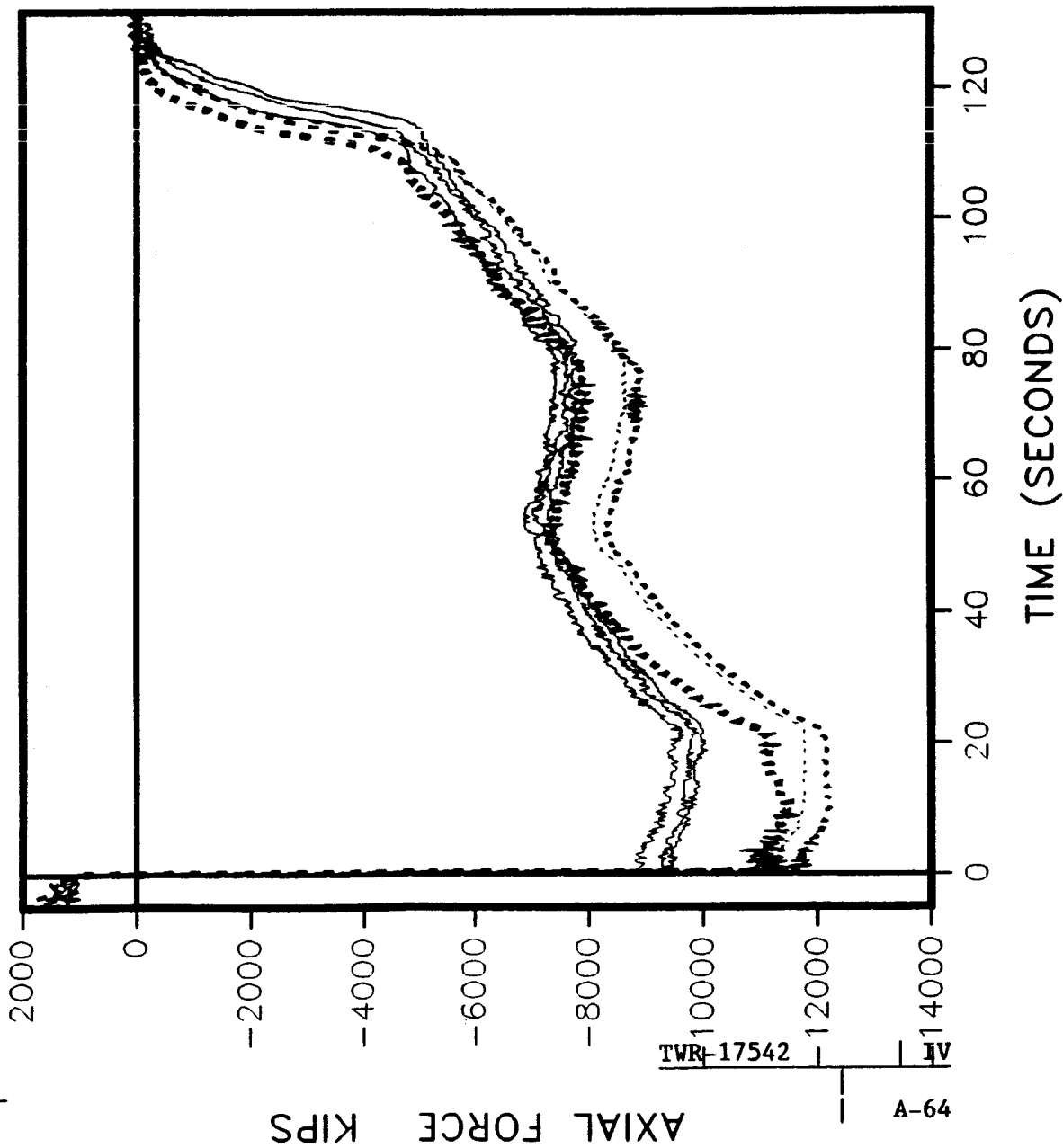
360L003 VS PREVIOUS FLIGHTS

AXIAL FORCE RIGHT SRB



360L003 VS PREVIOUS FLIGHTS

AXIAL FORCE RIGHT SRB



- - -	360L003	STATION 1196
- - -	360L002	STATION 1196
· · ·	360L001	STATION 1196
—	STS-1	STATION 1251
—	STS-2	STATION 1251
—	STS-3	STATION 1251

A

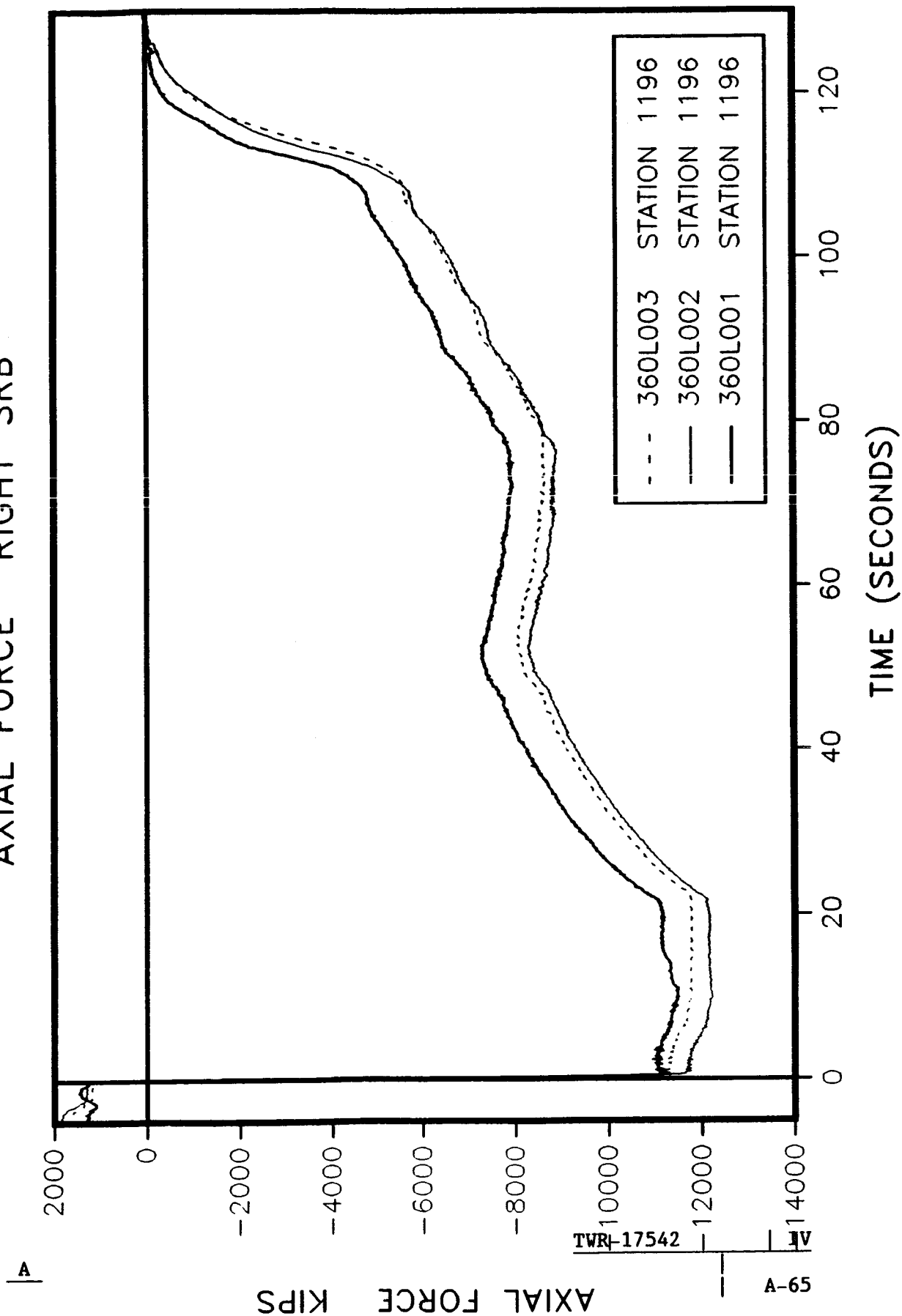
AXIAL FORCE KIPS

A-64

TWR-17542

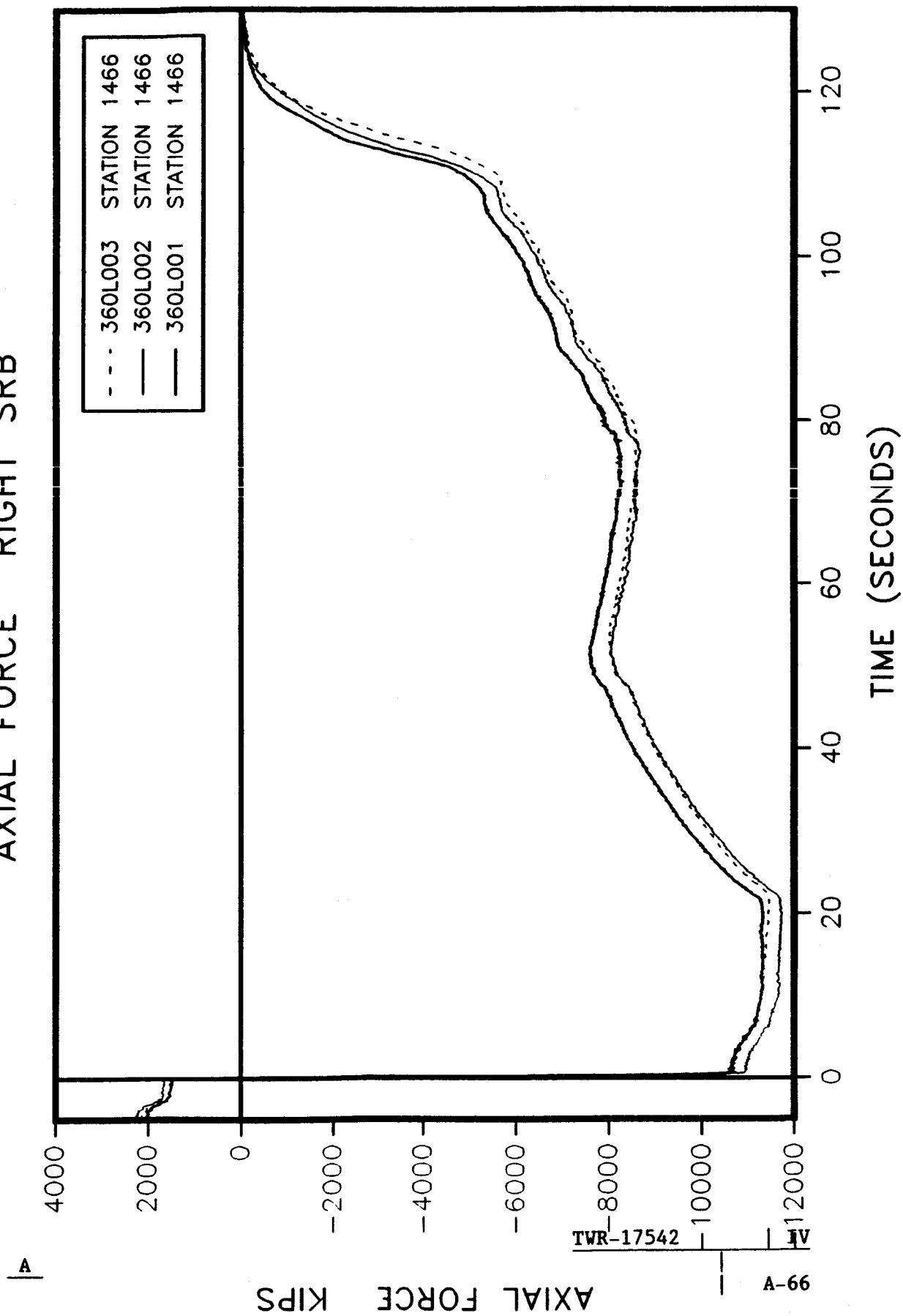
360L003 VS PREVIOUS FLIGHTS

AXIAL FORCE RIGHT SRB



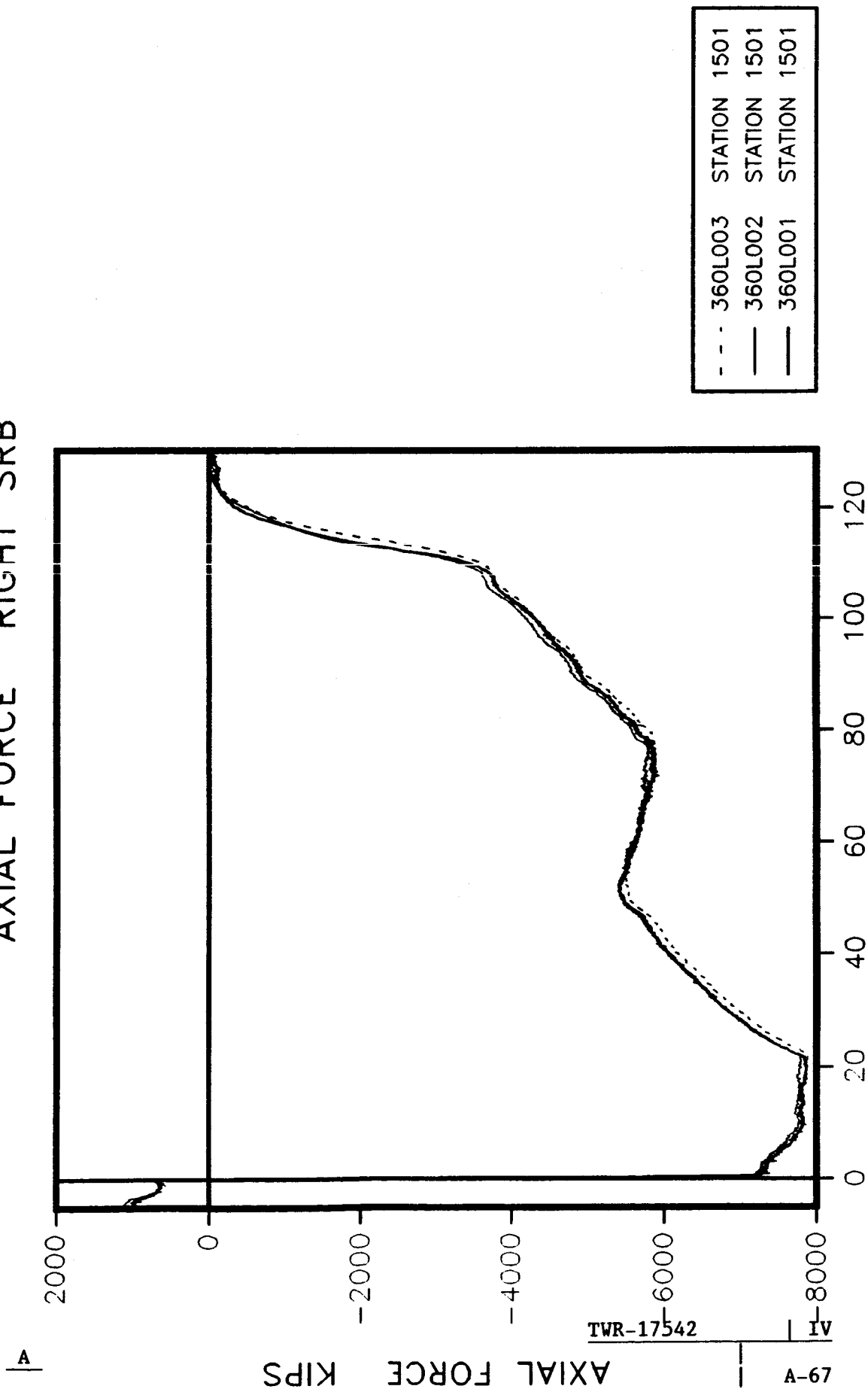
360L003 VS PREVIOUS FLIGHTS

AXIAL FORCE RIGHT SRB



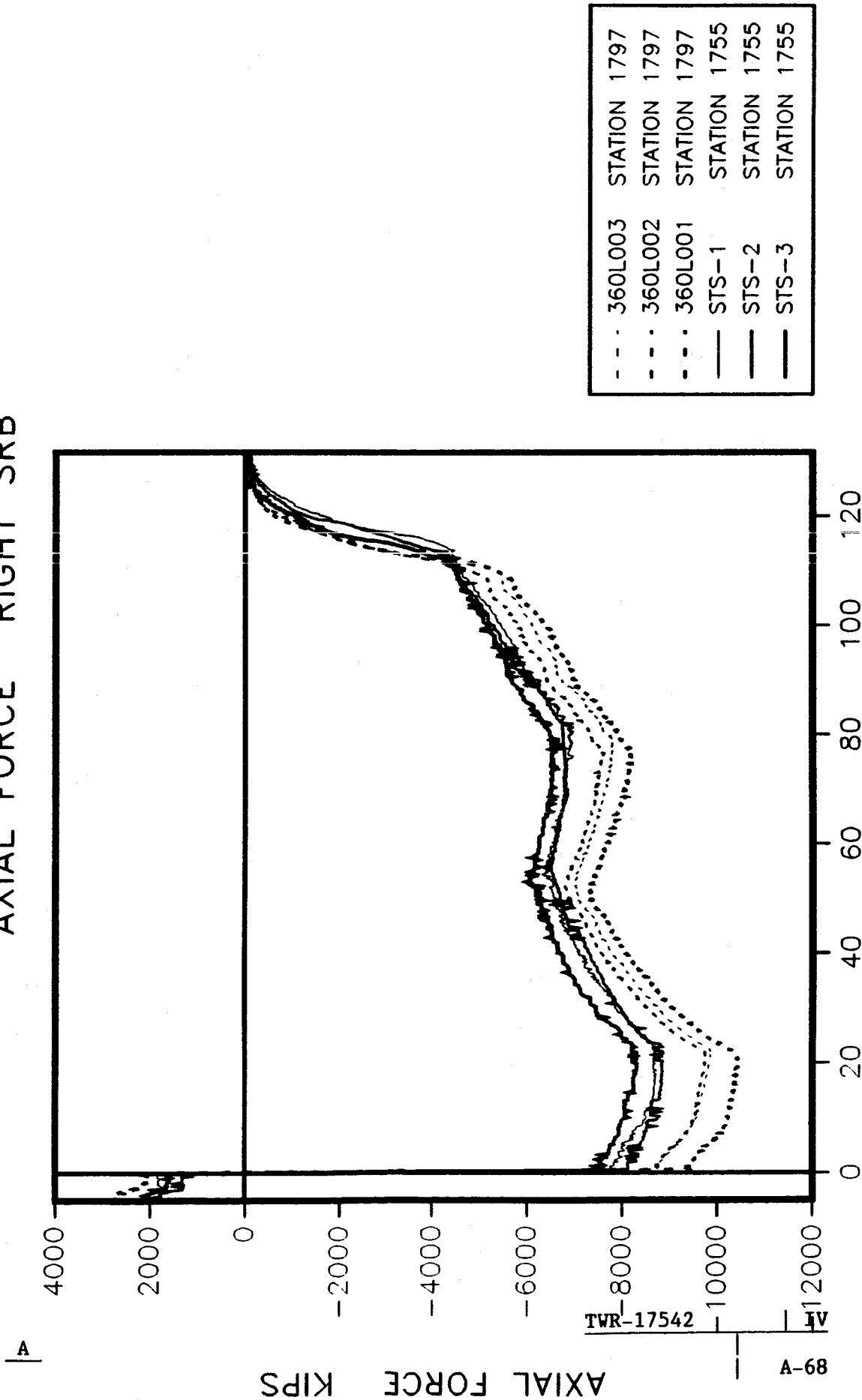
360L003 VS PREVIOUS FLIGHTS

AXIAL FORCE RIGHT SRB



360L003 VS PREVIOUS FLIGHTS

AXIAL FORCE RIGHT SRB

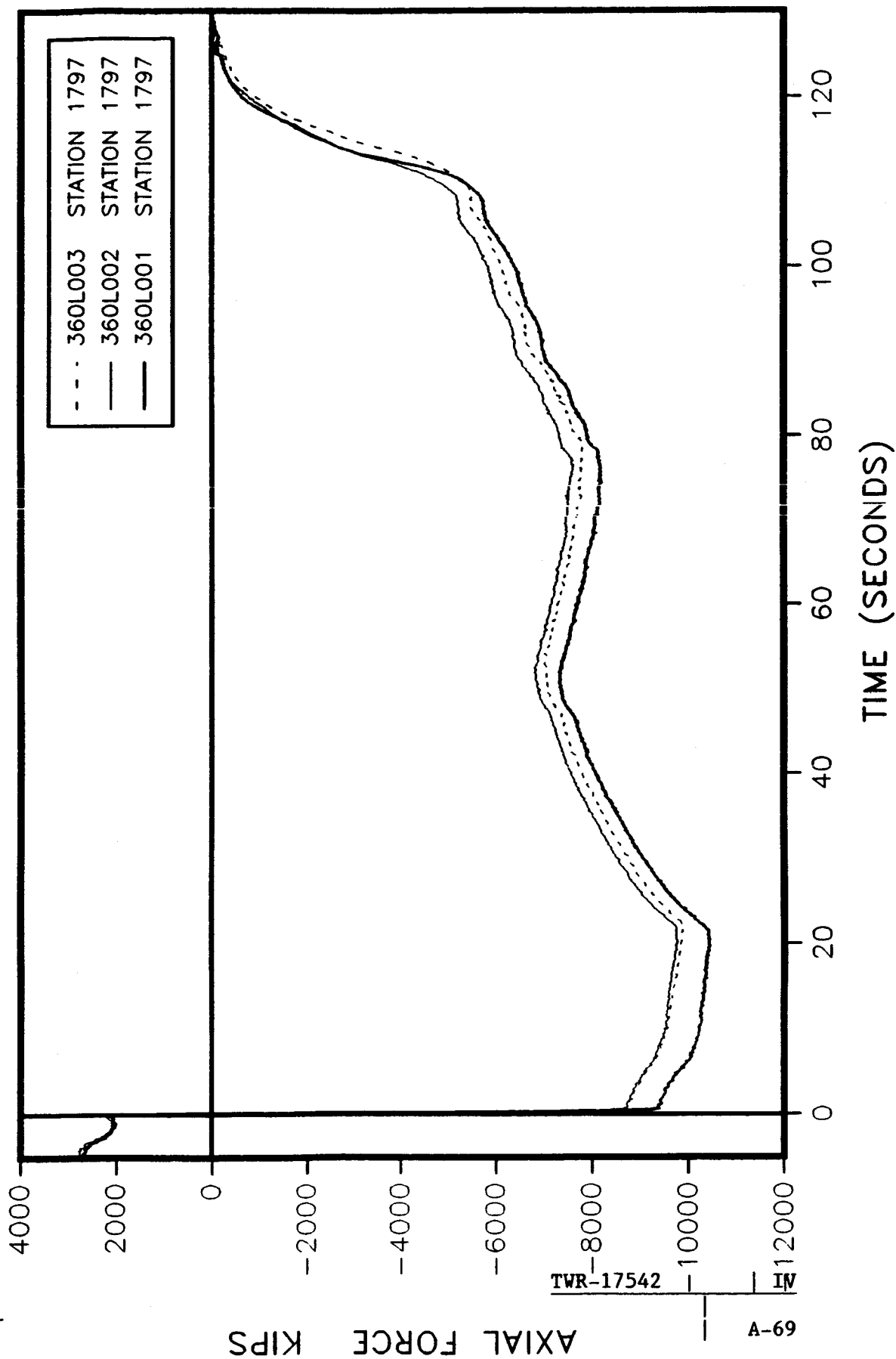


A-68

TWR-17542

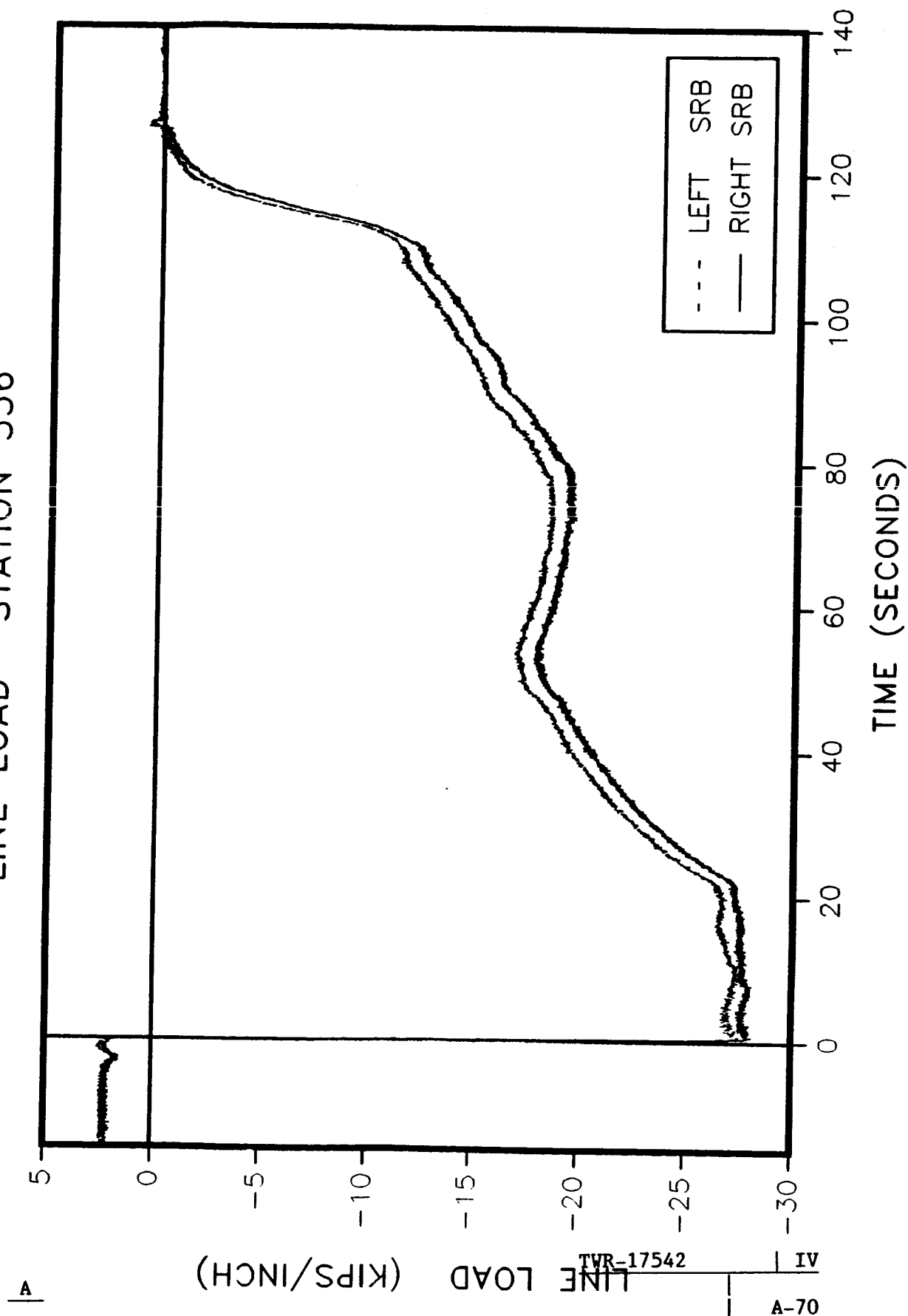
360L003 VS PREVIOUS FLIGHTS

AXIAL FORCE RIGHT SRB



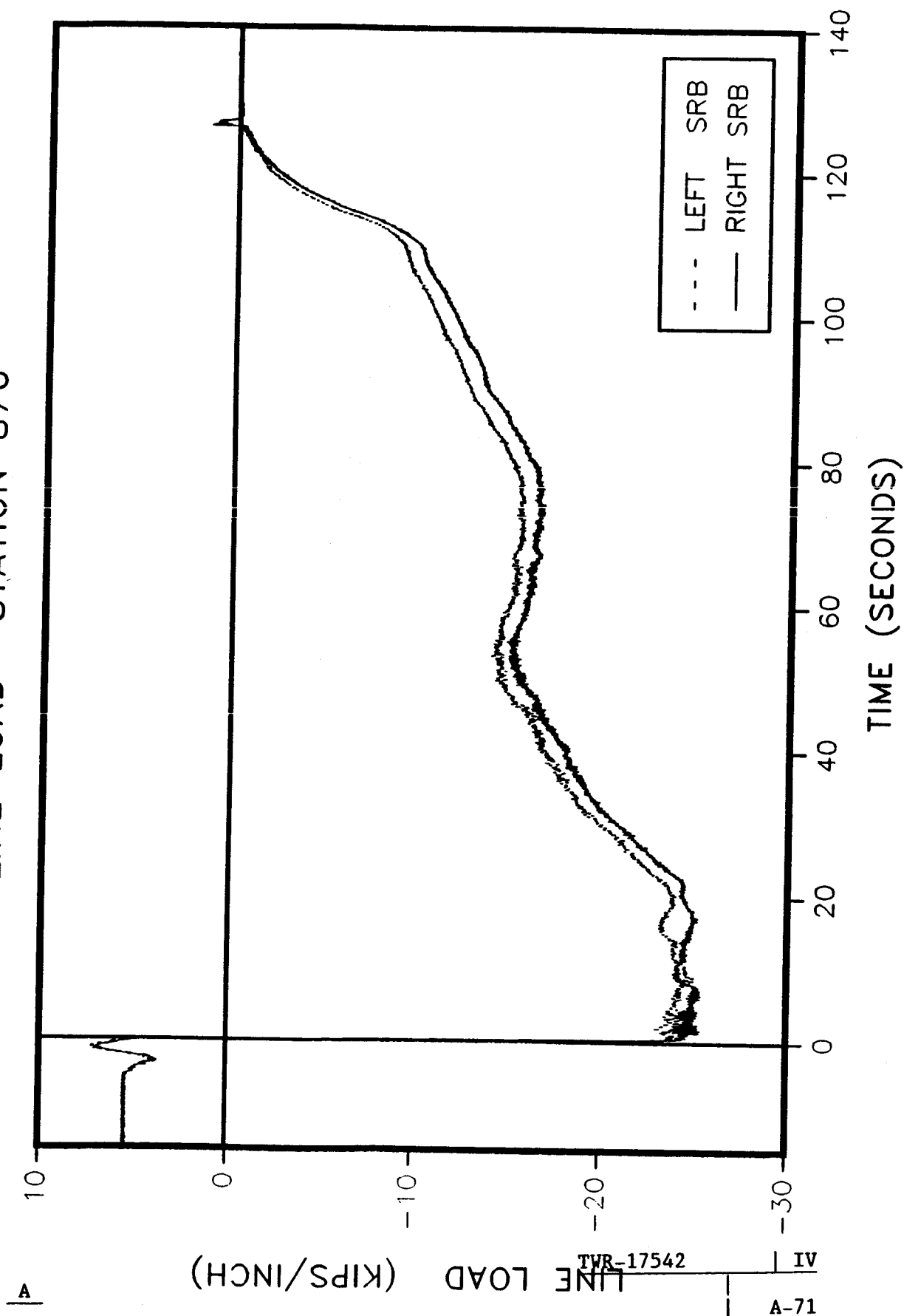
360L003

LINE LOAD STATION 556



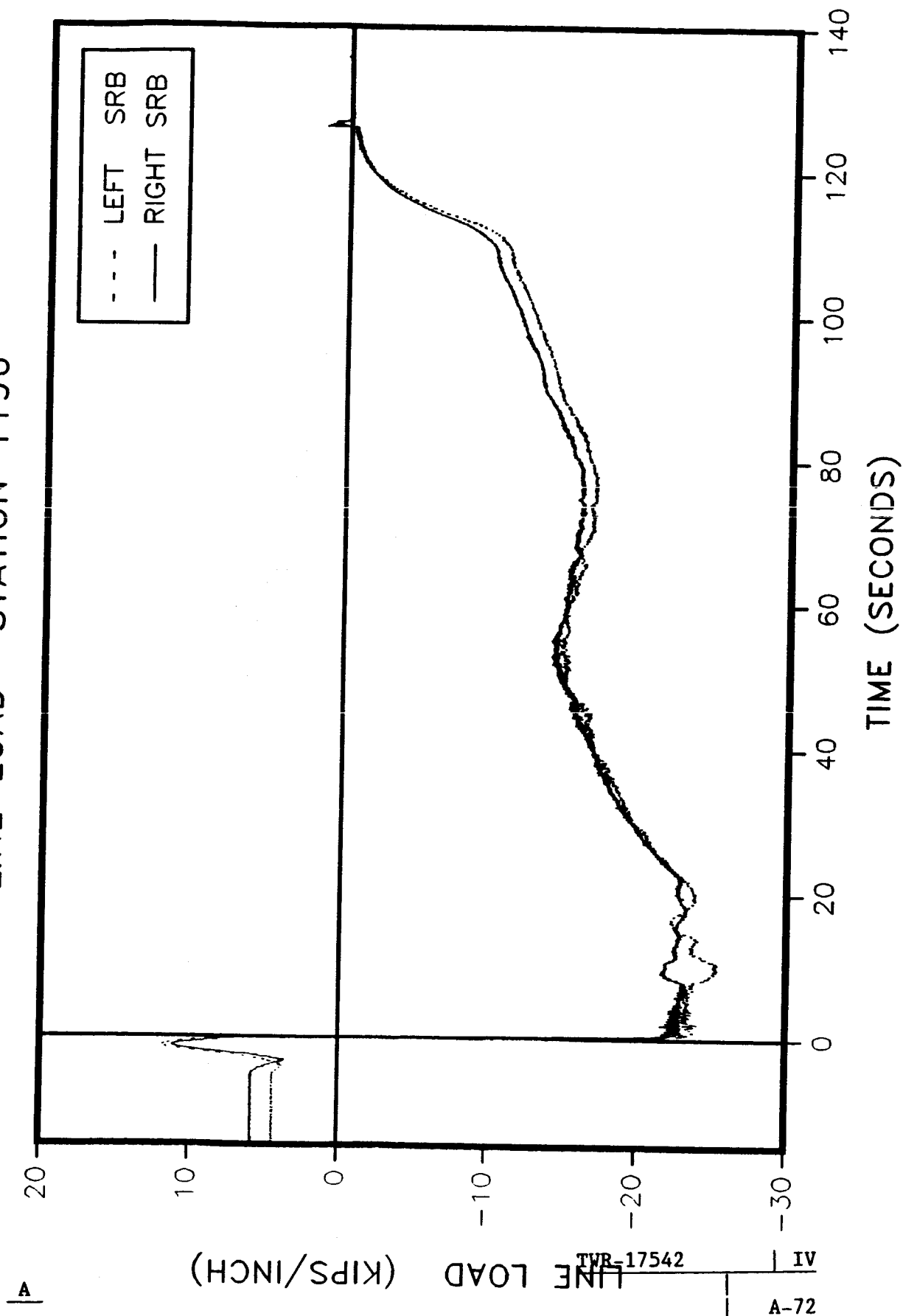
360L003

LINE LOAD STATION 876



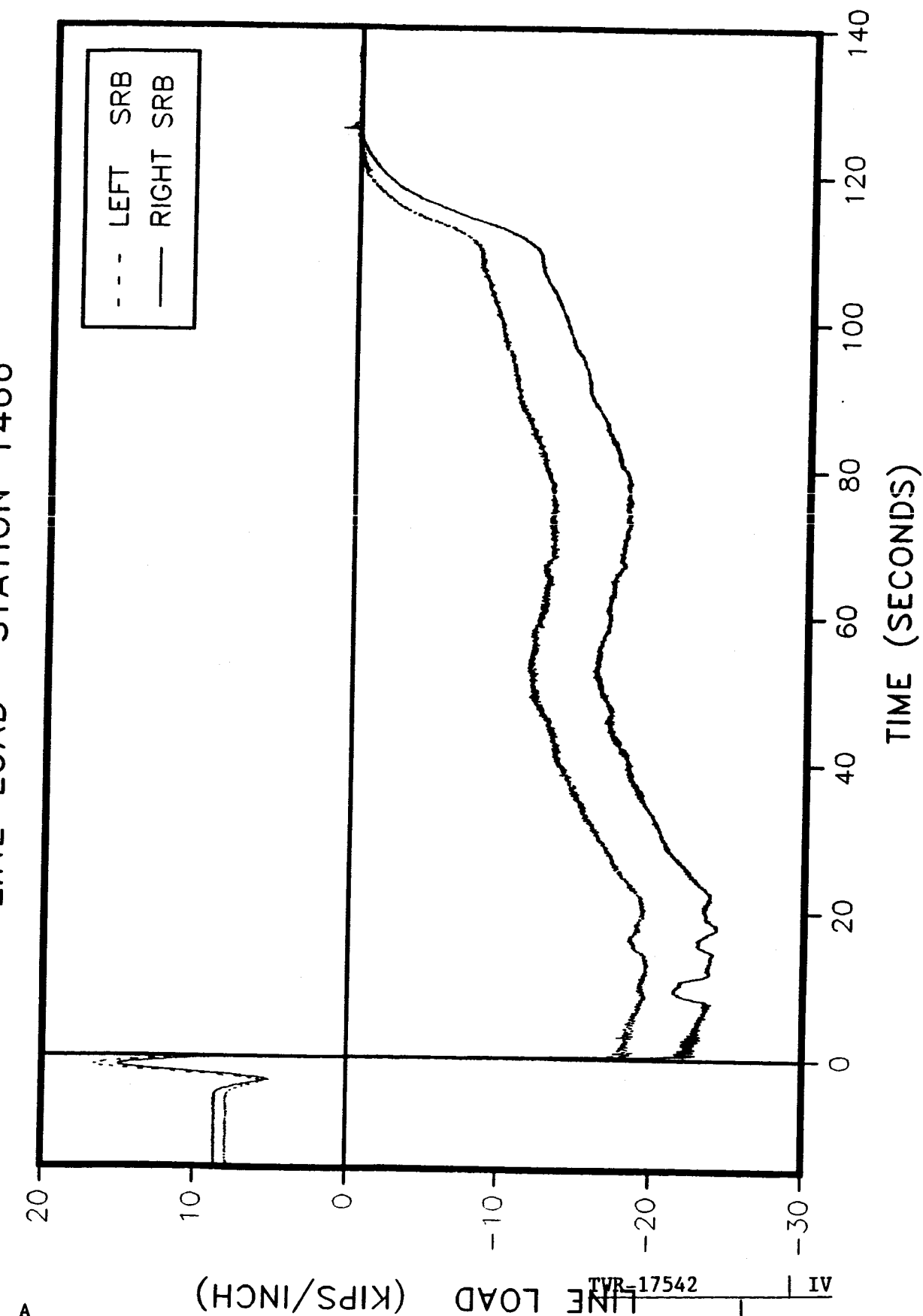
360L003

LINE LOAD STATION 1196



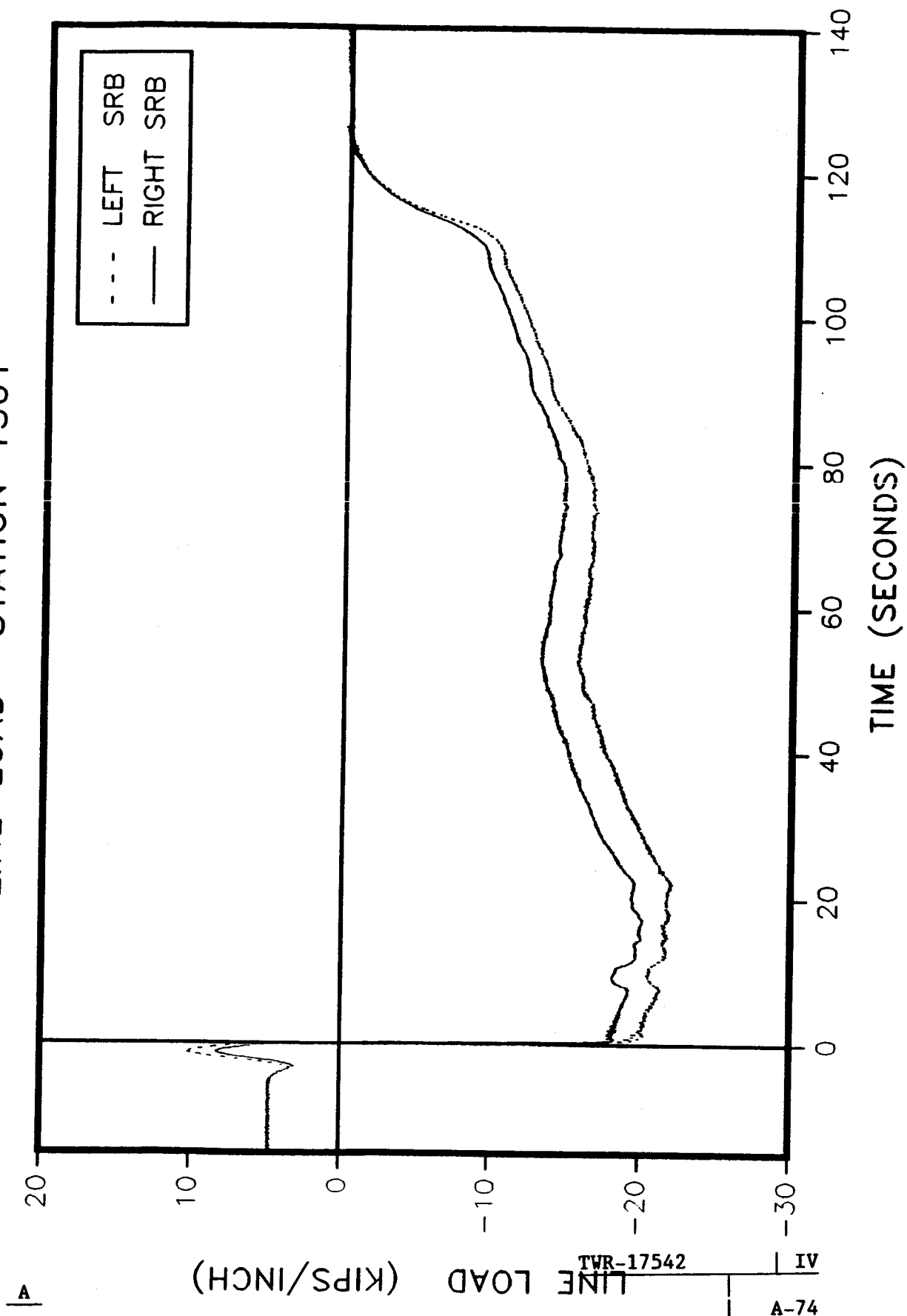
360L003

LINE LOAD STATION 1466



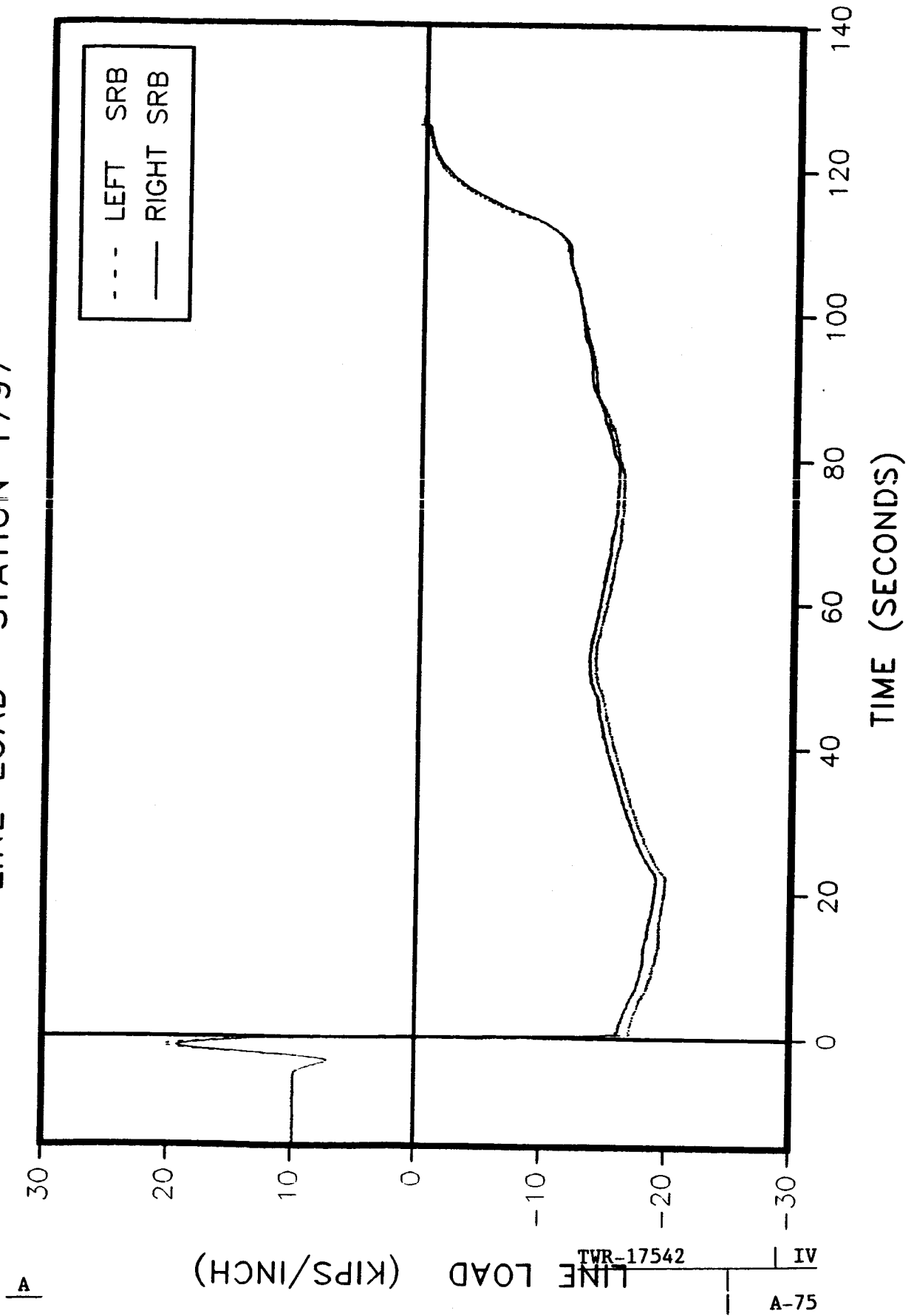
360L003

LINE LOAD STATION 1501



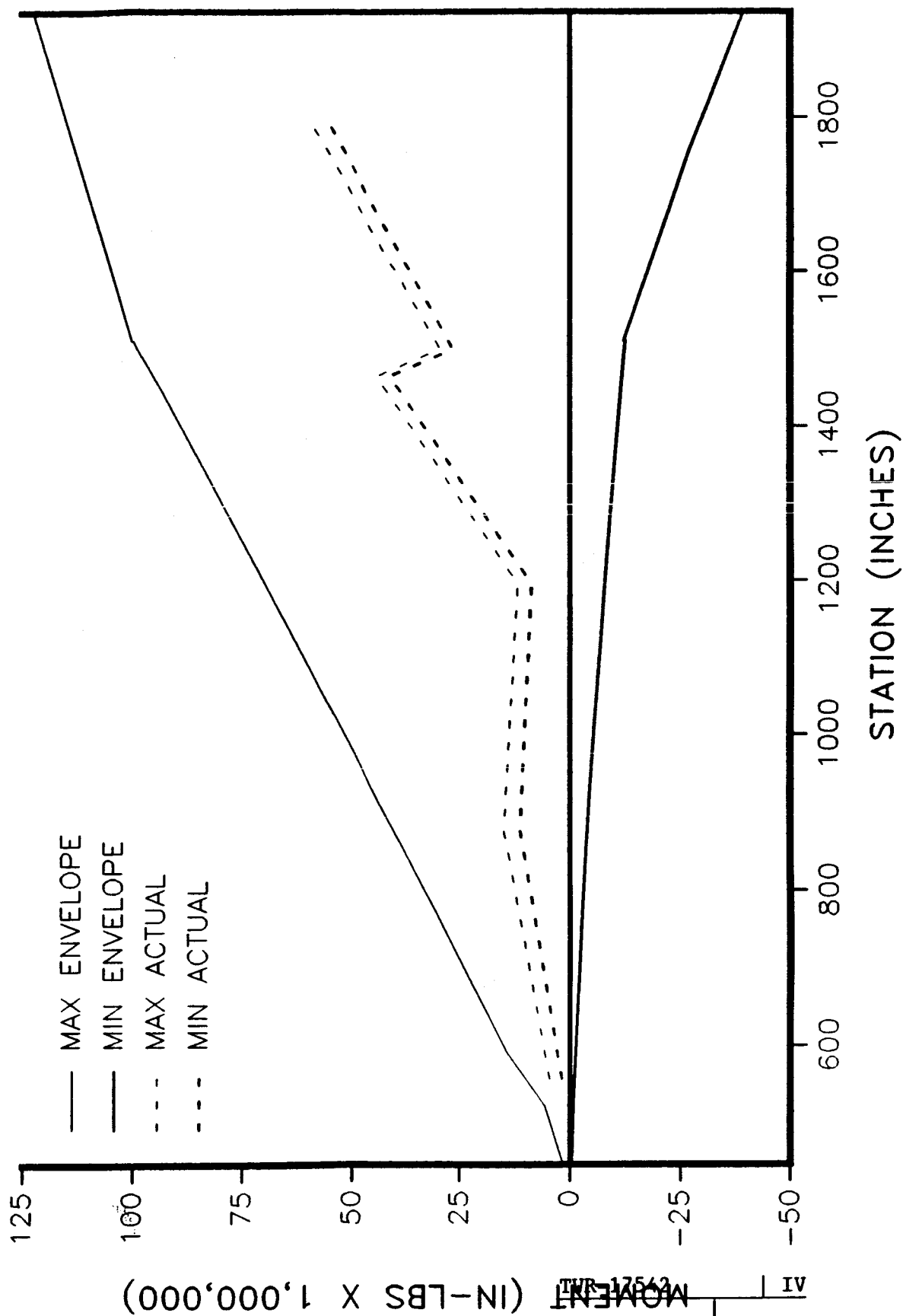
360L003

LINE LOAD STATION 1797



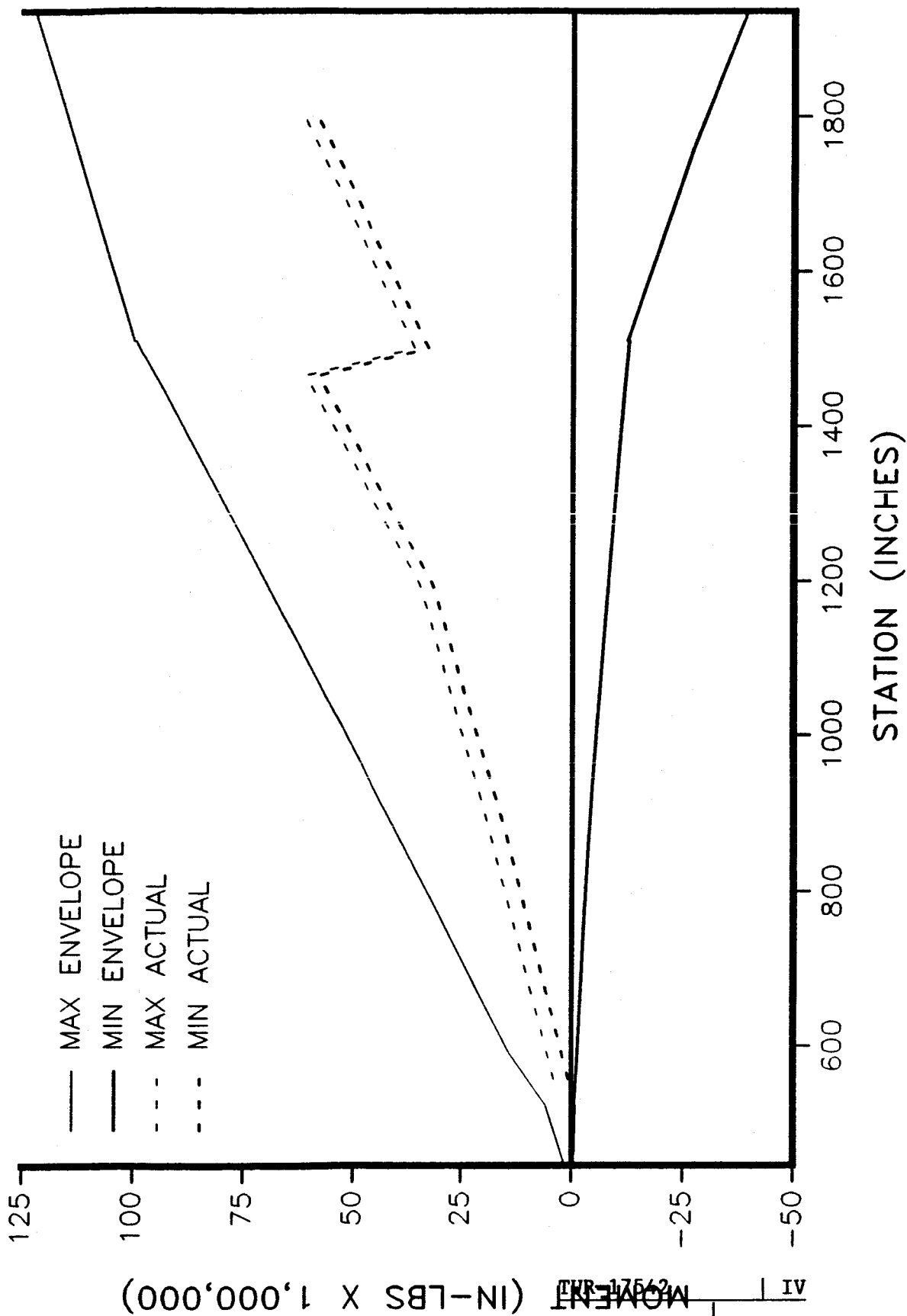
360L003 PRE-LAUNCH ENVELOPE

BENDING ABOUT THE Y AXIS LEFT SRB



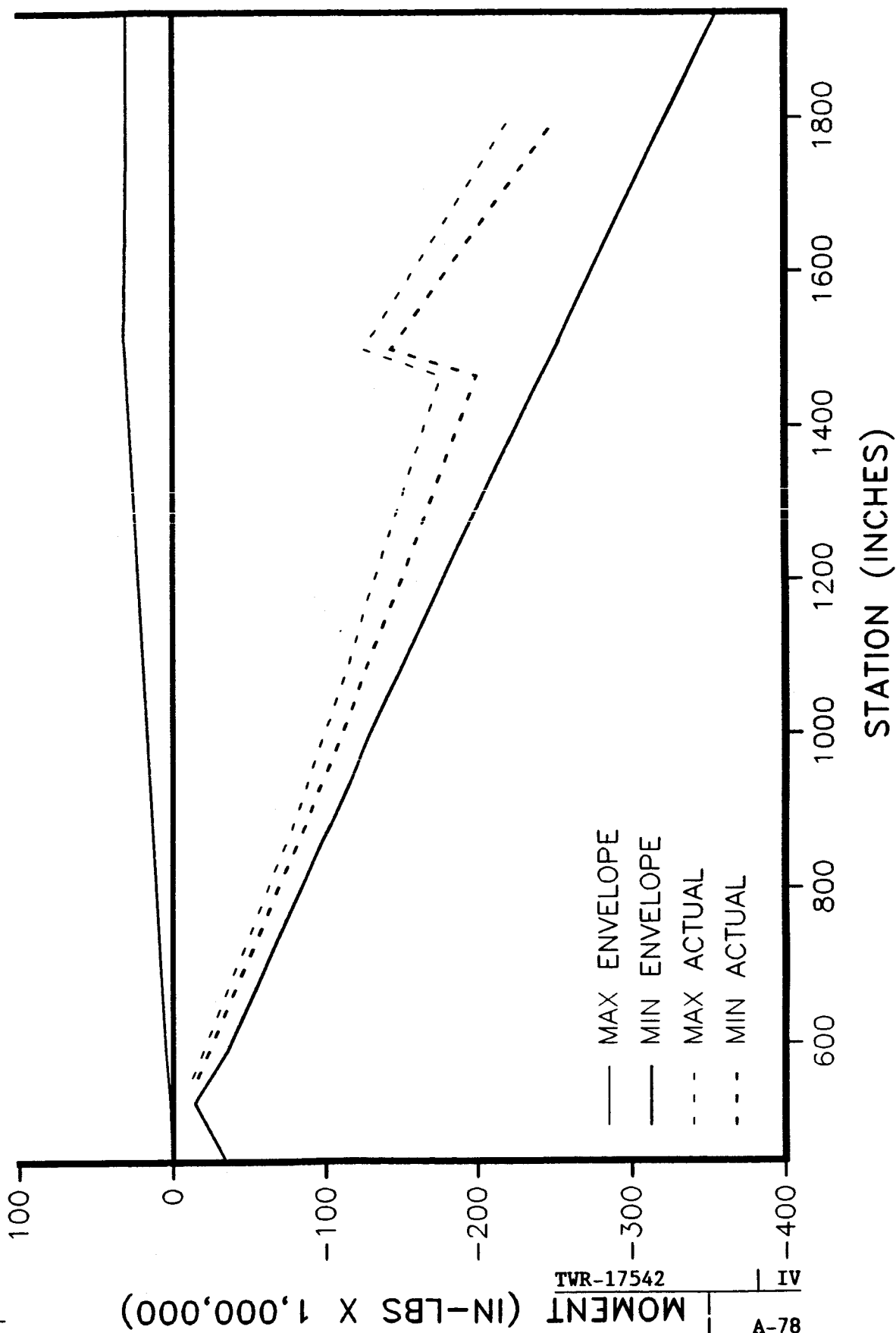
360L003 PRE-LAUNCH ENVELOPE

BENDING ABOUT THE Y AXIS RIGHT SRB



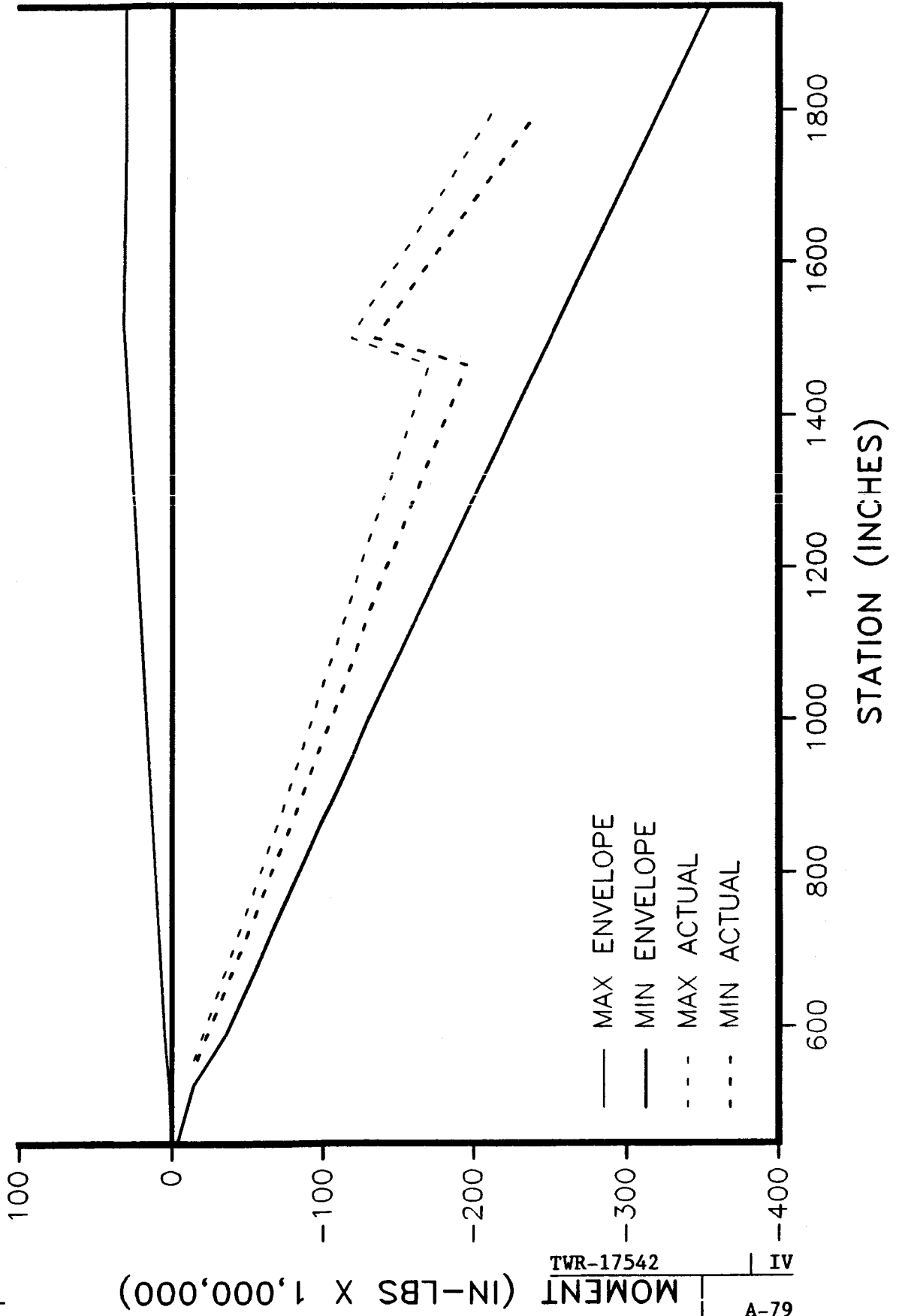
360L003 BUILD-UP ENVELOPE

BENDING ABOUT THE Y AXIS LEFT SRB



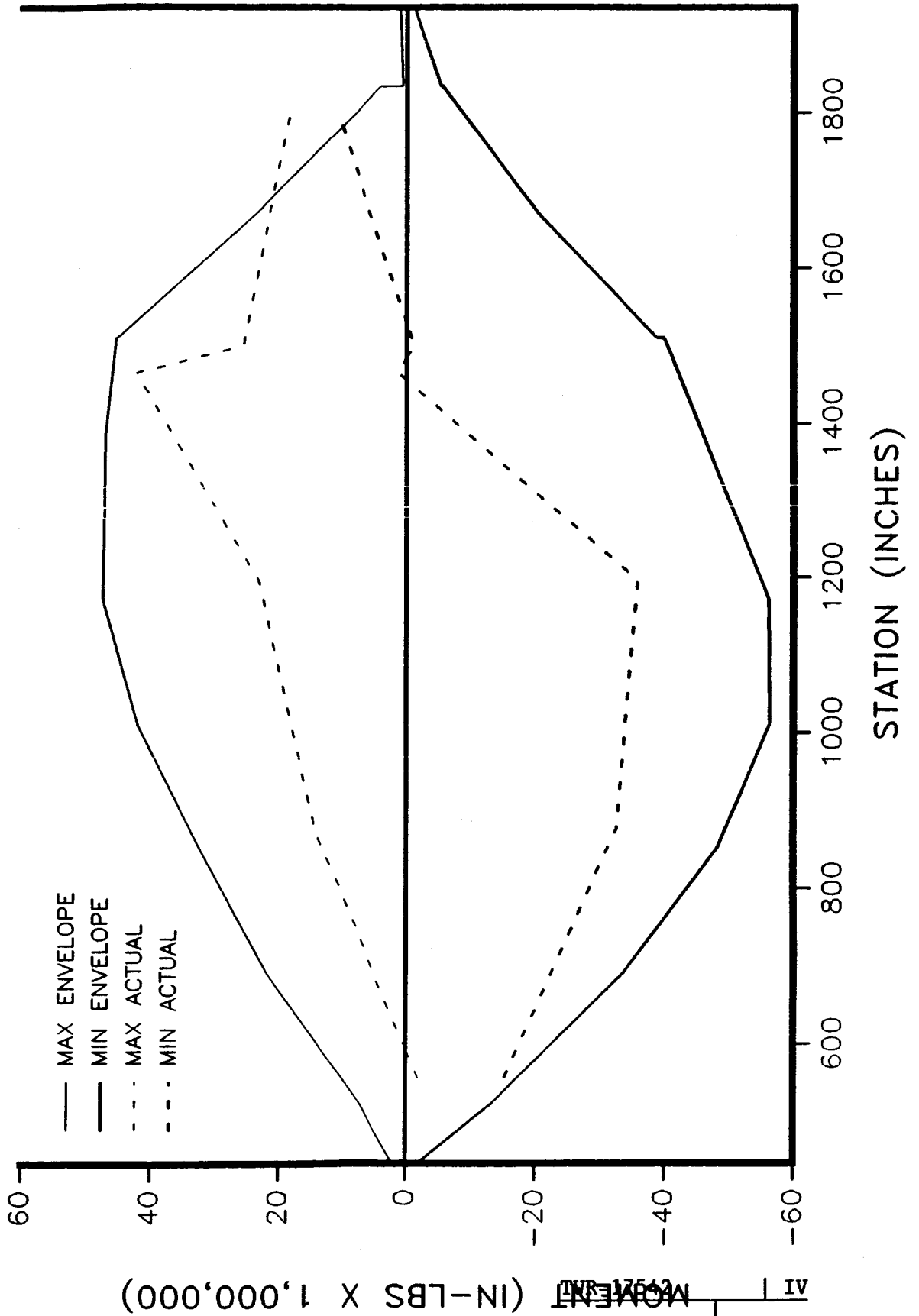
360L003 BUILD-UP ENVELOPE

BENDING ABOUT THE Y AXIS RIGHT SRB



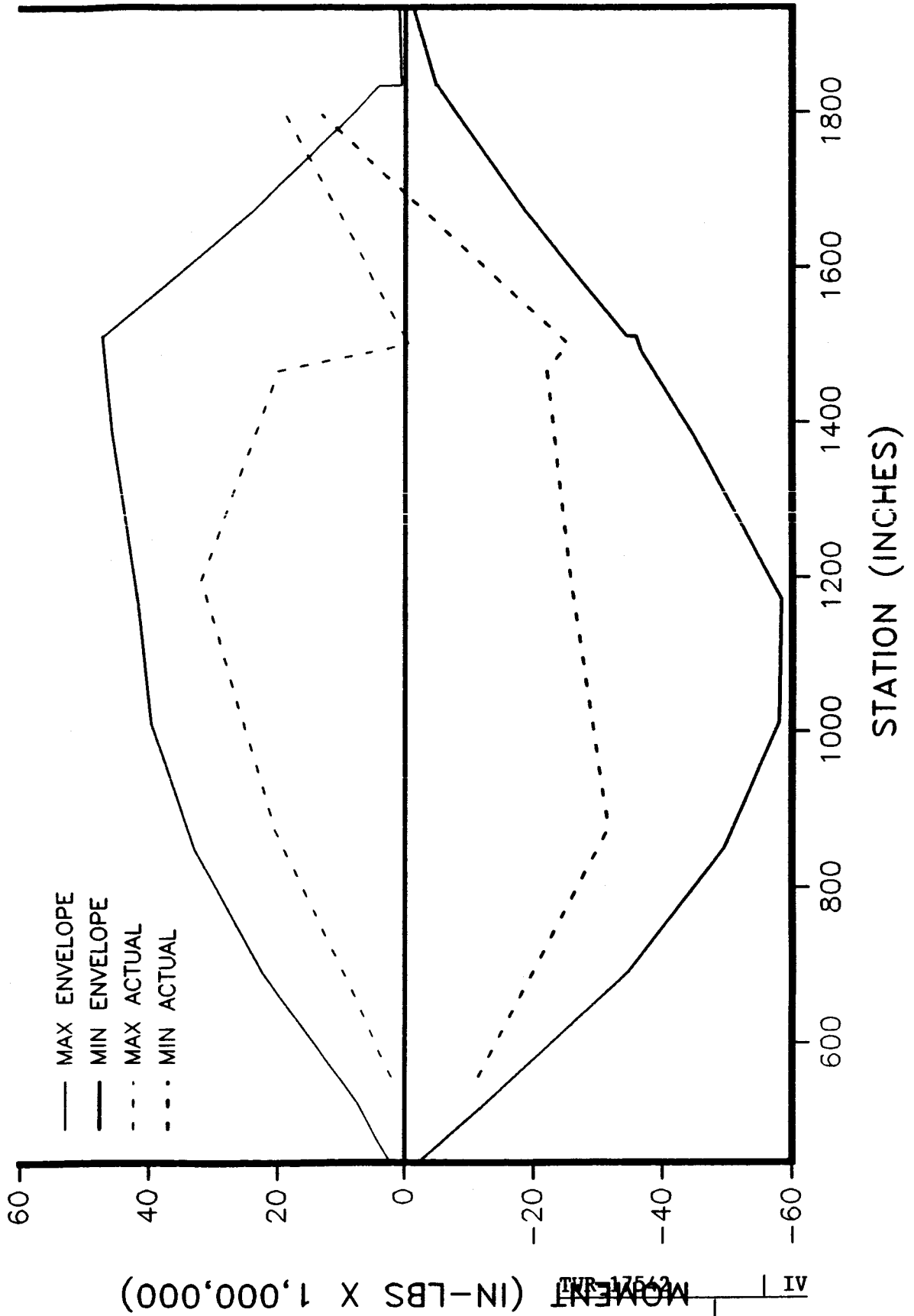
360L003 LIFT-OFF ENVELOPE

BENDING ABOUT THE Y AXIS LEFT SRB



360L003 LIFT-OFF ENVELOPE

BENDING ABOUT THE Y AXIS RIGHT SRB



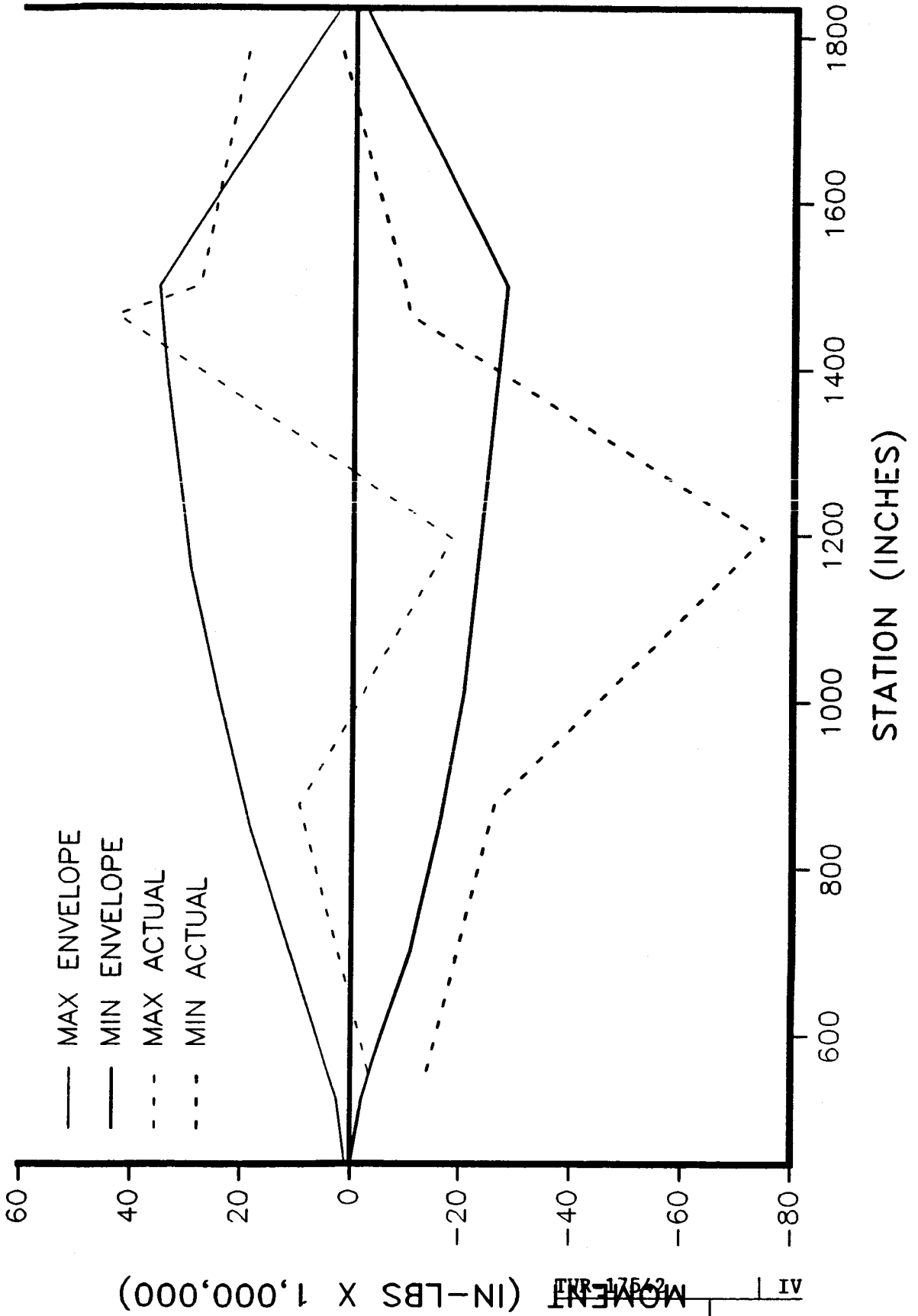
A

TWP-17562

IV
A-81

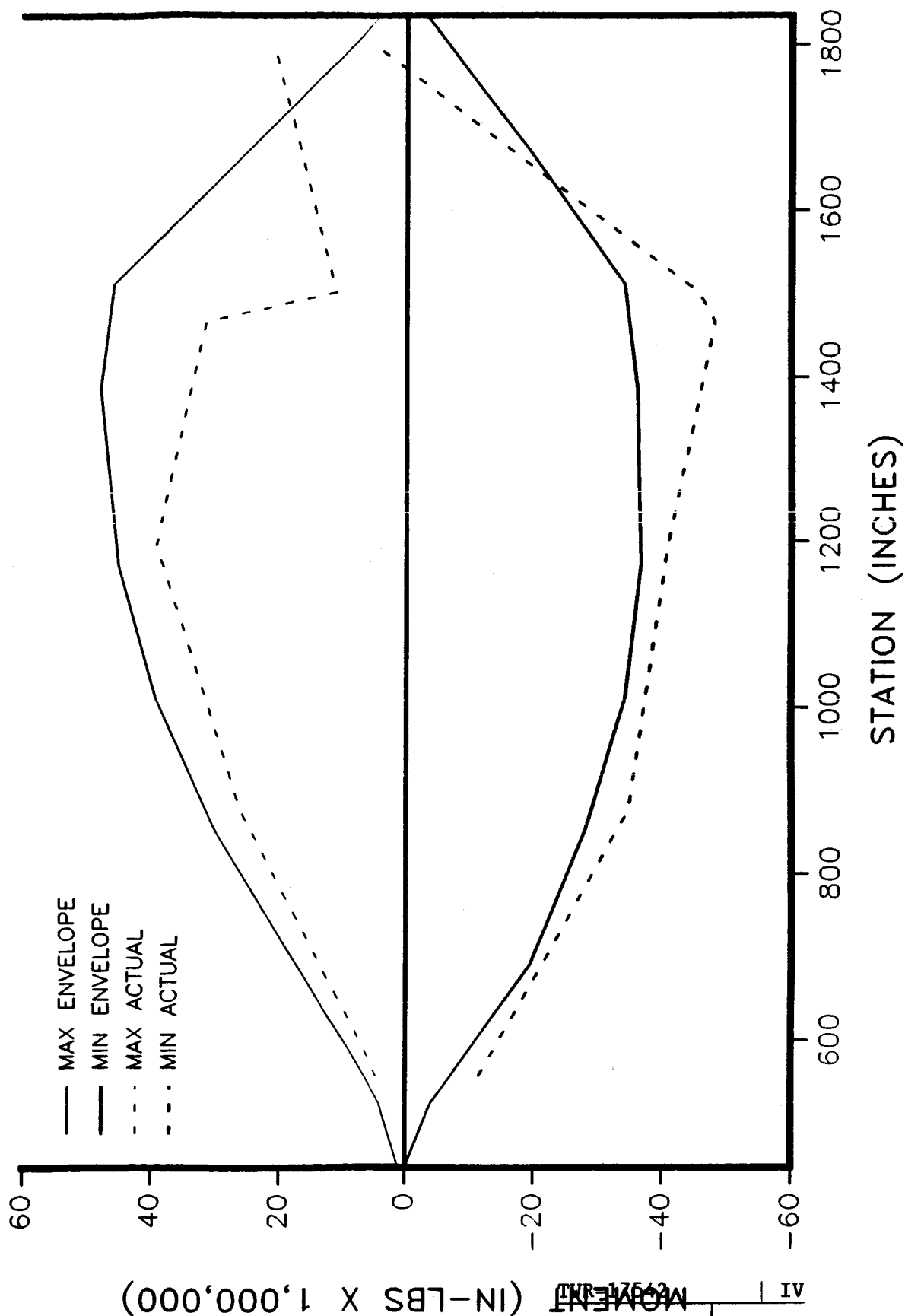
360L003 ROLL ENVELOPE

BENDING ABOUT THE Y AXIS LEFT SRB



360L003 ROLL ENVELOPE

BENDING ABOUT THE Y AXIS RIGHT SRB



A

MOMENT (IN-LBS X 1,000,000)

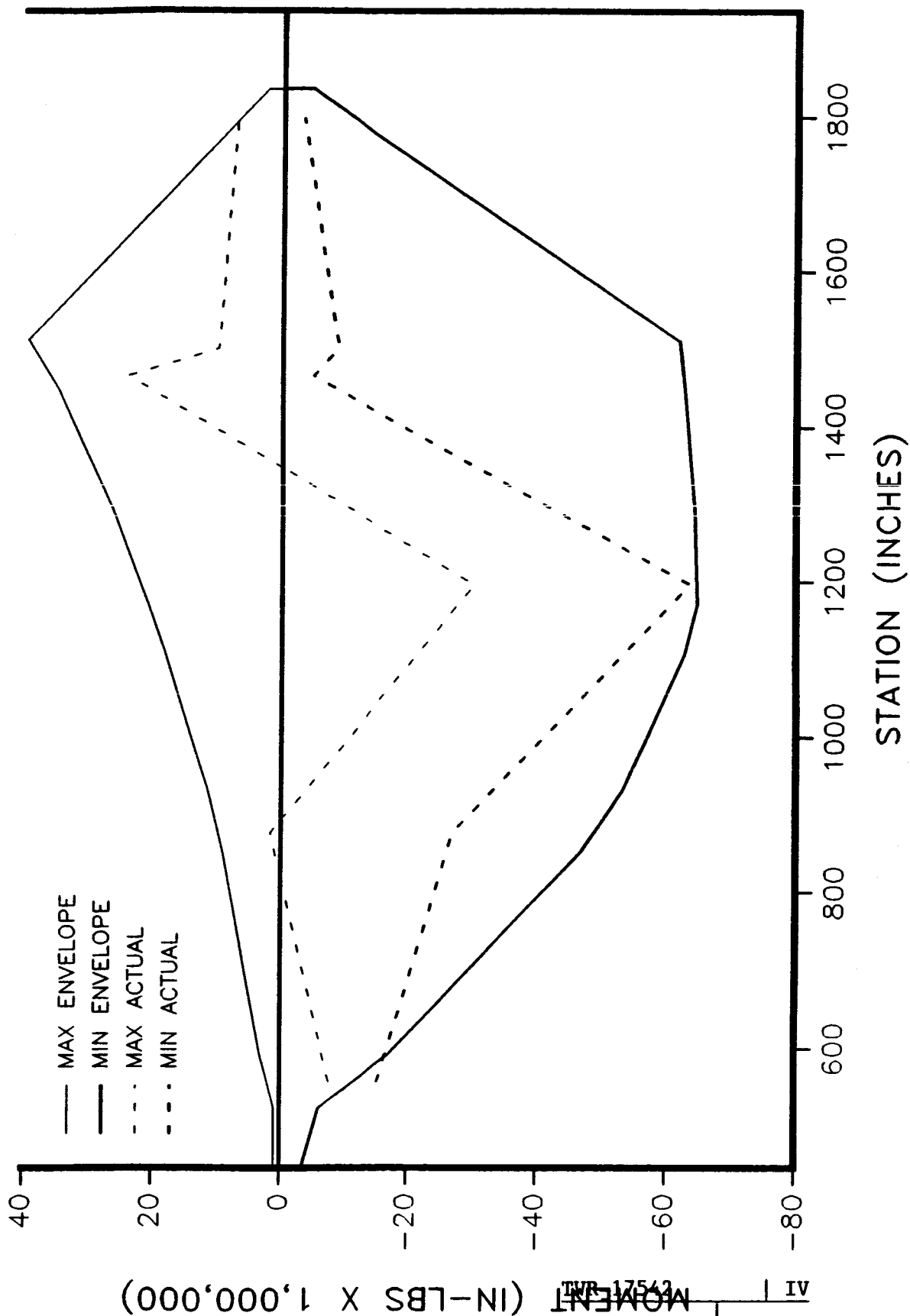
A-83

IV

TPR-17562

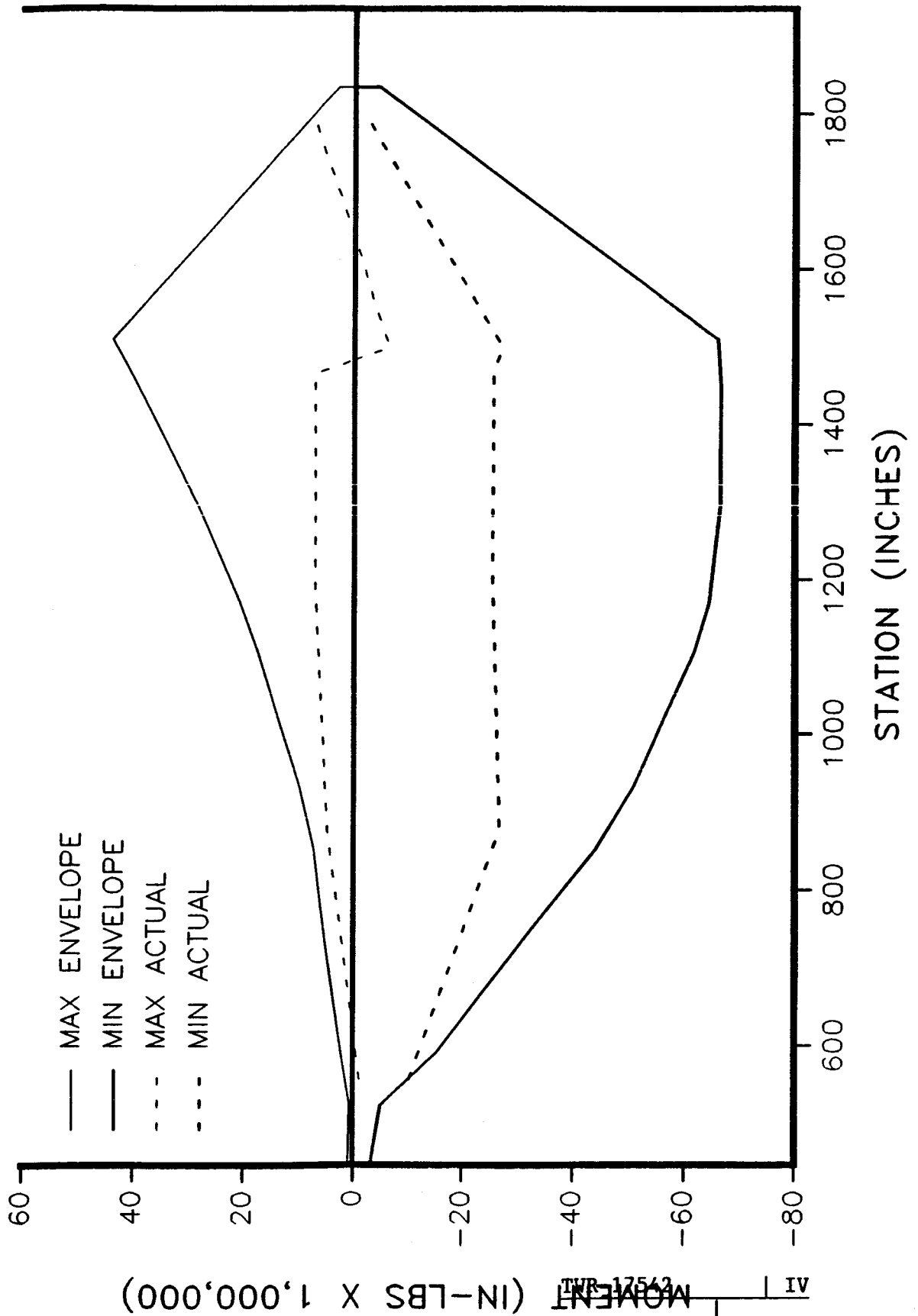
360L003 MAX Q ENVELOPE

BENDING ABOUT THE Y AXIS LEFT SRB



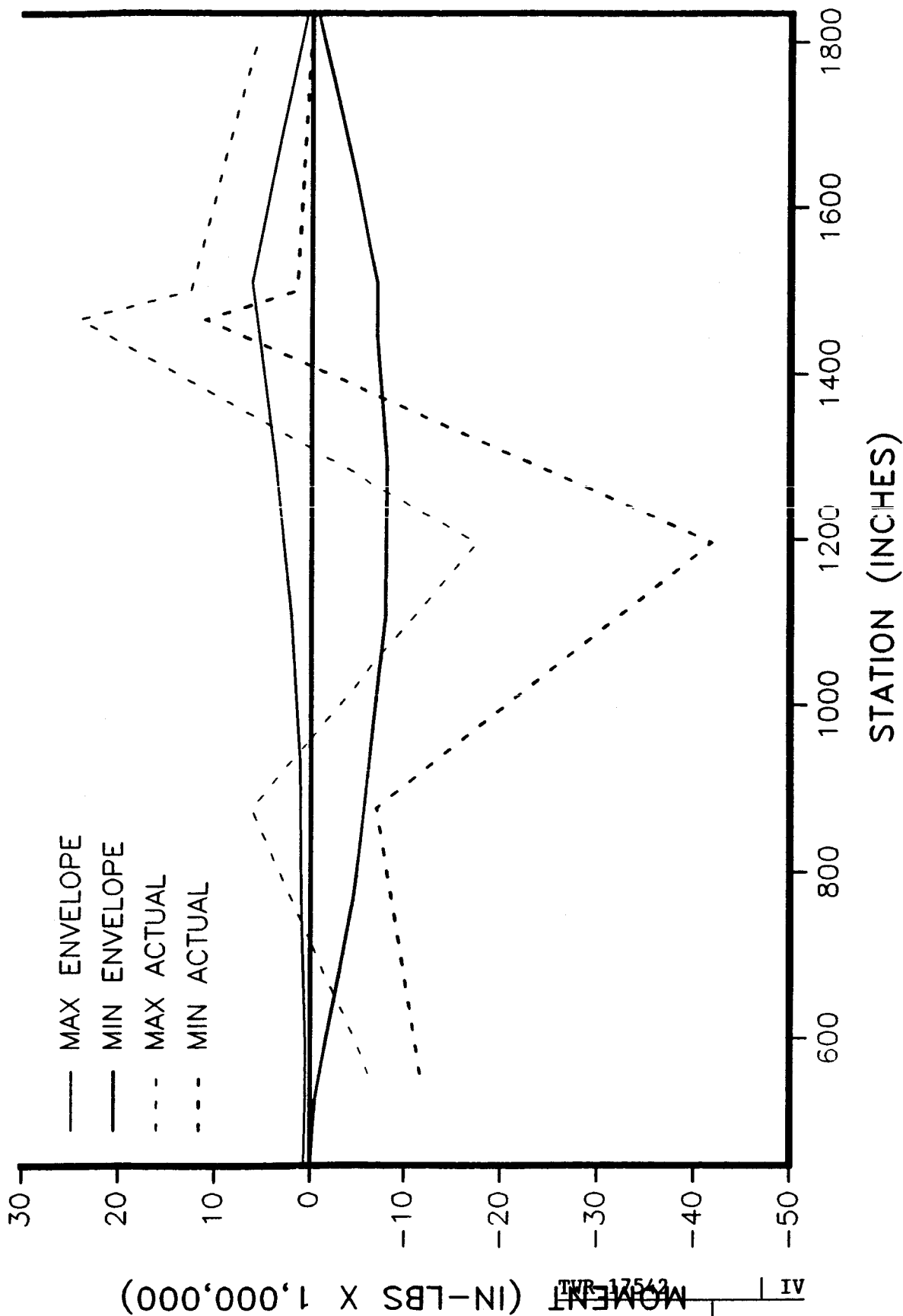
360L003 MAX Q ENVELOPE

BENDING ABOUT THE Y AXIS RIGHT SRB



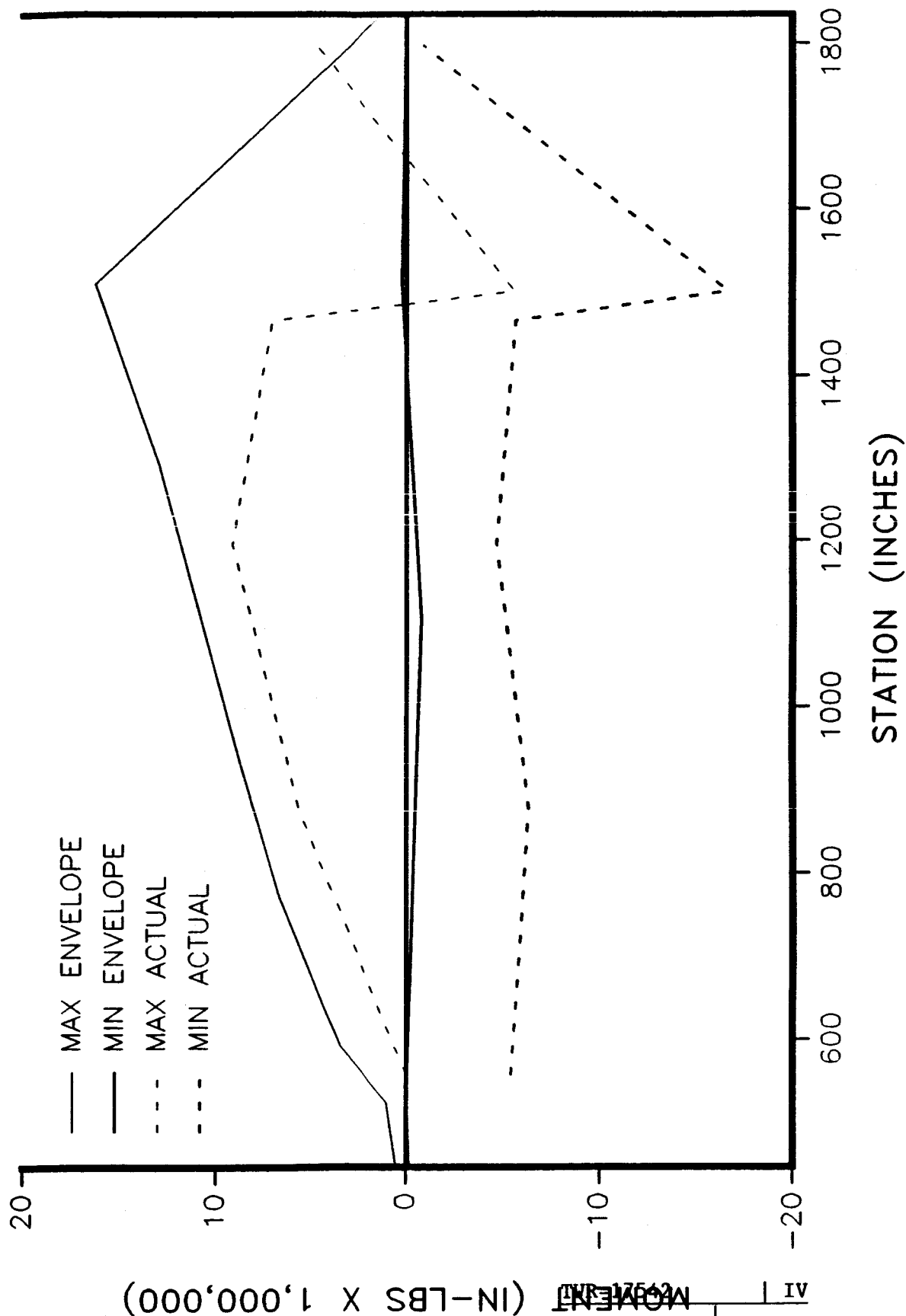
360L003 MAX G ENVELOPE

BENDING ABOUT THE Y AXIS LEFT SRB



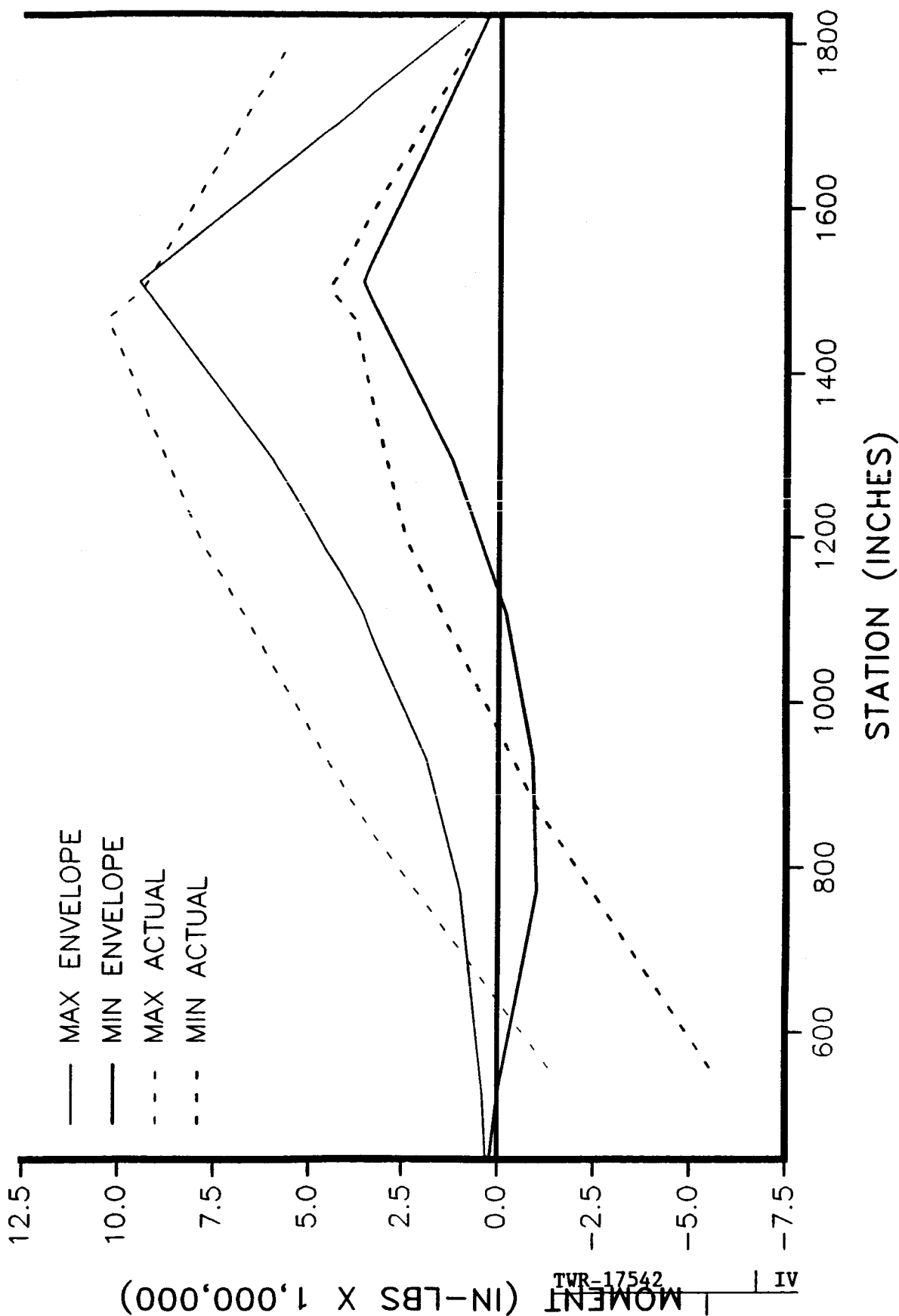
360L003 MAX G ENVELOPE

BENDING ABOUT THE Y AXIS RIGHT SRB



360L003 PRE-STAGING ENVELOPE

BENDING ABOUT THE Y AXIS LEFT SRB



A

MOMENT (IN-LBS X 1,000,000)

TVR-17542

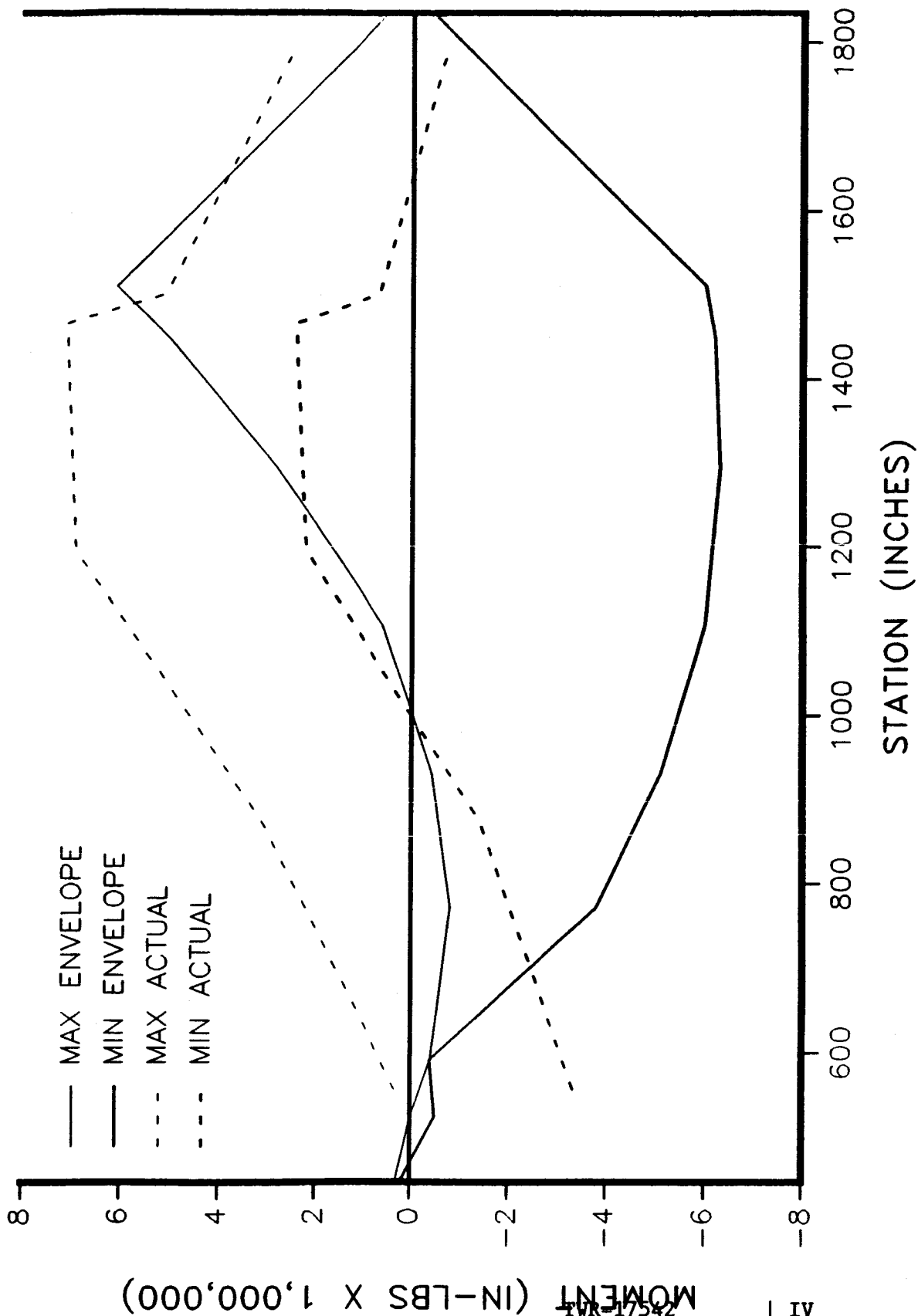
A-88

IV

STATION (INCHES)

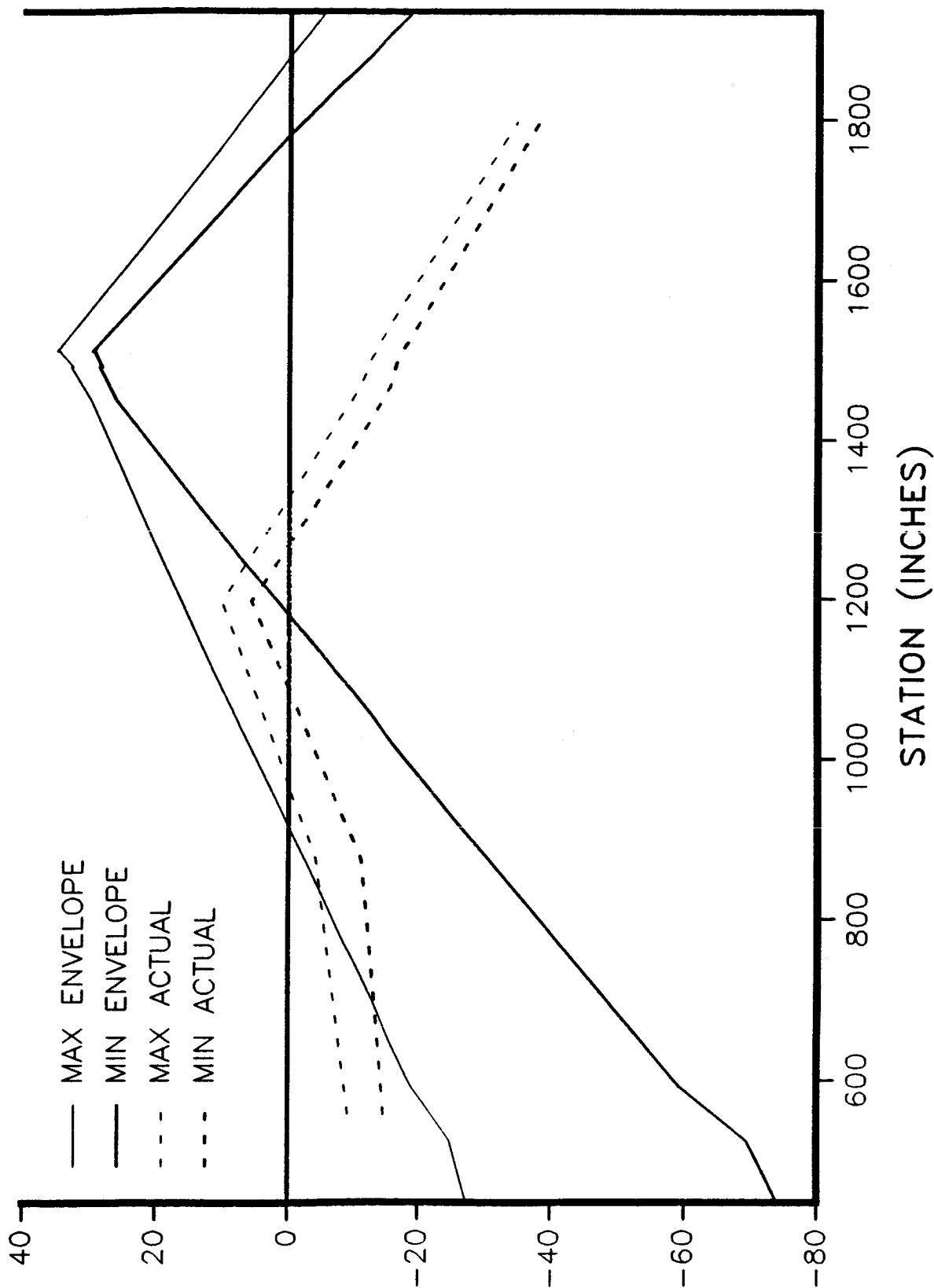
360L003 PRE-STAGING ENVELOPE

BENDING ABOUT THE Y AXIS RIGHT SRB



360L003 BUILD-UP ENVELOPE

BENDING ABOUT THE Z AXIS LEFT SRB



A

MOMENT (IN-LBS X 1,000,000)

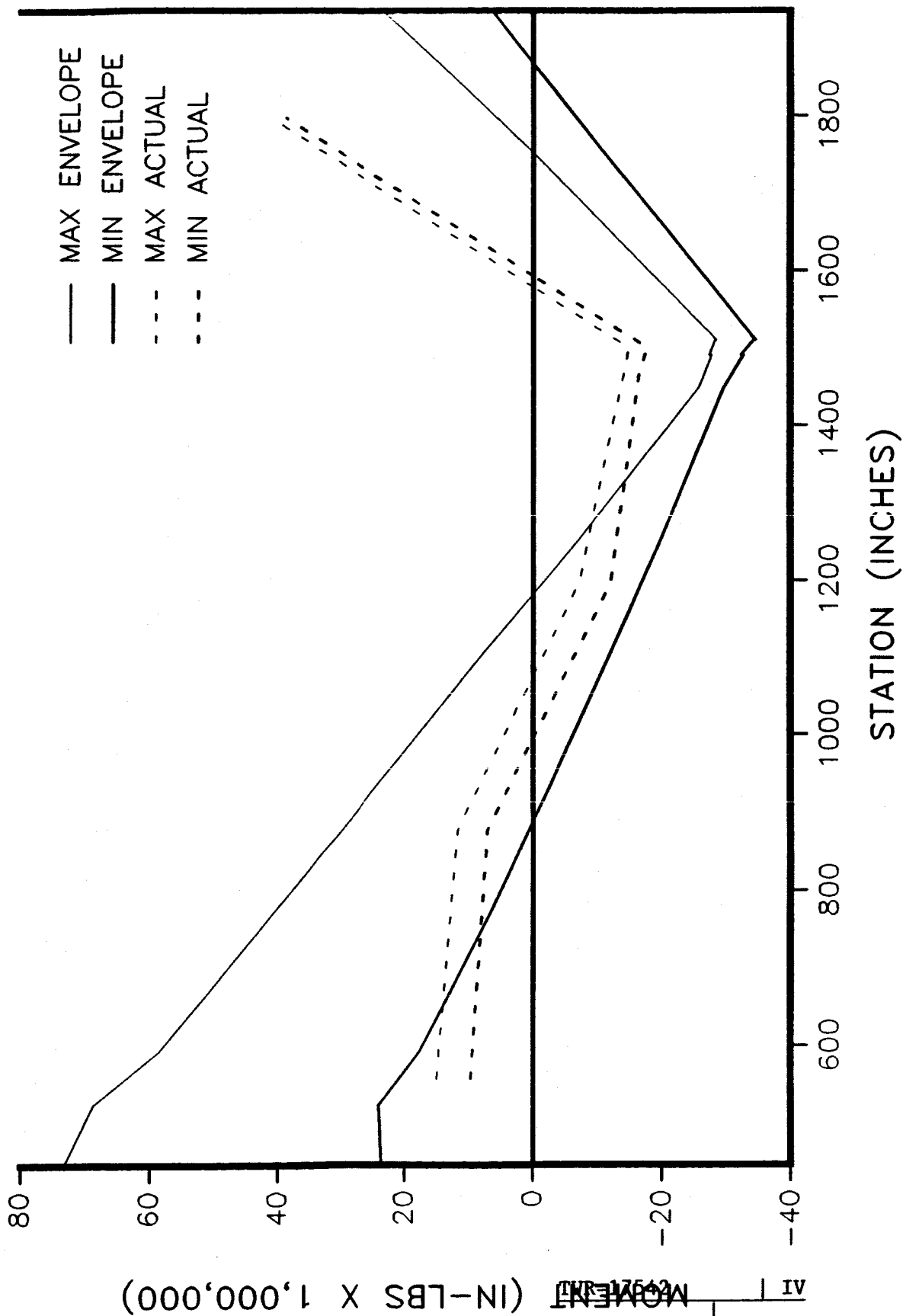
A-90

IV

ENC-17562

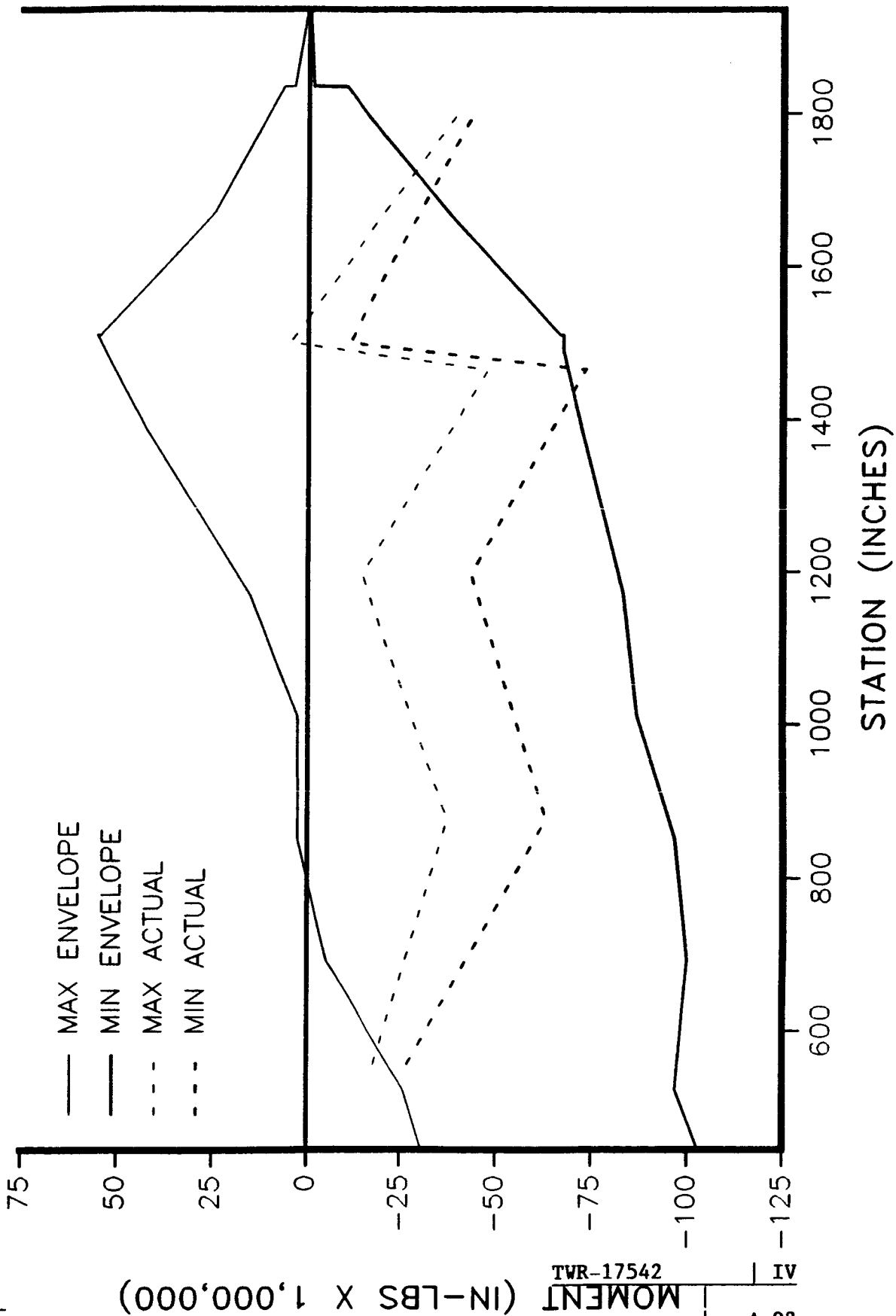
360L003 BUILD-UP ENVELOPE

BENDING ABOUT THE Z AXIS RIGHT SRB



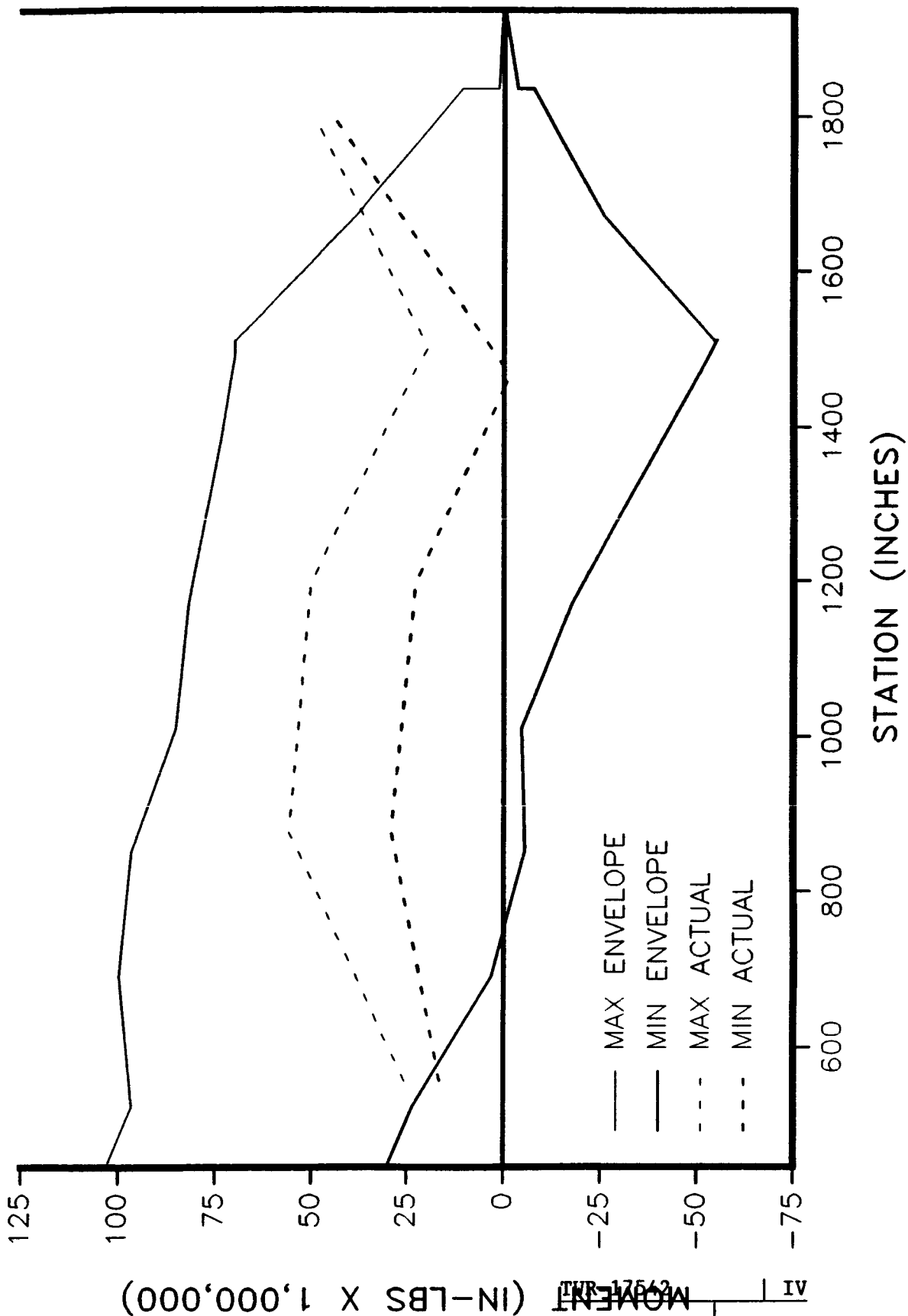
360L003 LIFT-OFF ENVELOPE

BENDING ABOUT THE Z AXIS LEFT SRB



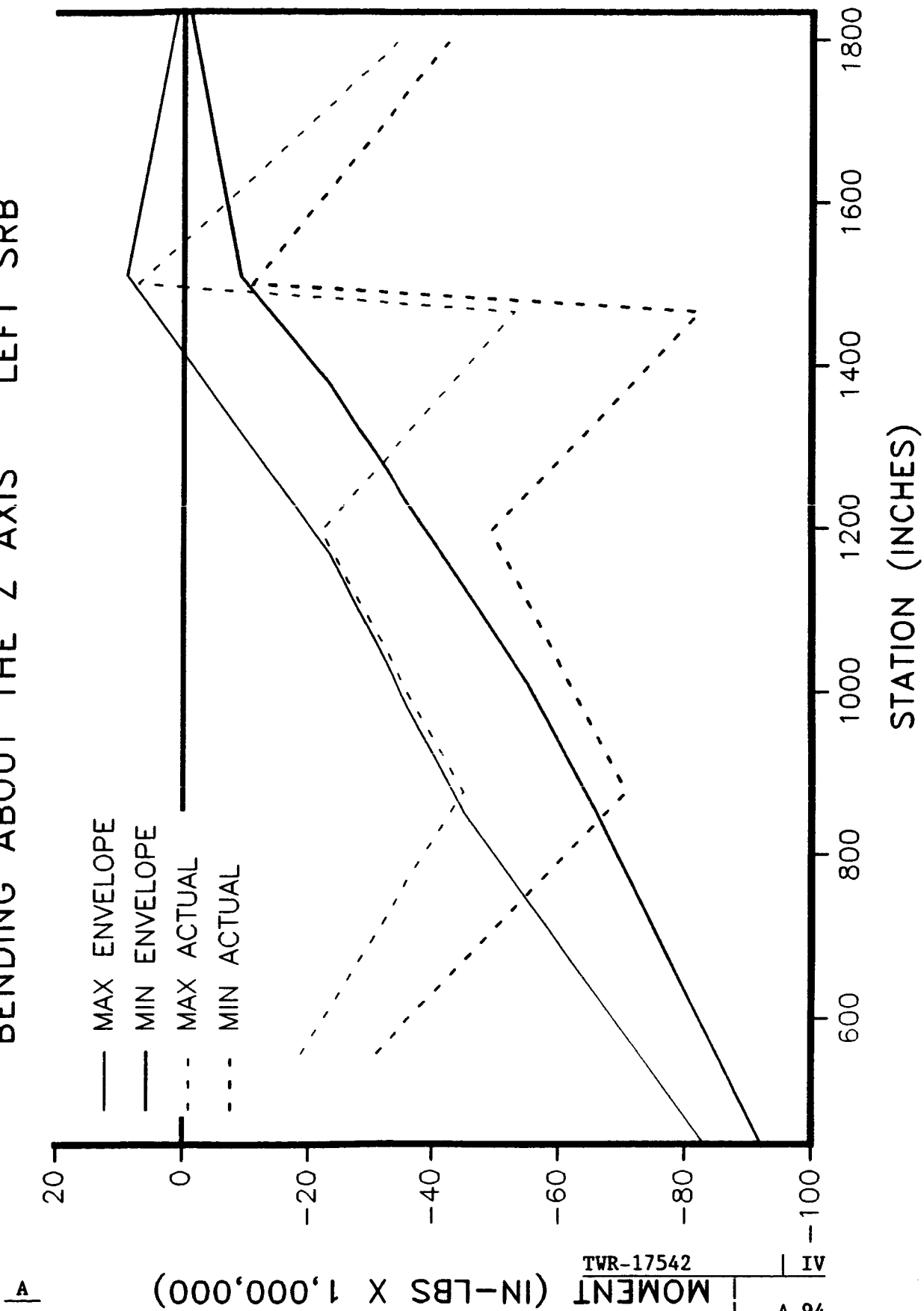
360L003 LIFT-OFF ENVELOPE

BENDING ABOUT THE Z AXIS RIGHT SRB



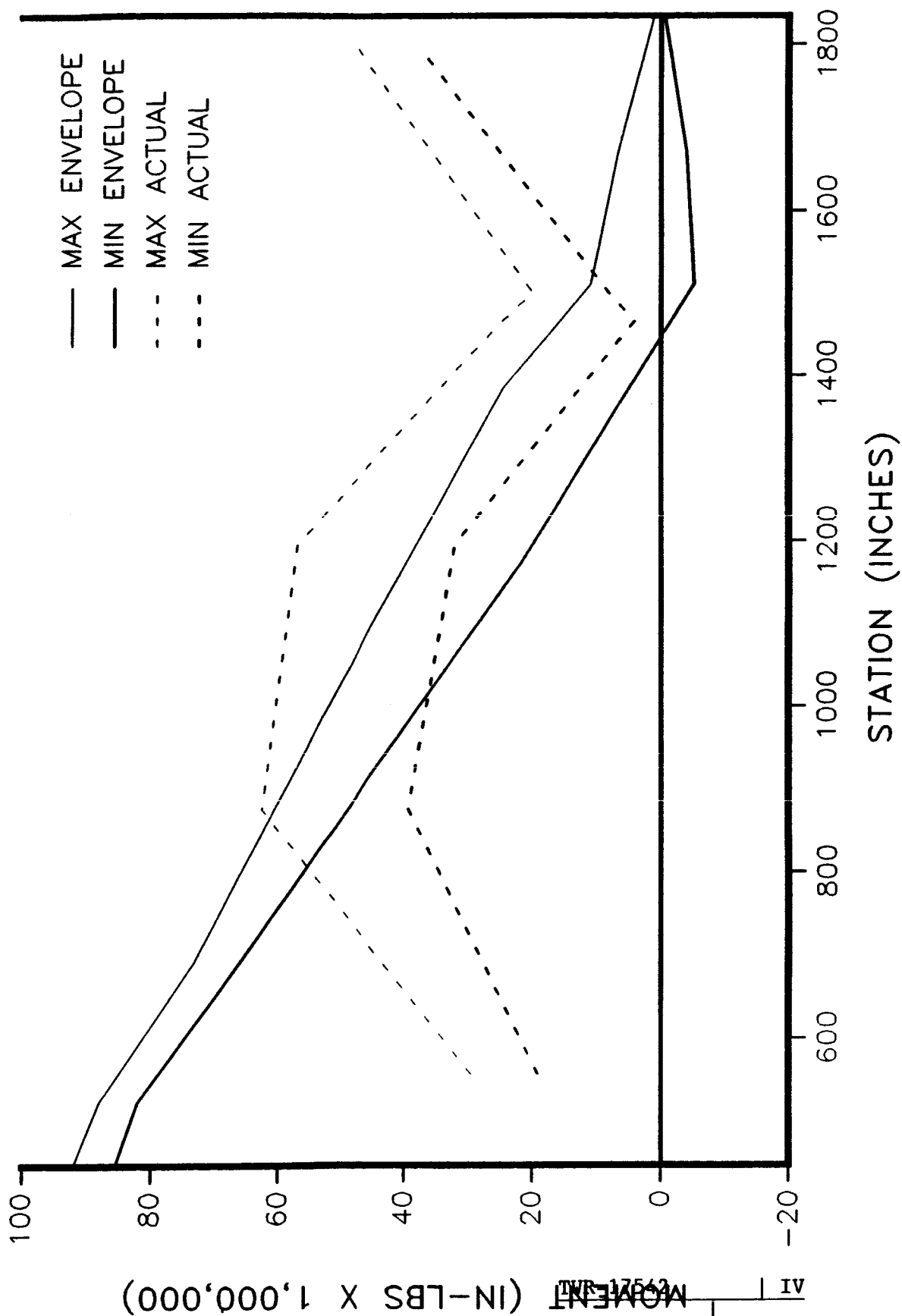
360L003 ROLL ENVELOPE

BENDING ABOUT THE Z AXIS LEFT SRB



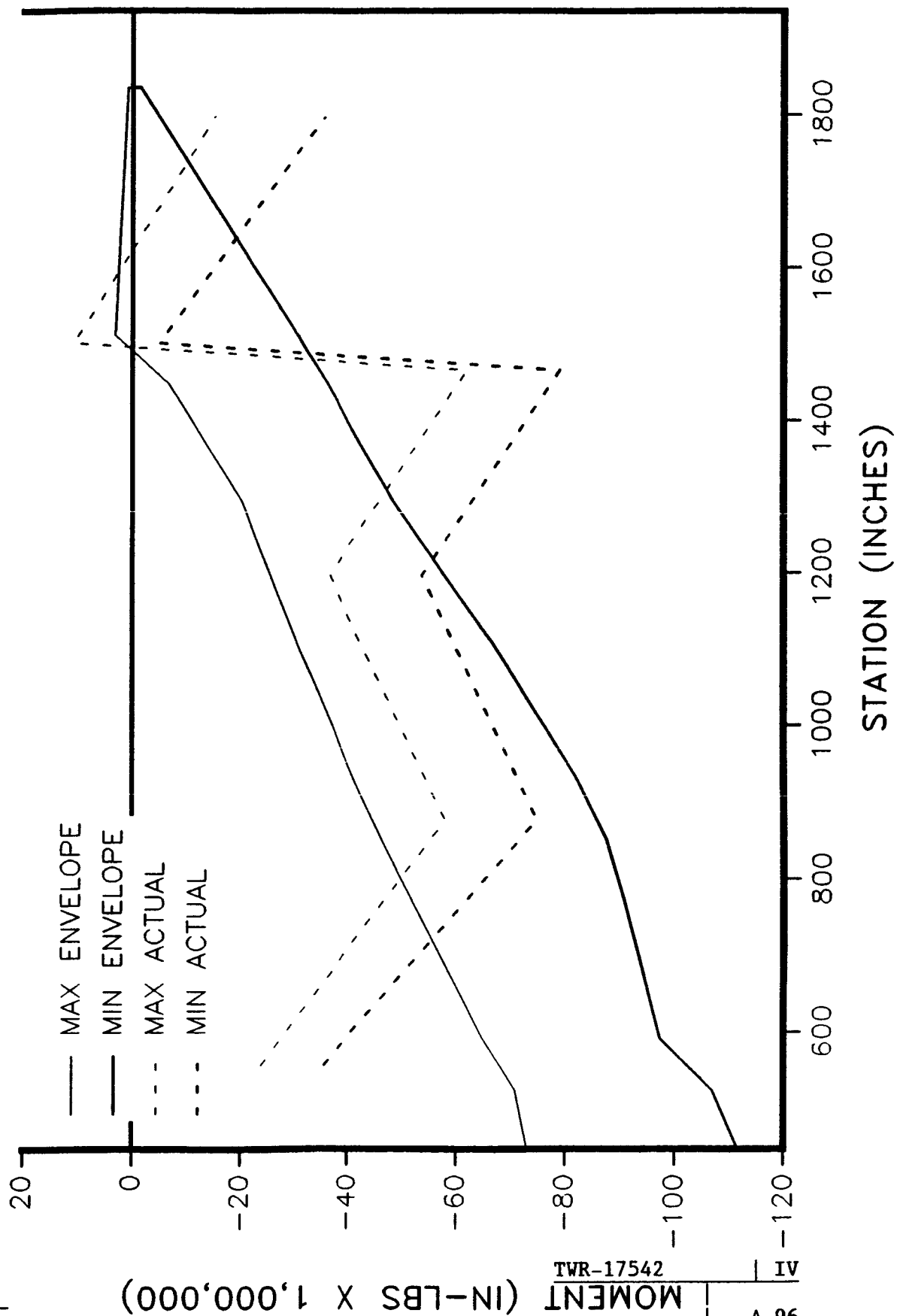
360L003 ROLL ENVELOPE

BENDING ABOUT THE Z AXIS RIGHT SRB



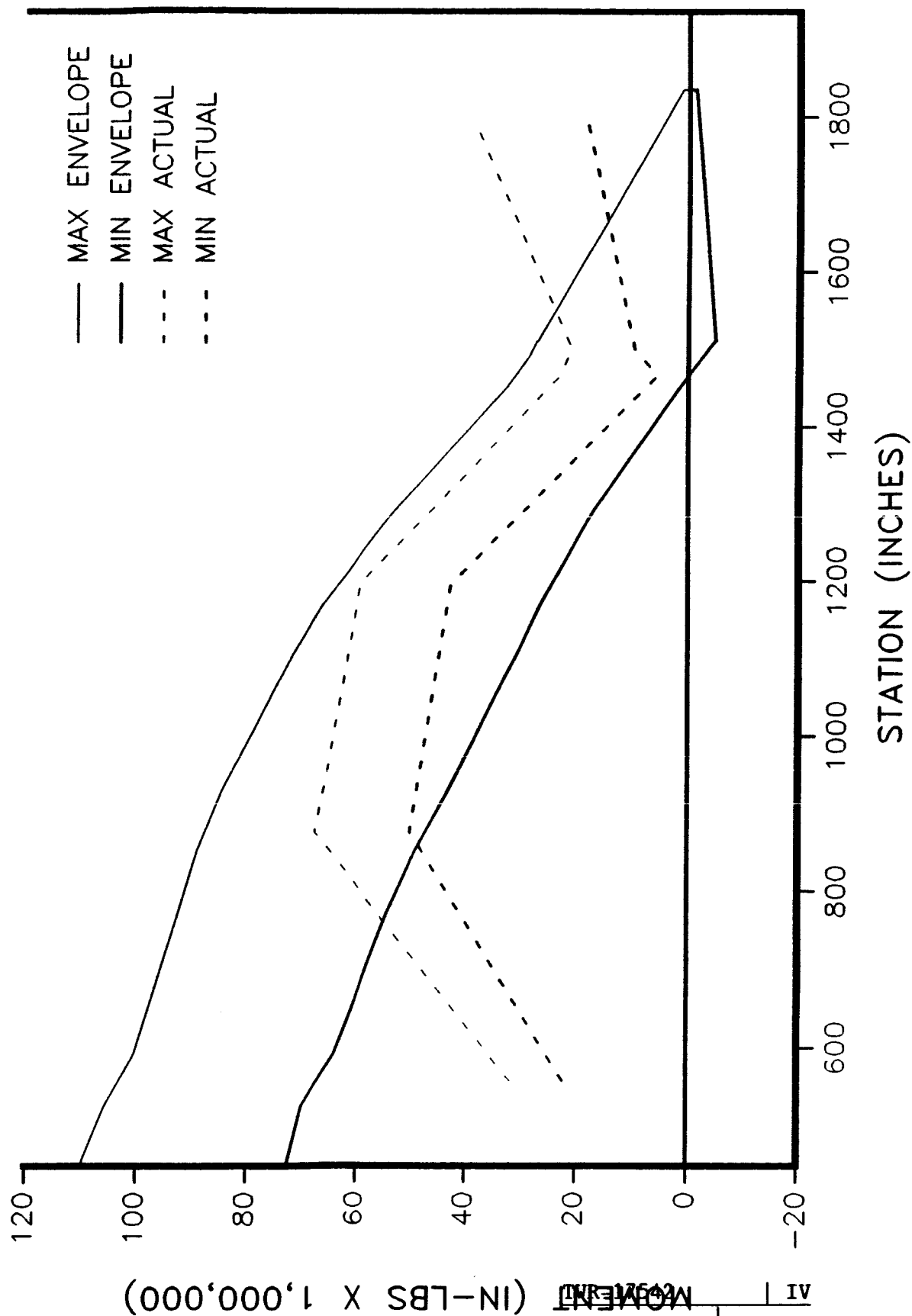
360L003 MAX Q ENVELOPE

BENDING ABOUT THE Z AXIS LEFT SRB



360L003 MAX Q ENVELOPE

BENDING ABOUT THE Z AXIS RIGHT SRB



A

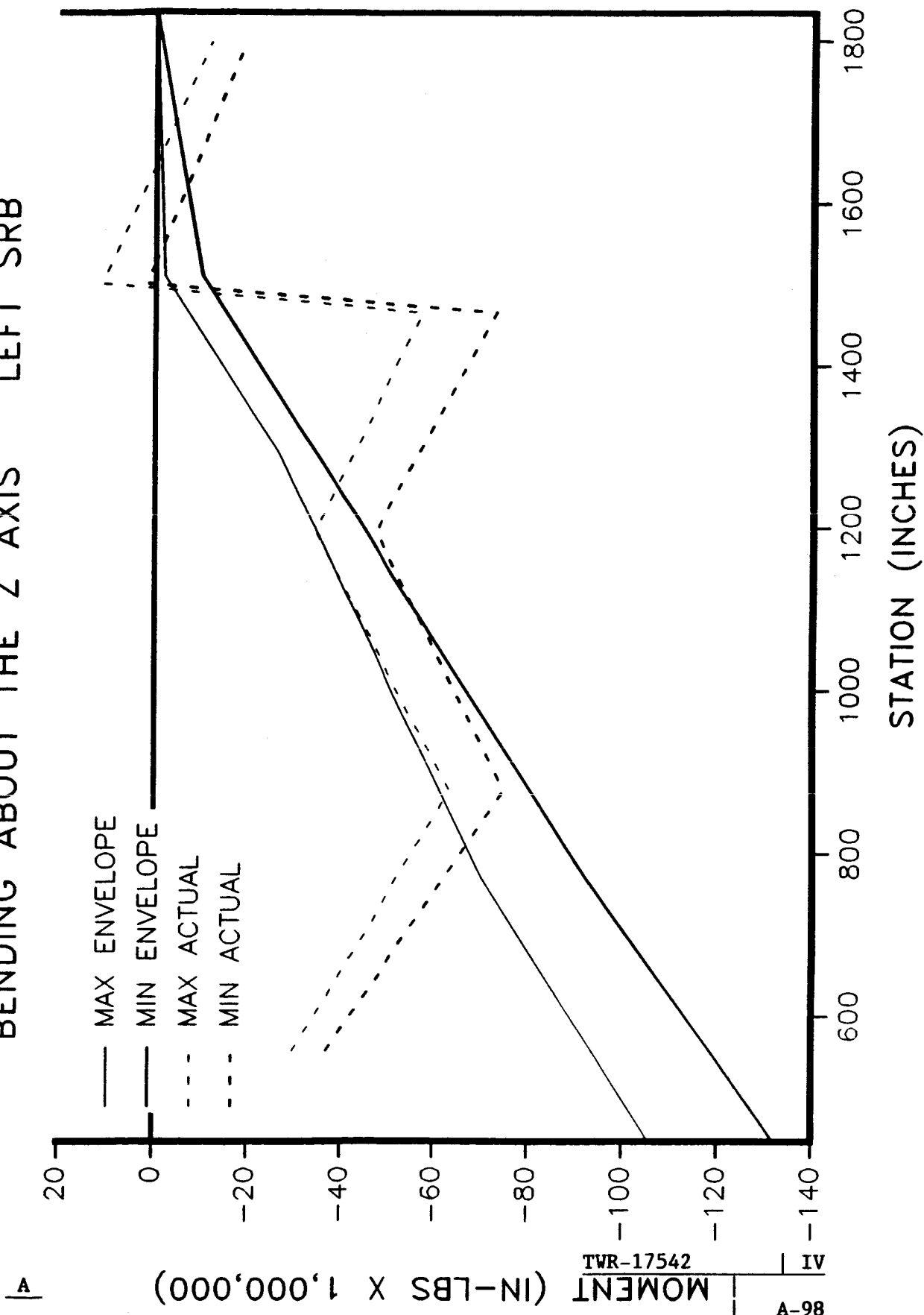
MOMENT (IN-LBS X 1,000,000)

A-97

IV

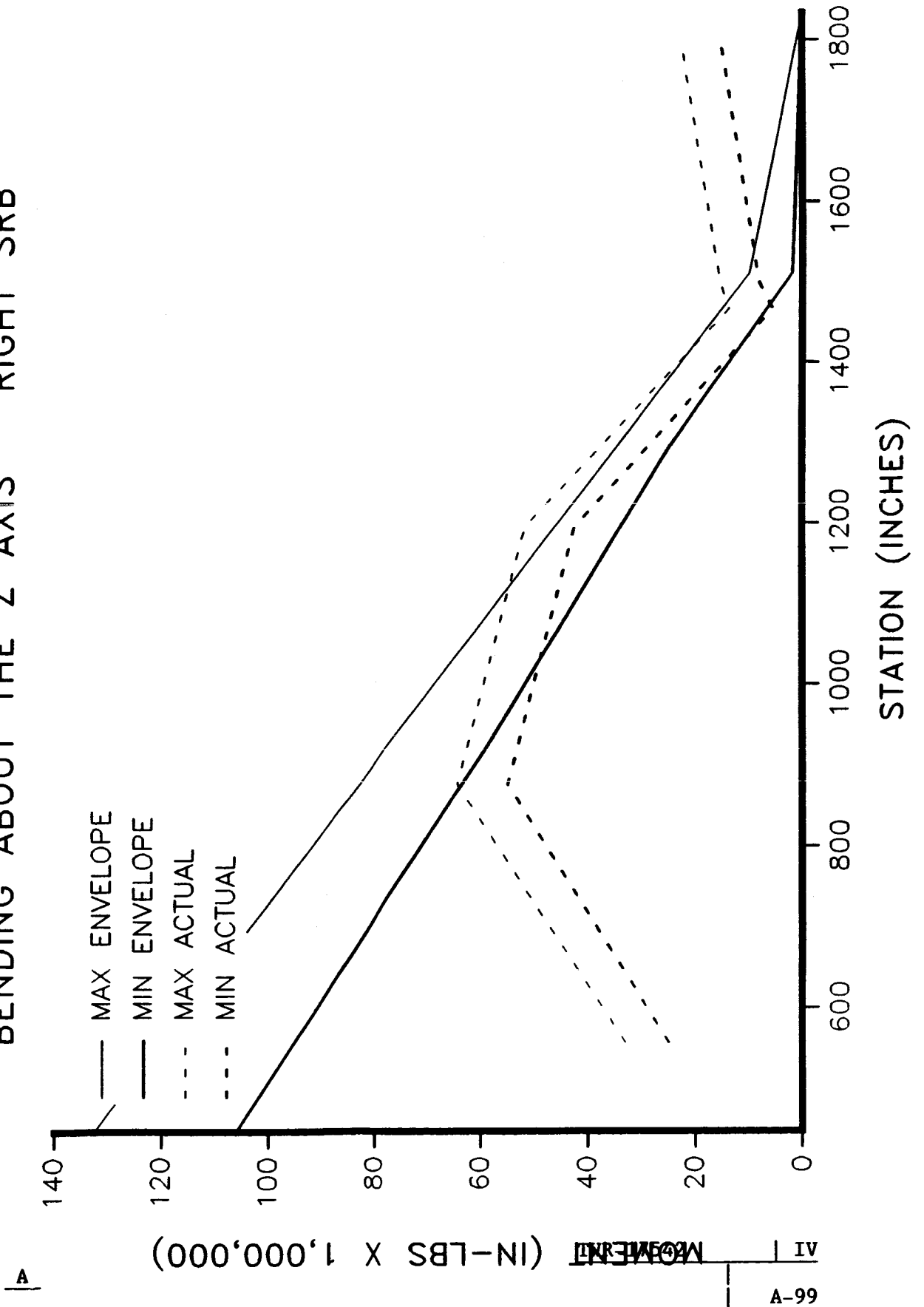
360L003 MAX G ENVELOPE

BENDING ABOUT THE Z AXIS LEFT SRB



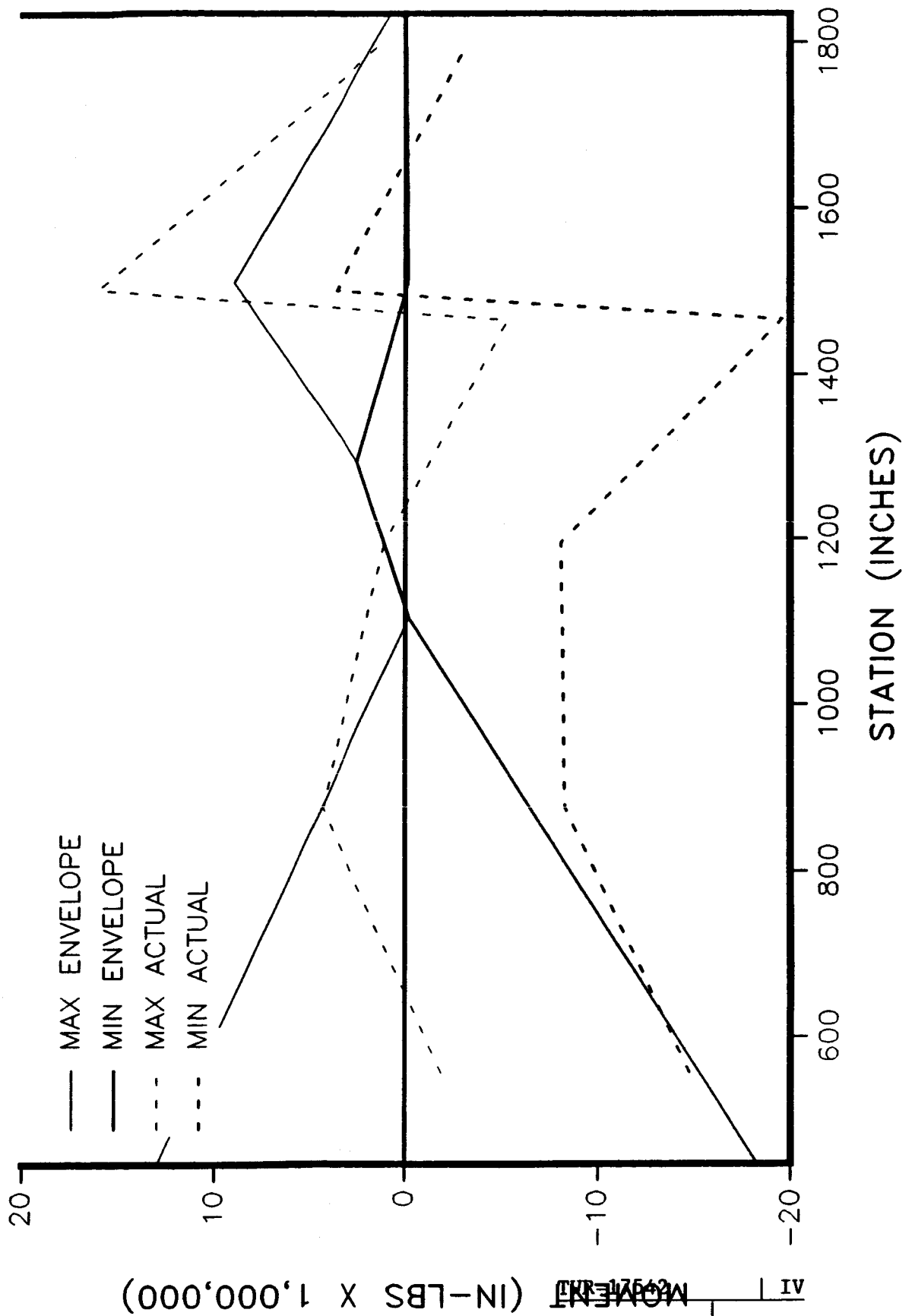
360L003 MAX G ENVELOPE

BENDING ABOUT THE Z AXIS RIGHT SRB



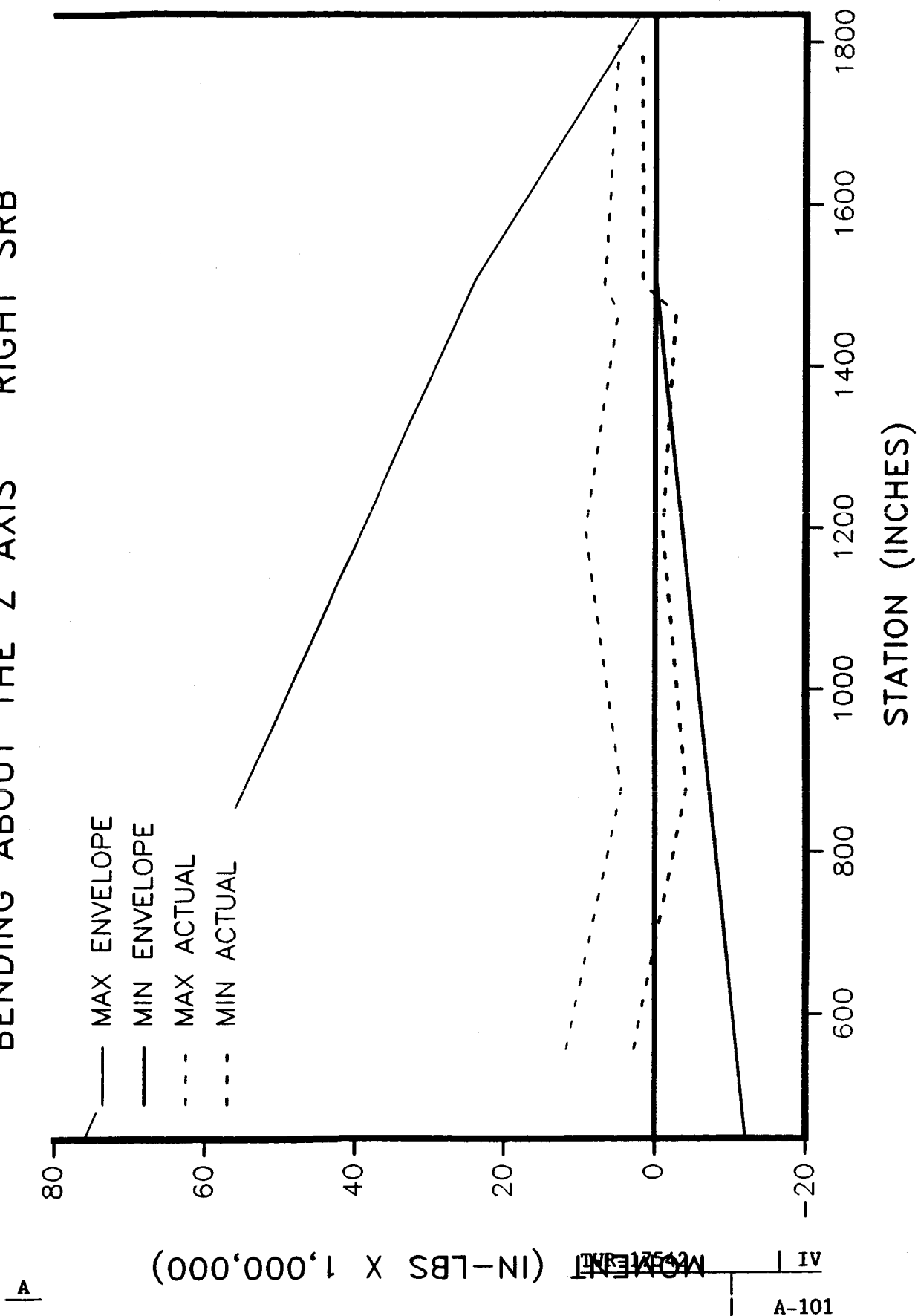
360L003 PRE-STAGING ENVELOPE

BENDING ABOUT THE Z AXIS LEFT SRB



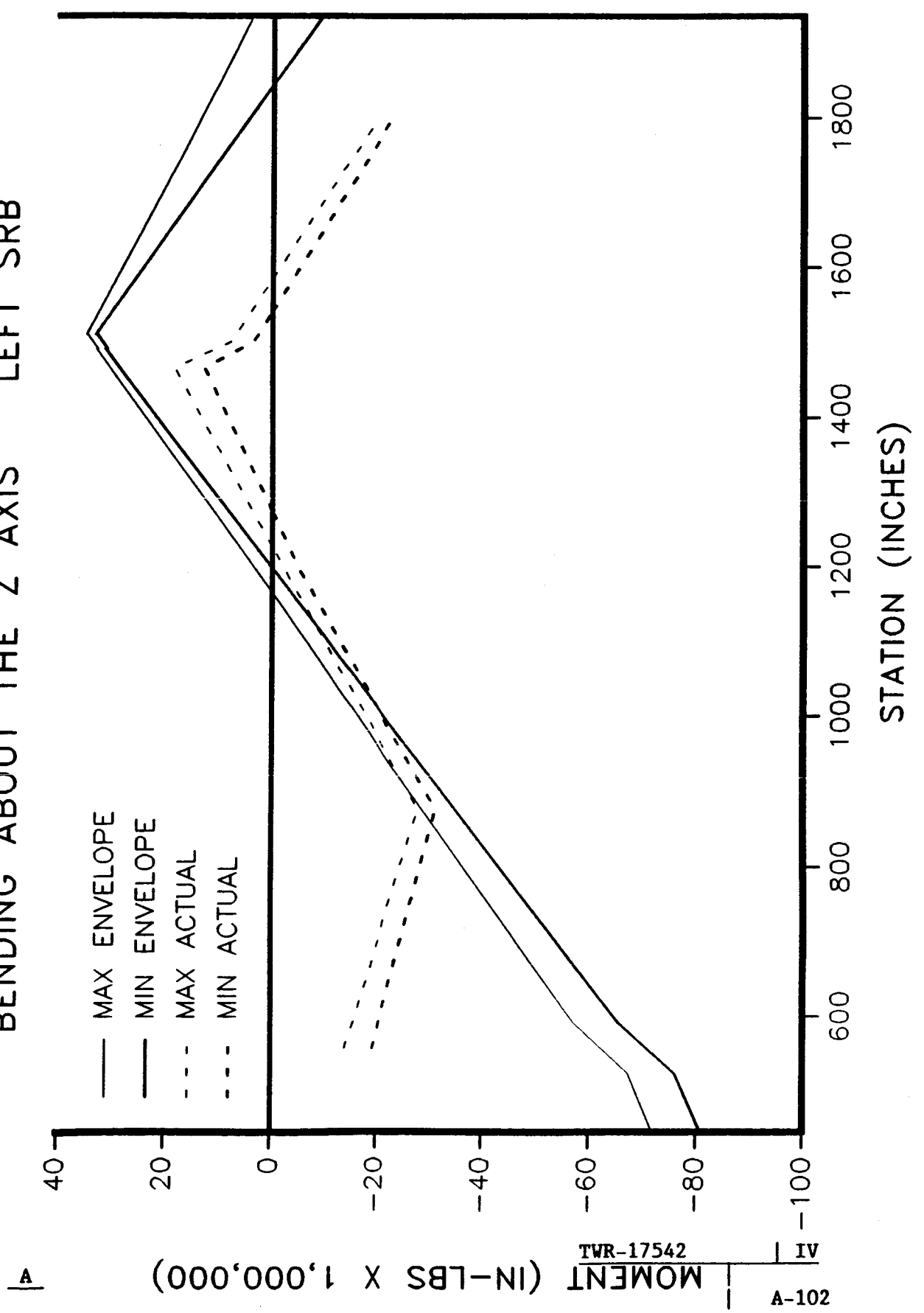
360L003 PRE-STAGING ENVELOPE

BENDING ABOUT THE Z AXIS RIGHT SRB



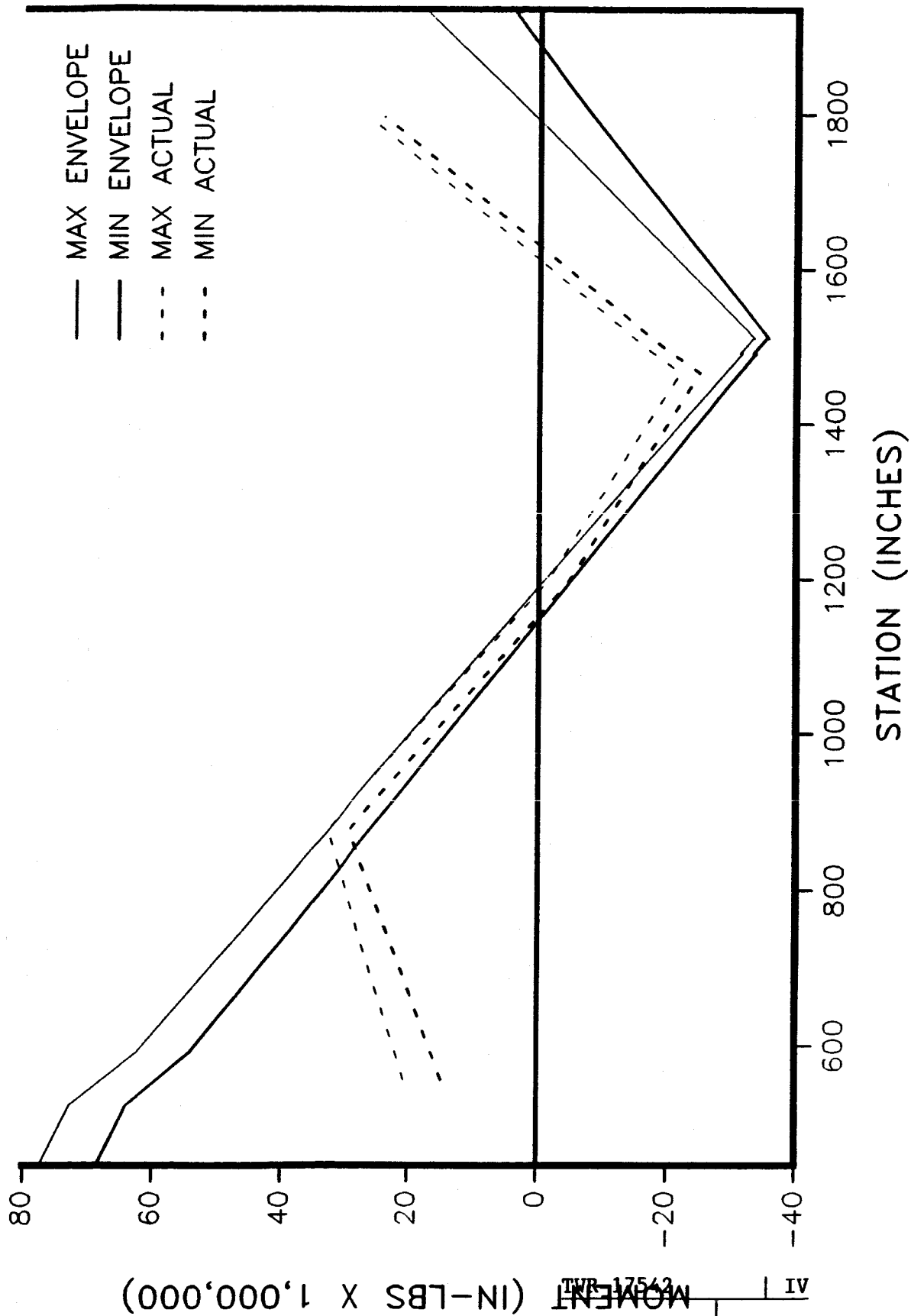
360L003 PRE-LAUNCH ENVELOPE

BENDING ABOUT THE Z AXIS LEFT SRB



360L003 PRE-LAUNCH ENVELOPE

BENDING ABOUT THE Z AXIS RIGHT SRB



A

MOMENT (IN-LBS X 1,000,000)

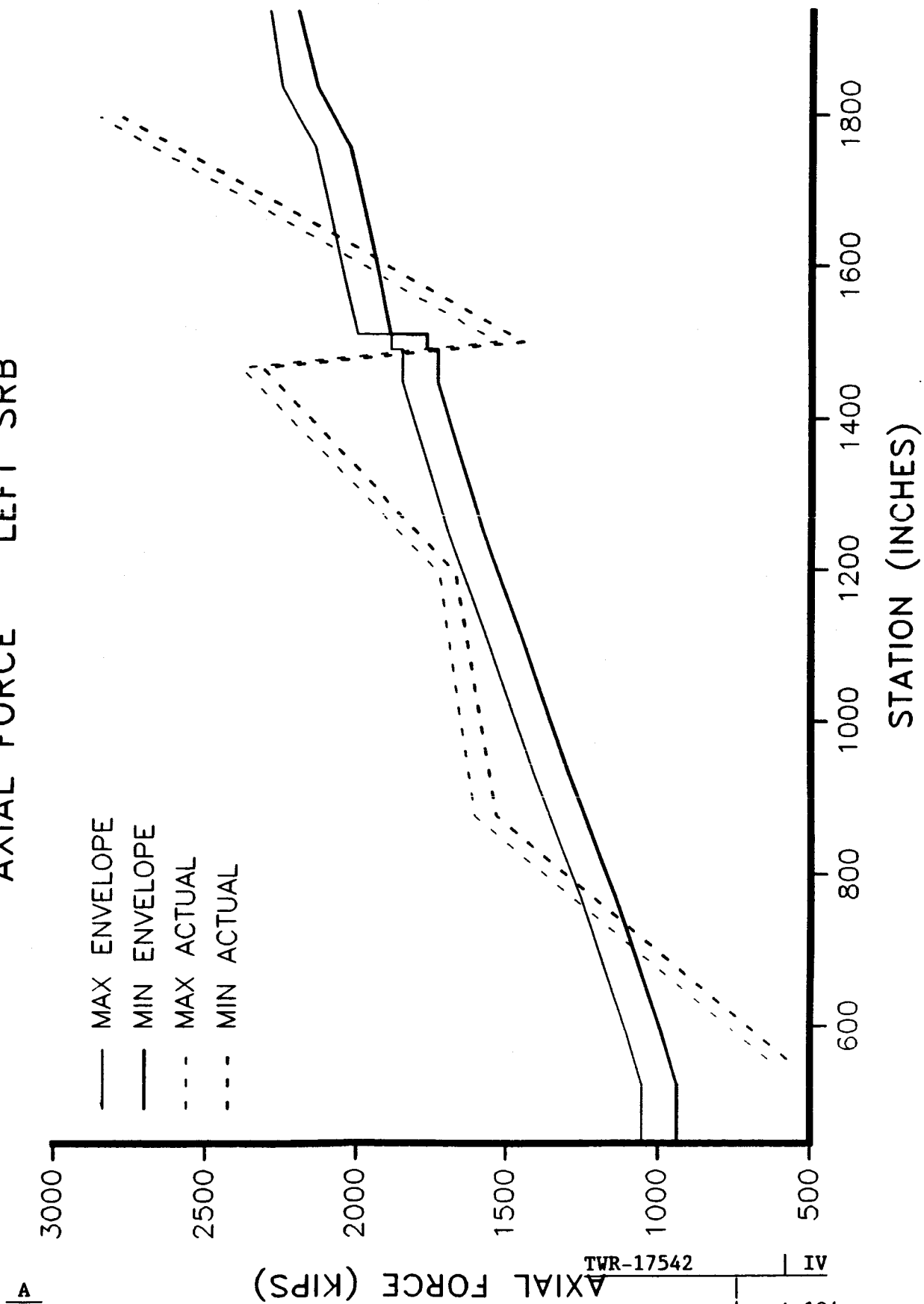
TWR-17543

IV

A-103

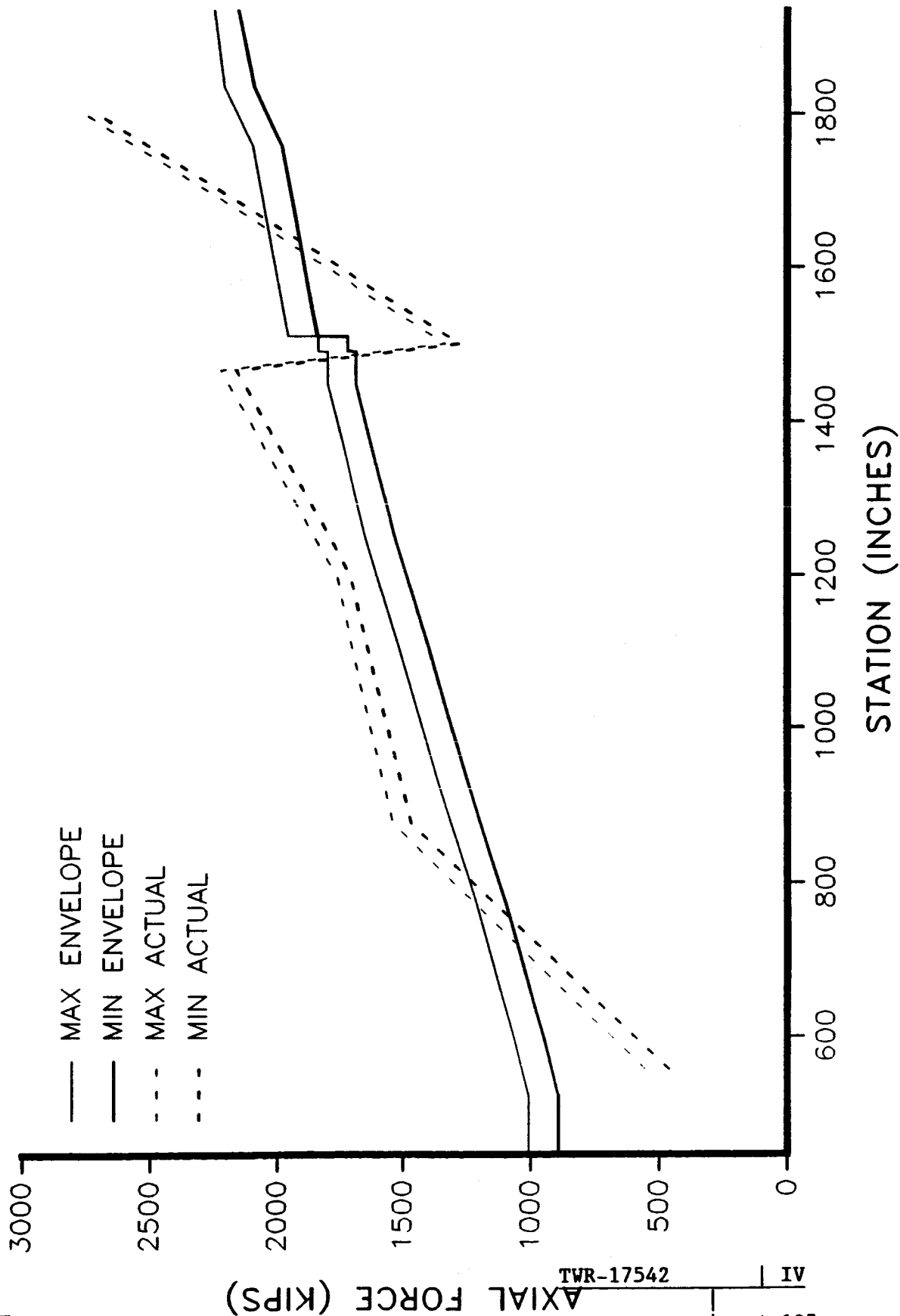
360L003 PRE-LAUNCH ENVELOPE

AXIAL FORCE LEFT SRB



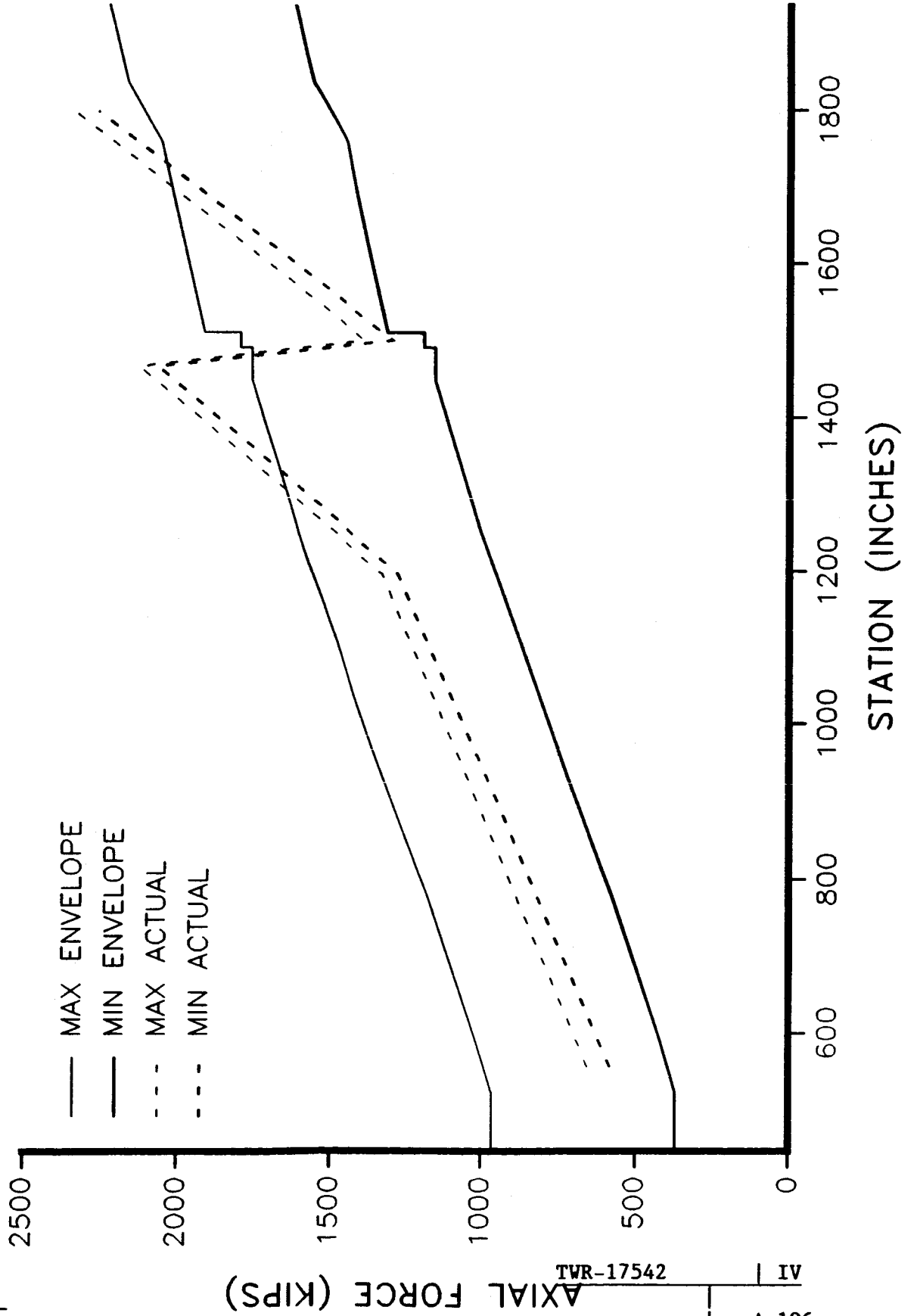
360L003 PRE-LAUNCH ENVELOPE

AXIAL FORCE RIGHT SRB



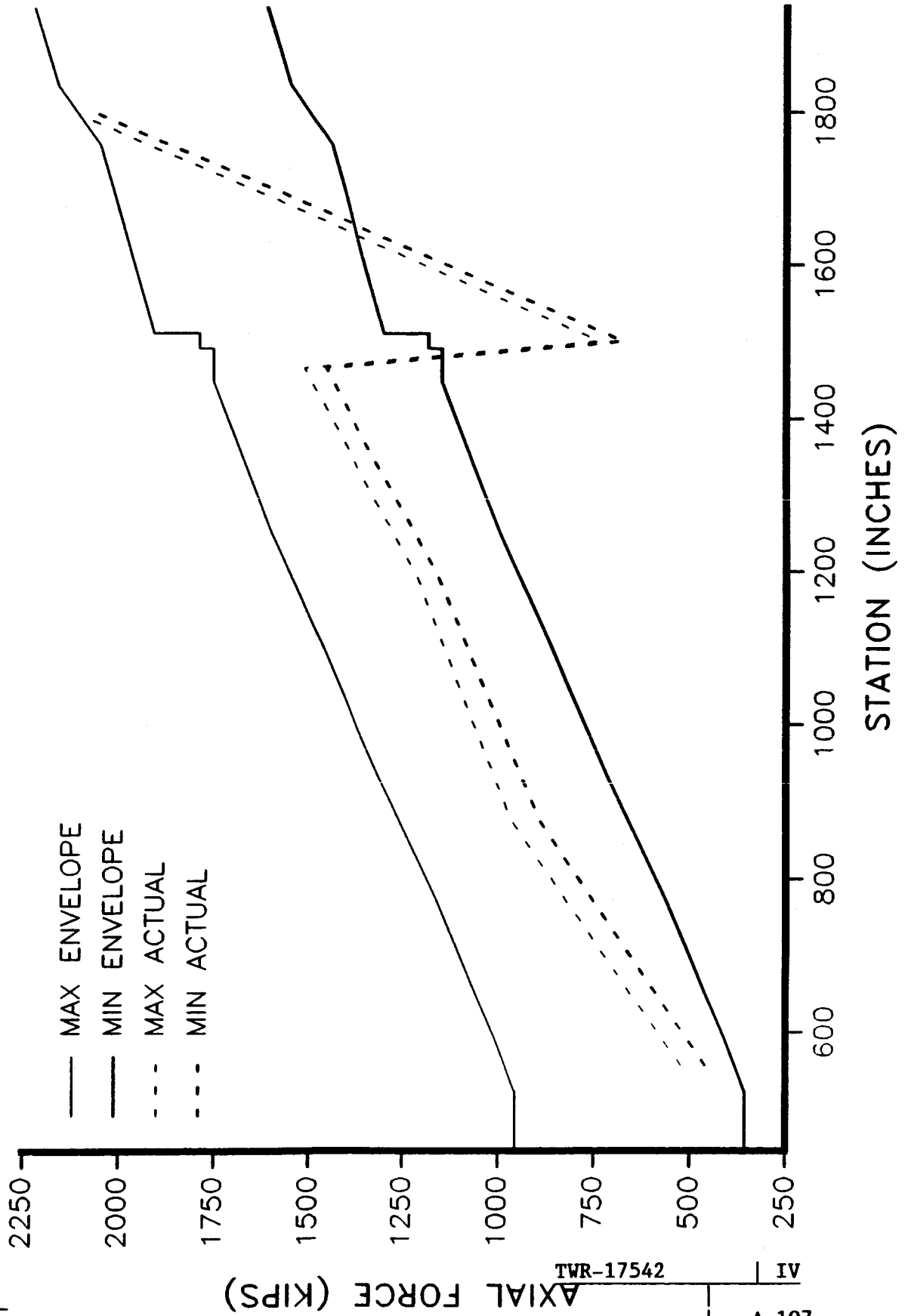
360L003 BUILD-UP ENVELOPE

AXIAL FORCE LEFT SRB



360L003 BUILD-UP ENVELOPE

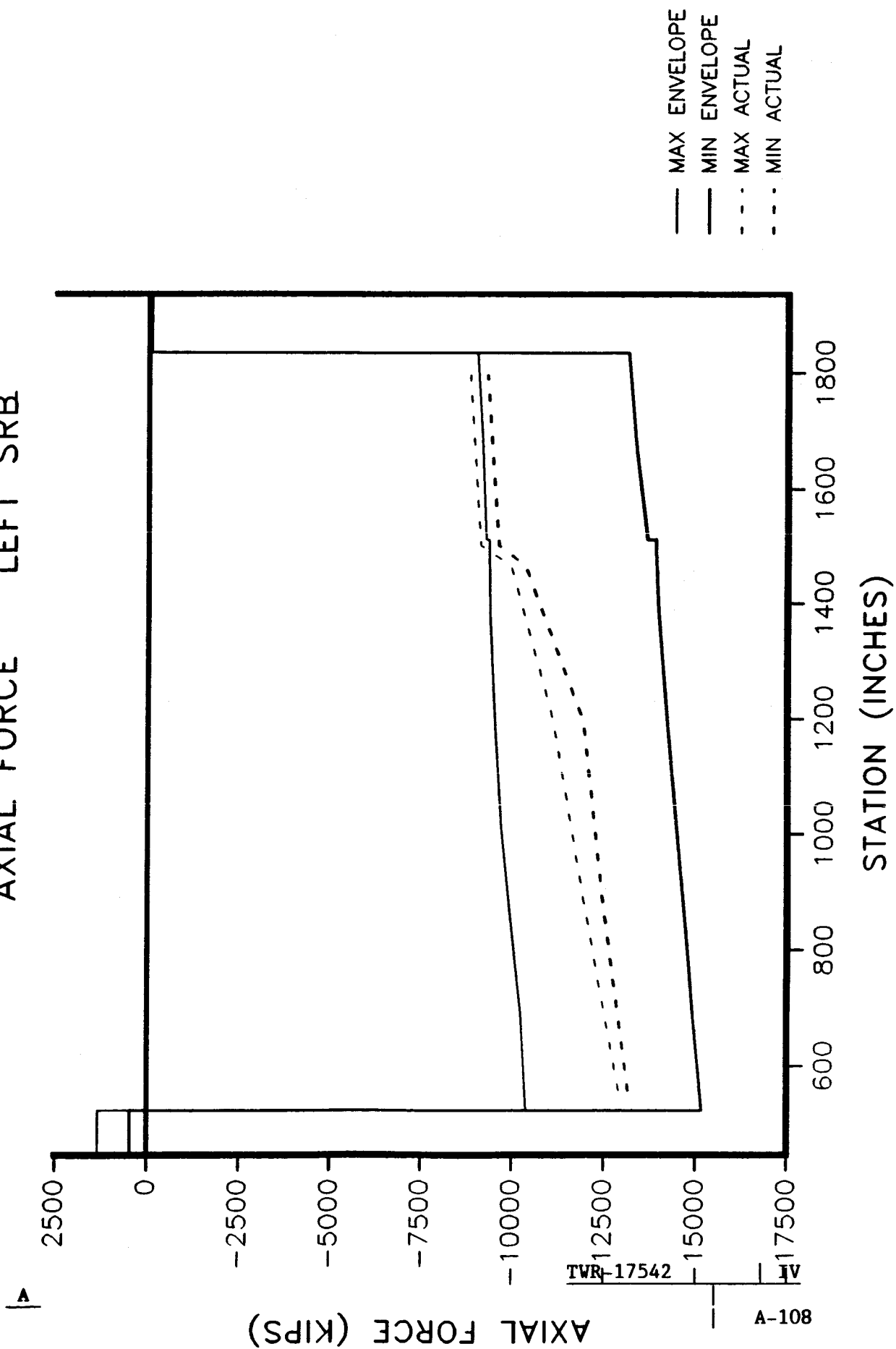
AXIAL FORCE RIGHT SRB



TWR-17542

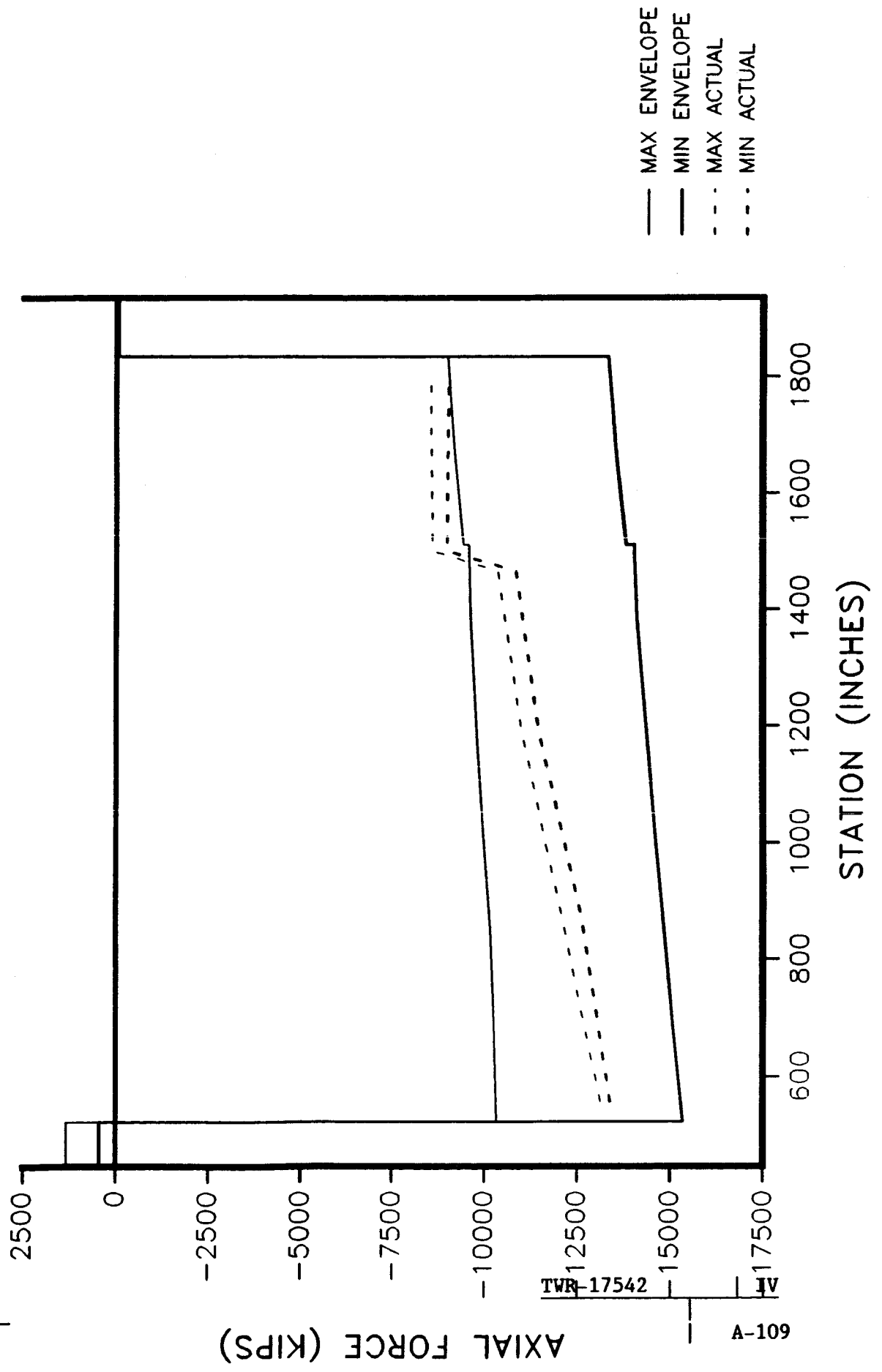
360L003 LIFT-OFF ENVELOPE

AXIAL FORCE LEFT SRB



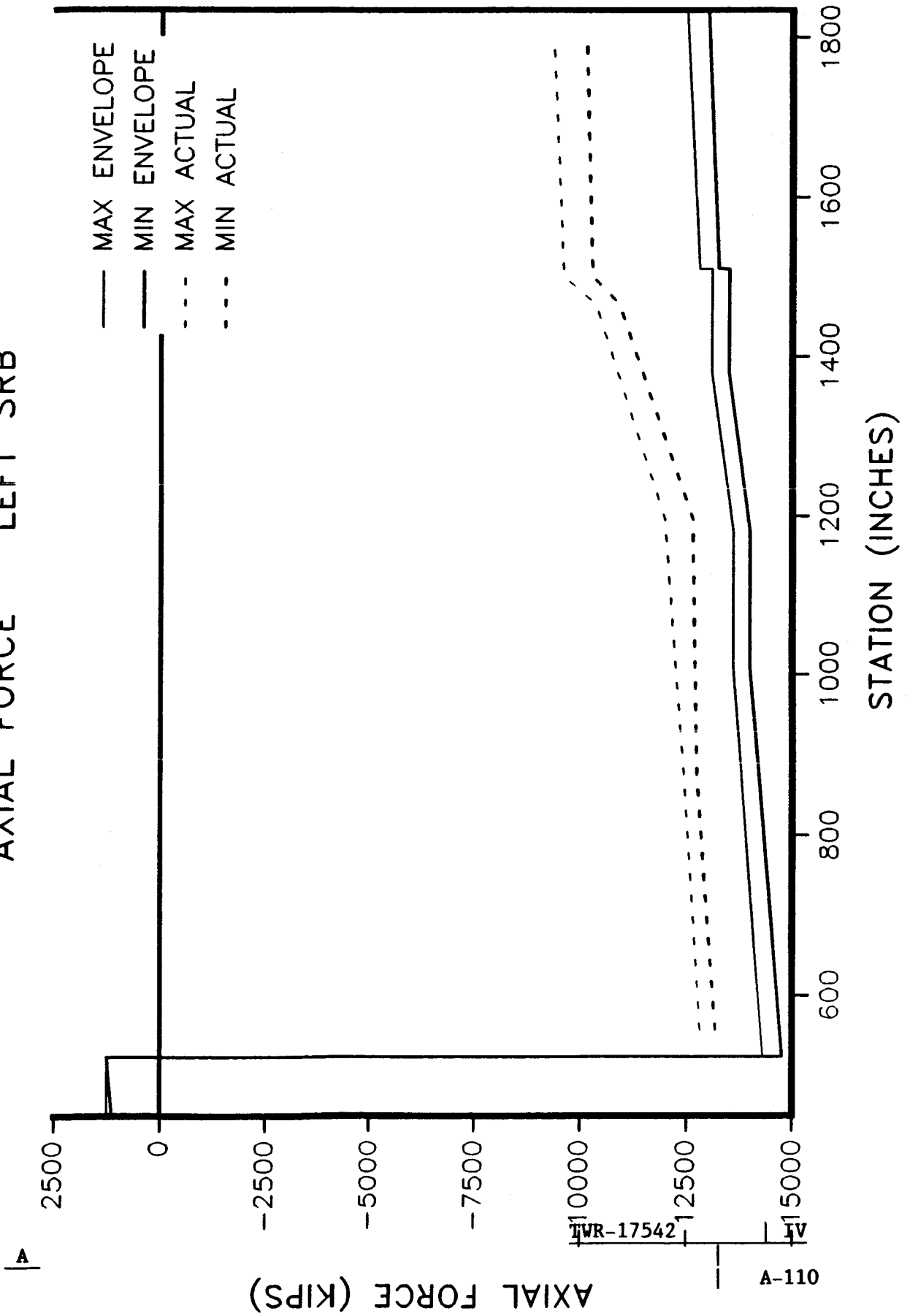
360L003 LIFT-OFF ENVELOPE

AXIAL FORCE RIGHT SRB



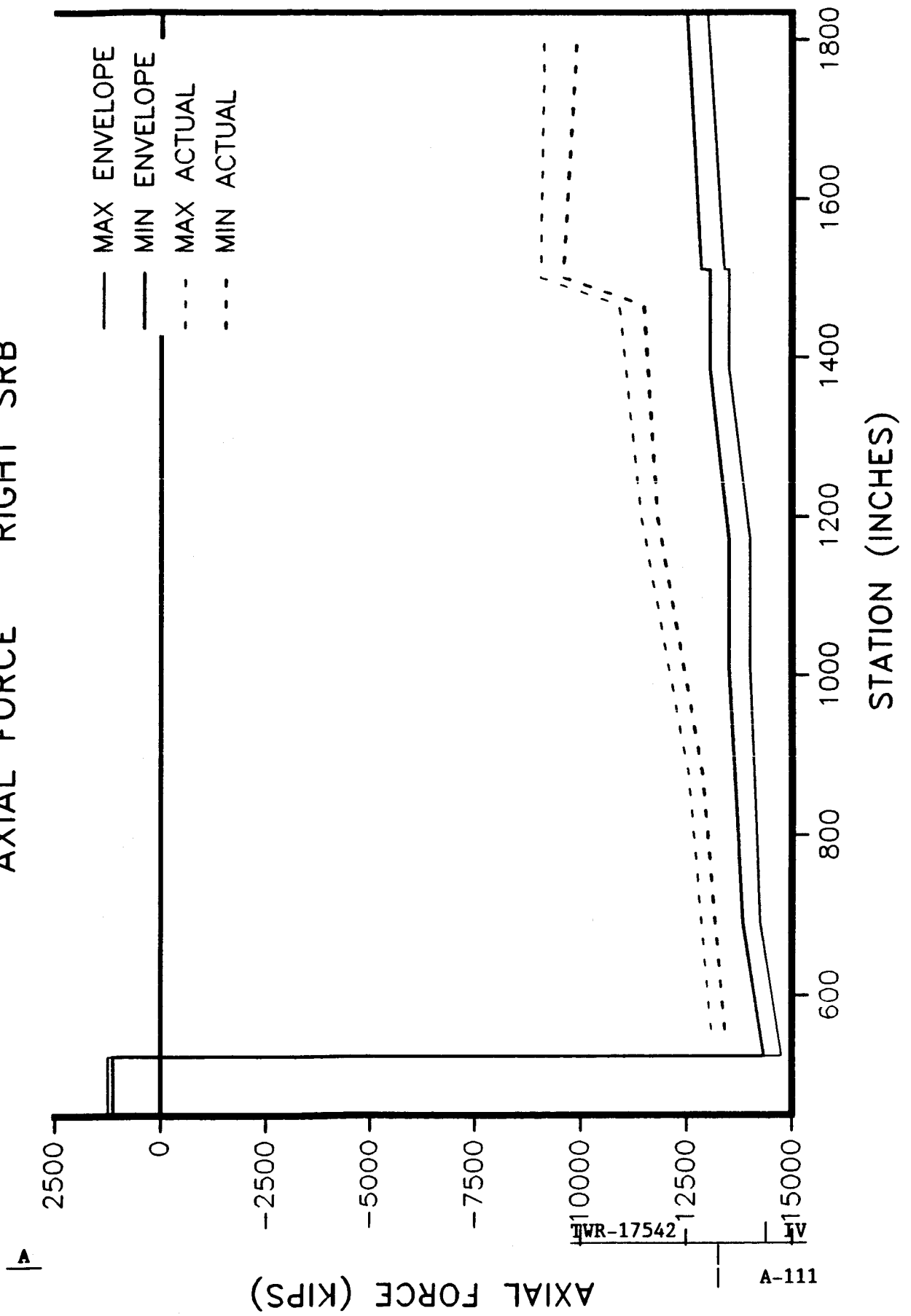
360L003 ROLL ENVELOPE

AXIAL FORCE LEFT SRB



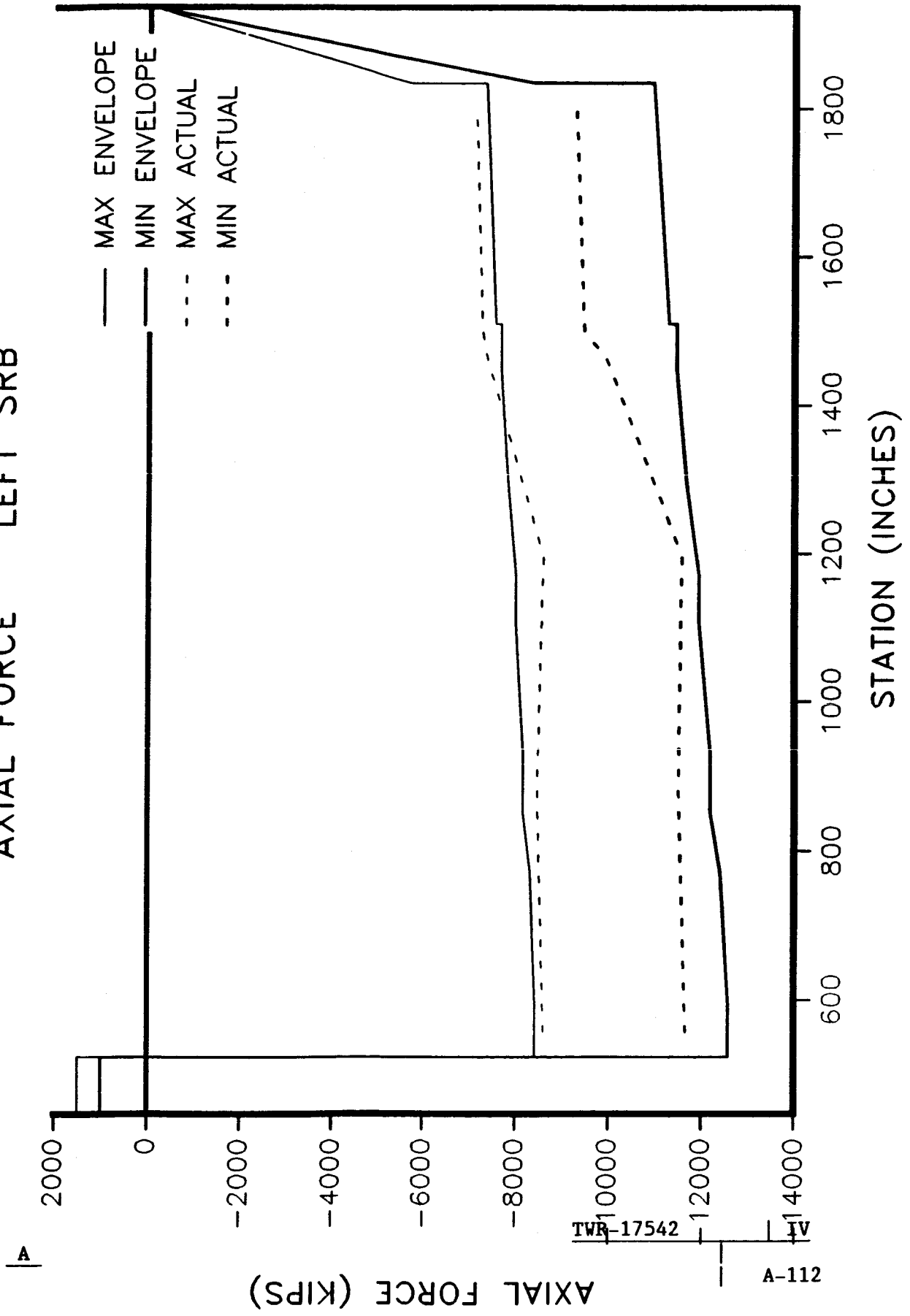
360L003 ROLL ENVELOPE

AXIAL FORCE RIGHT SRB



360L003 MAX Q ENVELOPE

AXIAL FORCE LEFT SRB



A

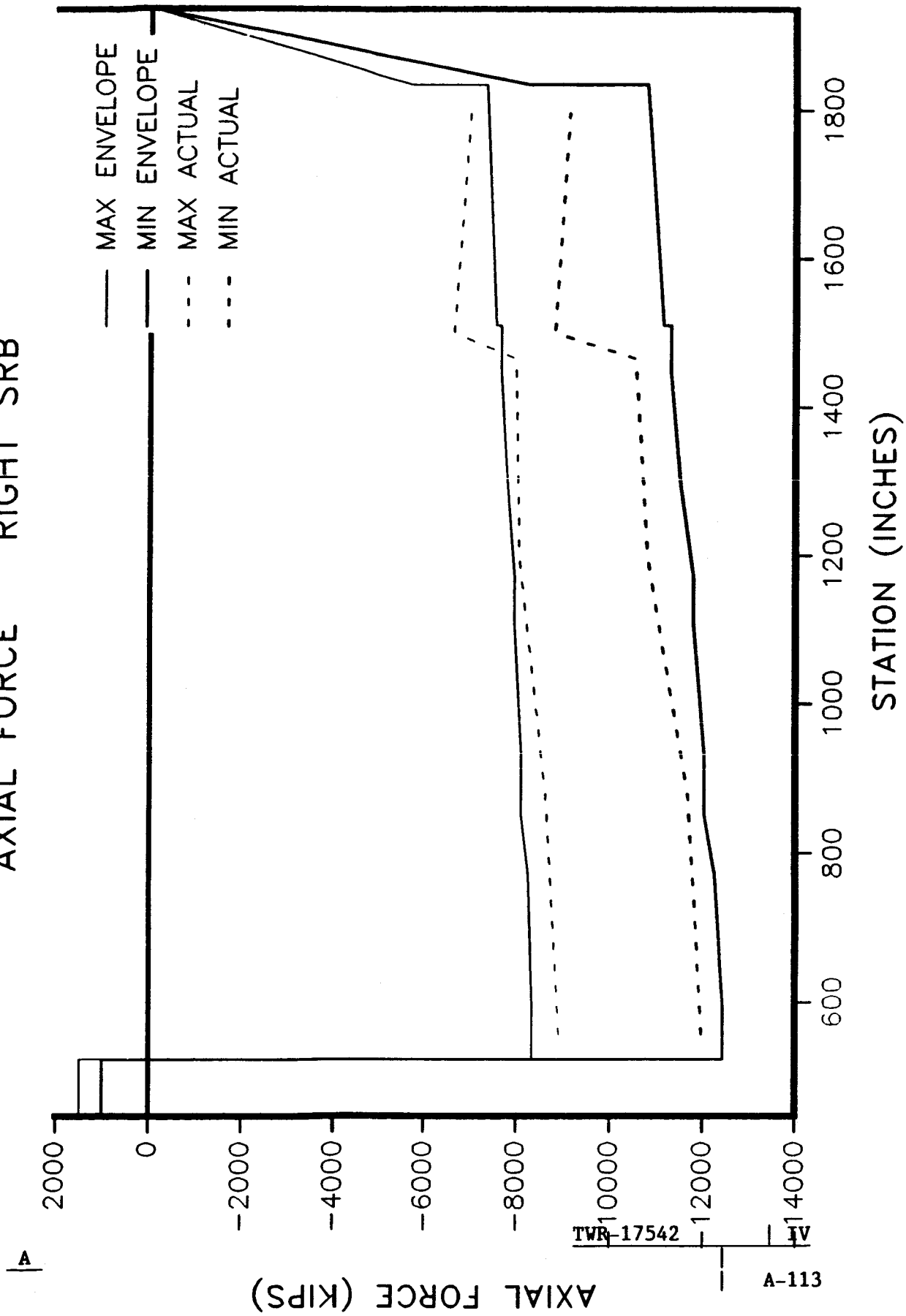
AXIAL FORCE (KIPS)

TWR-17542

A-112

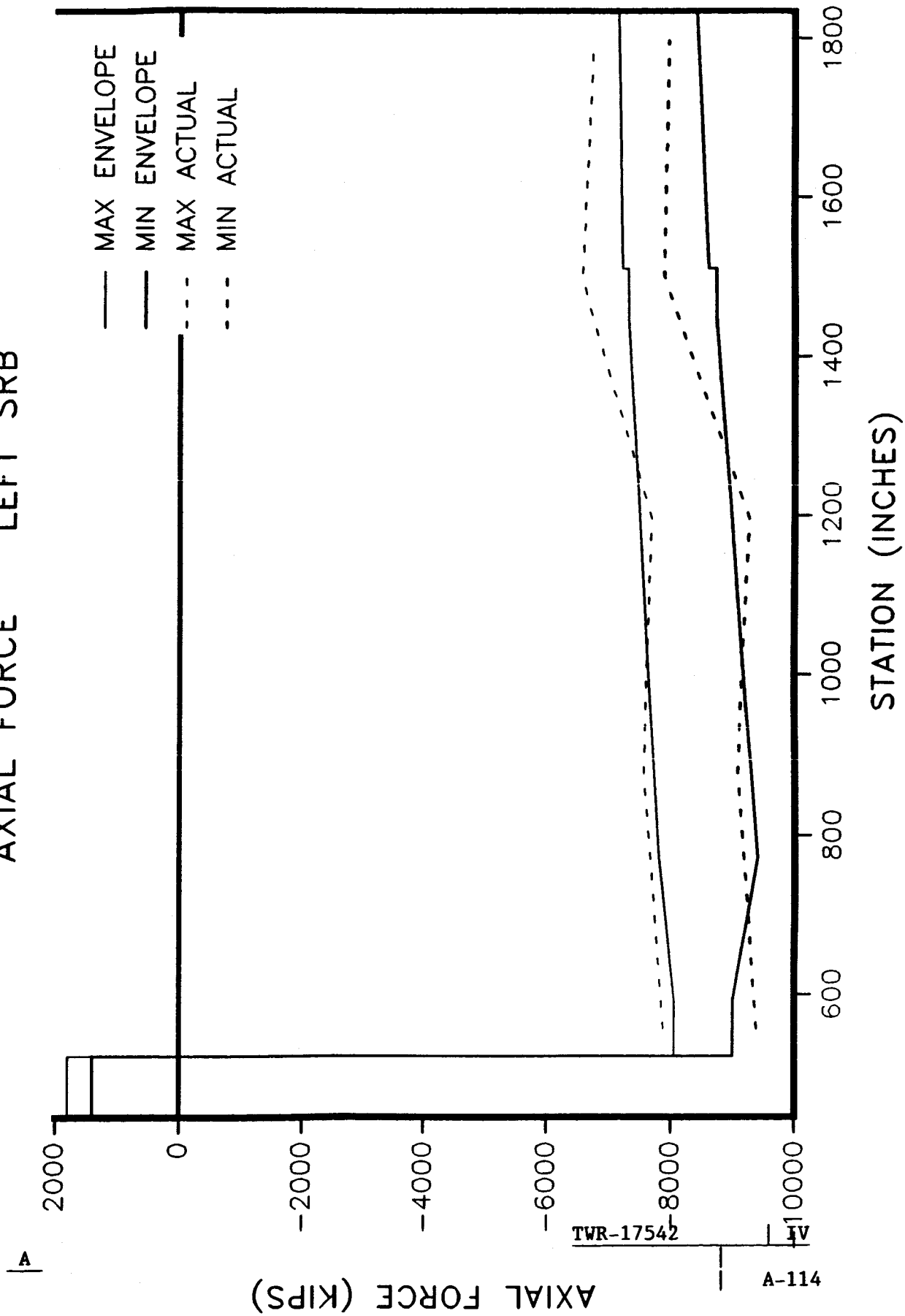
360L003 MAX Q ENVELOPE

AXIAL FORCE RIGHT SRB



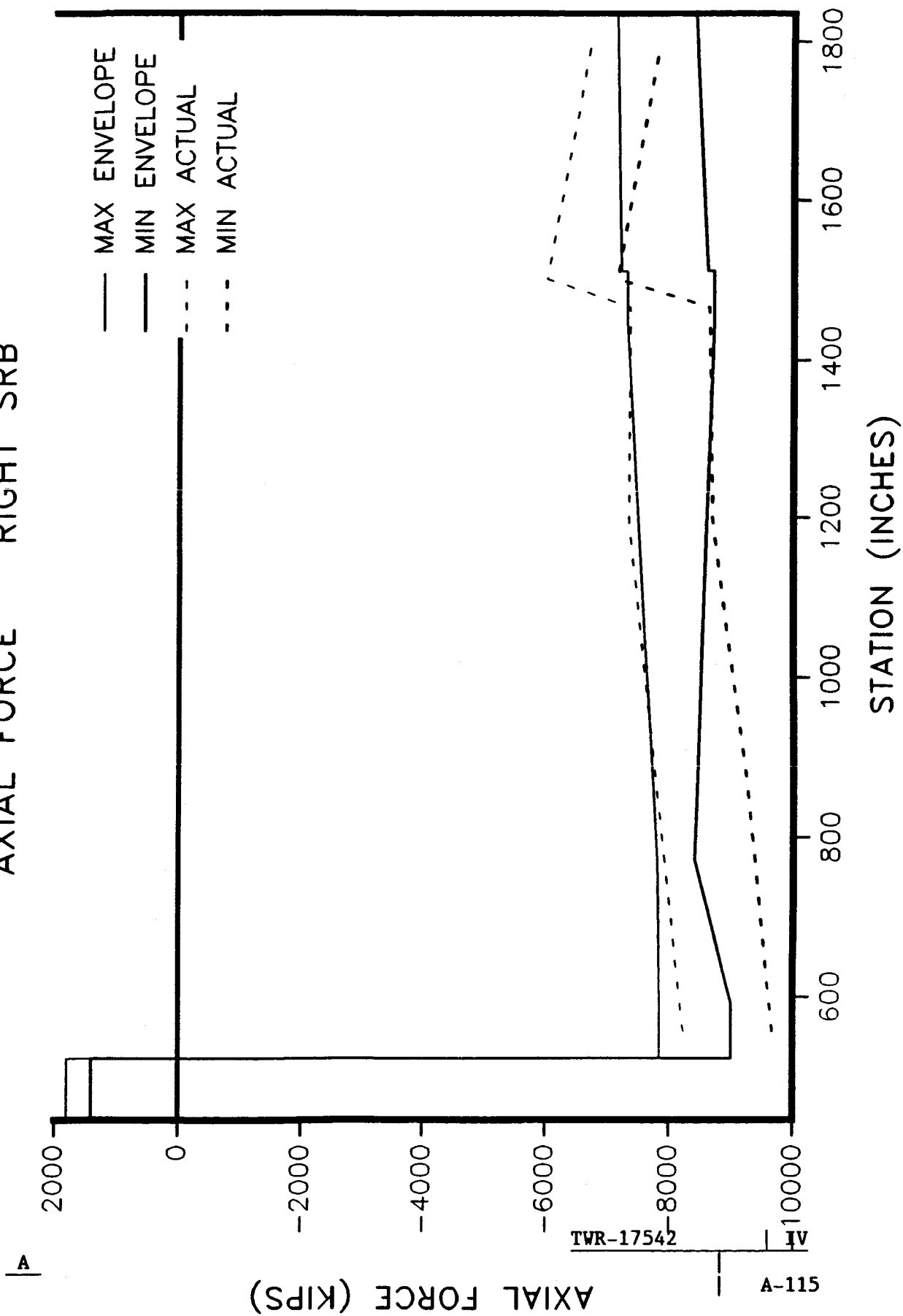
360L003 MAX G ENVELOPE

AXIAL FORCE LEFT SRB



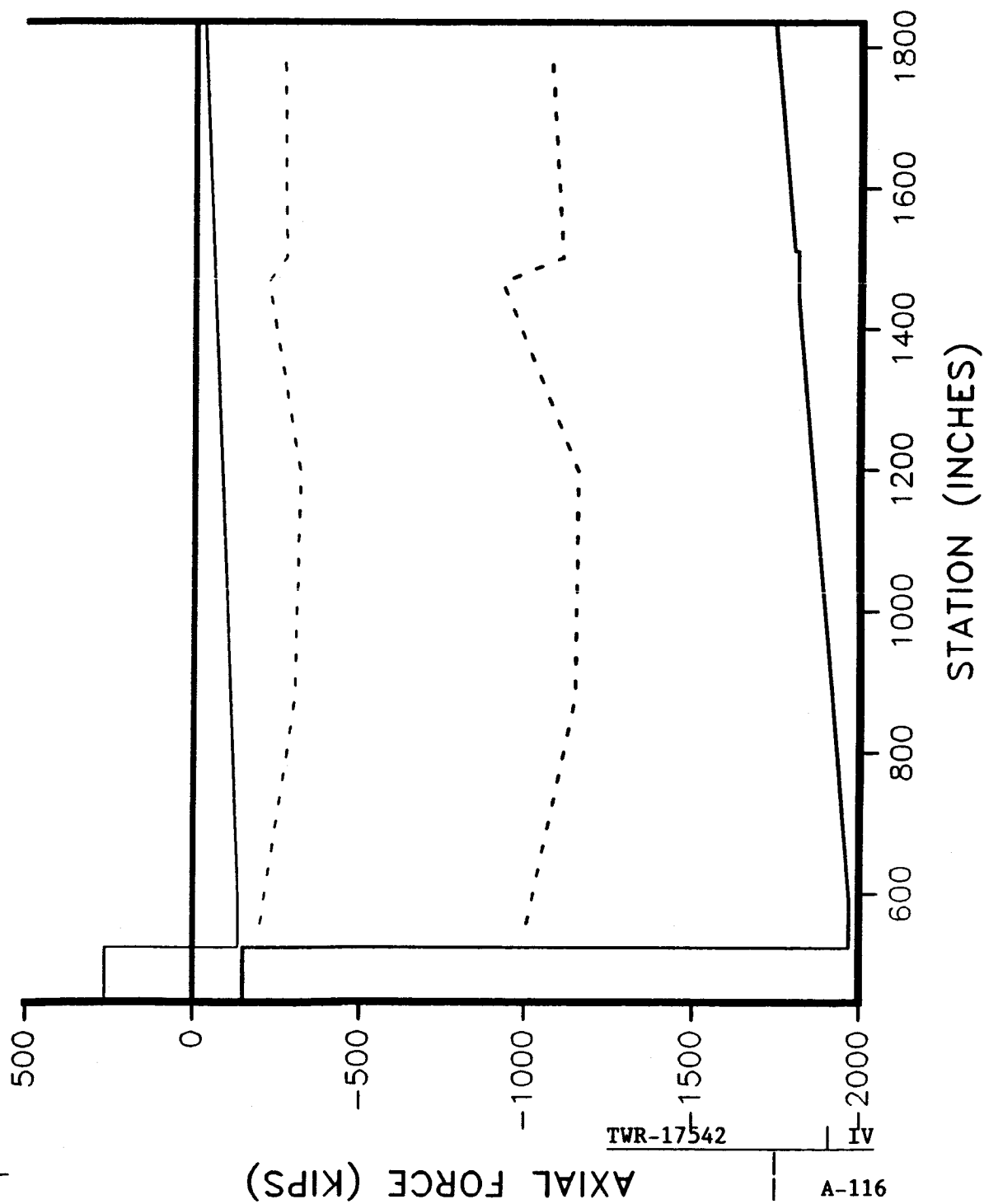
360L003 MAX G ENVELOPE

AXIAL FORCE RIGHT SRB



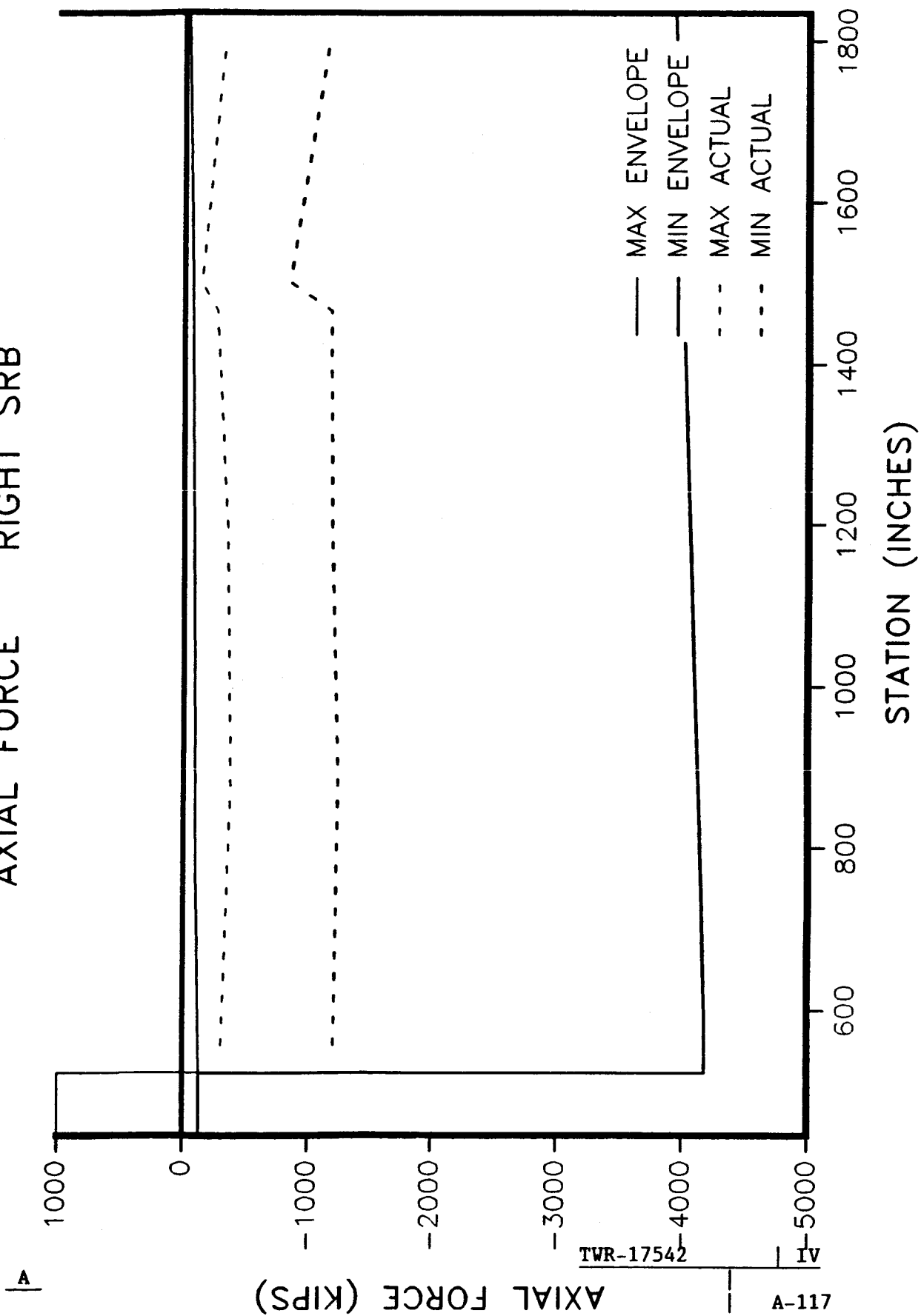
360L003 PRE-STAGING ENVELOPE

AXIAL FORCE LEFT SRB



360L003 PRE-STAGING ENVELOPE

AXIAL FORCE RIGHT SRB



APPENDIX B
RPRB PRESENTATIONS

REVISION **A**

DOC NO.	TWR-17541	VOL	IV
SEC	PAGE	B	

Rev A

360L003 POST-FIRE TEAM ASSESSMENT

SEALS COMPONENT INTERIM REPORT

Kelly Kobayashi

5 April 1989

Coordinated With:

PM - Brent Crosble

PE - Kelly Kobayashi

DE - Gary Nelson

SE - Neil Townsend

MORTON THIOKOL, INC.

Space Operations

INFORMATION ON THIS PAGE WAS PREPARED TO SUPPORT AN ORAL PRESENTATION
AND CANNOT BE CONSIDERED COMPLETE WITHOUT THE ORAL DISCUSSION

Doc

No. TWR-17542 Vol IV

SEAL COMPONENT INTERIM REPORT - 360L003 (Continued)

Rev A

0 360L003 SEAL COMPONENT INTERIM POST-FIRE ASSESSMENT

0 SEAL COMPONENT TEAM REVIEW HELD 31 MARCH 1989

0 TEAM MEMBERS IN ATTENDANCE

Project Engineering - Kelly Kobayashi
Design Engineering - Jeff Curry, Dave Rowsell
Reliability - Jeff Richards
Quality Assurance - Greg Nielson, Carl Shupe
Systems Engineering - Neil Townsend

0 TEAM REVIEW COVERED ALL OBSERVATIONS FROM 360L003 DISASSEMBLY AT KSC

MORTON THIOKOL, INC.
Space Operations

Doc
No. TWR-17542 Vol 1 IV

INFORMATION ON THIS PAGE WAS PREPARED TO SUPPORT AN ORAL PRESENTATION
AND CANNOT BE CONSIDERED COMPLETE WITHOUT THE ORAL DISCUSSION

2

SEAL COMPONENT INTERIM REPORT - 360L003 (Continued)

Rev A

0 FIVE SQUAWK REPORTS WERE WRITTEN AT KSC

0 ONE SQUAWK REPORT WAS ELEVATED TO KSC PROBLEM REPORT.
SECONDARY O-RING DAMAGE ON A CUSTOM VENT PORT PLUG.

0 THREE SQUAWK REPORTS WERE WRITTEN AGAINST SPLASHDOWN
DAMAGES TO SEALS AND SEALING SURFACES ON THE LEFT MOTOR AFT
EXIT CONE JOINT. RESULTED IN ONE KSC PROBLEM REPORT ASSIGNED TO
NOZZLE COMPONENT TEAM.

0 ONE SQUAWK REPORT WAS WRITTEN AGAINST DISASSEMBLY DAMAGE ON
THE RIGHT HAND MOTOR NOZZLE-TO-CASE JOINT WIPER O-RING. SQUAWK
WAS WRITTEN FOR DOCUMENTATION PURPOSES ONLY AT THE CUSTOMER
REQUEST. DISASSEMBLY DAMAGE TO THE WIPER O-RING IS ACCEPTABLE
PER PEEL DOCUMENT.

MORTON THIOKOL, INC.

Space Operations

Doc
No. TWR-17542 Vol IV

SEAL COMPONENT INTERIM REPORT - 360L003 (Continued)

Rev A

- 0 OBSERVATIONS AND ASSESSMENTS DOCUMENTED IN TWR-17542, VOLUME IV.
- 0 ONE OBSERVATION CATEGORIZED AS "POTENTIAL ANOMALY"
- 0 "POTENTIAL ANOMALY" CLASSIFIED AS "MINOR ANOMALY"

Doc
No. TWR-17542 Vol IV

Page B-4

MORTON THIOKOL, INC.
Space Operations

INFORMATION ON THIS PAGE WAS PREPARED TO SUPPORT AN ORAL PRESENTATION
AND CANNOT BE CONSIDERED COMPLETE WITHOUT THE ORAL DISCUSSION

SEAL COMPONENT INTERIM REPORT - 360L003 (Continued)

Rev

PROBLEM REPORT

KSC PR No. PV-6-125083

DESCRIPTION

SECONDARY O-RING FROM RIGHT MOTOR, AFT FIELD JOINT, CUSTOM VENT PORT PLUG (1U76386-32) HAD EXTRUSION DAMAGE ON THE O.D. OF THE O-RING.

HISTORY

EXTRUSION DAMAGE WAS FOUND ON 360L001B NOZZLE-TO-CASE JOINT CUSTOM VENT PORT PLUG SECONDARY O-RING. CLASSIFIED AS "MINOR ANOMALY" 11 NOVEMBER 1988.

TEAM CLASSIFICATION

MINOR ANOMALY, NO CONSTRAINT FOR NEXT LAUNCH.

MORTON THIOKOL, INC.

Space Operations

Doc

No. TWR-17542 Vol IV

SEAL COMPONENT INTERIM REPORT - 360L003 (Continued)

Rev A

RELIABILITY

SPR IS NOT BEING WRITTEN AT THIS TIME.

JUSTIFICATION

EXTRUSION DAMAGE IS FROM AN O-RING OVERFILL CONDITION IN THE SHOULDER SEAL GLAND DUE TO A DIMENSIONALLY DISCREPANT PORT. REFERENCE DRs 163057, AND 174472.

RECOMMENDATION

REWORK 135 DEGREE PORT ON 1U52982-02 S/N 00032 LIGHTWEIGHT CAPTURE FEATURE CYLINDER TO BLUEPRINT SPECIFICATIONS. REFERENCE DR 174472.

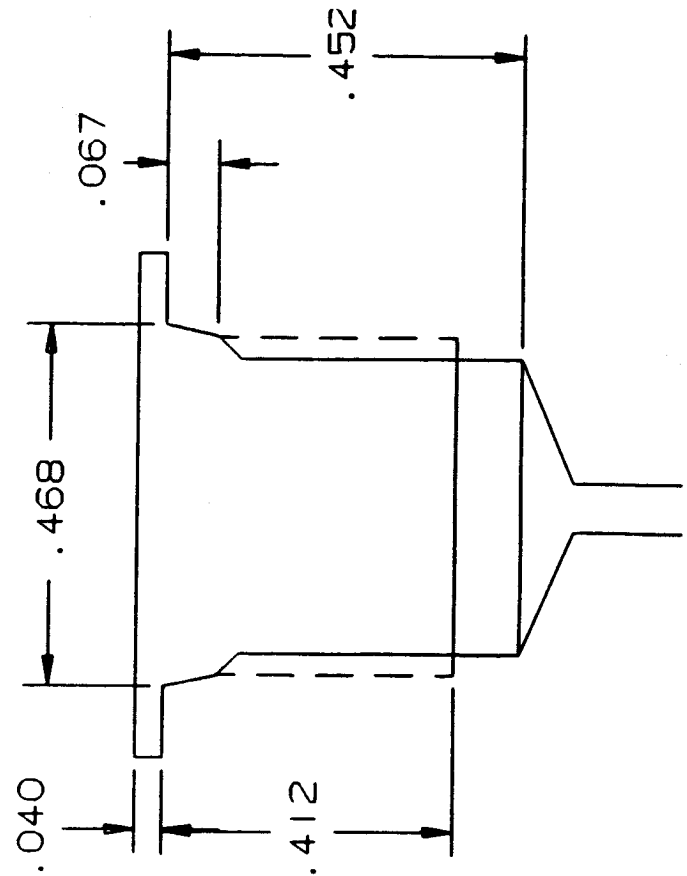
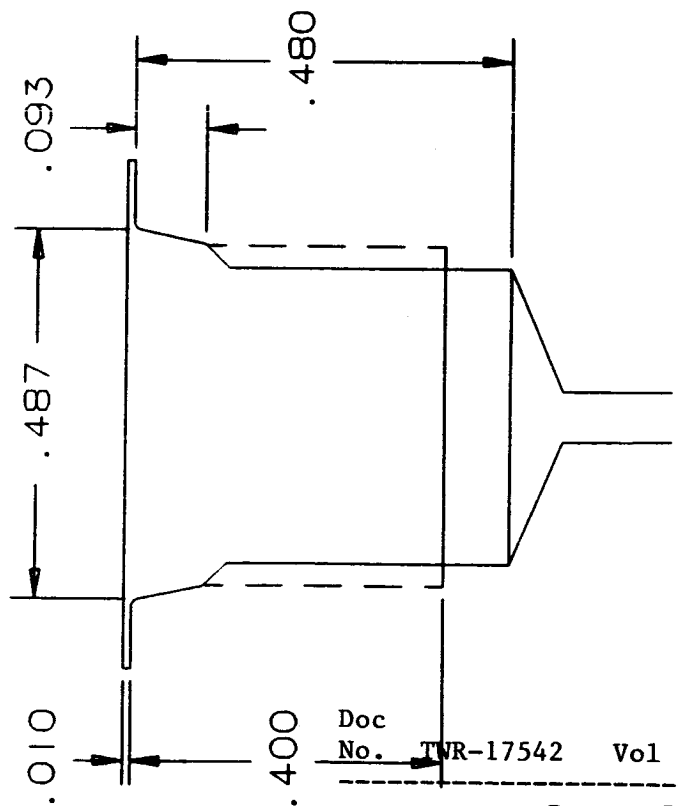
MORTON THIOKOL, INC.
Space Operations

Doc
No. TWR-17542 Vol IV

INFORMATION ON THIS PAGE WAS PREPARED TO SUPPORT AN ORAL PRESENTATION
AND CANNOT BE CONSIDERED COMPLETE WITHOUT THE ORAL DISCUSSION

Rev A

DR 174472



PORT CONFIGURATION (Min)

EXISTING CONDITIONS

RPRB PRESENTATION FOR S&A/B-B PORT PLUG ANOMALIES

Bryan Spaulding
Structural Applications

17 May, 1989

TEAM RECOMMENDATION

Coordinated with:

Program Management -- Brent Crosbie
Project Engineering -- Kelly Kobayashi
Design Engineering -- Gary Nelson, Dave Rowse, Scott Eden
Systems Engineering -- Neal Townsend
Quality Assurance -- Carl Shupe
Reliability -- Jeff Richards

INTRODUCTION

Rev

A

This presentation will inform the RPRB members on the post-flight and test inspection findings concerning the Safe and Arm leak check plugs used on 360L001, 360L002, 360L003, TEM-1, TEM-2, and QM-8.

- Presentation states team findings, corrective actions, and recommendations for PFAR closure.

- Observations made during the A-2 Seal Inspection
- Observations categorized as "Potential Anomaly"
- "Potential Anomaly" classified as "Minor Anomaly"

MORTON THIKOL, INC.

Space Operations

INFORMATION ON THIS PAGE WAS PREPARED TO SUPPORT AN ORAL PRESENTATION AND CANNOT BE CONSIDERED COMPLETE WITHOUT THE ORAL DISCUSSION

2

DOC
NO.

TWR-17542

VOL IV

Page B-9

BACKGROUND

Rev

A

There are two leak check port plugs used on the Barrier-Booster portion of the Safe and Arm device.

- 1 -- Rotor Shaft and Initiator Leak Check Plug
- 2 -- S&A to Igniter Adapter Gasket Leak Check Plug

- Standard MS9902-01 plugs are used.
- ECC initially installs both plugs with O-rings into a B-B prior to shipment to MTI.
- The rotor shaft and initiator plug is removed and reinstalled at MTI prior to KSC shipment.
 - The original O-ring is replaced with a new one.
- The S&A to Igniter Adapter plug is removed and reinstalled at KSC.
 - The original O-ring is replaced with a new one.
- The scratches found were suspected to have occurred during removal of the original O-ring.

MORTON THIOKOL, INC.

Space Operations

INFORMATION ON THIS PAGE WAS PREPARED TO SUPPORT AN ORAL PRESENTATION AND CANNOT BE CONSIDERED COMPLETE WITHOUT THE ORAL DISCUSSION

3

DOC
NO.

TWR-17542

VOL IV

Page B-10

LEAK CHECK PORT PLUG PICTURE

Rev

A

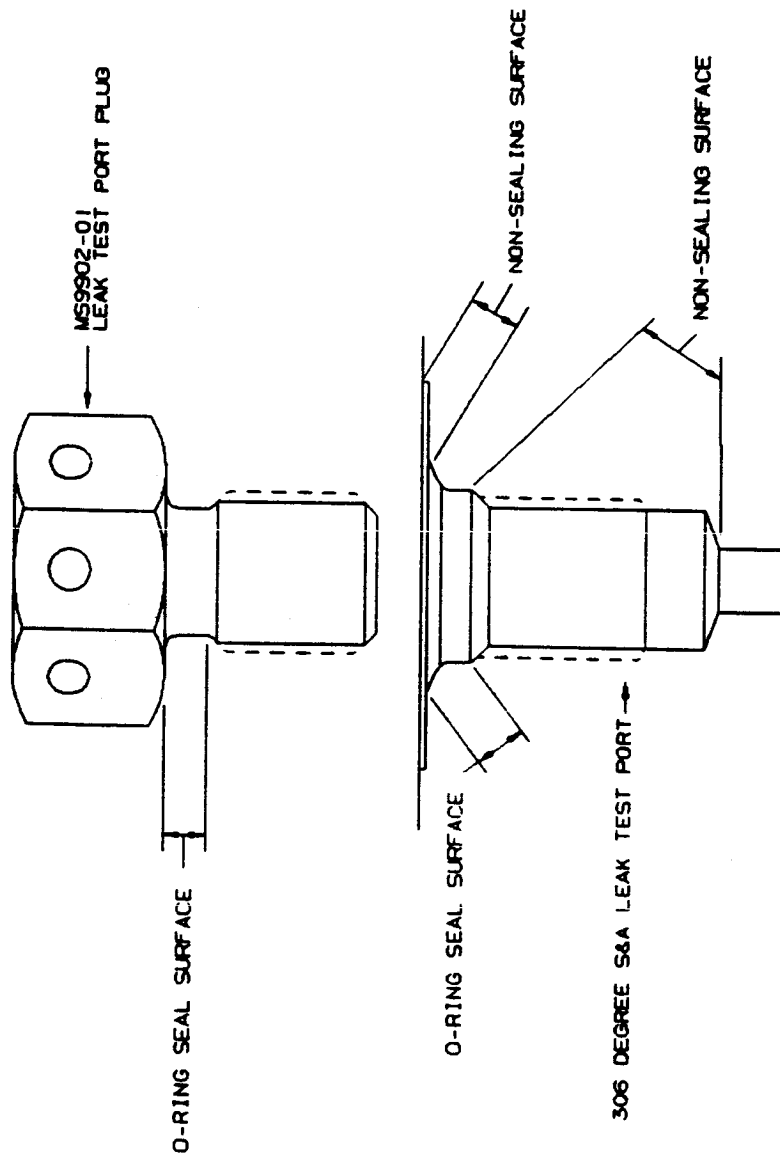


FIGURE 19- - LEAK TEST PLUG/PORT SEALING SURFACES
(FOR REFERENCE ONLY)

MORTON THIOKOL, INC.

Space Operations

INFORMATION ON THIS PAGE WAS PREPARED TO SUPPORT AN ORAL PRESENTATION
AND CANNOT BE CONSIDERED COMPLETE WITHOUT THE ORAL DISCUSSION

4

DOC
NO.

TWR-1754 2 VOL IV

Page B-11

BACKGROUND (Cont'd)

Rev

A

PROBLEM DESCRIPTION

Five of the nine Safe and Arm devices inspected had scratches across the sealing surface of the leak check plug (2B, 3A, 3B, TEM-1, and TEM-2).

- Scratches have been found on both plugs.
- The first scratches were found on Flight 3.
- Reinspection of other plugs showed the same type (less severe) scratches.

TEAM EVALUATION

- Worst case 3rd flight plug tests showed no leakage.
 - Plugs were hand tightened.
- Planning was inadequate at MTI and KSC.
 - Allowed the use of any type of removal tool.
 - Did not provide adequate plug inspection criteria.
 - MTI had no plug reinspection called out after removal of the original O-ring.

HISTORY

- No past history on this anomaly.

MORTON THIOKOL, INC.

Space Operations

INFORMATION ON THIS PAGE WAS PREPARED TO SUPPORT AN ORAL PRESENTATION AND CANNOT BE CONSIDERED COMPLETE WITHOUT THE ORAL DISCUSSION

5

DOC
NO.

TWR-1754 2 VOL IV

Page B-12

RESULTS

Rev

A

TEAM CLASSIFICATION

- Minor anomaly, no constraint for Flight 5 or subsequent

JUSTIFICATION

- Significant departure from documented historical data base.
 - Departure was not due to a change in production practices or engineering.
 - Probable that similar scratches occurred on any unit previously produced.
- Requires corrective action, but no impact on performance or schedule.

DOC
NO.

TWR-1754 2

Page B- 13

MORTON THIOKOL, INC.

Space Operations

INFORMATION ON THIS PAGE WAS PREPARED TO SUPPORT AN ORAL PRESENTATION
AND CANNOT BE CONSIDERED COMPLETE WITHOUT THE ORAL DISCUSSION

RECOMMENDATIONS

Rev

A

SHORT TERM TO CLOSE PFAR

- Suspect plugs on Flight 5 units will be replaced.
- Suspected plugs will be returned to MTI for evaluation.
- O-rings will be replaced.
- Units still at MTI will have the suspect plugs replaced just as Flight 5.
- Planning changed at MTI and KSC to eliminate the possibility of a scratch in the plug sealing surface. (COMPLETED)
 - MTI and KSC will use a brass or non-metallic O-ring removal tool.
 - MTI and KSC will visually inspect each plug in a well illuminated area.
- Close PFAR upon completion of the above recommendations.
- All corrective actions will be completed.

MORTON THIOKOL, INC.

Space Operations

INFORMATION ON THIS PAGE WAS PREPARED TO SUPPORT AN ORAL PRESENTATION
AND CANNOT BE CONSIDERED COMPLETE WITHOUT THE ORAL DISCUSSION

DOC
NO.

TWR-17542

VOL 1V

Page B- 14

RECOMMENDATIONS (Cont'd)

Rev A

LONG TERM IMPROVEMENT

- Change drawing number 1U52293 to install plastic plugs at ECC.
- Change drawings 1U52294 and 1U52295 to install the MS9902-01 plugs at MTI and KSC.
- Install the MS9902-01 plugs after the leak tests at MTI and KSC.
 - Does not require removal of plugs or O-rings.
 - Minimizes the possibility of scratches on the plug sealing surfaces.
- Speeds processing of units at ECC, MTI, and KSC.

MORTON THIOKOL, INC.

Space Operations

INFORMATION ON THIS PAGE WAS PREPARED TO SUPPORT AN ORAL PRESENTATION
AND CANNOT BE CONSIDERED COMPLETE WITHOUT THE ORAL DISCUSSION

DOC
NO.

TWR-17542

VOL IV

Page B-15

DISTRIBUTION

<u>Recipient</u>	<u>No. of Copies</u>	<u>Mail Stop</u>
K. S. Baker	1	L61C
J. Burn	1	L61C
F. W. Call	14	E05
R. B. Crosbie	1	E66
J. B. Daines	1	L61
G. Johnson	1	337A
M. K. Loosle	1	850A
T. W. Morgan	1	L52
K. Sperry	1	L61
W. Starrett	1	L52